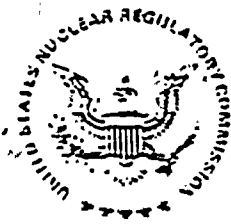


Control # 8204280230

Steam Generator Evaluation
Ginna Steam Generator Tube Failure Incident
January 25, 1982
R. E. Ginna Nuclear Power Plant
Docket No. 50-244

REGULATORY DOCKET FILE COPY

April 26, 1982



UNITED STATES
NUCLEAR REGULATORY COMMISSION
WASHINGTON, D. C. 20555

MEMORANDUM FOR: TERA CORPORATION
FROM: US NRC/TIDC/DOCUMENT MANAGEMENT BRANCH
SUBJECT: Special Document Handling Requirements

- ☒ 1. Please use the following special distribution list for the attached document.

*See Attached.
List*

- ☐ 2. The attached document requires the following special considerations:

- ☐ Do not send oversize enclosures to the NRC PDR.
- ☐ Only one oversize enclosure was received - please return for Regulatory File storage.
- ☐ Proprietary information - send only non-proprietary portions to the NRC PDR.
- ☐ Other: (specify)

cc: DMB Files

TIDC/DMB Authorized Signature

Subject: Steam generator tube rupture

ORB # 5 BC - 5cys

Req File - 1

NRC POR - 1

LPOR - 1

NSIC - 1

NTIS - 1

I & E - 1

NRR/RSB - 1

NRR/ICSB - 1

NRR/MTEB - 1

NRR/CSB - 1

NRR/MEB - 1

NRR/PTRB - 1

NRR/HFEB - 1

NRR/OLB - 1

IE/EPLB - 1

NRR/DL/ORAB - 1

NRR/DSI/AEB - 1

NRR/OSI/RAB - 1

NRR D/DL - 1

NRR D/DE - 1

NRR D/DHFS - 1

IE D/DEP - 1

DENTON/CASE - 1

Speis, T. - 1

Rubenstien - 1

Johnston, W. V. - 1

Knight, J. R. - 1

Houston, R. W. - 1

NRR D/DST - 1

ACRS - 6

Dist per

James E. Lyons 4/19/82

TABLE OF CONTENTS

	PAGE
1.0 <u>INTRODUCTION</u>	
1.1 General	1.1-1
1.2 Inspections	1.2-1
1.3 Repairs	1.3-1
1.3.1 Phase I	1.3-1
1.3.2 Phase II	1.3-1
1.4 Failure Analysis	1.4-1
1.5 Post Repair Program	1.5-1
1.6 Conclusions	1.6-1
1.6.1 Initial Plugging	1.6-1
1.6.2 Subsequent Degradation	1.6-1
1.6.3 Tube Rupture	1.6-2
1.6.4 Adequacy of Repairs	1.6-2
2.0 <u>STEAM GENERATOR CONFIGURATION AND OPERATING HISTORY</u>	
2.1 Configuration	2.1-1
2.2 Operating History	2.2-1
2.2.1 Chemistry	2.2-1
2.2.2 Plugging	2.2-2
2.2.3 Secondary Side Modifications	2.2-3
3.0 <u>STEAM GENERATOR INSPECTION RESULTS</u>	
3.1 Eddy Current Examination	3.1-1
3.2 Profilometry Examination	3.2-1
3.3 Fiber Optics Inspection	3.3-1
3.4 Television Video Inspection	3.4-1
3.5 Foreign Objects	3.5-1
3.5.1 A-Steam Generator	3.5-1
3.5.2 B-Steam Generator	3.5-1
4.0 <u>STEAM GENERATOR TUBE FAILURE ANALYSIS PROGRAM</u>	
4.1 Introduction	4.1-1
4.1.1 General	4.1-1
4.1.2 Program	4.1-1

TABLE OF CONTENTS (continued)

	PAGE
4.2 Postulated Failure Mechanisms	4.2-1
4.2.1 Initial Plugging	4.2-1
4.2.2 Collapse	4.2-1
4.2.3 Severance	4.2-1
4.2.4 Wear	4.2-2
4.2.5 Summary	4.2-2
4.3 Data Review	4.3-1
4.3.1 Purpose	4.3-1
4.3.2 Examination and Repair History	4.3-1
4.3.3 Evaluation	4.3-4
4.4 Metallurgical Review	4.4-1
4.5 Analysis	4.5-1
4.5.1 Design Parameters	4.5-1
4.5.2 Thermal Hydraulic Evaluation	4.5-4
4.5.3 Axial Loads	4.5-9
4.5.4 Lateral Impact Loads	4.5-12
4.5.5 Collapse	4.5-15
4.5.6 Flow Induced Vibration	4.5-18
4.5.7 Fatigue	4.5-22
4.5.8 Wear	4.5-26
4.6 Model Tests	4.6-1
4.6.1 Test Objectives	4.6-1
4.6.2 Test Apparatus	4.6-1
4.6.3 Test Procedure and Results	4.6-2
4.6.4 Conclusions	4.6-4
4.7 Laboratory Tests	4.7-1
4.7.1 Collapse Test	4.7-1
4.7.2 Fatigue Test	4.7-2
4.8 Conclusions	4.8-1
5.0 <u>STEAM GENERATOR REPAIR PROGRAM</u>	
5.1 Access Holes	5.1-1
5.1.1 Description	5.1-1
5.1.2 Installation	5.1-1
5.1.3 Design	5.1-1
5.2 Tube Removal	5.2-1
5.2.1 Summary	5.2-1
5.2.2 Categorization of Tubes	5.2-1
5.2.3 Tube Removal	5.2-2
5.2.4 Severed Tube Removal	5.2-2
5.2.5 Tube Pull	5.2-2
5.2.6 U-Bend Restraint	5.2-2
5.2.7 Remaining Tubes	5.2-2

TABLE OF CONTENTS (continued)

	PAGE
5.3 Loose Parts Removal	5.3-1
5.4 Mechanical Plug Removal	5.4-1
5.5 Material Control	5.5-1
5.6 Post Repair Inspections/Tests	5.6-1
5.7 Radiation Exposure	5.7-1
5.7.1 Planning	5.7-1
5.7.2 Tube Removal	5.7-1
5.7.3 Exposure	5.7-1
 6.0 <u>TECHNICAL BASIS FOR REPAIRS</u>	
6.1 Introduction	6.1-1
6.2 Analyses	6.2-1
6.2.1 Access Ports	6.2-1
6.2.2 Thermal/Hydraulic Evaluation	6.2-2
6.2.3 Structural Evaluation	6.2-4
 7.0 <u>FUTURE ACTIVITIES</u>	
7.1 Metallurgical Examination	7.1-1
7.2 Testing	7.2-1
7.2.1 Westinghouse	7.2-1
7.2.2 Combustion Engineering	7.2-1
7.3 Loose Parts Monitoring System	7.3-1
7.3.1 Summary	7.3-1
7.3.2 Description	7.3-1
7.4 Intermediate Outage	7.4-1
 Appendix A Metallurgical Examination of Ginna Steam Generator Tubes	
 Appendix B EPRI/CE Analyses and Tests, Steam Generator Tubing Structural Analysis	
 Appendix C Ginna Steam Generator External Tube Loading Test	

LIST OF TABLES

TABLE NO.	TITLE
2.1	A-Steam Generator Tube Plugging History
2.2	B-Steam Generator Tube Plugging History
2.3	B-Steam Generator Periphery Area Defects
3.4-1	Data Review B-Steam Generator Hot Leg
4.3-1	Number 6 Wedge Area Plugged Tubes - Inspection History
4.3-2	Number 4 Wedge Area Plugged Tubes - Inspection History
4.5.2-1	Nominal and Between Tube Crossflow Velocities
4.5.3-1	Summary of Worst Case Axial Loads on a Plugged Tube
4.5.4-1	Foreign Object Induced Loads
4.5.6-1	Basic Analysis Model Geometry
4.5.6-2	Tube Fundamental Frequencies for the Various Cases Analyzed
4.5.6-3	Vortex-Shedding Induced Loads on Protrusions for a Fluid Velocity of W.O. Ft./Sec.
4.5.7-1	Calculated Stresses (KSI) - Nominally Plugged Tube
4.5.7-2	Principal Stresses (KSI) - Nominally Plugged Tube
4.5.7-3	Usage Factor for a Nominally Plugged Tube
4.5.7-4	Usage Factor for a Nominally Plugged Tube With Notch or Stress Riser
4.5.7-5	High Cycle Fatigue Curve
4.5.7-6	High Cycle Fatigue Curve
4.8-1	Conclusions about Collapse
4.8-2	Conclusions about Fatigue
4.8-3	Conclusions about Wear
4.8-4	Conclusions about Burst

LIST OF TABLES

TABLE NO.	TITLE
5.1	B-Steam Generator Recovery Exposure
6.2.1-1	Stress Summary for 3 Inch diameter Access Port
6.2.2-1	Between Tube Crossflow Velocities in and Near the Tubes Removed Region
6.2.3-1	Summary of Maximum Tube Gap Velocities
6.2.3-2	Summary of Vortex Shedding & Turbulence Analyses

LIST OF FIGURES

FIGURE NO.	TITLE
2.1	Series 44 Steam Generator
2.2	Wedge Area Configuration
2.3	A-Steam Generator Plugged Tube Map
2.4	B-Steam Generator Plugged Tube Map
3.4-1	Secondary Side Tube Sheet Periphery Video
3.4-2	B-Steam Generator Hot Leg
4.2-1	Postulated Failure Mechanism Sequence
4.3-1	Number 4 Wedge Area: Plugging History
4.5.1-1	Schematic Showing Hot Leg Span Geometry
4.5.2-1	Charm Model
4.5.2-2	Three Dimensional (WECAN) Hydraulic Model of Tube sheet to First Support Plate Region
4.5.2-3	R-Z Distribution of Nodes for 3-D Hydraulic Analysis
4.5.2-4	R- θ Distribution of Nodes for 3-D Hydraulic Analysis
4.5.2-5	Computed Average Velocities
4.5.2-6	Base Case Computed Average Velocities
4.5.2-7	Velocity Vector and Quality Distributions
4.5.2-8	Velocity Vector and Quality Distributions
4.5.2-9	Velocity Vector and Quality Distributions
4.5.2-10	Velocity Vector and Quality Distributions
4.5.2-11	Fluid Velocities in the Node 11 Cell
4.5.4-1	Dynamic Model of Foreign Object Impact
4.5.4-2	Steam Generator Tube Spring Force Time History - Case 1

LIST OF FIGURES

FIGURE NO.	TITLE
4.5.4-3	Foreign Object and Steam Generator Tube Displacement Time History - Case 1
4.5.4-4	Steam Generator Tube Spring Force Time History - Case 2
4.5.4-5	Foreign Object and Steam Generator Tube Displacement Time History - Case 2
4.5.4-6	Steam Generator Tube Spring Force Time History - Case 3
4.5.4-7	Foreign Object and Steam Generator Tube Displacement Time History - Case 3
4.5.5-1	External Pressure and Axial Load Required for Incident Yielding
4.5.5-2	Computer Model for Uniform Pressure Loading
4.5.5-3	Model Used for Concentrated Loading
4.5.5-4	Boundary Conditions for Concentrated Load Model
4.5.5-5	Concentrated Radial Loads
4.5.5-6	Axial Distance from Load
4.5.6-1	Basic Analysis Model Geometry
4.5.6-2	Fluidelastic Stability Ratio of Tubes - Fixed-Fixed
4.5.6-3	Fluidelastic Stability Ratio of Tubes - Fixed-Pinned
4.5.6-4	Fluidelastic Stability Ratio Comparison
4.5.6-5	Cylindrical Cross Section Tube - Cross Flow Velocity
4.5.6-6	Flat Cross Section Tube - Cross Flow Velocity
4.5.6-7	Tear Model for Calculating
4.5.6-8	Illustration of Alternating Lift and Frequency vs. Fluid Velocity for a Tear

LIST OF FIGURES

FIGURE NO.	TITLE
4.5.6-9	Illustration of Alternating Lift and Frequency vs. Fluid Velocity for a Tear
4.5.6-10	Illustration of Alternating Lift and Frequency vs. Fluid Velocity for a Tear
4.6.2-1	Plan view of Flow Test Model
4.6.2-2	Section View of Flow Test Model
4.6.2-3	Rear Elevation View of Flow Test Model
4.6.2-4	Photograph of Tube Bundle Used in Flow Test Model
4.6.2-5	Region of Test Simulation
4.6.2-6	Test Simulation Detail
4.6.2-7	Cold Flow Loop
4.6.2-8	Biaxial Accelerometer Orientation
4.6.2-9	Force Transducer Orientation & Installation Assembly
4.6.2-10	Photograph of Force Transducer Mounted in Tube Support Plate
4.6.3-1	Foreign Object
4.6.3-2	Tube Accelerometer Response Time Histories for Foreign Object Impact
4.6.3-3	Tube Force Transducer Time Histories for Foreign Object Impact
4.6.3-4	Tube Response for Foreign Object Impact
4.6.3-5	Tube Accelerometer Response Time Histories for Instrumented Impact Hammer
4.6.3-6	Tube Force Transducer Response for Instrumented Hammer Impact
4.6.3-7	Accelerometer Calibration Data
4.6.3-8	Force Transducer Calibration Data

LIST OF FIGURES

FIGURE NO.	TITLE
4.6.3-9	Tube Wear Photograph
4.6.3-10	Tube Wear Photographs
4.6.3-11	Tube Accelerometer Response Envelopes
4.6.3-12	Tube Accelerometer Response with Tube Degradation
4.6.3-13	Severed Tube Accelerometer Response
4.7.1-1	Test Fixture for Collapse of Steam Generator Tubes
4.7.1-2	Photograph Showing the Test Set Up for Tube Collapse Test
4.7.1-3	Photograph Showing Instrumentation Details for the Tube Collapse Test
4.7.2-1	View of Test Set Up
4.7.2-2	View of Test Set Up
4.7.2-3	Close View of Fatigue Test Set Up
4.7.2-4	Close View of Fatigue Test Set Up
4.7.2-5	Instrumentation Block Diagram
4.8-1	Postulated Failure Mechanism Sequence
5.1	Three inch access hole cross sectional view
5.2	Number 4 Wedge Area
5.3	Number 6 Wedge Area
5.4	Access Hole Cover Plate Assembly Details
5.5	Categorization of Defects, B-Steam Generator
6.2.1-1	Location of Access Ports
6.2.1-2	Finite Element Model
6.2.2-1	Charm Lateral and Axial Velocity Values
6.2.2-2	Charm Lateral and Axial Velocity Values

LIST OF FIGURES

FIGURE NO.	TITLE
6.2.2-3	Charm Lateral and Axial Velocity Values
6.2.2-4	Charm Lateral and Axial Velocity Values
6.2.2-5	Quality Distribution
6.2.2-6	Quality Distribution
6.2.3-1	Collapse Pressure of Tubing with Elliptical Wastage
6.2.3-2	Collapse Pressure of Axially Stalled Tubing
6.2.3-3	Collapse Pressure of Uniformly Thinned Tubing
6.2.3-4	Schematic of a Partial Tube
7.1	Steam Generator Loose Part Monitor Sensor Locations
7.2	Electrical One Line Steam Generator Loose Part Detection System
B.1	Worst Load Conditions Prior to Tube Plugging
B.2	Worst Load Conditions After Tube Plugging
B.3	First Mode Natural Frequency as a Function of Axial Compressive Load
B.4	Fluid-Elastic Vibrations
B.5	Temperature Distributions for Various Loading Conditions
B.6	Computer Print Pattern of the Element Layout
B.7	Element Layout
B.8	Temperature vs. Time Curves
B.9	Downcomer Temperature Distribution for Hot Standby
B.10	Downcomer Temperature Distribution for 100% Power Steady State
B.11	Downcomer Temperature Distribution for Cold Feed at Hot Standby
B.12	Transient Downcomer Annulus Outlet Temperature Vs. Time Plot

LIST OF FIGURES

FIGURE NO.	TITLE
B.13	Mass Quality at 7 Inches Above Tube Sheet
B.14	Radial Velocity at 7 Inches Above Tube Sheet
B.15	Axial Velocity at 14 Inches Above Tube Sheet
B.16	Void Fraction at 7 Inches Above Tube Sheet
B.17	Mass Quality at 20 Inches Above Tube Sheet
B.18	Radial Velocity at 20 Inches Above Tube Sheet
B.19	Axial Velocity at 27 Inches Above Tube Sheet
B.20	Mass Quality at 33 Inches Above Tube Sheet
B.21	Radial Velocity at 33 Inches Above Tube Sheet
B.22	Mass Quality at 91 Inches Above Tube Sheet
B.23	Radial Velocity at 46 Inches Above Tube Sheet
B.24	Axial Velocity at 51.8 Inches Above Tube Sheet
B.25	Mass Quality at 46 Inches Above Tube Sheet
B.26	Radial Velocity at 91 Inches Above Tube Sheet
C.1	External Tube Loading Test Apparatus

Steam Generator Evaluation

1.0 INTRODUCTION

1.1 General

At 9:25 a.m. on January 25, 1982, a tube ruptured in the B-Steam Generator at Ginna Station. A report summarizing the sequence of events, operator actions, emergency procedures, equipment performance, radiological assessment, and recommendations relative to the transient itself was submitted to the NRC by letter dated April 13, 1982. This report provides information specifically related to the tube failure. The work described in this report is a culmination of work performed by several organizations including Rochester Gas and Electric, Westinghouse, EPRI, and Combustion Engineering.

Shortly following the achievement of cold shutdown conditions on January 26, 1982, a comprehensive corrective action program was developed for the B-Steam Generator. The objectives established for this program were:

- a) determine the full extent of defects,
- b) determine the tube failure mechanism(s),
- c) restore the steam generator to a condition which is safe to operate while maintaining radiation exposures as low as reasonably achievable, and
- d) obtain NRC concurrence for return to power.

To accomplish these objectives, an extensive series of inspections, tests, repairs, and analyses have been performed.

1.2 Inspections

The elevation of the tube rupture was determined by filling the secondary side of the steam generator with water, and observing the wide range level as the generator was drained. The level dropped to below the bottom level tap before stopping. Since the tap is centered 12 inches above the tube sheet, this meant that the rupture was at the lower end of the tube. Observation of the tube sheet from the primary side manways as a small amount of water was added showed water leaking from the inlet, or hot leg, side of tube Row 42 Column 55 (R42 C55). Subsequent fiber optic inspection of the inside diameter (I.D.) of the tube confirmed the presence of the burst.

Extensive eddy current, fiber optics, video, and visual inspections have been performed in both the A and B steam generators. Eddy current examinations have been performed in 100% of the hot leg tubes and a random sample of cold leg tubes in each steam generator. Profilometry examination was performed in a random sample of tubes in the B-Steam Generator. A combination of fiber optic and video inspections were performed on the secondary side of each steam generator at the tube sheet. These inspections included viewing the tube bundles from the periphery of both the hot and cold legs, and from the tube lane in the B-Steam Generator. Additional fiber optic and video inspections of the Number 4 and Number 6 wedge areas in the B-Steam Generator were performed through access holes drilled in the shell of the steam generator. Visual inspections of the upper internals or steam drum of each steam generator were also performed.

1.3 Repairs

1.3.1 Phase I

The repairs to the B-Steam Generator were performed in two phases. Phase I included plugging of R42 C55; drilling two, 3 inch diameter access holes in the secondary shell; and removing metallurgical samples of selected tubes. The removal of metallurgical samples involved the cutting of several sections of tubing from the Number 4 wedge area; and pulling the hot leg side of R45 C47 from the top of the tube bundle. The results of the metallurgical examination of these tubes are reported in Appendix A to this report.

1.3.2 Phase II

The Phase II repairs included removal of structurally degraded tube sections from between the tube sheet and first support plate, and removal of mechanical plugs from 3 acceptable tubes surrounding R42 C55. These 3 tubes had been preventatively plugged prior to performing the secondary side video inspections. Metallurgical examination of the tube sections removed during this phase is presently in progress. Tube ends were restrained in the U-bend region where sections of tubing had been removed. Foreign objects were removed from both steam generators; and tubing fragments were removed from the B-Steam Generator during the repairs.

1.4 Failure Analysis

The failure analysis program has consisted of metallurgical examinations, analyses, and testing. The metallurgical examinations included visual inspections, photography, radiography, metallography, and scanning electron microscopy. Analyses have been performed to quantify the potential effect of lateral loads, flow induced vibration, local fluid loads, and axial loads on tube failure. Laboratory testing is being performed to demonstrate the effect of lateral loads, fatigue, and axial loads on steam generator tubing. Model testing has been performed to study the behavior and interaction of foreign objects and tubing in a simulated flow environment.

1.5 Post Repair Program

A series of inspections and tests will be performed in the B-Steam Generator following completion of repairs. This will include eddy current examination of tubing adjacent to any area involved in the repairs, another secondary side video inspection at the tube sheet, and primary and secondary side hydrostatic tests. A loose parts monitoring system will be installed on the primary and secondary side of each steam generator prior to start-up. An intermediate outage is scheduled to perform another set of steam generator inspections.

1.6 Conclusions

1.6.1 Initial Plugging

The eddy current examinations of periphery tubes in the B-Steam Generator showed both I.D. and O.D. defects. The metallurgical examinations of the tube pulled in 1978 showed evidence of O.D. surface cold working and an O.D. bulge. The metallurgical examinations of the periphery tube sections removed from the steam generator during the present outage have also found cold working of O.D. surfaces. These examinations have also found O.D. surface defects. None of the examinations to date has found any evidence of corrosion or I.D. defects.

Axial load analysis shows that there is insufficient force developed to initiate the tube damage. Model testing has demonstrated that foreign objects are very mobile in the flow field at the bottom of the generator. This testing also showed that the flow velocities are high enough to cause relatively large foreign object impact loads on steam generator tubes. The magnitude of the loads has been corroborated by analysis. Therefore, the most probable cause of the initial tube plugging appears to have been defects resulting from foreign object impacts. However, axial load may have been a contributing factor in the initial plugging of some tubes.

1.6.2 Subsequent Degradation

Video and subsequent metallurgical examination has shown varying degrees of degradation of previously plugged tubes. In addition to minor dings and similar small defects, this degradation included collapse, severing, and wear. The structural degradation of tubes (collapse, severing, or through wall wear) occurred only in the Number 4 and Number 6 wedge areas. Analysis and test results show that external operating pressures alone will not collapse a plugged tube. The results show that weakening of the tube by wall thinning or ovalization, and/or additional stress from lateral or axial loads, must exist in combination with external pressure, to cause collapse. The metallurgical examinations found significant cold working of the collapse surfaces.

Model testing and calculations have been performed which show that a foreign object can impose the magnitude of lateral loads required to contribute to collapse or severing. The fatigue analysis and testing show that a collapsed tube under sufficient lateral and axial load will fail (sever). Axial load analysis shows that, assuming lockup at the first support plate, axial loads are significantly higher in wedge area tubes. Severing of collapsed tubes in the Number 4 wedge area, but not the Number 6 wedge area, appears to be related to a foreign object residing there for a longer period of time. Vibration analysis shows that collapsed tubes are subject to flow induced vibration, and that severed tubes vibrate with an amplitude sufficient to interact with adjacent tubes.

1.6.3 Tube Rupture

Review of the eddy current data and metallurgical examination results for tube R42 C55 shows that it went from less than 40% to 84% wall thinning between May 1981 and January 25, 1982. Wear calculations for one Inconel tube rubbing on another are consistent with this rate. The metallurgical examinations show that R42 C55 had a ductile, tensile overload failure. Burst strength calculations, assuming nominal ultimate strength for Inconel tubing, show that 0.875 inch O.D. tubes will burst at 87% uniform, circumferential wall thinning. The metallurgical examinations show no evidence of corrosion or surface irregularities on R42 C55. All of the available evidence shows that tube R42 C55 ruptured due to excessive hoop stress from internal pressure. The excessive hoop stress was caused by thinning of the tube wall from wear by an adjacent tube. The adjacent tube was able to vibrate against R42 C55 since it had severed as a result of the failure sequence described above.

1.6.4 Adequacy of Repairs

All structurally degraded tube sections have been removed from the B-Steam Generator. An extensive program of inspection and removal has been performed to assure that no loose parts remain in the generator. The inspection, analysis, and test results show that the structural degradation of tubes which led to the rupture of R42 C55 was caused by the presence of a relatively large foreign object in a hot leg wedge area. The results indicate that a foreign object will not cause structural degradation of tubes outside the wedge areas of the steam generator. Removal of the foreign objects will preclude additional structural degradation of active or plugged tubes, and potential rupture of an active tube. In addition, the analyses and tests show that, in the absence of a foreign object, the plugged tubes with minor O.D. defects will not experience further degradation.

2.0 STEAM GENERATOR CONFIGURATION AND OPERATING HISTORY

2.1 Configuration

Ginna Station's steam generators are Westinghouse Series 44 vertical shell and U-tube units of the recirculating design and operation. They are rated at 3,130,000 lbs/hr. steam flow at 725 psig. The steam generator tubing is mil-annealed Inconel 600 conforming to ASTM Specification SB-163-61T. The 3260 tubes are partially rolled into the tube sheet and seal-welded, leaving an approximately 19 inch crevice in the 22 inch tube sheet. The support plates are carbon steel of the drill hole design. Attachment of the support plates to the wrapper and shell is accomplished by wedging the support plate against the wrapper and welding the wedges in place at six equally spaced locations around the periphery of the support plate. There are twelve (12) locations around the circumference of the support plate where wedges could be applied. However, by design, only six (6) of these locations are used for attachment of each support plate. The support plate in these locations is free of the 0.375 inch diameter flow holes for several rows into the bundle. These areas of the support plate are called "wedge areas". See Fig. 2.1 and 2.2 for details of the configuration.

2.2 Operating History

2.2.1 Chemistry

When Ginna Station began hot functional testing in November 1969, the secondary water chemistry control recommended by Westinghouse Electric Corporation was phosphate buffering control. From start-up through 1970, emphasis was placed on pH control only. As a result, the Marcy/Halstead ratio of sodium to phosphate (NaPO_4) generally ranged between 2.8 to 6.0. In 1971 through 1972, recommended chemistry was modified to maintain the Marcy/Halstead ratio to less than 2.6. Early in 1973, when stress corrosion cracking (SCC) had become evident at several plants, a further reduction of the Marcy/Halstead ratio to 2.1 was recommended. However, as Na/PO_4 was concentrating in the sludge at the lower ratios, an acidic condition was being formed which resulted in wastage attack of the tubing. Therefore, a new Marcy/Halstead ratio range of 2.3 to 2.6 was recommended in late 1973.

During the period of phosphate type control, steam generator blowdown rate was a maximum of 16 gallons per minute per steam generator. Other coordinated phosphate control parameters were as follows:

pH	-	8.5 to 10.6
PO_4	-	10 to 80 ppm
Free OH^-	-	0
Chloride	-	under 75 ppm

Since the phosphate buffering chemistry control was difficult to maintain without concentrating an aggressive environment in the sludge-saturation zone of the tube sheet, Westinghouse recommended in September 1974 that all their operating plants switch from phosphate control to the all volatile treatment (AVT) chemistry control. Ginna had experienced some acidic wastage type attack which was identified by an eddy current examination in the spring of 1974. In November 1974, Ginna was shut down for steam generator inspection, water lancing, and conversion of water chemistry control to AVT. Steam generator blowdown was increased to 64 gallons per minute per steam generator to assure that cation conductivity would be as low as achievable.

During subsequent operation, cation conductivity progressively improved, decreasing from 2.5 μmhos in December 1974 to approximately 0.7 μmhos by 1977. Typical 1977 blowdown chemistry was as follows:

cation conductivity	-	0.70 μmhos
chloride	-	<50 ppb
sodium (Na)	-	<10 ppb

In order to provide assurance that feedwater purity was maintained on AVT, condenser integrity was continually monitored by eddy current examination and preventative plugging of damaged tubes during shutdowns. As a further measure, full flow, deep bed condensate polishers were installed and put into operation in January 1978. Blowdown rates were increased to 70 gallons per minute per steam generator in February 1979.

The following blowdown chemistry comparison demonstrates the continued improvement in bulk water chemistry over the last eight years:

<u>Parameter</u>	<u>1974-1977</u>	<u>1978</u>	<u>1981</u>
Cation Cond., μ mhos	0.7-2.5	0.2-0.4	0.12-0.2
Chloride, ppb	< 50	< 10	3-5
Sodium, ppb	5-15	5-15	3-8
Silica, ppb	20-50	15-30	5-10
pH	8.6-9.0	8.7-8.9	8.7-8.9

Since November 1969, oxygen concentration has generally been less than 5 ppb. There have been several times over the last twelve years when dissolved oxygen has been as high as 40 ppb for several days. From July 1978 to the present, feedwater dissolved oxygen has been less than one (1) ppb.

Operating chemistry has been closely monitored throughout plant life and has progressively improved over the operating history of Ginna Station. Participation in the Steam Generator Owners' Group with the Electric Power Research Institute has provided valuable information regarding operating chemistry. Presently, Ginna Station's secondary water chemistry and feedwater purity are well within the Owners' Group Guidelines.

2.2.2 Plugging

Ginna Station's first pluggable defects were identified in March 1974 by an eddy current examination of both steam generators. The pluggable defects were found only in the A-Steam Generator and were confirmed to be wastage of the Inconel 600 tubing. Within three years after conversion to the AVT water chemistry, the plugging of tubes in the A-Steam Generator for secondary side attack was essentially eliminated. See Table 2.1 and Fig. 2.3 for further definition of the A-Steam Generator tube plugging history.

The B-Steam Generator has had a different plugging history. Its first pluggable defect did not occur until after the AVT conversion. The first pluggable defects were identified in March 1975 and were characterized as stress corrosion cracking (SCC). SCC occurred because of the molar ratio shift (Na/PO_4) resulting in the sludge after conversion from phosphate control to the all volatile treatment (AVT) chemistry control. This shift resulted in a caustic environment being formed in previously phosphated

sludge since, on AVT, there is no addition of phosphate to buffer the sodium hydroxide. As with the A-Steam Generator, within a few years after AVT conversion, secondary side corrosion indications subsided. However, beginning in 1976, defects were found in the periphery area. These defects were mainly in the wedge areas (areas where the support plates are attached to the shell of the steam generator) within the first four (4) inches above the tube sheet. However, four (4) tubes adjacent to the Number 4 wedge area were found to have indications about 24 inches above the tube sheet. The majority of these defects were interpreted as internal diameter indications based on the eddy current signals.

In the spring of 1979, the first indications of tubesheet crevice intergranular attack (IGA) were identified in the B-Steam Generator. Since that time, a total of 74 indications of crevice IGA have been identified, 16 of which have been sleeved and the others plugged. Table 2.2 and Figure 2.4 provide further definition of the B-Steam Generator tube plugging history. Table 2.3 is a detailed listing of the periphery defects including tubes that have been plugged one or two rows in from the periphery.

2.2.3 Secondary Side Modifications

In March 1975, modifications were made to the steam generators to improve the lateral flow velocities across the tube sheet and to improve blowdown efficiency. The purpose of increased flow velocity and blowdown was to reduce the sludge pile area and volume on the tube sheet, thereby reducing the concentrating medium where corrosion of the tubes had been seen.

The modifications consisted of the following:

- a) Modification of the feedring so that 80% of the feedwater would flow down the hot leg side of the steam generator and the remaining 20% would flow down the cold leg side.
- b) Removal of the downcomer flow resistance plate to increase the recirculation ratio from 2.36 to 4.73.
- c) Replacement of the moisture separator swirl vane orifice rings with smaller diameter rings to increase the moisture separator efficiency.
- d) Installation of blowdown lane flow blockers to prohibit flow from bypassing the tube bundle and coming into the blowdown lane directly from the wrapper annulus.

Due to the increased recirculation ratio, the total moisture carryover was higher than desired. Therefore, a modification was performed in February 1976 consisting of the installation of perforated plates on the moisture separator demister end plates.

To provide further assurance that water hammer due to feedring drainage would not occur, another modification of the feedrings was performed in February 1979. This modification involved plug-welding all the bottom drain holes on the feedring and installing J tubes on top of the feedring. The J tubes were located so as to maintain the 80% to 20% feedwater flow split between the hot and cold legs, respectively.

During the March 1982 refueling and maintenance outage, further moisture separation equipment modifications have been implemented to increase their effectiveness and efficiency. These modifications involved installation of upper deck plate relief with directional chimneys and steam flow redirection pagodas over the swirl vanes, and the addition of larger demister drains.

TABLE 2.1

GINNA STATION
A-STEAM GENERATOR
TUBE PLUGGING HISTORY

<u>DATE</u>	<u>WASTAGE</u>	<u>SCC*</u>	<u>PITTING</u>	<u>MANUF.</u>	<u>TOTAL</u>
In Factory				1	1
March, 1974	19				19
November, 1974	2				2
March, 1975***		46**			46
February, 1976	39				39
April, 1977	13				13
April, 1978			1		1
April, 1980	<u> </u>	<u> </u>	<u>1</u>	<u> </u>	<u>1</u>
TOTALS	73	46	2	1	122

* - SCC (caustic stress corrosion cracking.)

** - one tube leak of less than 0.1 gallons per minute

*** - plugging criteria changed from 50% to 40% wall penetration

TABLE 2.2

GINNA STATION
B-STEAM GENERATOR
TUBE PLUGGING HISTORY

<u>DATE</u>	<u>WASTAGE</u>	<u>SCC+</u>	<u>IGA++</u>	<u>PERIPHERY</u>	<u>TOTAL</u>
March, 1975+++		11			11
January, 1976	(2)*			(2)	2
February, 1976	2				2
April, 1976				15*	15
April, 1977	1				1
July, 1977	1			5*	6
January, 1978	6			2*	8
April, 1978				15	15
February, 1979	2		2	2	6
December, 1979			11	2*	13
April, 1980	1		31**	2	34
November, 1980			3**		3
May, 1981			14**	1	15
January, 1982			13	3***	16
TOTALS	15	11	74**	49	147

(2) - these 2 tubes were wastage indications below the top of the tube sheet on the periphery

* - 5 tube leaks less than 0.1 gallons per minute

** - 28 tubes of 74 were not above plugging limit of 40% wall penetration

*** - R42 C55 tube rupture

+ - SCC (caustic stress corrosion cracking)

++ - IGA (tube sheet crevice intergranular attack of the tubes)

+++ - plugging criteria changed from 50% to 40% wall penetration

TABLE 2.3

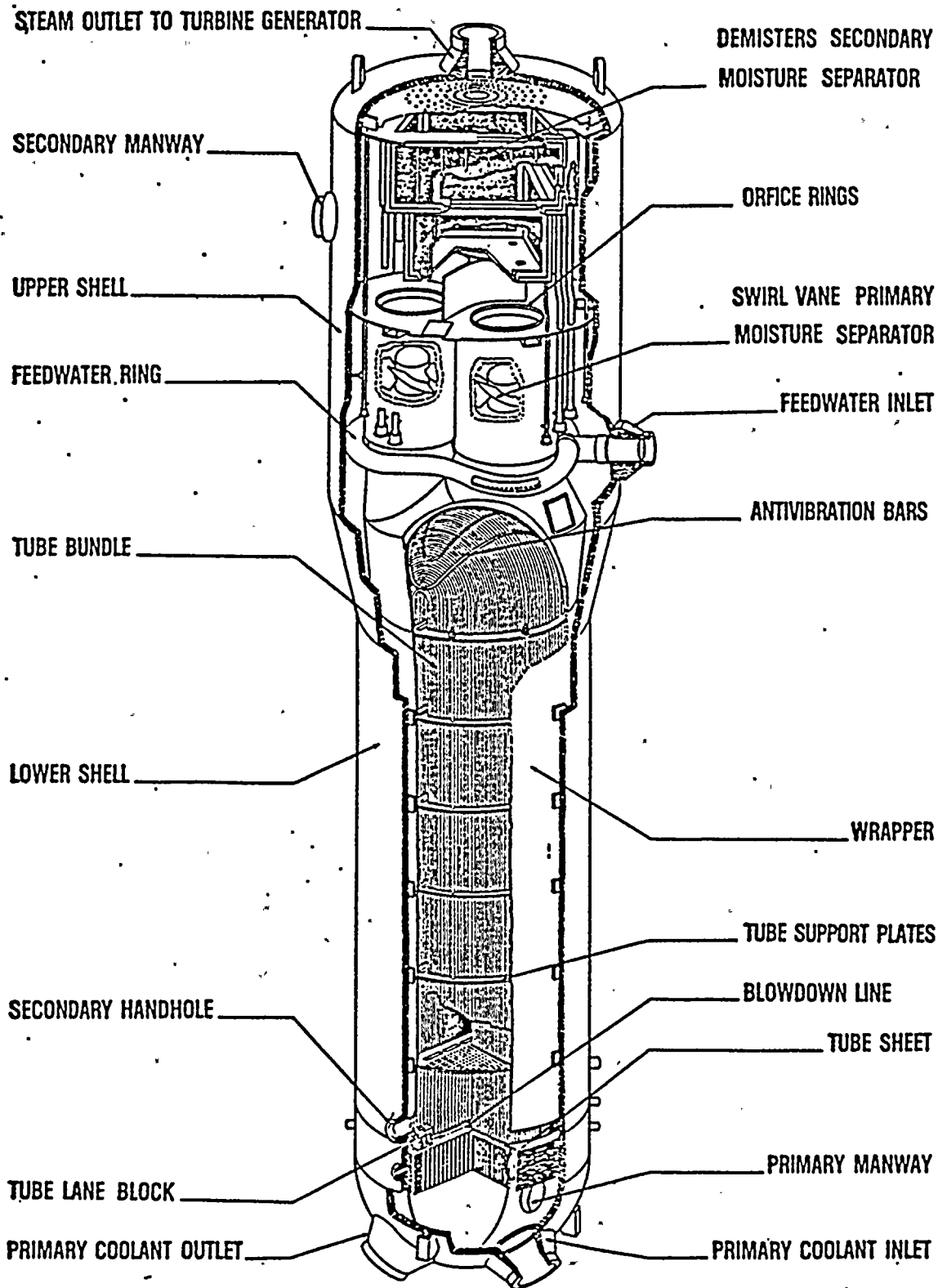
GINNA STATION
B-STEAM GENERATOR
PERIPHERY AREA DEFECTS
ORIGINAL EDDY CURRENT INTERPRETATION

January 76	-	R39 C69	-	O.D.'s top of tube sheet (TTS)
		<u>R40 C68*</u>	-	I.D.'s 2" below TTS
May 76	-	R8 C92	-	I.D. at TTS
		R9 C91	-	I.D. 3" above TTS
		R10 C91	-	I.D. 2"-4" above TTS
		R11 C91	-	I.D. at TTS
		<u>R12 C91*</u>	-	I.D. at TTS
		R13 C90	-	Distorted tube sheet entry
		R14 C90	-	I.D. 2"-4" above TTS
		R15 C90	-	I.D. 2" above TTS
		R15 C89	-	OK (No Defect)
		R16 C89	-	I.D. 2" above TTS
		R17 C89	-	I.D. 2" above TTS
		R30 C15	-	47% O.D. 2" above TTS
		R31 C15	-	43% O.D. 3" above TTS
		R32 C15	-	I.D. at TTS
		R33 C15	-	I.D. at TTS
July 77	-	<u>R45 C54*</u>	-	Bulge and I.D. signal 2"-4" above TTS
		<u>R44 C55</u>	-	Bulge and I.D. signal 2"-4" above TTS
		R44 C56	-	Bulge and I.D. signal 2"-4" above TTS
		R44 C57	-	Bulge and I.D. signal 2"-4" above TTS
		R44 C58	-	Bulge 2"-4" above TTS
		R12 C2	-	O.D. above TTS
January 78	-	R45 C53	-	Bulge and I.D. 2"-4" above TTS
		<u>R44 C54*</u>	-	100% Defect (July 77 I.D. above TTS)
April 78	-	R45 C50	-	I.D. at TTS
		R45 C51	-	I.D. at TTS
		R45 C52	-	Bulge 2"-4" above TTS, Defect below TTS
		R44 C52	-	Damaged when R45 C52 was pulled
		R44 C53	-	Distorted TTS
		R43 C58	-	I.D. at TTS
		R43 C59	-	I.D. at TTS
		R43 C60	-	Noisy I.D. signal at TTS
		R43 C61	-	Noisy I.D. signal at TTS
		R41 C66	-	Many I.D. signals at TTS
		R40 C67	-	I.D. at TTS
		R39 C68	-	O.D. and I.D. above TTS
		R39 C70	-	I.D. at TTS
		R38 C71	-	I.D. at TTS
		R38 C72	-	I.D. at TTS

TABLE 2.3 (continued)

February 79	-	R43 C55	-	Distorted tube sheet entry
		R43 C56	-	O.D. and I.D. above TTS
		R35 C75	-	63% O.D. at #2 Support plate (cold leg)
		R28 C12	-	47% O.D. at #1 Support plate (cold leg)
December 79	-	R43 C54*	-	100% Defect
		R43 C57	-	80% O.D. above TTS
April 80	-	R45 C48	-	46% O.D. 24" above TTS
		R45 C49	-	36% O.D. 24" above TTS
		R32 C16	-	41% O.D. 2" above TTS
April 81	-	R43 C53	-	80% O.D. above TTS
February 82	-	R42 C55	-	Burst
		R45 C46	-	41% O.D. 24" above TTS
		R45 C47	-	49% O.D. 24" above TTS

* - leaks less than 0.1 gallons per minute



W SERIES 44 STEAM GENERATOR

NOT TO SCALE
9189

FIGURE 2.1

RG&E Steam Generator
HOT LEG (INLET)

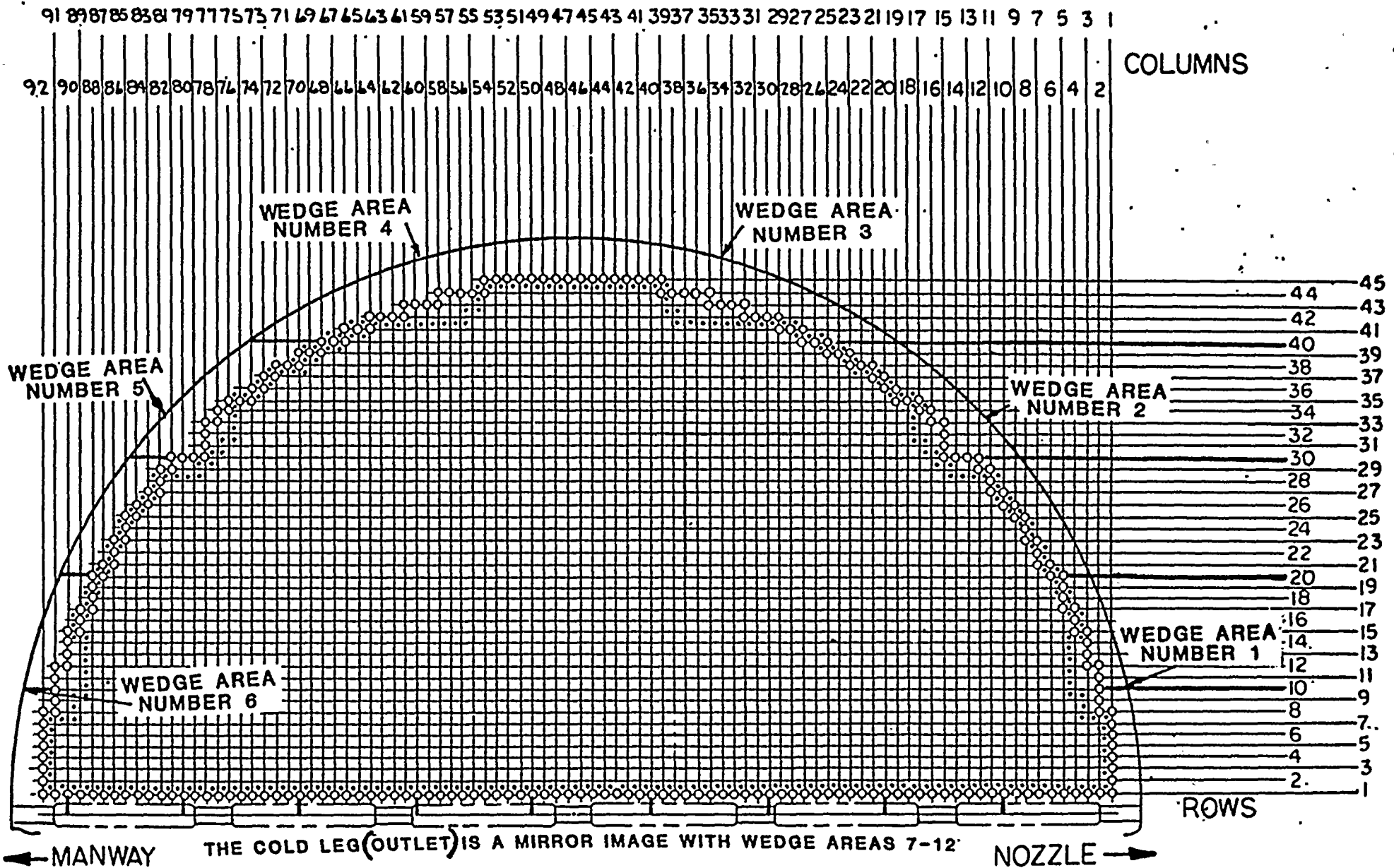


FIGURE 2.2

A S/G

RG&E Steam Generator A INLET PLUGGED TUBE MAP

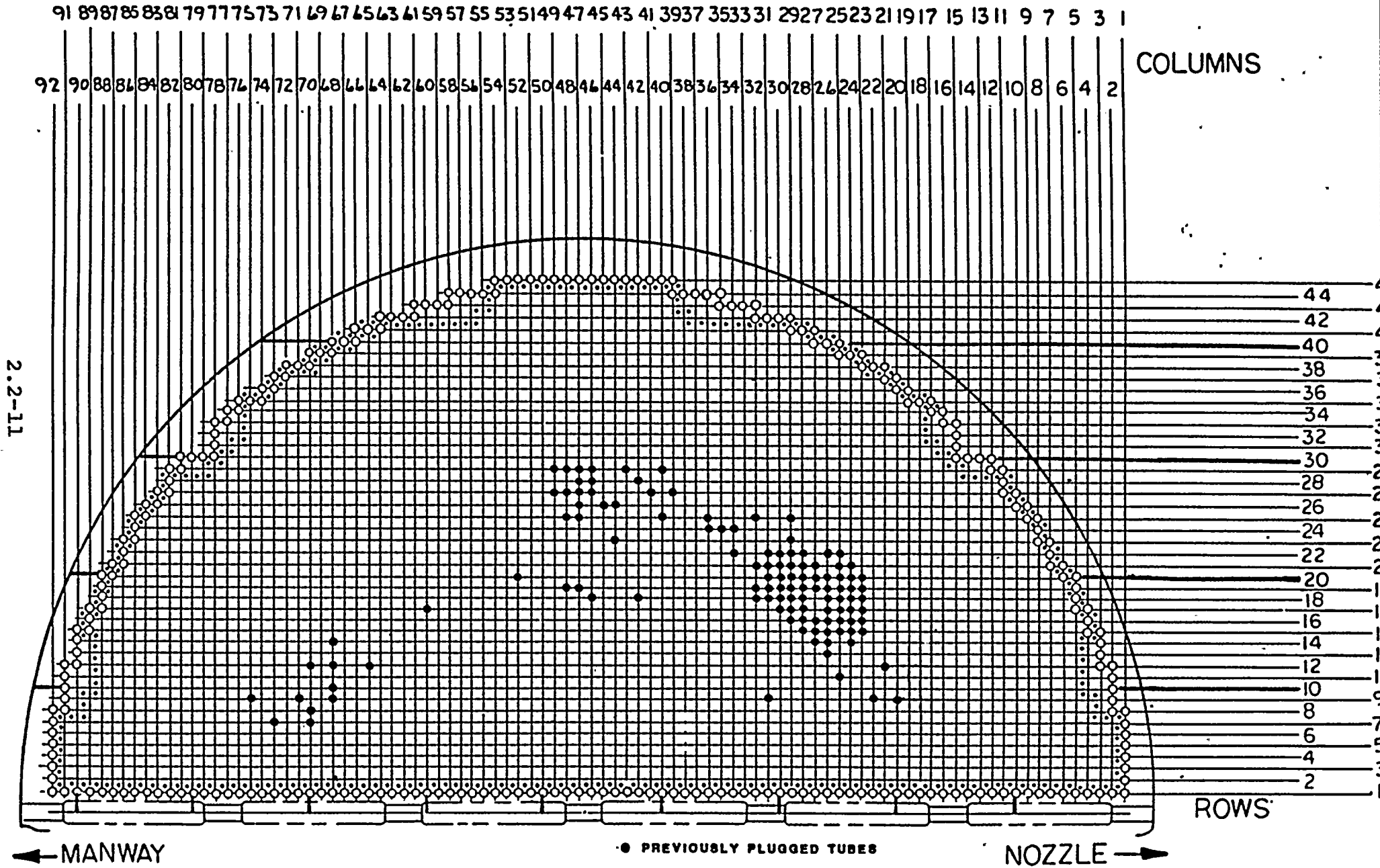


FIG. 2.3

B S/G

RG&E Steam Generator
B INLET PLUGGED TUBE MAP

91 89 87 85 83 81 79 77 75 73 71 69 67 65 63 61 59 57 55 53 51 49 47 45 43 41 39 37 35 33 31 29 27 25 23 21 19 17 15 13 11 9 7 5 3 1

COLUMNS

92 90 88 86 84 82 80 78 76 74 72 70 68 66 64 62 60 58 56 54 52 50 48 46 44 42 40 38 36 34 32 30 28 26 24 22 20 18 16 14 12 10 8 6 4 2

2.2-12

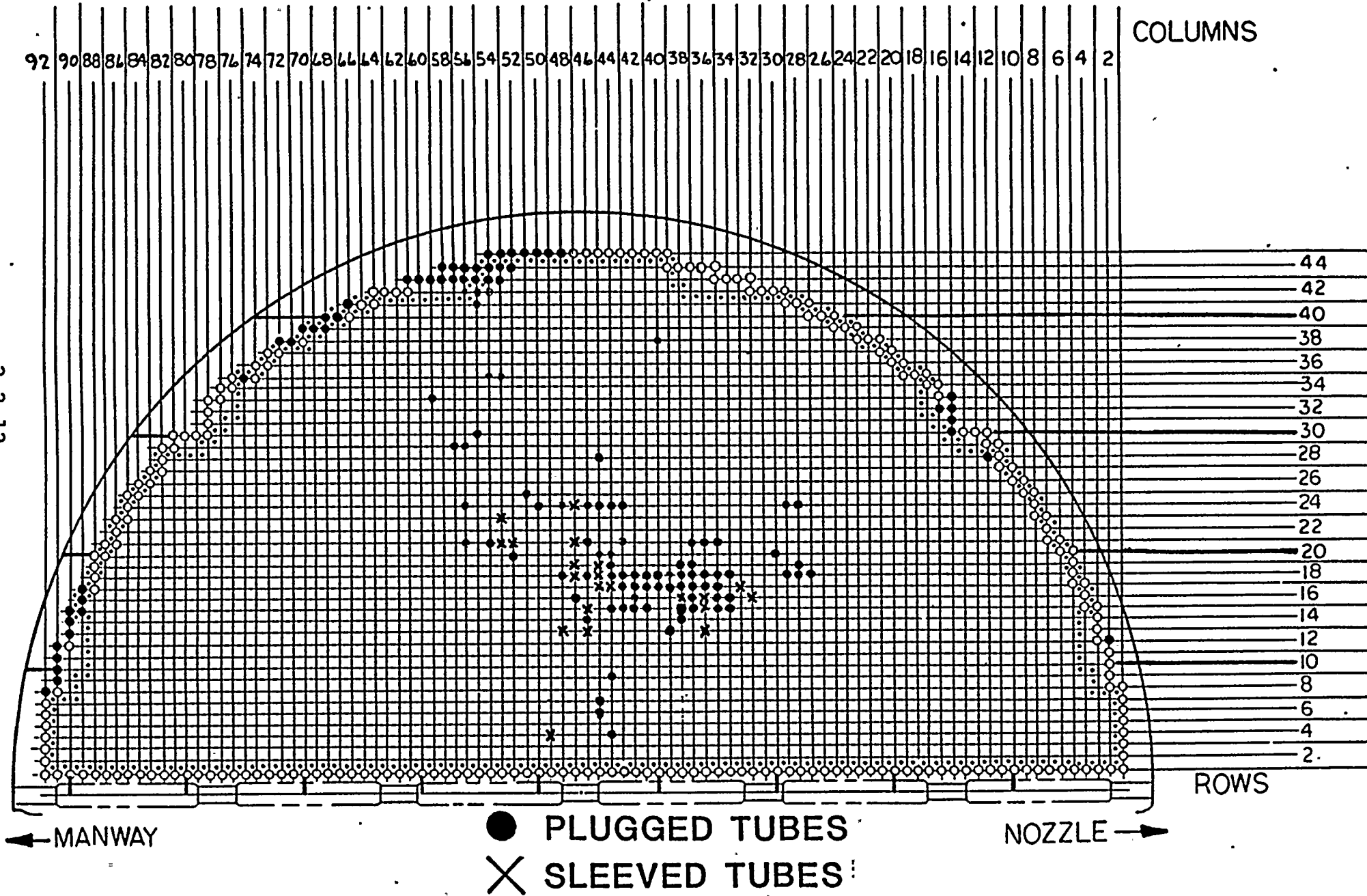


FIG. 2.4

3.0 STEAM GENERATOR INSPECTION RESULTS

3.1 Eddy Current Examination

The inspection of the B-Steam Generator after the January 25th tube rupture started with a hydrostatic leak test to identify the burst tube. By visual inspection during the leak test, tube R42 C55 in the B hot leg (inlet) was identified as the leaking tube. No other tubes were found to be leaking from this leak test. After visual verification, a single frequency 400 kHz eddy current examination was made of the leaking tube by hand probing from the primary manway. A large volume defect was found approximately 5 inches in length running from 3 to 8 inches above the tube sheet.

The method used for the multifrequency eddy current examination of the total steam generator was the same method that has been used for the last four inspections. This state-of-the-art method includes techniques that provide maximum sensitivity to the types of damage which are being identified in steam generators throughout the industry. Specifically, both differential and absolute techniques are used as follows:

- a) 400 kHz differential
- b) 200 kHz differential
- c) 210 kHz absolute
- d) 100 kHz absolute

In order to increase the sensitivity in areas where support plates and tube sheet indications normally mask actual tubing defects, mixing of both the differential and absolute frequencies respectively, was utilized.

The scope of the multifrequency eddy current examination included 100% of both steam generators' hot leg (inlet) tubes, all periphery tubes, and a sampling of the cold leg (outlet) tubes of both steam generators. A tube examination consists of examining a tube from at least the first support plate through the tube sheet. A sampling of tubes over the U-bends and to the sixth support plate level was also examined.

Results of the multifrequency eddy current examination of the A-Steam Generator hot and cold legs (inlet and outlet) and the B-Steam Generator cold leg (outlet) revealed no pluggable indications or any noticeable changes from previous inspections. There were no pluggable indications or any noticeable changes from previous inspection results above the first support plate in either steam generator. However, the B-Steam Generator hot leg (inlet) did reveal that further degradation had occurred in several tubes since the last inspection. There were no indications found similar to the burst tube R42 C55. Two tubes, R45 C46 and R45 C47, had indications 24 inches above the tube sheet of 41% and 49% through the wall, respectively. These indications were approximately mid-span between the tube sheet and the first

support plate. Thirteen tubes were found with defects in the crevice, similar to the defects from crevice IGA which have been identified in the past. The following is a list of those tubes:

1. R9 C44 - 14 inches below the top of tube sheet (TTS)
2. R16 C42 - 12 to 14 inches below TTS
3. R18 C39 - 4 to 12 inches below TTS
4. R20 C45 - 10 inches below TTS
5. R20 C44 - 10 inches below TTS
6. R21 C56 - 10 inches below TTS
7. R21 C43 - 4-12 inches below TTS
8. R24 C56 - 4 inches below TTS
9. R24 C48 - 6-10 inches below TTS
10. R33 C59 - 17 inches below TTS to rolled transition
11. R35 C54 - 16 inches below TTS to rolled transition
12. R35 C53 - 12 inches below TTS to rolled transition
13. R38 C40 - 16 inches below TTS to rolled transition

Five of these crevice indications have not changed since the Spring 1981 inspection.

3.2 Profilometry Examination

Assessment of any geometric conditions that may have been associated with the burst tube, or other tubes in the vicinity of the burst tube, was accomplished by use of the Babcock and Wilcox Company's profilometry equipment. This procedure utilizes strain gauges with fingers attached which are calibrated to known deflections of larger or smaller diameters than the nominal inside diameter of the tubes.

Approximately 75 tubes were examined including the burst tube (R42 C55), tubes around the burst tube, and a sampling of tubes on the periphery.

The results of this inspection revealed about 20 tubes that had a dent at the first support plate. These dents were generally less than 10 mils. In addition, the burst tube had bulged in the area of fracture as had been expected. These results did not provide any insight into the cause of the burst.

3.3 Fiber Optics Inspection

As part of the inspection program, fiber optics inspections were performed from the primary and the secondary side of the burst tube. The secondary side inspection included probing the columns on either side of the burst tube, and then coming around the periphery of the steam generator on the tube sheet and viewing into the bundle in the area of the burst tube.

The primary side probing of the burst tube revealed a diamond shaped burst approximately 4 inches long and 0.75 inches wide at its widest point. Secondary side inspection results from the column probing revealed no abnormal observations.

As the inspection was progressing around the periphery, abnormal damage was observed to previously plugged tubes around rows 44 and 45, columns 58 to 53. Also, as the fiber optics equipment was being removed from the steam generator, a foreign object was identified around the area of R25 C85. The foreign object identified was a carbon steel plate 0.5 inches thick by 4.18 inches wide by 6.31 inches long. This plate was removed along with another piece of carbon steel approximately 0.050 inches thick by 0.6 inches wide by 4 inches long. Because of these results, further inspection was deemed necessary, utilizing equipment and procedures that would allow for a greater field of vision with higher resolution of the steam generator periphery tubes.

3.4 Television Video Inspection

After the fiber optics inspection results became available on February 10 and 11, equipment was located capable of performing a video inspection within the geometric constraints of the steam generator periphery. A Westinghouse Underwater Reactor Vessel Inspection Video System was selected for the inspection. After three days of mock-up work and procedure development, the inspection technique was implemented in the B-Steam Generator on February 14.

The video inspection consisted of, first, scanning the periphery tubes around the total circumference of the steam generator hot and cold legs and then, second, scanning the columns perpendicular to the tube sheet blowdown lane. These two areas were inspected in both the A and B-Steam Generators, as defined by Fig. 3.4-1.

Scanning the columns perpendicular to the tube sheet blowdown lane did not reveal any abnormalities in either steam generator. Foreign objects were found in both steam generators. Tube damage was only found in the B-Steam Generator hot leg. The tube damage identified was mainly associated with previously plugged tubes in the Number 4 and 6 wedge areas. In addition, some minor scrapes and dings were identified on tubes located near R40 C68. No defects were found on tubes in the Number 2 wedge area. (This was confirmed by subsequent, more detailed, fiber optics examination.) Complete inspection results for the B-Steam Generator hot leg are documented in Table 3.4-1.

TABLE 3.4-1

DATA REVIEW B-STEAM GENERATOR HOT LEG

<u>Tube</u>	<u>Results</u>	<u>Location</u> (see Fig. 3.4-2)
R1C92	OK	
R2C92	OK	
R3C92	OK	
R4C92	OK	
R5C92	OK	
R6C92	OK	
R7C92	OK	
R8C92	COLLAPSED WITH HOLE - PLUGGED	A
R9C91	O.D. DAMAGE (Ripples on surface) - PLUGGED	B
R10C91	O.D. DAMAGE - WIPED AREA - SCRAPED (Ripples) PLUGGED	C
R11C91	COLLAPSED WITH HOLE (Ripped) 4-5" above T.S. - PLUGGED	D
R12C91	COLLAPSED WITH HOLE 4" Above T.S. - PLUGGED	E
R13C90	O.D. DAMAGE - PLUGGED	F
R14C90	COLLAPSED WITH O.D. DAMAGE - DEPRESSION - PLUGGED	G
R15C90	O.D. DAMAGE WITH HOLE (Collapsed & Ripples) PLUGGED	H
R16C89	MINOR O.D. DAMAGE - PLUGGED	I
R17C89	O.D. DAMAGE - PLUGGED	J
R18C88	OK	
R19C88	OK	
R20C88	OK	
R21C87	OK	
R22C86	OK	
R23C86	OK	
R24C85	OK	
R25C85	OK	
R26C84	OK	
R27C83	OK	
R28C82	OK	
R29C82	OK	
R30C81	OK - SMALL SHREAD OF TUBING ON TUBE SHEET	K
STAY ROD	OK	
R33C78	OK	
R34C77	OK	
R34C76	OK	
R35C76	OK	
R35C75	OK - PLUGGED	
R35C74	OK	
R36C74	OK	
R36C73	OK	
R37C73	OK	
R37C72	OK	
R38C72	OK - MINOR O.D. DAMAGE - PLUGGED	L
R38C71	OK - MINOR O.D. DAMAGE - PLUGGED	M
R38C70	OK	

DATA REVIEW B-STEAM GENERATOR HOT LEG

<u>Tube</u>	<u>Results</u>	<u>Location</u> (see Fig. 3.4-2)
R39C70	OK - O.D. DAMAGE - PLUGGED	N
R39C69	OK - O.D. DAMAGE - PLUGGED	O
R39C68	OK - O.D. DAMAGE - PLUGGED	P
R40C68	OK - PLUGGED	Q
R40C67	OK - PLUGGED	R
R41C66	OK - PLUGGED	S
R41C65	OK - O.D. DAMAGE - DINGS	T
R41C64	OK - O.D. DAMAGE - DINGS	U
R42C64	OK - O.D. DAMAGE - DINGS	V
R42C63	OK - O.D. DAMAGE - DINGS	W
R42C62	O.D. - O.D. DAMAGE - DINGS	X
R43C61	SCRAPED ON O.D. - PLUGGED	Y
R43C60	SCRAPED ON O.D. - PLUGGED	Z
R43C59	O.D. DAMAGE - PLUGGED	AA
R44C58	COLLAPSED, O.D. DAMAGE - PLUGGED	AB
R44C57	COLLAPSED, O.D. DAMAGE - PLUGGED	AC
R44C56	COLLAPSED, MISSING - PLUGGED	AD
R44C55	COLLAPSED, O.D. DAMAGE - PLUGGED	AE
R45C54	COLLAPSED, MISSING - PLUGGED	AF
R45C53	COLLAPSED, O.D. DAMAGE - PLUGGED	AG
R45C52	PULLED TUBE	AH
R45C51	OK - MOTTLED (RIPPLED O.D.) - PLUGGED	AI
R45C50	OK - PLUGGED	
R45C49	OK - PLUGGED	
R45C48	OK - PLUGGED	
R45C47	OK - PLUGGED	
R45C46	OK - PLUGGED	
R45C45	OK	
R45C44	OK	
R45C43	OK	
R45C42	OK	
R45C41	OK	
R45C40	OK	
R45C39	OK	
R44C38	OK	
R44C37	OK	
R44C36	OK	
R44C35	OK	
R43C34	OK - PIECE OF WIRE, AND PLATE 3.5" X 1.5" X .5"	AJ
R43C33	OK	
R43C32	OK	
R42C31	OK	
R42C30	OK	

DATA REVIEW B-STEAM GENERATOR HOT LEG

<u>Tube</u>	<u>Results</u>	<u>Location</u> (see Fig. 3.4-2)
R42C29	OK	
R41C28	OK	
R41C27	OK	
R40C26	OK	
R40C25	OK	
R39C24	OK	
R39C23	OK	
R38C21	OK	
R37C20	OK	
R36C19	OK	
R35C18	OK	
R35C17	OK	
R34C16	OK	
R33C16	OK	
R33C15	OK - PLUGGED, SMALL SHREAD OF TUBING BETWEEN R32C15 & STAY BAR	AK
STAY BAR	OK	
R30C13	OK	
R30C12	OK	
R29C11	OK	
R28C11	OK	
R27C10	OK	
R26C9	OK	
R25C8	OK	
R24C8	OK	
R23C7	OK	
R22C7	OK	
R21C6	OK	
R20C5	OK	
R19C5	OK	
R18C5	OK	
R17C4	OK	
R16C4	OK	
R15C3	OK	
R14C3	OK	
R13C3	OK	
R12C2	OK - PLUGGED	AL
R11C2	OK	
R10C2	OK	
R9C2	OK	
R8C1	OK	
R7C1	OK	
R6C1	OK	
R5C1	OK	
R4C1	OK	
R3C1	OK	
R2C1	OK	
R1C1	OK	

Secondary Side Tube Sheet Periphery Video Inspection Program

- [illegible]

B-Steam Generator

3.4-6

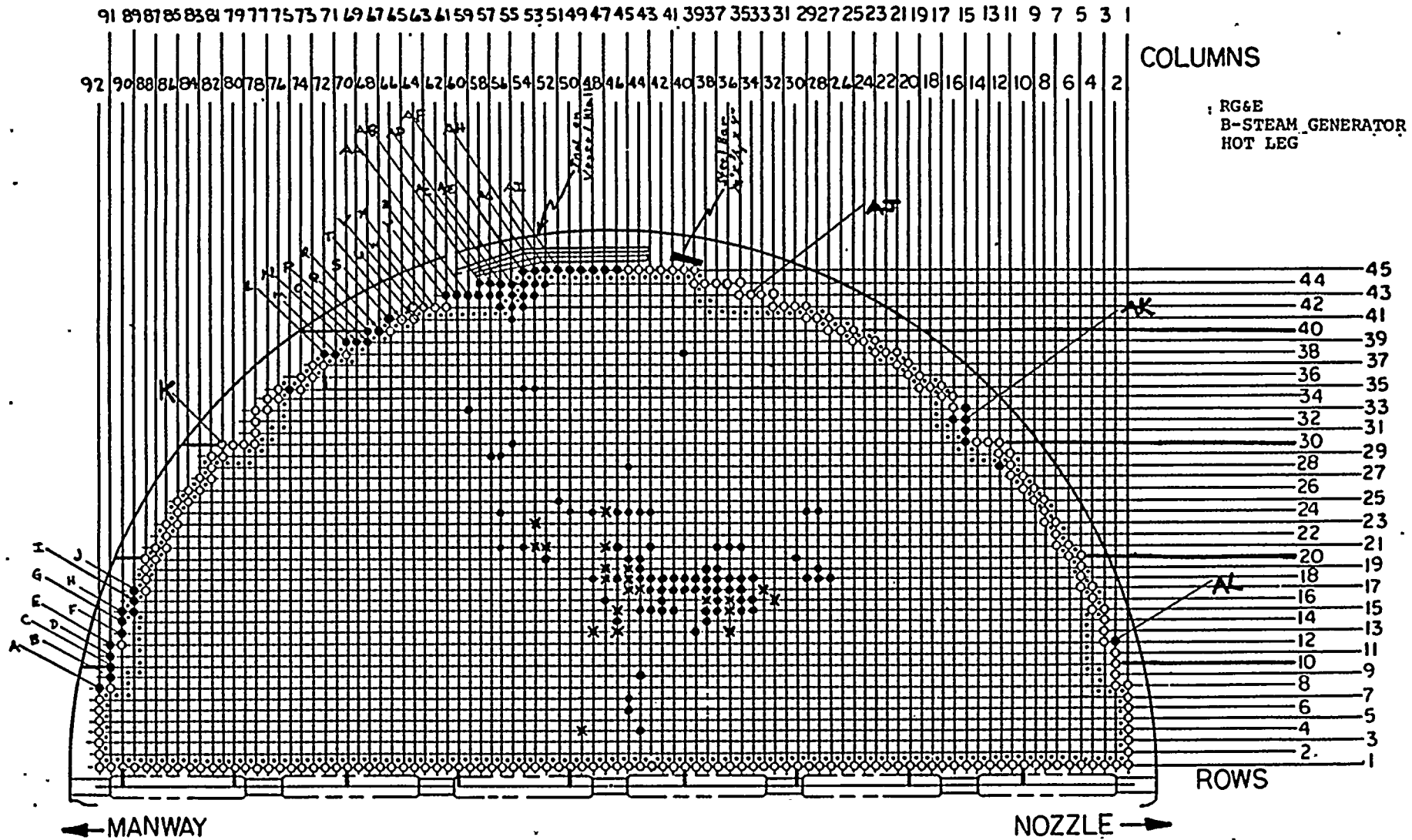


FIGURE 3.4-2

3.5 Foreign Objects

3.5.1 A-Steam Generator

No foreign objects were found in the A-Steam Generator hot leg. The following foreign objects were found in the A-Steam Generator cold leg.

- a) A piece of wire 0.0375 inches in diameter, 11.125 inches long, non-magnetic, stainless steel located near R34 C77.
- b) A piece of wire 0.1265 inches in diameter 4.5625 inches long, magnetic, carbon steel weld rod, located near R44 C38.
- c) Piece of metal with portion of weld. Irregular shape approximately 0.5 inches thick by 0.75 inches wide by 1 inch long. Magnetic material, carbon steel plate segment. Located near R44 C38.

3.5.2 B-Steam Generator

The following is a listing of foreign objects found in the B-Steam Generator. Figure 3.4-2 illustrates the primary locations where the foreign objects were found in the B-Steam Generator hot leg.

- a) Piece of magnetic carbon steel plate 0.5 inches thick by 4.18 inches wide by 6.31 inches long. Located near R25 C85 area.
- b) Piece of magnetic carbon steel plate 0.5 inches thick by 1.5 inches wide by 3.5 inches long. Initially located near R45 C46 area.
- c) Piece of magnetic carbon steel plate oval shape 0.5 inches thick, minor axis 2.0 inches with major axis 2.375 inches. Located wedged between R45 C53 and R44 C53.
- d) Piece of magnetic carbon steel strip 0.050 inches thick by 0.6 inches wide by 4 inches long. Located near R25 C85 area.
- e) Piece of copper tubing, approximately 0.25 inches in diameter by 1.062 inches long. Located near R45 C47 area.
- f) Piece of welding electrode 0.18 inches in diameter by 2 inches long. Located near R43 C34 area.
- g) Four pieces of welding slag small ball shapes less than 0.5 inches in diameter.
- h) Two pieces of material small ball shapes less than 0.25 inches in diameter.

- i) Small pieces of Inconel tubing were also identified from damaged tubes of various lengths. These were located in the Number 4 wedge area. Two other pieces were identified, one near R30 C81 the other near R33 C15.

4.0 STEAM GENERATOR TUBE FAILURE ANALYSIS PROGRAM

4.1 Introduction

4.1.1 General

An extensive failure analysis program has been developed to determine the mechanisms which resulted in the rupture of tube R42 C55 on January 25, 1982. The purpose of this program is to provide analytical and experimental information relative to the role that various, postulated failure mechanisms had in the tube rupture. This information is then used to establish the most probable failure mechanisms, and take the corrective actions necessary to preclude recurrence.

4.1.2 Program

The failure analysis program was developed based on the operating history of the B-Steam Generator, inspection results, and previous analysis and test results. The program was designed to assess the various mechanical mechanisms which may have been involved in the tube failures. These include buckling, collapse, fatigue, severing, wear, and burst. The program includes assessment of the effect that foreign objects may have had in the failure mechanism.

The program consists of the following elements:

- a) postulated failure mechanism
- b) data review
- c) metallurgical examinations
- d) analyses
- e) model testing
- f) laboratory testing

The majority of the analysis and testing work has been performed by Westinghouse. The collapse and fatigue testing is being performed at the Research and Development Laboratories in Churchill, Pennsylvania. The flow model testing was performed at the Westinghouse Engineering Test Facility in Tampa, Florida. Sections 4.5 through 4.8 of this report contain a detailed description of the analyses and tests performed by Westinghouse together with the associated results and conclusions from that work.

In addition to Westinghouse, analysis and testing has been performed by Combustion Engineering. The analysis work was performed under contract to the Electric Power Research Institute, Inc. (EPRI) and the Steam Generator Owners Group. Appendix B to this report contains a summary of that work. Testing relative to the effects of axial load and loose part impacting on a steam generator tube's propensity for local buckling is presently in progress at Combustion Engineering's Chattanooga, Tennessee facilities. A description of the test equipment, parameters, and methodology is included in Appendix C to this report. The results of this work will be provided as an Addenda when they are available.

4.2 Postulated Failure Mechanisms

4.2.1 Initial Plugging

As stated in Section 2.2.2 of this report, plugging of tubes in the B-Steam Generator periphery began in 1976. The tubes were plugged for a combination of internal and outside diameter eddy current indications. The indications occurred between the tube sheet and first support plate. Since many of the indications were internal diameter, and these tubes were in a region of the steam generator where very little sludge can accumulate, corrosion is not postulated to be a mechanism involved in the failure. Therefore, the most probable cause of the initial tube plugging is postulated to be some adverse lateral or axial mechanical loading mechanism on the tubes.

4.2.2 Collapse

Video inspection and subsequent tube removals have shown the presence of collapse areas on several plugged tubes on the B-Steam Generator hot leg periphery. Based on the location of these tubes in the outermost tube rows, and the time at which they were originally plugged, it appears that collapse was the next step in tube degradation following the initial plugging. The factors which may have contributed to the collapse are external pressure, lateral impact, and axial load. Lateral impact of the tube could have resulted in ovalization, wall thinning, or cyclic stresses. Axial load could have resulted in additional stresses in the tube. Since the tubes were previously plugged, they were under external pressure during normal plant operation. Ovalization, wall thinning, and/or mechanical stress could have weakened the tube to the point where it collapsed under normal operating pressures.

4.2.3 Severance

Several tubes in the Number 4 wedge area of the B-Steam Generator were found to be severed. This included tubes both with and without evidence of collapse. The two outermost tubes which had collapse areas were severed at the tube sheet and first support plate. The remaining tubes were located primarily in inner rows and had been severed at the tube sheet only. Therefore, it appears that severing was the next step in the failure process following collapse. Severing of the tube is postulated to have occurred as a result of either wear or fatigue loadings from flow induced vibration and/or lateral impact. The lateral impact could have been either from another severed tube or a foreign object. Flow induced vibration could have resulted from weakening of the tube due to a collapse area, and/or lowering of natural frequency as a result of the collapse and/or axial load.

4.2.4 Wear

Many tubes, particularly in the Number 4 wedge area, were found to have outside diameter (O.D.) wear. The wear appears to be primarily the result of one tube rubbing on another. This is postulated to have occurred from the severed tubes. In a few cases, very localized wear areas were seen. These appear to have been caused by a foreign object. Wear on a previously plugged tube could have weakened it to the point where it severed and subsequently caused impact or wear on additional tubes. Wear on an active tube would result in either a defect which was detected by eddy current and the tube plugged; or enough wall thinning over a sufficient area to cause the tube to burst from internal pressure.

4.2.5 Summary

Figure 4.2-1 illustrates the various failure mechanisms, and their sequence, which are postulated to have resulted in the rupture of R42 C55. A foreign object, axial loads, and pressure are postulated to have combined in leading to a sequence of events which led to plugging of many tubes on the B-Steam Generator periphery, and eventually to the rupture of one of them. The intermediate steps leading to the rupture appear to have included collapse, severing, and wear. Most of this intermediate tube degradation occurred subsequent to plugging and, therefore, could not be detected by eddy current examination. The analyses and tests which are described in the following sections have been performed to substantiate the postulated failure mechanisms described here.

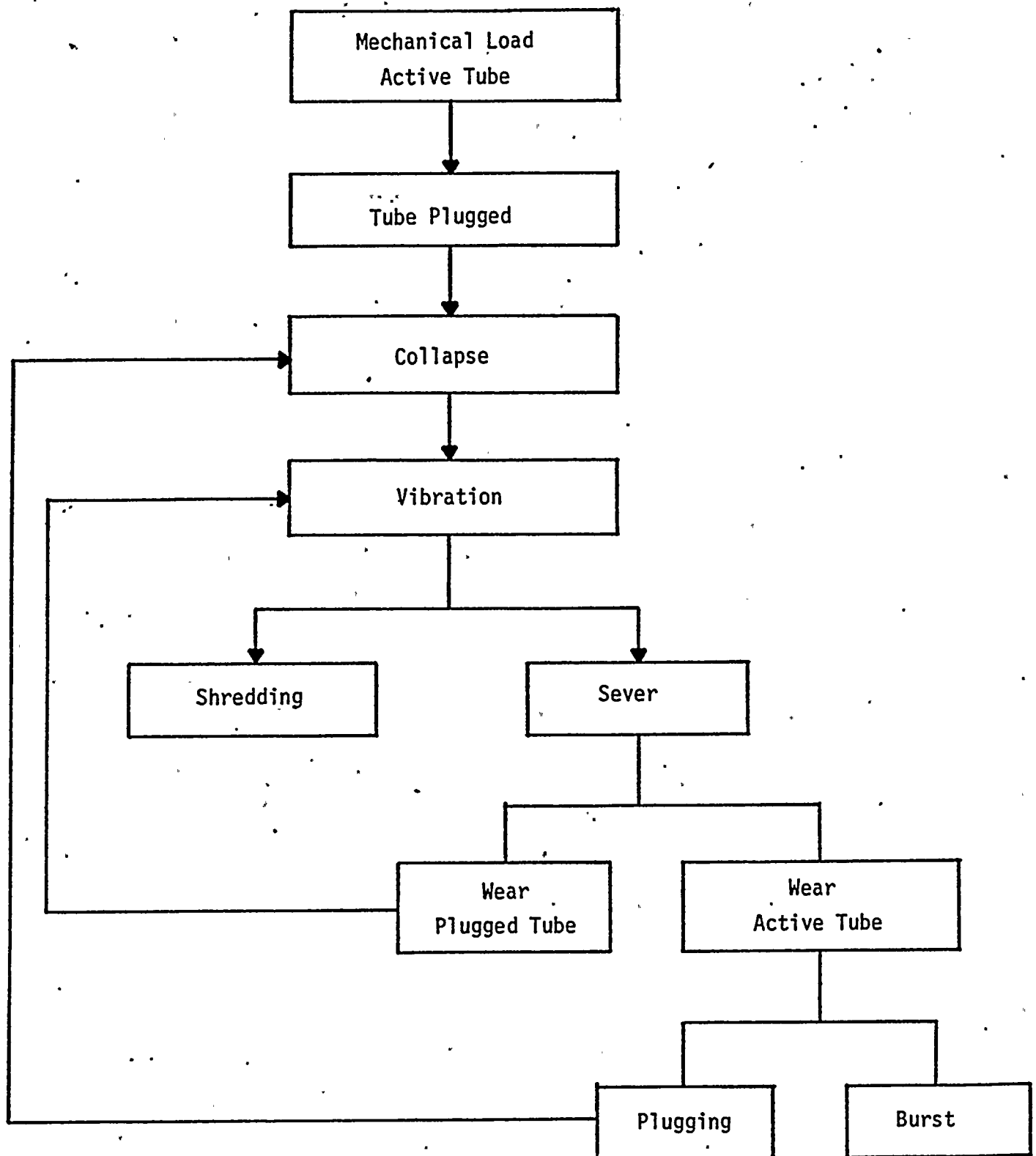


Figure 4.2-1
Postulated Failure Mechanism Sequence

4.3 Data Review

4.3.1 Purpose

The purpose of this section is to review the examination and repair history of the peripheral tubes in the B-Steam Generator. The results of this review are then related to the results of the February 1982 examinations. Only one peripheral tube in the A-Steam Generator has been plugged, and that tube was plugged during steam generator fabrication. No peripheral tubes have been plugged in the A-Steam Generator during operation.

4.3.2 Examination and Repair History

Ginna Station began operation in late 1969. Steam generator eddy current inspections were performed in April 1972, March 1974, November 1974, and March 1975. There were no indications of any tube degradation in any peripheral tubes found during any of these inspections.

In January 1976, the plant was shut down with a periphery tube leak in the B-Steam Generator. The leakage, through tube R40 C68, was less than 0.1 gpm. R40 C68 was determined to have I.D.-type indications 2 inches below the top of the tube sheet and was plugged. R39 C69 had O.D. indications at the top of the tube sheet and was also plugged.

In February 1976, the plant was shutdown for refueling, maintenance, and steam generator inspection. There were no eddy current indications in the B-Steam Generator peripheral tubes.

In April 1976, shortly after startup from the February 1976 outage, a tube leak occurred in the B-Steam Generator. The leak rate was less than 0.1 gpm from the tube R12 C91, near the tube lane on the manway side of the bundle in the Number 6 wedge area.* Eddy current inspection revealed I.D.-type indications at the top of the tube sheet. Neighboring tubes on the periphery in this wedge area were shown by eddy current inspection to contain signals which were characterized also as I.D.-type. These also were located at, or just above the top of, the tube sheet. In addition, a few tubes in the Number 6 wedge area also produced eddy current signals at the first tube support plate. These were characterized as dents of various sizes, all less than 10 mils. All peripheral tubes with any I.D.-type indications in this area

* A tube sheet map of the hot leg side of the B-Steam Generator is found in Figure 2.4. Wedge area locations are defined in Figure 2.2.

were plugged during this outage. (Also plugged at this time were 4 tubes on the opposite side of the bundle, in Column 15, Rows 30-33, which is in the Number 2 wedge area. Two of these, R30 C15 and R31 C15, exhibited O.D. indications, 45% through-wall, about 2 inches above the top of the tube sheet. The other 2 tubes displayed I.D.-type of signals at the top of the tube sheet.)

Eddy current inspection of selected tubes in the Number 4 wedge area (90° to the tube lane and furthest from it, at the periphery) showed no significant indications during the April 1976 outage. During the April 1976 inspection, an individual reached into the secondary side of the B-Steam Generator through the 6 inch blowdown lane handhole to probe the Number 6 wedge area. No evidence of external distress was felt on the peripheral tubes and no unusual conditions or foreign objects were noted between the tubes and the steam generator shell.

The plant then operated until April 1977. In April 1977, inspections of the Number 4 wedge area revealed one tube, R45 C54, to have two I.D.-type indications, one slightly above and one slightly below the top of the tube sheet. Three neighboring tubes did not exhibit recordable indications at this investigation. The unit was returned to service in mid-May 1977.

Shortly thereafter, on July 5, 1977, a minor leak (0.09 gpm) occurred in the B-Steam Generator. The leaking tube was identified as R45 C54, which had been identified as having indications the preceeding April. In the July inspection, R45 C54 exhibited bulge and I.D.-type indications. Inspection of neighboring tubes in the Number 4 wedge area indicated that four tubes in Row 44 (Columns 55-58) also contained bulge type indications and I.D.-type signals in the tube sheet area. These five tubes plus the tube at R12 C2, which had an O.D. indication above the tube sheet, were plugged and the unit was returned to service.

In January 1978, a leak occurred in the Number 4 wedge area at tube R44 C54, adjacent to the columns that were plugged the preceding July. Following the plugging of this tube and the adjacent tube (R44 C53), which displayed a bulge signal and an I.D.-type indication above the tube sheet, the unit was returned to service and operated until the refueling and maintenance outage of April 1978.

In April 1978, several tubes in the Number 4 wedge area were identified by eddy current testing to exhibit I.D.-type signals near the top of the tube sheet. Several dent-type indications at the first support plate were identified on some (but not all) tubes containing I.D.-type signals. The dents were all less than 10 mils. Several additional peripheral tubes in an area centered at R40 C69 (about 3/4 of the peripheral distance from the Number 6 wedge area to the Number 4 wedge area) also exhibited the I.D.-type signals.

During the April 1978 outage, one of the Number 4 wedge area tubes, R45 C52, was removed for laboratory investigation. Metallurgical, microanalytical, and metallographic studies were performed and are reported in an Electric Power Research Institute Report (Ref. 4.3-1). No evidence of I.D.-type degradation (such as primary water stress-corrosion cracking, other corrosion phenomena, or I.D. mechanical processes) was detected in this analysis. The tube exhibited a 15-mil diametral "bulge" above the top of the tube sheet in an area containing many small peen-like marks and "ripples" on the outside diameter (O.D.) surface. The rippled area also displayed a slight amount of wall thinning (approximately 15% maximum) and a slight increase in micro-hardness.

The features that were observed on the O.D. surfaces were mechanical appearing in nature and, except for the "bulge", are of the type which could have been caused by a "peening-like" action of a solid object interacting with the O.D. surface. Information available to the analysts was that the O.D. mechanical features faced the tube lane and not the periphery of the bundle. (It is conceivable, however, that the orientation of the investigated tube sections may not have been unambiguously established.)

Following plugging in April 1978 of all I.D.-type indications in the Number 4 wedge area and in the R40 C69 area (15 total tubes), the plant returned to service.

Inspections in February and December 1979 resulted in plugging several more tubes in the Number 4 wedge area. The tube at R43 C56 (February 1979) and the tube at R43 C57 (December 1979) exhibited large O.D.-type indications 2-3 inches above the top of the tube sheet. In April 1980 and May 1981, three Number 4 wedge area tubes were plugged for O.D. indications. The 1980 tubes, R45 C48 and R45 C49, exhibited approximately 40% O.D. indications about 24 inches above the top of the tube sheet.

Following the January 1982 event in the B-Steam Generator, the original eddy current findings from the Number 6 and Number 4 wedge areas plugging were reviewed and reevaluated. The peripheral tubes were also characterized by a video tape examination conducted in February 1982. Tables 4.3-1 and 4.3-2 present the results of the recent reevaluation for the Number 6 wedge area and the Number 4 wedge area, respectively. Table 4.3-2 also presents eddy current interpretations from inspections prior to the plugging date for the Number 4 wedge area. (Tubes in the Number 6 wedge area yielded no eddy current indications at inspections prior to the outage at which they were plugged). Also provided in both tables is a summary of the February 1982 video and visual inspections. Figure 4.3-1 is a schematic representation of the plugging history in the Number 4 wedge area.

4.3.3 Evaluation

Many of the plugged tubes in both the Number 4 and Number 6 wedge areas were observed to be externally damaged during the February 1982 videoscans inspections of the bundle periphery. Eddy current data was interpreted at the time of plugging, and have been confirmed through reevaluation now, as being a bulge or I.D.-type indication. It is concluded that the defects which caused the original tube plugging in the Number 4 and Number 6 wedge areas cannot be established from a review of the eddy current inspection data alone. The I.D.-type of eddy current indications that were observed in the 1976 inspection of the Number 6 wedge area were of appreciable amplitude. Such signals could be attributable to:

- (a) Actual I.D. discontinuities such as cracks (axial or circumferential) pits, thinning, magnetite deposition (on the I.D.), or permeability variations.
- (b) A localized bulge or diametral increase.
- (c) The presence on the O.D. of a highly conducting layer, such as copper.

Examination of the Number 6 wedge area tubes is currently in progress using metallurgical failure analysis techniques, including radiography and metallographic sectioning. Radiography of tubes R14 C90, R15 C90 and R12 C91 (the 1976 leaker) has not indicated any cracks which could have accounted for the original I.D.-type signals. Sectioning of tube R15 C90 over a length from 1 to 6 inches above the top of the tube sheet did not reveal any I.D. discontinuities which could have generated the 1976 eddy current signals.

The observations of O.D. indications of hot leg peripheral tubes in the Number 4 wedge area was made after the I.D.-type of indications were first observed in the same wedge area. The first observation of indications in this area was in February 1979. Later indications occurred on tubes in the row adjacent to the peripheral tubes.

TABLE 4.3-1

PLUGGED TUBES IN NUMBER 6 WEDGE AREA, B-STEAM GENERATOR, HOT LEG
INSPECTION HISTORY AND CURRENT CONDITION

TUBE (ROW-COLUMN)	DATE PLUGGED	EDDY CURRENT RESULTS AT PLUGGING DATE (1982 REVIEW)		CONDITION FOLLOWING JANUARY 1982 EVENT. VIDEO TAPE INSPECTION, VISUAL EXAMINATION
		NEAR TUBE SHEET TOP	SP 1	
8-92	4/76	Very large I.D. 2" above TTS	Indication	Collapsed and penetrated
9-91	4/76	Small I.D., not significant	Dent	Rippled O.D. surface
10-91	4/76	Small I.D. types \approx 3" above TTS	Dent	Wiped (Scraped) O.D.
11-91	4/76	Many I.D.s at TTS	Dent	Collapsed and torn open 4-5" above TTS
12-91 (LEAKER)	4/76	Large I.D. indications 4" above TTS	Dent	Collapsed and penetrated hole at 4" above TTS
13-90	4/76	TS distortion	Dent	O.D. damaged
14-90	4/76	Large I.D. 4" above TTS, TS dent signal	Small dent distorted	Collapsed and dented
15-90	4/76	Large I.D. 3" above TTS, smaller I.D.'s	Distorted	Collapsed rippled, and penetrated
15-89	4/76	No confirmed indication	Distorted	
16-89	4/76	No indications	Distorted	Minor O.D. damage
17-89	4/76	Large I.D. 3" above TTS	Clean	O.D. damage

Notes: TTS = Top of Tube Sheet
 SP 1 = Support Plate No. 1
 I.D. = Inside Diameter Type of Signal
 O.D. = Outside Diameter

TABLE 4.3-2

PLUGGED TUBES IN NUMBER 4 WEDGE AREA, B-STEAM GENERATOR, HOT LEG
INSPECTION HISTORY AND CURRENT CONDITION

TUBE (ROW-COLUMN)	DATE PLUGGED	EDDY CURRENT RESULTS AT PLUGGING DATE		EDDY CURRENT RESULTS AT INSPECTIONS PRIOR TO PLUGGING	CONDITION FOLLOWING JANUARY, 1982 EVENT, VIDEO TAPE INSPECTION ± VISUAL EXAMINATION
		NEAR TUBE SHEET TOP	SP 1		
45-46	2/82	41% O.D. 24" above TS	Clean	None	OK
45-47	2/82	49% O.D. 24" above TS	Clean	None	OK
45-48	4/80	1 O.D. - ~ 20" above TS	Clean	None	OK
45-49	4/80	1 O.D. - ~ 20" above TS	Distorted	None	OK
45-50	4/78	No significant indication		1/78 1 I.D. at TTS	OK
45-51	4/78	1 I.D. at TTS		1/78 1 I.D. at TTS	Mottled (rippled) O.D. surface
45-52	4/78*	Small I.D.s; possible bulge at TTS, one I.D. about 5" below TTS	Clean	7/77 Tube OK, 1/78 1 I.D. at TTS	*Removed in 4/78
45-53	1/78	Many I.D.s, large amplitude, TTS bulge signal	Clean	7/77 Large, saturated signals at TTS	Collapsed, O.D. damage
45-54	7/77	Large I.D. signals; TTS location = ? possibly due to a bulge	Distorted	4/77 1 I.D. above TTS 1 I.D. below TTS SP1 = Clean	Collapsed, O.D. damage Severed at SP 1 Missing
44-52	4/78	No indication	Clean		
44-53	4/78	Unidentified signal at TTS	Clean	1/78 Tube OK	

TABLE 4.3-2 (Continued)

TUBE (ROW-COLUMN)	DATE PLUGGED	EDDY CURRENT RESULTS AT PLUGGING DATE		EDDY CURRENT RESULTS AT INSPECTIONS PRIOR TO PLUGGING	CONDITION FOLLOWING JANUARY, 1982 EVENT, VIDEO TAPE INSPECTION ± VISUAL EXAMINATION
		NEAR TUBE SHEET TOP	SP 1		
44-54	1/78	1 I.D. near TTS	Clean	4/77 Tube OK 7/77 Large, ~ 100% indication at TTS	Severed at TTS
44-55	7/77	Large I.D. signals; TTS location = ? possible bulge	Distorted	4/77 OK	Collapsed, O.D. damage, severed at TTS.
44-56	7/77	Large, saturated I.D. signals possible bulge	Distorted	4/76 SP1 = Clean Dent between TTS and SP1 4/77 Tube OK, SP1 Clean	Collapsed, O.D. damage severed at SP1 missing
44-57	7/77	Large I.D. signals at TTS, possible bulge	Clean	4/76 TS Distortion signal	Collapsed, O.D. damage
44-58	7/77	Large I.D. at TTS possible bulge	Clean	4/76 O.D. but TS distortion 4/77 Tube OK	Collapsed, O.D. damage
43-53	4/81	1 O.D. signal	Distorted		
43-54	12/79	100% signal above TTS + Dent at TTS	Clean		
43-55	2/79	Possibly a small dent or tube sheet distortion at TTS	Distorted		Severed at TTS
43-56	2/79	O.D. signal 3" above TTS and large I.D. signals at TTS	Distorted		
43-57	12/79	Large O.D. signal above TTS and TS distortion	Dented	2/79 1 I.D. at TTS SP1 = Dented	

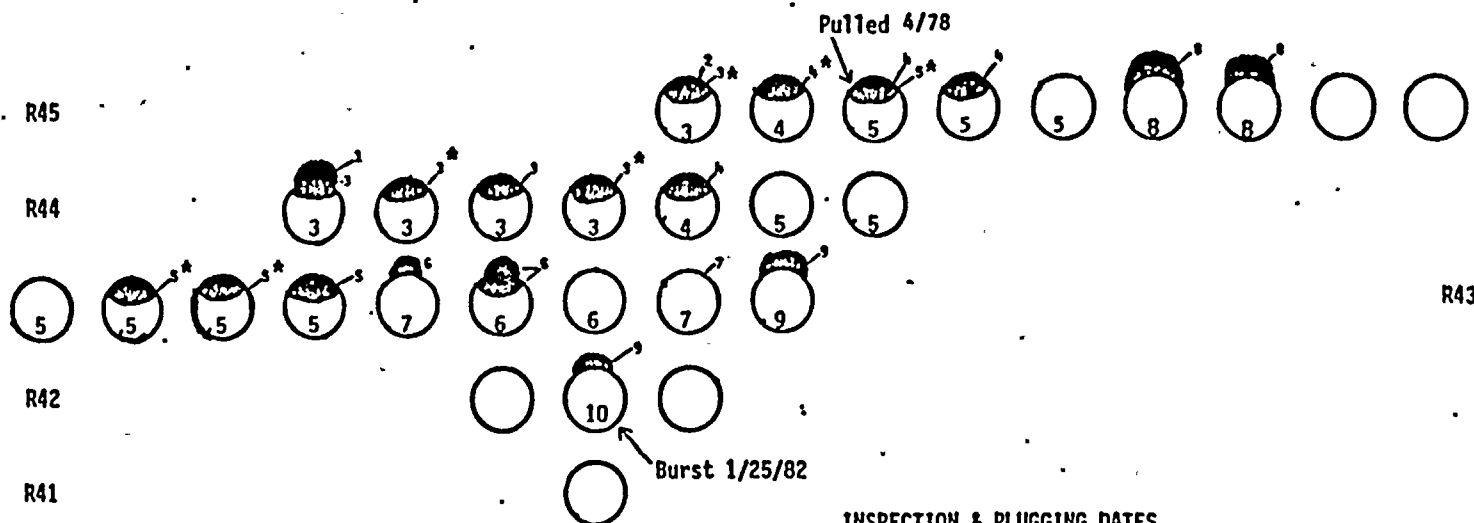
4.3-7

TABLE 4.3-2 (Continued)

TUBE (ROW-COLUMN)	DATE PLUGGED	EDDY CURRENT RESULTS AT PLUGGING DATE		EDDY CURRENT RESULTS AT INSPECTIONS PRIOR TO PLUGGING	CONDITION FOLLOWING JANUARY, 1982 EVENT, VIDEO TAPE INSPECTION ± VISUAL EXAMINATION
		NEAR TUBE SHEET TOP	SP 1		
43-58	4/78	1 insignificant I.D. -1" above TTS	OK		
43-59	4/78	Very small I.D., possible bulge, TTS	Dented		O.D. damage
43-60	4/78	Small I.D., 5" above TTS, possible bulge at TTS	Dented	7/77 Tube OK, SP1 = Clean	Scraped on O.D.
43-61	4/78	Nothing detectable	Dented		Severed at TTS
42-55	2/82	Burst 4.1 inches x 0.75 inches		4/81 <40% Axial O.D. Indication; SP1 = Distorted	Burst

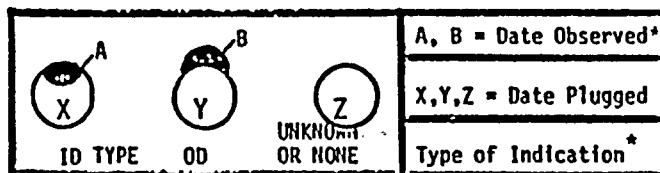
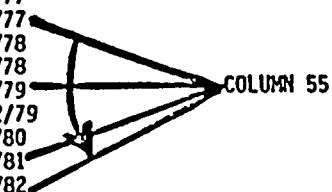
NOTES - TTS = Top of Tube Sheet
 SP 1 = Support Plate No. 1
 I.D. = Inside Diameter Type of Signal
 O.D. = Outside Diameter
 * = R45 C52 was pulled in April 1978

C60 C59 C58 C57 C56 C55 C54 C53 C52 C51 C50 C49 C48 C47 C46



INSPECTION & PLUGGING DATES

1	4/76
2	4/77
+ 3	7/77
4	1/78
5	4/78
+ 6	2/79
7	12/79
8	4/80
+ 9	4/81
+ 10	2/82



* Indicates possible Bulge accompanying ID - Type Signal.

B STEAM GENERATOR HOTLEG, NUMBER 4 WEDGE AREA: PLUGGING HISTORY

Figure 4.3-1

4.4 Metallurgical Review

An extensive metallurgical evaluation is currently in progress on a number of tube specimens which have been removed from the Number 4 and 6 wedge areas of the B-Steam Generator. The purpose of these investigations is to provide documentation on what caused R42 C55 to burst, what are the failure mechanisms involved in the damage to tubes, and to help clarify why a number of periphery tubes have been plugged in the B-Steam Generator since April 1976. The results of the investigations to date are presented in Appendix A. The following is a synopsis of those results.

Extensive investigations have been conducted to date of 5 tube segments from the Number 4 wedge area. These include tube R42 C55 (which burst on January 25, 1982), R44 C54, R43 C54, R43 C55, R44 C55, and R43 C56. The techniques have included nondestructive examinations, dimensioning, macrophotography, optical metallography, scanning electron microscope (SEM), fractography, and microhardness determinations. In general, all degradation processes observed are exclusively mechanical in nature and are not in any way related to any properties of the Inconel 600 tubing material or to any environmental degradation of a corrosion nature. The physical properties of the tubing sections are normal for Inconel 600 and no evidence has been found of any stress corrosion cracking, pitting, or corrosion wastage. The elemental analysis of tube R44 C55 was typical of Inconel 600 (for Fe, Ni, Cr), and both this tube and tube R42 C55 gave mechanical property values which are typical of virgin, mil-annealed Inconel 600 (normal hardness, yield strength, and elongation).

Tube R42 C55, which suffered an axial burst, was shown to be worn axially in two long wear scars, one of which reduced the original 0.050 inch wall thickness to approximately 0.008 inches for approximately 4 inches in length. The resultant burst at this thinned point was a purely ductile failure. The fracture face was pure shear (dimpled rupture), the normal fracture mode for tensile overload in annealed Inconel 600. The burst is explicable exclusively in terms of a reduction (by wear) to a thickness which was insufficient to sustain the I.D.-to-O.D. differential pressure.

Severed, previously plugged tubes, R44 C54, R43 C55, and R44 C55, were shown to have been worn through in several areas. Fractures on these tubes were, in two cases, of a fatigue mode, the SEM fractographs revealing typical situations. This breakage process of axial fractures is consistent with a wear process having reduced the remaining axial ligaments to the point where these ligaments did fatigue and tear. Some of the other areas of breakage were not discernable, due to the fact that the fracture faces were obliterated by the damage process to the extent that details were lost to the SEM investigation. However, the evidence does support the fatigue or tensile overload of minimum ligaments which appear to have operated to complete the damage process.

Tubes R43 C54 and R44 C56 both showed wear areas consistent with those seen on the burst tube R42C 55. These tubes had been previously plugged. R43 C54 had leaked prior to plugging and had sustained further damage, opening up a rather large area, due to wear and tube impacting.

All five tubes removed from the Number 4 wedge area showed wear areas. These areas of wear were axial, several inches in length, and exhibited circumferential grinding marks or striations. The wear areas were shown by metallography to have cold worked surface layers. These were verified by taking microhardness traverses across the cold work areas. Typical cold work on the wear surfaces was less than 0.001 inches in depth. Other wear areas, such as the burst wear surface, does not show any evidence of cold work.

Tube R44 C55, which was collapsed on the lower two inches of the specimen, was also analyzed for cold work by metallography and microhardness traverses. The results of these analyses documented extensive cold work (up to 0.008 inches in depth) in the collapsed area. A comparative analysis done at Battelle Columbus Laboratories on a specimen from tube R45 C54 also showed extensive cold work in the collapsed area of that tube.

Damage, for the most part, to both plugged tubes and to the burst tube R42 C55 appears to have originated in wear from the secondary side (O.D.). The worn surfaces then suffered additional degradation from tensile overload in the case of the active tube, and from fatigue and/or overload in the case of plugged tubes. Attempts to align the wear surfaces on the burst tube with wear surfaces on adjacent, previously plugged tubes demonstrated that the adjacent tubes were relatively free to move since they had been severed near the top of the tube sheet. On the burst tube, for example, the wear scar associated with the burst faced the backside of the neighboring tube R43 C55, and faced the wrapper. There was, however, a second wear scar on R42 C55 which was displaced circumferentially by an amount which confirms that severed tube R43 C55, which caused the wear, was mobile. Examination of other worn, previously plugged tubes, also revealed multiple wear scars (axially oriented), suggestive again of the mobility of the severed wearing members.

In addition to these results for tubes from the Number 4 wedge area, which are detailed in the appended report, examinations are continuing on three tubes from the Number 6 wedge area. Zones which contained the 1976 eddy current indications have been radiographed on tubes R12 C91 (the 1976 leaker), R14 C90 and R15 C90. No evidence of I.D. anomalies or discontinuities was discernible from the radiographs. Additionally, the destructive (metallographic) examination of the I.D. surface of tube R15 C90 in the zone from 1 to 6 inches above the tube sheet has not revealed any characteristics which could account for the 1976 type of eddy current signals. These laboratory investigations remain in progress to verify the structural damage these tubes suffered as well as their original plugging defect origins.

4.5 Analysis

This section describes the results of analysis programs performed to establish the nature and magnitude of loads acting on steam generator tubes; and evaluates analytically the role that these loads played relative to the postulated failure mechanism described in Section 4.2. Consistent with the observed degradation of tubing in the B-Steam Generator, the tubing of primary interest is the tube spans between the tube sheet (TS) and the first tube support plate (TSP) in the neighborhood of the wrapper support blocks on the hot leg side of the steam generator. Accordingly, where applicable, the localized conditions associated with this tubing were utilized in the evaluation. Figure 4.5.1-1 shows schematically this region of the bundle. The figure also includes the pertinent dimensions of the tube and interacting components.

The analyses included thermal mechanical loads due to normal operating transients, lateral loads due to a foreign object impact, and hydraulic loads including consideration of vortex shedding, cross-flow turbulence and fluid-elastic excitation. Axial and bending loads were included in the evaluations to account for axial tube restraint at the TSP and possible offset between the TS and TSP holes. If tubes are axially restrained at their ends (tube sheet and TSP), axial loads can develop due to thermal growth mismatch of a plugged tube relative to the stub barrel and/or surrounding active tubes. Axial bending stresses result from (1) an initial offset between the TS and TSP holes and radial thermal growth mismatch between the TS and TSP, and (2) rotation or bowing of the tube sheet due to the primary-secondary pressure differential. The initial maximum offset was assumed to be 0.1 inch based on the fabrication practice and experience with Model 44 and similar design steam generators. These axial loads were developed conservatively assuming full restraint of tubes in the wedge areas; away from the wedge areas, axial restraint would be significantly lower due to the TSP flexibility.

Following the load determination, a structural evaluation of tubing subjected to these loads is presented considering the potential of collapse, fatigue, wear and burst.

4.5.1 Design Parameters

Steam generator and tubing design parameters, and transient descriptions are presented in the following:

4.5.1.1 Steam Generator

No load steady-state conditions

$$T_{\text{hot}} = T_{\text{cold}} = T_{\text{av}} = T_{\text{stm}} = 547^{\circ}\text{F}$$

$$P_p = 2250 \text{ psia}$$

$$P_s = 1020 \text{ psia}$$

100 Percent Full-Power Condition

$$T_{hot} = 603.8^{\circ}F$$

$$T_{cold} = 547.7^{\circ}F$$

$$T_{av} = 572.5^{\circ}F$$

$$T_{stm} = 516.3^{\circ}F$$

$$P_p = 2250 \text{ psia (hot leg)}$$

$$P_s = 777 \text{ psia}$$

$$T_{FW} = 414.7^{\circ}F$$

$$\text{Steam flow} = 3.1 \times 10^6 \text{ lbs /hr}$$

$$\text{Feedwater flow} = 3.18 \times 10^6 \text{ lbs /hr}$$

$$\text{Recirculation ratio} = 4.73$$

Tube Bundle Parameters

$$\text{Pitch} = 1.234 \text{ inches}$$

$$\text{Wrapper I.D.} = 117.00 \text{ inches}$$

$$\text{Wrapper opening} = 14.00 \text{ inches}$$

$$\text{Tube span between tube sheet and first support plate} = 51.81 \text{ inches}$$

Ferrous Materials and Pertinent Properties

Tube sheet - SA-336

Stub Barrel - SA-302 GR B

Support plate, shear lugs, spacers and wedges - Carbon Steel

$$E_{70}^* = 27.9(10)^3 \text{ ksi}$$

$$E_{600}^* = 25.7(10)^3 \text{ ksi}$$

$$\alpha_{70}^{**} = 6.07(10)^{-6} \frac{\text{in.}}{\text{in.}^{\circ}F}$$

$$\alpha_{600}^{**} = 7.23(10)^{-6} \frac{\text{in.}}{\text{in.}^{\circ}F}$$

* = Youngs Modulus at the indicated temperature

** = mean coefficient of linear expansion in going from 70°F to the indicated temperature.

4.5.1.2 Tubing

Steam generator tubing material is mill-annealed Inconel-600. The nominal tube dimensions are 0.875 inch O.D. x 0.050 inch wall. The design minimum wall is 0.045 inch and the maximum specified ovality in the straight legs of the tubing is two percent.

Pertinent material properties for the evaluation are listed below:

$$E_{70} = 31.7(10)^3 \text{ ksi}$$

$$E_{600} = 29.2(10)^3 \text{ ksi}$$

$$\alpha_{70*} = 7.13(10)^{-6} \frac{\text{in.}}{\text{in.}^{\circ}\text{F}}$$

$$\alpha_{600} = 7.90(10)^{-6} \frac{\text{in.}}{\text{in.}^{\circ}\text{F}}$$

$$S_y^* = 35.5 \text{ ksi at } 550^{\circ}\text{F}^{**}$$

$$S_a = 26.0 \text{ ksi} = \text{Section III fully reversed alternating stress limit at } 10^6 \text{ cycles for } E = 26(10)^3 \text{ ksi}$$

4.5.1.3 Transient Description

In the following transient description, active tubes are assumed to interact with both primary and secondary fluid; plugged tubes are considered to interact only with the secondary fluid and as such are assumed to be in thermal equilibrium with the secondary fluid.

a) Plant Heat-Up (200 cycles)***

This transient is initiated from the cold shut-down condition. At the end of the transient, the primary pressure and temperature are 2250 psia and 547°F, respectively. The heat-up rate is such that continuous thermal equilibrium is maintained between the primary and secondary fluids. Accordingly, at the end of the transient, the secondary fluid is at the no-load (hot standby) steady-state temperature of 547°F and the secondary pressure equals the saturation pressure, 1020 psia.

* Material yield strength

** This is the code minimum value. Acceptable range at room temperature for yield strength is 40.00 - 65.00 ksi per applicable specifications.

*** Numbers in parenthesis are design basis cycles for 40-year plant life.

b) Plant Cool-down (200 cycles)

This transient is an exact reverse of the plant heat-up transient in a) above.

c) Plant Loading (14,500 cycles)

This transient initiates from hot standby conditions. The primary pressure during this transient remains at 2250 psia, while T_{hot} increases from 547°F at no-load to 604° at full load. The secondary side temperature and pressure drop to 517°F and 780 psia, respectively.

d) Plant Unloading (14,500 cycles)

This transient initiates from 100 percent full power conditions and is an exact reverse of plant loading transient in c) above.

e) Step load transients of + 10 percent full power (4,000 cycles).
For fatigue evaluation, these transients are conservatively enveloped by the plant loading/unloading transients.

f) Reactor Trip (400 cycles)

For fatigue evaluation, this transient is enveloped by the plant unloading transient.

g) 50 percent Step Load Decrease (200 cycles)

Also enveloped by the plant unloading transient.

h) Hot Standby with 70°F Feedwater Cycling (200 cycles)

This transient deviates from the Design Specification in that for Ginna plant, since early 1980 the feed is continuous at a rate of about 35 gpm (as opposed to a cyclic slug-feed at 300 gpm in the Design Specification). Although normally only one occurrence per year is expected for this transient (during plant start-up following refueling), for analysis purposes, 200 cycles of the transient are conservatively assumed, consistent with the number of heat-up cool-down transients.

4.5.2 Thermal-Hydraulic Evaluation

4.5.2.1 Purpose

The purpose of this sub-section is to determine fluid velocities for use in evaluating fluid induced loads on steam generator tubes near the tube bundle entrance region.

The plugging of tubes in the periphery of the tube bundle will lead to a redistribution of the flow in the plugged tube region. The flow velocities resulting from this redistribution must be evaluated to

determine if flow induced loads on the steam generator tubes in and near the plugged region are significantly affected.

The CHARM computer program (reference 4.5.2-1) was used to perform a thermal-hydraulic analysis of the tube bundle region between the tube sheet and the first support plate. Two cases were considered: a) nominal, and b) one block of tubes plugged in the periphery of the bundle.

The two-dimensional CHARM analysis was performed for the plane of symmetry perpendicular to the tube lane which divides the hot and cold legs into equal halves. At nominal conditions, there is no flow across this plane.

Because the CHARM analysis was two-dimensional (axial and radial) a separate three-dimensional hydraulic analysis of the tube sheet-to-first support plate region was performed to determine circumferential changes in the fluid flow patterns due to plugging. This analysis used the WECAN hydraulic conductance element (reference 4.5.2-2) and a pressure-forced boundary condition, rather than the flow-forced assumption inherent in the CHARM analysis.

4.5.2.2 CHARM Analysis

CHARM is a Westinghouse Proprietary two-dimensional analysis code used to compute the fluid flow conditions in a two-dimensional domain. The basic variables computed are the pressure, velocity, density and enthalpy by use of multidimensional characteristics in which a system of fluid flow compatibility equations are formulated and numerically integrated along bicharacteristic curves. The region analyzed is divided into rectangular cells of sizes ΔX and ΔY along the two (X, Y) coordinate axes. Velocity and pressure at the boundaries are specified and the code calculates the pressure, velocities (lateral and vertical), temperature, density, enthalpies, and quality distributions inside the model. Other input data required are the flow resistances (either input or calculated internally by the code) and heat load in each cell of the model.

Since the code does not recognize the presence of obstructions inside a cell, the tubes in the model were simulated by flow resistances. The input velocity to the model was adjusted to account for the reduction of the free volume available for the fluid as a result of tubes being present. The output velocity was then corrected to restore its physical meaning.

4.5.2.3 RGE Steam Generator Model and Input Data

The region modeled for the CHARM calculation was the area between the tube sheet and the first tube support plate (1st TSP). The plane of analysis was the vertical diametral plane perpendicular to the tube lane axis of the steam generator. The model, therefore, consisted of the hot side and the cold side of the unit with the centerline of the SG located at the middle of the model plane as shown in Figure 4.5.2-1.

The tubing inside the cells of the model was represented by radial and axial flow resistances. The input data were the tube O.D. and pitch. The numerical values of the resistances were computed internally by the code. When the tubes in a certain area were plugged, the heat load in the cell was set to zero.

Relevant geometrical data used in the CHARM calculations were:

Tube O.D. = 0.875 inch
Tube Pitch = 1.234 inches
Wrapper I.D. = 117 inches.
Wrapper Opening = 14 inches
Tube sheet-to-First Support Plate Height = 51.81 inches

The flow inlet velocity at the wrapper opening on the hot side was taken to be 2.38 ft/sec and that on the cold side to be 2.14 ft/sec. These velocities were consistent with the split of the total flow between the hot side and the cold side at the tube bundle inlet being taken to be .65 and .35, respectively, which accounted for some mixing and swirling in the downcomer annulus.

As mentioned previously, the code does not recognize the porosity of a cell. As a result, the input velocity to the boundary cells of the model was adjusted to account for a reduction in area due to the presence of tubing using the appropriate tube pitch and diameter.

4.5.2.4 Three-dimensional (WECAN) Analysis

The WECAN hydraulic conductance analysis model was based on the subdivision of the tube sheet-to-first support plate region into the cells shown in Figure 4.5.2-2. The extent of the plugged tube region was assumed to be five tube pitches deep (radially) and 20° wide (circumferentially). This corresponds to approximately 80 plugged tubes or more than twice the actual number of plugged tubes in the Number 4 wedge area. The model consisted of 100 internal nodes, each at the center of one of the cells shown in Figure 4.5.2-2. Five boundary nodes (201, 206, 211, 216, and 221) were used to represent the fluid just upstream of the wrapper opening. Twenty-five boundary nodes (101-125) were used to represent the boundary at the first support plate.

Figures 4.5.2-3 and 4.5.2-4 show the nodal distribution in the $\theta = 10^\circ$ and $Z = 7$ -inch planes, respectively. Node numbers in the remaining θ and Z planes were such that the node-spacing in the circumferential direction was 5 and that in the axial direction was 25. In the radial direction, the node spacing was made smallest in the vicinity of the region where the tubes were plugged, and varied in a geometric progression radially inward. The circumferential spacing of nodes was a constant 20° and allowed for two nodes per axial level on each side of the sector in which tubes were plugged.

The WECAN hydraulic conductance model calculates the flow rate between any two nodes according to the formula:

$$\text{FLOW RATE} = C \times \sqrt{\Delta p}$$

where C is the hydraulic conductance and Δp is the difference in pressure between two nodes. The hydraulic conductances between internal nodes were determined from CHARM - calculated cross-flow and axial flow friction factors according to the following:

$$C \text{ (axial)} = A \sqrt{\frac{2 \cdot D_H \cdot g}{f_{ax} L \rho}}$$

$$C \text{ (circumferential and radial)} = A \sqrt{\frac{2 \cdot D_T \cdot g}{f_{cr} L \rho}}$$

where ρ = fluid density ($.7812 \times 10^{-4}$ lb-sec²/in⁴)
 D_H = axial flow hydraulic diameter (1.3406 in)
 D_T = tube O.D. (.875 in)
 f_{ax} = axial flow friction factor = .03095
 f_{cr} = cross flow friction factor = .99043
 g = 386 in/sec²
 L = distance between nodes
 A = flow path area between nodes

In the wrapper opening flow paths (nodes 201-1 through 221-21) the hydraulic conductance included both the tube crossflow component and the hydraulic loss due to the expansion and turning of the flow as it exits the downcomer through the wrapper opening. To simulate the low fluid velocities indicated by CHARM in the plugged-tube region above the wrapper opening, the axial hydraulic conductances in this region were set equal to very small numbers.

Calculations were performed by setting the pressures in the downcomer nodes (201-221) equal to .96 psi and those at the first support plate (101-125) equal to 0.0 psi to approximately simulate the appropriate pressure drop in this region. By pressure-forcing, rather than flow forcing the calculations, the circumferential flow velocities can be estimated. The downcomer and first support plate were chosen as boundary points for pressure-forcing because the pressure at each of these two points should be relatively constant.

4.5.2.5 Results

The CHARM calculations included the following cases: a) Ginna nominal base case at 100 percent power, and b) a perturbed case simulating a plugged tube region in which the heat load in all cells along the columns X=2 and X=20 were set to zero. The widths of these columns are 5.85 inches, or approximately five tube pitches.

Figures 4.5.2-5 and 4.5.2-6 show the CHARM computed average velocities in the cells for the nominal and plugged cases at the hot side entrance. The interpretation of the output is as follows:

1. To obtain the physical lateral velocity (U_L):

$$U_L = U_{\text{CHARM}} \left(\frac{p^2 - \frac{\pi}{4} D^2}{p^2} \right)$$

where U_{CHARM} is the CHARM computed velocity.

2. To obtain the physical axial (or vertical) velocity V : No change
3. To obtain the maximum lateral velocity between tubes ($U_{\text{max, gap}}$):

$$U_{\text{max, gap}} = U_{\text{CHARM}} \left(\frac{p^2 - \frac{\pi}{4} D^2}{p^2} \right) \left(\frac{p}{p-D} \right)$$

Figures 4.5.2-7 through 4.5.2-10 show the velocity vector and quality distributions for both cases. The major effect of tube plugging was the appearance of a reduced fluid velocity field and a low quality region in the area between the bottom of the wrapper and the first support plate where the tubes were plugged. Because the density of the fluid in this region was lower, the resulting pressure gradients tended to be such that the fluid entering the tube bundle through the wrapper opening does not expand as quickly as it did in the nominal case. This tended to increase fluid cross flow velocities in the plugged-tube region near the wrapper opening.

In the CHARM model, circumferential fluid velocities were neglected. Figure 4.5.2-11 illustrates the behavior of the flow field in the plugged-tube region near the wrapper opening (node 11 cell) as predicted by the 3-D WECAN analysis. Because of the flow restriction produced by the deadwater region above the wrapper opening, the fluid entering the plugged-tube region expanded circumferentially (face C) instead of axially. The flow restriction also resulted in a reduction of the incoming velocity on face A. On face B, the velocity was below the CHARM-predicted value because of the efflux through faces C.

Conservative estimates of the limiting cross-flow velocities required that the significant effects of both the CHARM and WECAN analyses be considered. The major result from the CHARM analysis was an increase above nominal values of the radial velocities in and near the plugged tube region. The major results of the WECAN analysis were the prediction of a reduced flow out of the plugged tube region (face B) and of a circumferential crossflow velocity component (between tubes) of approximately 3.5 ft/sec (through face C). A limiting location on faces A and C, therefore, was their intersection, where the effects of both radial and circumferential components were present. On face B, however, it was more conservative to take the CHARM-predicted value rather than the WECAN value, because the latter is significantly lower due to the efflux through faces C. The CHARM-value on face B, however, will be, in addition, conservatively adjusted to reflect the fact that the area of face B is less than that of face A. Mathematically, these maximum cross flow velocity estimates are summarized below:

$$\text{Face A: } U_{CR} = \sqrt{U_{nom}^2 + U_C^2}$$

$$\text{Face B: } U_{CR} = U_B^{CHARM} \left(\frac{\text{area of face A}}{\text{area of face B}} \right)$$

Face C: U_{CR} = Same as on face A

where U_{CR} is the cross flow velocity and U_B^{CHARM} is the CHARM velocity at face B.

Table 4.5.2-1 summarizes the results of these calculations for nominal and plugged tube conditions. Circumferential crossflow velocities were used only in the plugged tube cell; calculations indicated that circumferential velocities elsewhere are negligible. The face B crossflow velocities are all CHARM-predicted values adjusted for the area reduction. Also given are adjusted CHARM crossflow velocities on face B for several cells downstream (radially inward) of the first cell. The nominal between-tube crossflow velocity is 8.2 ft/sec and occurs at the outer periphery of the tube bundle.

In summary, the presence of a block of plugged tubes approximately five tube pitches deep (approximately 80 tubes) had the following effects:

- a) A reduced fluid velocity field and a low quality region appeared between the wrapper opening and the first support plate in the region where the tubes are plugged. This tended to increase fluid crossflow velocities in the plugged tube region near the wrapper entrance.
- b) The highest between-tube crossflow velocity increased from 9.01 ft/sec in the no-plugged tube case, to 9.11 ft/sec in the plugged tube case, or slightly more than one percent, which is not significant.

4.5.3 Axial Loads

The development of axial loads as set forth herein is limited to plugged tubes since evaluations which follow that utilize this information focus on plugged tubes. Axial loads on steam generator tubing are dependent on the degree of tube-to-TSP restraint and could result from any of the following three considerations:

- a) External Pressure: If the tube is free to move axially through the TSPs, a net compressive load is developed on the tube due to the difference in projected areas of the outer and inner U-bend surfaces. This load is a maximum at no-load condition. The magnitude of this load is

$$F = \pi/4 D_o^2 P_s = 604 \text{ lb (compression)}$$

where

$$\begin{aligned} D_o &= 0.875 \text{ inch, outside tube diameter, and} \\ P_s &= 1005 \text{ psig, maximum secondary side pressure} \end{aligned}$$

- b) Tube-to-Stub Barrel Thermal Interaction: If a plugged tube in the wedge area is axially restrained at the TSP, axial loads in the tube result due to the differences in stub barrel/shell and tubing thermal displacements. The range of axial load on a plugged tube in a wedge area on hot leg is calculated for the significant transients and full power steady-state conditions.

Hot Standby with 70°F Feedwater

Minimum shell temperature for this transient was calculated to be 476°F assuming slug-feeding at the 300 gpm maximum rate per Reference Specifications*. The plugged tube was conservatively assumed to remain at the no-load steady-state temperature of 547°F. The maximum tube load is:

$$F = E \delta A_t$$

where

$$\begin{aligned} E &= 29.4 \times 10^6 \text{ lb/in}^2, \text{ elastic modulus of tube} \\ A_t &= \pi/4 (D_o^2 - D_i^2) = 0.12 \text{ in}^2, \text{ cross sectional area of tube, and} \\ \delta &\text{ is the tube restraint per unit length due to thermal growth mismatch with the stub-barrel and is given by} \\ \delta &= (\alpha \Delta T)_{\text{SG}} = 7.67 \times 10^{-6} \times (467 - 547) = -0.00055 \text{ in/in maximum} \end{aligned}$$

Thus, the maximum resulting tube load is

$$F = -1940 \text{ lb (compression)}$$

This load reduces to zero as the unit reaches the no-load steady-state condition. During this transient, since only the minimal flow velocities exist, the load is not relevant for flow-induced vibration analyses, but should only be considered in fatigue evaluation.

Plant Loading/Unloading

For these transients, the mean shell temperature was conservatively assumed to remain at its corresponding value at the initiation of the transient. The plugged tube temperature, however, closely follows the actual secondary fluid temperature. Consequently, at the end of the plant loading transient, the tubing is subjected to an axial tensile load due to the temperature differential of $\Delta T = 547 - 517 = 30^\circ\text{F}$. Or,

$$F = E (\alpha \Delta T)_{\text{SG}} A_t = 825 \text{ lb (tension)}$$

* The Ginna procedure since early 1980 has utilized continuous feed at a nominal rate of 35 gpm, and results in significantly less severe transient conditions than analyzed here.

Upon reaching steady-state full power conditions, the mean shell temperature is about 20°F lower than the bulk secondary temperature due to subcooling between the wrapper and the shell. Therefore, even though the plant unloading transient is an exact reverse of the plant loading transient, the tube is subjected to an axial compressive load corresponding to $\Delta T = - (30 + 20)^\circ\text{F}$, or

$$F = 50/30 \times 825 = - 1375 \text{ lb (compression)}$$

Full-Power Steady-State

As explained above, the tube is under a constant compressive load corresponding to $\Delta T = - 20^\circ\text{F}$ due to the subcooling effect on the mean shell temperature. Hence,

$$F = - 20/30 \times 825 = - 550 \text{ lb (compression)}$$

- c) Plugged-Tube-to-Active Tube Interaction: If a plugged tube is surrounded by a cluster of active tubes, and if the tubes are axially restrained at the TSP, the plugged tube motion is essentially controlled by the active tubes. The load in a plugged tube that exists at 100 percent power condition can be calculated as follows:

Assuming no thermal loading at the no-load, uniform steady-state conditions of $T = 547^\circ\text{F}$, the difference in thermal growth is:

$$\delta = (\alpha\Delta T)_A - (\alpha\Delta T)_P = 0.0004 \text{ in/in where}$$

mean metal temperature variations for the active (A) and plugged (P) tubes and linear coefficient of thermal expansion are:

$$\Delta T_A = 565 - 547 = 18^\circ\text{F}$$

$$\Delta T_P = 517 - 547 = -30^\circ\text{F and}$$

$$\alpha = 7.80 \times 10^{-6} \text{ in/in}$$

The resulting force (tension) on the plugged tube is:

$$F = E\delta A_t = 1410 \text{ lb}$$

Summary

In addition to the above conditions, axial loads due to other transients can be calculated in a similar fashion once the temperature differentials between the tube(s) and stub barrel/shell are established. In using these loads for the various analyses, the following should be noted:

- o Axial loads due to pressure and thermal growth mismatch cannot occur simultaneously on a given tube, as these loads result from independently assumed tube end conditions at the TSP.

- o At the no-load, steady-state condition, all components are at a uniform temperature of 547°F and, hence, axial tube loads following the hot standby and plant unloading transients approach zero as the temperatures approach steady-state conditions. These loads are, therefore, applicable to fatigue analyses, but would have a minimal influence on collapse as a result of lateral impact loading, and flow-induced vibration analyses due to the short period of time they would be acting.
- o During full power steady-state conditions, the compressive axial load on a tube exists due to the subcooling effect on the mean shell temperature. However, the load due to tube-to-tube interaction is significantly higher, although tensile. The steady-state compressive load is important from the viewpoint of increased susceptibility to fluid-elastic instability; and the tensile load is important from the viewpoint of increased susceptibility to collapse.

Maximum calculated axial loads for a wedge area on hot leg and their analytical applicability are summarized in Table 4.5.3-1. Axial loads in a nonwedge area would be less.

4.5.4 Lateral Loads

4.5.4.1 Purpose

Lateral loads on steam generator tubes in addition to a pressure differential between the O.D. and I.D. surfaces can result from interaction of the tubing with an external source such as the fluid or a solid object. Loading due to fluid effects will be discussed in 4.5.6 and the affects of a pressure differential is well established. The purpose of this sub-section will be to estimate analytically the magnitude of the lateral impact load that a solid object, similar to that removed from the Ginna steam generator could input to a tube.

4.5.4.2 Analysis

A schematic of the tube bundle entrance region with a foreign object present is shown in Figure 4.5.4-1. Fluid forces acting on the solid object can accelerate it toward a tube resulting in impact and tube motion. After coming to a halt, the elastic forces of the tube then force the foreign object in the direction opposite to that from which it came and disengagement of the solid object and tube can occur. If this happens, one or more additional impacts can occur. The analysis of this phenomenon proceeds as follows:

4.5.4.3 Foreign Object

When the foreign object is disengaged from the tube the force acting on it is strictly hydrodynamic. The magnitude of this force is estimated from

$$F \text{ (fluid)} = C_D \rho_f A |U_f - \dot{x}_p| (U_f - \dot{x}_p) / 2$$

where

ρ_f = fluid density = $.7812 (10^{-4}) \text{ lb-sec}^2/\text{in}^4$
 A = projected area of loose part (assumed to be a triangle 6.5 in by 4.19 in).
 U_f = Fluid Velocity
 \ddot{x}_p = foreign object velocity
 C_D = Drag Coefficient

The drag coefficient is estimated from Reference 4.5.4-1 to be equal to unity. The equation of motion of the foreign object is then

$$M_p \ddot{x}_p = F (\text{fluid})$$

where M_p = foreign object mass (assumed to be $.0074798 \text{ lb-sec}^2/\text{in}$), and \ddot{x}_p is the foreign object acceleration.

The fluid velocity U_f is assumed to have the following form:

$$U_f = U_{ss} + U_A \cos (2 \pi f t)$$

where

U_{ss} = A steady state component of velocity
 U_A = Alternating component of velocity
 f = Frequency of alternating velocity component
 t = time

The reason for including the alternating velocity component is to simulate the type of alternating velocity fluctuations that would be expected downstream of a support block in the downcomer. It is estimated that, for a 6.5 inch wide support block in a 15.5 ft/sec stream and a Strouhal number of 0.2, the frequency of such fluctuations is approximately 5.72 HZ.

4.5.4.4 Steam Generator Tube

The steam generator tube is simulated as a simple spring-mass system initially at rest. Two spring-mass combinations are considered. In the first model (Model 1) the deformation of the tube is assumed to follow the mode shape of the first fixed-fixed beam mode between the tube sheet and the first support plate. As such the applied loading is related to the mass per unit length of the tubing between the tube sheet and first support plate. The spring constant based on a deflection four inches above the tube sheet is 3717 lb/in and the effective mass is $.03767 \text{ lb-sec}^2/\text{in}$. In the second model (Model 2), the spring constant and mass are 19439 lb/in and $.01068 \text{ lb-sec}^2/\text{in}$, respectively, and are based on the static deflection profile of a fixed-fixed beam with an applied point load four inches above the tube sheet. This second model is more representative of a lateral impact load being applied to a tube such as occurred at Ginna. Shell stiffnesses have been neglected.

The tube equation of motion is obtained from Newton's Second Law using the nomenclature of Figure 4.5.4-1 and is:

$$(M_{SG} + E M_p) \ddot{x} + K_{SG} x = 0$$

where $E = 0$ corresponds to the situation when tube and foreign object have independent motions, and $E = 1$, to the situation when they move together.

Both foreign object and tube velocities at time zero are set equal to zero, as is the initial position of the tube. The foreign object and tube equations of motion are numerically integrated in time.

4.5.4.5 Results

Figures 4.5.4-2 through 4.5.4-7 illustrate the Model 1 steam generator tube force history, and the displacement histories of both the steam generator tube and foreign object for three cases. These cases are summarized below:

Case	$x_p(0)$	U_{ss}	U_A
1	-5 inches	2.3 ft/sec	0.0 ft/sec
2	0.0 inches	.69 ft/sec	.69 ft/sec
3	0.0 inches	.345 ft/sec	.69 ft/sec

Case 1 considers the translation of the foreign object from a position near the shell to the steam generator tube as a result of fluid forces associated with a nominal fluid velocity of 2.3 ft/sec. Cases 2 and 3 simulate the type of behavior which might be expected, when the steady fluid velocities are lower than nominal and alternating velocities exist because of a disturbance produced by an object like a support block. The alternating velocity was assumed to be 30 percent of the nominal steady-state value, or .69 ft/sec.

Foreign object induced loads associated with each of the above cases are provided in Table 4.5.4-1. The impact forces are on the order of 26-107 lb in Case 1. In cases 2 and 3, it is notable that the impact forces are higher for the lower steady-state velocity (Case 3). This is because disengagement and impact can more readily take place when the steady hydrodynamic forces are small.

A comparison of the Model 1 and Model 2 results demonstrates the importance of the tube dynamic characteristics on the magnitude of the impact loads. In Case 1, the magnitude of the initial impact load will be approximately proportional to the square root of the ratio of the spring constant to the total mass (tube-effective plus foreign object) of the system. Consequently as verified by the analysis the Model 2 loads should be greater than the Model 1 loads because of the higher stiffness and lower mass associated with Model 2. The stiffness associated with impacting of a steam generator tube by a foreign object will be greatest near the top of the tube sheet because of the restraint provided by the tube sheet to a beam type deformation. If the primary

tube response to impact is a shell type rather than a beam-type of deformation, the high stiffnesses and low effective-mass associated with a shell mode can be expected to yield impact forces even greater than those given in Table 4.5.4-1.

In summary, this analysis demonstrates that foreign object impact loads in excess of 100 lb are possible even for beam-type only deformations of the impacted tube. In all probability, shell-type deformations will also be significant, and will lead to even higher impact loads.

4.5.5 Collapse

The purpose of this section is to analytically assess the potential for tube collapse due to possible thermal, mechanical and hydraulic loads identified for the Ginna steam generator in conjunction with the postulated failure mechanism described in Section 4.2.

In this analysis, the tube was assumed plugged and thus was subject to the secondary side external pressure. In addition, an axial load which arose from restraint at the first tube support plate was assumed to act on the tube. A radial load associated with a foreign object impacting the tube near its tube sheet end and causing local deformation of the tube wall was then superimposed on the pressure and axial restraint loadings. Random and repeated application of such a load can result in degradation of a local area of the tube surface and in progressive tube ovality such that, under the combined effects of the axial restraint, pressure, and impact, the tube would collapse when the ovality reaches a critical value.

In the following, a lower bound calculation using the von Mises criterion with only the external pressure and the axial load acting on the tube was performed first. Then, a finite element analysis of an ovalized tube is performed to include the effects of a radial concentrated loading.

4.5.5.1 The von Mises Criterion

One method that is often used to determine yield in a structure is the von Mises criterion. It is essentially a measure of the maximum distortion energy. For a cylindrical tube under external pressure and axial loading, the von Mises criterion may be written as:

$$2 S_y^2 = (\sigma_h - \sigma_a)^2 + (\sigma_a - \sigma_r)^2 + (\sigma_r - \sigma_h)^2 \quad (1)$$

Here:

$$\begin{aligned} S_y &= \text{yield strength of the tube material} \\ \sigma_r &= -P, \text{ the external pressure} \\ \sigma_h &= +p \frac{R_m}{t} \\ \sigma_a &= F/2\pi R_m t \end{aligned}$$

where:

σ_a = axial stress
 σ_r = radial stress
 σ_h = hoop stress
 R_m = mean radius of tube
 t = tube wall thickness
 F = total axial force

Equation (1) states that one half of the sum of the squares of the stress intensities can be taken equal to the square of the material yield strength at incipient yielding of the structure.

If D = O.D. of tube, then $R_m = \frac{D+t}{2}$ and Equation 1 becomes:

$$\sigma_a^2 - p \left(\frac{R_m}{t} - 1 \right) \sigma_a + p^2 \left(1 + \frac{R_m}{t} + \frac{R_m^2}{t^2} \right) - S_y^2 = 0 \quad (2)$$

For the Ginna steam generator tubing:

$$\begin{array}{ll}
 D = 0.875 \text{ in} & R_m/t = 8.25 \\
 t = 0.050 \text{ in} & A = \pi/4 (0.875^2 - 0.775^2) \\
 R_m = 0.4125 \text{ in} & = 0.12959 \text{ in}^2
 \end{array}$$

Thus, Equation 2 simplifies to

$$\sigma_a^2 - (7.25) \sigma_a + 77.3125 p^2 - S_y^2 = 0 \quad (3)$$

Since σ_a is due to the axial force (F), Equation 3 can be used to determine values of F .

Equation 3 is plotted in Figure 4.5.5-1 for Inconel tubing with yield strengths of 38 ksi and 55 ksi. For reference, the Euler's buckling load and a collapse test point due to external pressure only are indicated. It is seen that under usual values of pressure and axial force, the plugged tube with a nominal thickness will not collapse.

4.5.5.2 Stress Analysis of Ovalized Tubes

The stress analysis of ovalized tubes subjected to combined external pressure, localized radial loading, and axial loading is described in this section. The purpose of the analysis is to determine the magnitude of radial load required to produce elastic stresses equal to the yield point of the material, when such a load is superimposed upon a constant external pressure loading of 1000 psi and, in some cases, a constant axial tensile load of 1000 lb*. The analysis, though related

*As discussed in Section 4.5.3 and Table 4.5.3-1, during steady-state power operation, tensile loads of this order can be expected in a plugged tube near the hot leg wedge location due to the thermal growth mismatch under the assumption of axial restraint at the first TSP.

to the investigation of the collapse of plugged steam generator tubes, was not a true collapse load analysis. It only indicated the load at which yielding begins at the highest-stressed point. Prior to collapse, yielding must penetrate essentially through the thickness of the tube wall and far enough along the tube length to precipitate instability.

To account for this series of events would require a true collapse load analysis. Such an analysis, under these conditions would be much more extensive than the one described herein, involving complex modeling and iterative, large deflection, elastic-plastic stress calculations.

The analysis was performed for 0.875 inch O.D. tubes of two wall thicknesses, 0.05 and 0.03 inch, and four ovalities, 0.01, 0.02, 0.04 and 0.06. The tube material is Inconel 600 at 550°F, with a minimum yield strength of 35.5 ksi, an estimated maximum yield strength of 57.7 ksi and a modulus of elasticity of 29.4×10^6 psi.

Computer analysis was performed with the ANSYS program. The initial intent was to use a single structural model to handle both external pressure and localized loading. However, after experiencing problems with boundary condition simulation for pressure loading, it was decided to use a separate supplemental model that had previously been successfully employed in tube collapse pressure analysis. This model is shown on Figure 4.5.5-2. The model used for concentrated radial loading is shown on Figures 4.5.5-3 and 4.5.5-4. The effect of axial loading on stresses was superimposed upon computer results by means of hand calculations. The von Mises yield criterion was assumed to apply.

Results of the analysis are plotted on Figures 4.5.5-5 and 4.5.5-6. Figure 4.5.5-5 plots maximum von Mises stress vs. concentrated radial load for the two tube thicknesses. In Figure 4.5.5-5, it is seen that the maximum stress increases with increasing concentrated radial load, increases with increasing ovality, increases with decreasing tube wall thickness, and increases with application of a 1000 lb tensile load. For the nominal tube wall thickness of 0.050 inch, it is seen that the maximum stress in the tube exceeds the maximum yield stress of 57.7 ksi at an ovality of 0.01 and a concentrated radial load of approximately 75 pounds. Greater tube ovality reduces the radial load required to speed the maximum yield stress of 57.7 ksi; for example, at an ovality of 0.06, the maximum yield stress is reached at a concentrated radial load of approximately 60 pounds.

Figure 4.5.5-6 is a plot of hoop stress versus axial distance from the point of load application for a five pound concentrated radial load. This figure shows the localized nature of these stresses. Such localization would indicate that substantial yielding in the immediate vicinity of the load could probably be tolerated before tube collapse would be precipitated. The first phase of yielding is visualized as a local, surface effect, with a subsurface elastic core and fully elastic tube sections a short distance away from the load continuing to provide stability. Only when the yield zone had spread through-wall and over a substantial area, will collapse occur. Typically, plastic hinges along two diametrically opposite planes for a length of 2 to 3 tube diameters are required for collapse. Thus, for eventual collapse in addition to a larger than analytically calculated magnitude of radial load to cause

yielding, the radial load must act in an impacting manner over a distributed area spanning about 2 to 3 tube diameters along the tube axis.

4.5.5.3 Factors in the Collapse of the Ginna Tube

It is seen from the preceding sections that the Ginna tube can deform plastically under a combination of external hydraulic (secondary side) pressure, axial load and a concentrated radial load. The latter load can cause the tube wall to deform progressively with repeated applications resulting in increased ovality and eventually, the external pressure will collapse the tube.

4.5.6 Flow-Induced Vibration

The purpose of this sub-section is to determine the stability characteristics and magnitudes of the flow-induced vibrational displacements and/or loads for hot leg tubes between the tube sheet and the first support plate. This information is pertinent to assess the degree of fatigue usage as a result of fluid-solid interactions. Both gross and local hydraulic effects will be considered. Gross hydraulic effects are defined as those which act on a tube or group of tubes and are of interest relative to the overall response characteristics of a tube. The loading mechanisms are fluid-elastic excitation, vortex-shedding and turbulence. Effects of tube plugging, structural degradation and axial loading are considered in the analysis.

In the local hydraulic load analysis, the magnitude and frequency of lift, drag, and torque loads acting on a tubing protrusion are calculated and are of interest in assessing the propensity for shredding of a tube due to fluid loading. The primary mechanism for this is considered to be vortex-shedding.

4.5.6.1 Gross Fluid Effects

In this sub-sub-section, results of analyses performed to characterize the dynamic behavior of tubes with cylindrical and irregular cross sectional geometries, when influenced by secondary fluid cross-flow, are reported. The purpose of the analyses was to determine tube natural frequencies, stability to fluid elastic excitation, and amplitude of vibration in terms of cross sectional geometry and cross-flow velocities. The analyses were based on an undistressed cylindrical tube, and other tube configurations having flat, 10 percent ovalized, and kidney shaped distressed cross sections. Fluid elastic excitation, vortex shedding, and cross-flow turbulence were the vibration mechanisms evaluated for tubes with a fixed-fixed and fixed-pinned boundary.

4.5.6.1.1 Mathematical Model of the Tube Configurations

Specific parameters used in the analyses are presented in Table 4.5.6-1, and the basic model configuration between the tube sheet and the first tube support plate is shown in Figure 4.5.6-1. Individual mathematical models were generated to simulate either an undistressed cylindrical tube or cylindrical tubes having a distressed cross section four inches above the tube sheet and two inches in length. The distressed cross

sections were: totally flat, 10 percent ovalized, and a kidney shape. Since the tube was considered to be plugged, the total mass of the tube was the summation of the tube material mass and the mass of the secondary fluid displaced by the tube. Fixed-fixed boundary conditions constrained all degrees-of-freedom at the tube sheet and the first tube support plate. The fixed-pinned boundary constituted total fixity at the tube sheet, and constrained tube displacements at the first tube support plate, where rotation in the x-y plane was permitted. Natural frequencies and fluid-elastic stability ratios and amplitudes were computed using a lumped mass finite element computer program.

Fluid velocities of 10 ft/sec and 20 ft/sec were used in this evaluation. These velocities were equally distributed over a 14-inch length of tubing between the wrapper opening and the tube sheet. A fluid density of 50 lb/ft³ was used in the mathematic models.

4.5.6.1.2 Analysis

A tube is considered to be stable when the stability ratio is less than unity. The stability ratio (U_e/U_c) is defined as the ratio of the effective velocity (U_e) to the critical velocity (U_c). The effective velocity is a function of the distribution of secondary fluid flow velocity along the tube axis, fluid density, tube mass, and the mode shape of vibration. The critical velocity (U_c) is the threshold velocity above which the tube amplitude increases as the secondary fluid velocity is increased and the induced energy from the fluid exceeds the damping energy dissipated by the tube. Computed fluid-elastic stability ratios for four tube configurations are presented in Figure 4.5.6-2 and 4.5.6-3 for the the fixed-fixed and fixed-pinned boundary conditions, respectively. Based on these results, it can be seen that the undistressed cylindrical tube and the distressed flat tube bracketed the ten percent ovalized and kidney shaped configurations. The cylindrical tube was the more stable and the flat distressed tube the least stable. Figure 4.5.6-4 illustrates the marked increase in tube stability when the damping ratio for a fixed-pinned tube was increased from 0.01 to 0.025.

Presented in Table 4.5.6-2 are the computed bending mode fundamental frequencies for all tube cross sectional geometries. Since the cylindrical and the flat are limiting configurations, analysis was extended to investigate the influence of an assumed 1000 lb compressive load being applied to these two tube configurations. Analysis was done for both the fixed-fixed and fixed-pinned boundary conditions. Results indicated the fixed-pinned boundary condition to be the limiting condition for both tube geometries. The compressive load decreased the natural frequency of the cylindrical tube from 40.3 Hz to 38.5 Hz, and the natural frequency of the flat tube was reduced from 31.6 Hz to 27.9 Hz. In terms of fluid-elastic excitation, the reduction in natural frequency reduces the critical velocity and consequently reduces the stability margin. The reduced frequency also tends to increase the amplitude of vibration due to turbulence.

Cross-flow turbulence was evaluated, because it causes narrowband random vibration of tubes at about the natural frequency of tubes in the fluid. The vibration amplitudes vary randomly in time and direction. Turbulence is thought to be the main cause of tube vibration in steam generators when the possibility of fluid-elastic excitation has been eliminated (Reference 4.5.6-1 and 4.5.6-2). Presented in Figures 4.5.6-5 and 4.5.6-6 are the computed amplitudes of vibration due to cross-flow turbulence as a function of cross-flow velocity for the cylindrical and flat section tubes. These amplitudes correspond to the natural frequencies presented in Table 4.5.6-2.

Axial flow turbulence can cause a tube to vibrate; however, cross-flow turbulence excites the tube to larger amplitudes of vibration than does the axial flow condition. Amplitudes of vibration due to vortex shedding were not considered to be applicable, since vortex shedding is essentially a boundary layer phenomena and any condition that tends to disrupt the boundary layer will, in all probability, reduce the amplitude of vibration. Laboratory tests have shown no indications of resonance peaks due to vortex shedding in closely spaced tube arrays for the flow velocities considered relevant in the region of the wrapper opening and the tube sheet (Reference 4.5.6-1). In most of the research investigations regarding vortex shedding, the flow velocity approaching the tube and/or an array of tubes has a relatively uniform velocity profile and low level of turbulence. However, in an operating steam generator as the flow enters through the wrapper opening, the fluid flow becomes turbulent and the axial component of the velocity is thought to disrupt the boundary layer on the tube and the formation of vortices generated by the flow perpendicular to the tube. Although research continues to be done for vortex shedding in tube bundles, it may be considered a second order mechanism for inducing tube degradation in steam generators as the cross-flow impinges on only a small portion of the tube in the region of the tube sheet (Reference 4.5.6-1). Of the three mechanisms identified with flow induced vibration, amplitudes generated by turbulence are smaller in magnitude than those generated by fluid-elastic excitation or vortex shedding. In closely spaced tube arrays, the considered predominant mechanisms are turbulence and fluid-elastic excitation.

4.5.6.1.3 Results

In summary, the major results of this analysis are:

1. Cross-flow velocities in the range of 9 ft/sec can cause peak root mean square amplitude vibrations of .6 mils for a fixed-fixed cylindrical cross section tube and approximately 1 mil for a fixed-pinned cylindrical cross section tube. The application of a 1000 lb compressive force had a negligible effect. Maximum amplitudes of vibrations would be roughly a factor of seven higher than the peak root mean square vibrations.
2. Cross-flow velocities in the range of 9 ft/sec can cause peak root mean square amplitude vibrations of 1 mil for a fixed-fixed flat cross section tube and approximately 3 mils for a fixed-pinned flat cross section tube. The application of a 1000 lb compressive force had a small effect. Maximum amplitude vibrations would be roughly a factor of seven higher than the peak root mean square vibrations.

3. Fluid-elastic instability of the flat cross section tube for a fixed-fixed boundary condition will occur for fluid velocities in the range of 11.5-16 ft/sec. Since maximum cross-flow velocity is of the order of 9 ft/sec, fluid-elastic instability is not predicted analytically.
4. Fluid-elastic instability of the flat cross section tube for a fixed-pinned boundary condition will occur for fluid velocities in the range of 10-14 ft/sec. Since the maximum flow velocity is of the order of 9 ft/sec, fluid-elastic instability is not predicted analytically.

4.5.6.2 Local-Fluid-Effects

4.5.6.2.1 Purpose

A tear in a steam generator tube might result in a protrusion which could be acted upon by fluid-induced alternating lift and drag loads to further increase the extent of the tear. The purpose of this section is to estimate the magnitudes of these loads so as to establish the role that fluid effects might have played in the shredding of tubes. The primary mechanism for producing such loads is considered to be vortex-shedding.

4.5.6.2.2 Analysis

Figure 4.5.6-7 illustrates the tear model used in the analysis. A protrusion with a height H and with a projected width D was exposed to a fluid cross-flow velocity of U . Alternating lift, drag, and torque acted as shown on the figure and were computed from the following equations.

$$\text{LIFT} = C_L (\rho_f U^2 / 2) H D \exp(i\omega t)$$

$$\text{DRAG} = C_D (\rho_f U^2 / 2) H D \exp(i\omega t)$$

$$\text{TORQUE} = C_L (\rho_f U^2 / 2) (H D^2 / 8) \exp(i\omega t)$$

where ρ_f is fluid density, C_L and C_D are alternating lift and drag coefficients, and $\omega = 2\pi f$ is the circular frequency of vortex-shedding. The latter can be computed from:

$$\omega = 2 \pi f = 2 \pi S U / D$$

where S = Strouhal number. From Reference 4.5.6-3 a Strouhal number of 0.2 and a lift coefficient of 0.5 were found to be appropriate. From Reference 4.5.6-4, it was estimated that an alternating drag coefficient of approximately 0.1 times the alternating lift coefficient was appropriate.

4.5.6.2.3 Results

Figures 4.5.6-8 through 4.5.6-10 illustrate as a function of fluid velocity the variation of alternating lift, torque and drag loads acting on a tear whose dimensions are $H = 2.5$ inches and $D = 0.5$ inch. The

fluid velocity range covered is 0 - 20 ft/sec. This envelops the maximum between-tube cross-flow velocity which does not exceed 10 ft/sec (see Section 4.5.2).

Table 4.5.6-3 summarizes the alternating lift, drag and torque amplitudes and frequencies of excitation for a range of protrusion heights H and H/D values of 1.0 and 5.0. The fluid velocity is assumed to be 10.0 ft/sec

In summary, the major conclusion from this analysis is that oscillating lift, drag and torque loads were not large enough to accelerate the tearing of tubing protrusions at the fluid velocities present in the tube bundle (≤ 10 ft/sec).

4.5.7 Fatigue

This sub-section presents the results of analytical calculations performed to assess the fatigue characteristics of steam generator tubing. Cases analyzed were:

- a) a nominally plugged tube
- b) a plugged tube with a notch or stress riser type degradation due to foreign object impact
- c) a plugged tube with a locally collapsed section and notch or stress riser type degradation with and without continuous impact by a foreign object.

In the Case 3 analysis, lateral load magnitudes of 10, 25, and 50 lb were considered.

For the first two cases, no lateral impact loads were included and the fluid interaction loads were taken to be minimal, consistent with the results of sub-section 4.5.6. Consequently, Cases 1 and 2 were examined from the viewpoint of low cycle fatigue due to thermal-mechanical operating loads and cycles. On the other hand, Case 3 analysis considered fluid-interaction and cyclic lateral impact loads and as such is of primary interest from the viewpoint of high-cycle fatigue. For Case 3, worst case axial loads were assumed in conjunction with the fluid interaction analysis.

In addition to the gross fluid interaction evaluations discussed above, the case of a locally shredded tube is considered in sub-section 4.5.7.2 to evaluate the propensity of crack propagation and continued shredding under the influence of local fluid effects.

The following nomenclature is used in the remainder of this section.

P_p = Primary side pressure, psi

P_s = Secondary side pressure, psi

r_i = Inside radius of tube = 0.3925 in

r_o = Outside radius of tube = 0.4375 in

- E_T = Modulus of Elasticity for tube at operating temperature, psi
 D_o = Outside diameter of tube = 0.875 in
 D_i = Inside diameter of tube = 0.785 in
 L = Length of tube span = 52.2 in
 θ = Tube sheet rotation angle = 0.096°
 T_{TP} = Mean temperature of plugged tube, $^\circ F$
 T_{TA} = Mean temperature of active tube, $^\circ F$
 T_{SB} = Mean temperature of stub barrel, $^\circ F$
 α = Coefficient of thermal expansion, in/in $^\circ F$
 I = Moment of inertia for tube, in 4
 δ = Displacement, in or displacement per unit length, in/in

4.5.7.1 Tubing Evaluation

The following parameters are assumed for the fatigue evaluation of a plugged tube throughout this section.

- Design minimum tube wall = 0.045 in
- Maximum ovality = two percent for straight length tubing
- Stress concentration due to notch or stress riser type degradation = 4.0
- Initial TS and TSP holes offset = 0.1 in

Additionally, the evaluation included the worst case axial loads based on hot leg parameters. Tubes on the cold leg and/or away from the wedge areas would have significantly larger fatigue margins than that indicated from the analysis due to the increase in tube support plate flexibility away from the wedge areas.

Case 1: Nominally Plugged Tube

The stress categories used in calculating the stresses are listed below. The calculated stresses are tabulated in Table 4.5.7-1. The summation of the principal stresses is given in Table 4.5.7-2. The alternating stress and the usage factors are given in Table 4.5.7-3.

Stress Categories

- a) Pressure stress in the tube:

$$\sigma_{\text{hoop}} = \frac{(P_p - P_s) \cdot r_o}{t}$$

$$\sigma_{\text{radial}} = \frac{-(P_p + P_s)}{2}$$

- b) Bending stress in the tube due to rotation of tube sheet as a result of primary-to-secondary ΔP :

$$\sigma_{\text{bending}} = \frac{3E_T D_o \theta}{L}$$

- c) Bending stress due to in-plane thermal growth mismatch between tube sheet and support plate:

$$\sigma_{\text{bending}} = \frac{3E_T D_o \delta_{TH}}{L^2}$$

where:

δ_{TH} = Radial expansion differential between tube sheet and tube support plate.

$$= [(\alpha \cdot \Delta T)_{TS} - (\alpha \cdot \Delta T)_{TSP}] R$$

and

R = 56.5 in, the distance of the outermost tube from the steam generator centerline.

- d) Bending stress in the tube due to as-built offset δ_o

$$\sigma_{\text{bending}} = \frac{3E_T D_o \delta_o}{L^2}$$

- e) Axial stress in the tube due to thermal growth mismatch between tube and stub barrel.

$$\sigma_{\text{axial}} = E_T [(\alpha \cdot \Delta T)_{SB} - (\alpha \cdot \Delta T)_{TP}]$$

- f) Bending stress in the tube due to axial forces acting through tube offset, δ .

$$\sigma_{\text{bending}} = \frac{-F_A \cdot \delta \cdot D_o}{2I}$$

where:

$$F_A = (\sigma_{\text{axial}}) \cdot (\text{Area of tube})$$

$$\delta = \delta_{TH} + \delta_{TS \text{ ROT.}} + \delta_o$$

$$I = \frac{\pi \cdot (D_o^4 - D_i^4)}{64} = 0.01036 \text{ in}^4$$

- g) Axial stress in the tube due to thermal growth mismatch between plugged tube and active tubes.

$$\sigma_{\text{axial}} = E_T [(\alpha \cdot \Delta T)_{TA} - (\alpha \cdot \Delta T)_{TP}]$$

- h) Hoop bending stress due to two percent ovality. This was obtained from the results of finite element analysis in Section 4.5.5.

Case 2: Nominally Plugged Tube with a Notch

This case analysis is basically the same as the Case 1 analysis, except that a stress concentration factor of 4.0 was applied to the axial stresses to increase the stresses due to a notch or stress riser. The summation of principal stresses and the usage factor for this case are given in Table 5.3.7-4.

In both of the above cases, the hot standby feedwater cycling (following the plant heatup but prior to plant unloading) was analyzed for a maximum ΔT on the hot leg side. During a 300 GPM slug feed cycle, the maximum ΔT between the plugged tube and the stub barrel would be 71°F. Use of this ΔT in the case of the Ginna Steam Generator is conservative since the feedwater transient at Ginna since early 1980 is a 35 GPM continuous feed type cycle, which would result in a lower ΔT than a slug feed type cycle. The number of feedwater cycles, consistent with the plant heatup cycles, was assumed to be 200 over the 40 year design life of the plant.

Case 3: Plugged Tube with Locally Collapsed Section

This section presents the results of the evaluation of a plugged tube with a locally collapsed section and notch or stress riser type degradation with and without continuous impact by a foreign object. For the analysis, the tube was assumed to be locally collapsed over a 2.0-inch length beginning at 4.0 inches above the tube sheet. An analysis, as described in Section 4.5.6 was performed to obtain the frequency and the root mean square stresses, due to cross-flow turbulence. A 1000 lb axial load on the tube was considered in this analysis to simulate the effect of thermal growth mismatch loads due to axial restraint at the first tube support plate.

The uncollapsed portion of the tube was assumed to have a nominal two percent ovality. Hoop stresses on oval tubes under the combined effects of external pressure and various magnitudes of lateral loads were obtained from the detailed finite element analysis described in Section 4.5.5.

For a fixed-pinned condition, the maximum peak stress*, due to cross-flow turbulence with a fluid velocity of 10.0 ft/sec and including a

*The analytically calculated stresses correspond to a root mean square (RMS) excitation. For an actual flow field in a typical steam generator, cross-flow turbulence causes narrow-band random vibration of tubes. Based on experimental data, the ratio of peak to RMS stress is approximately 7.0 and is used in this evaluation.

stress concentration factor of 4.0 for a notch, was equal to + 11.24 ksi which is less than the material endurance limit of approximately 13 ksi at 10^{11} cycles. Hoop stress due to two percent ovality and various impact loads was:

0 lb impact	=	15.0 ksi
10 lb "	=	19.5 ksi
25 lb "	=	26.0 ksi
50 lb "	=	39.0 ksi

Using a high-cycle fatigue curve, the allowable cycles for the above loads are as summarized in Tables 4.5.7-5 and 4.5.7-6. This high-cycle fatigue curve is proposed to ASME to include the alternating stresses representing 10^{11} cycles for Inconel material. The times to failure (cumulative usage factor = 1.0) in Table 4.5.7-6 are based on an impact frequency of 38.5 Hz (3.3×10^6 cycles/day) which is the fundamental vibration frequency of a fixed-pinned tube with a 1000 lb axial compressive load.

Based on results of the fatigue analysis above, both nominal and degraded plugged tubes without a lateral impact have acceptable margin to fatigue due to the worst case thermal-mechanical and hydraulic loadings over the design life of the plant. A plugged tube under axial compression, with a locally collapsed section and a notch or stress riser, subjected to a continual lateral impacting load will fail in fatigue; the calculated failure time for this case varies from about a day to a few weeks depending on the magnitude of the impact loading.

4.5.7.2 Shred-Evaluation

A tear in a tube could result in a protrusion which could be acted upon by fluid-induced alternating lift and drag loads to further increase the extent of the tear. For this case, the hydraulic load calculations were discussed in the previous section (4.5.6). Even for significantly large tears (0.5 inch wide x 2.5 inches high), the calculated loads were very small, resulting in maximum tube stresses well below 10.0 ksi. Thus, based on a high-cycle endurance limit of approximately 13 ksi at 10^{11} cycles as previously given, no crack propagation is expected.

4.5.8 Wear

The purpose of this section is to calculate the period of time for sufficient wear to occur that bursting of a tube would result. The calculation will consider potential ranges of wear for Inconel tubes rubbing against other Inconel tubes.

Deweese (Reference 4.5.8-1) previously gave the value of 582 in²/lb as the specific wear coefficient for Inconel sliding on Inconel in 500°F water and 8540 in²/lb in 300°F water. He also presented data for other material combinations and deduced that fretting wear is about 1/10 that of continuous sliding wear. This would mean that the range for fretting wear of Inconel on Inconel should be 58 in²/lb to 854 in²/lb or an average of 456 in²/lb.

4.5.8.1 Wear Calculations

The empirical wear formula according to Archard's theory on wear is given as:

$$V = CFT \times 10^{-12}$$

where: V = wear volume, in^3

C = specific wear coefficient, $(\text{psi})^{-1}$ or in^2/lb

F = force, lb

T = total travel or rubbing distance, in

It can be shown that a uniformly-thinned 7/8" O.D. tube will burst when the wall is reduced to approximately 6.6 mils under the normal Ginna operating conditions, assuming an ultimate strength of 89.7 ksi. (See Section 4.5.8.3.)

Therefore, if the rub area is 8.00 inches x 0.10 inch and the wear depth is 0.0434 inch which is reasonably similar to the Ginna situation, $V = 8 \times 0.1 \times 0.0434 = 0.0349 \text{ in}^3$.

For purposes of establishing a contact force for one tube rubbing on another, it is assumed that a severed tube is catilevered from the tube support plate and is 50 inches long. Under fluid drag forces, the severed tube will lean against a neighboring tube that is supported both at the tube sheet and at the tube support plate.

The drag force, F_D , is computed as follows:

$$F_D = 1/2 \rho AU^2 C_D$$

where: ρ = density of water = 1.94 slugs/ ft^3

$$= 0.001123 \text{ slugs/in}^3$$

A = projected area of the severed tube in the wrapper opening

$$= 12 \times 7/8 = 10.5 \text{ in}^2$$

U = flow velocity = 3 ft/sec

$$\approx 36 \text{ in/sec}$$

C = drag coefficient

$$\approx 0.8 \text{ (assumed turbulent)}$$

$$F_D = 1/2 \times 0.001123 \times 10.5 \times 36^2 \times 0.8 = 6.11 \text{ lb}$$

Under this load, the severed tube deflection is 0.5548 inch.

Since the neighboring tube is 0.31 inch away, the deflection of the tube is limited to this clearance. The contact force F can be estimated as:

$$F = \frac{0.5548 \times 0.31}{0.5548} \times 6.11 = 2.7 \text{ lb}$$

A value of $F = 3 \text{ lb}$ will be used.

With $C = 456 \text{ (psi)}^{-1}$ and $F = 3 \text{ lb}$,

$$T = \frac{V}{CF \times 10^{-12}} = \frac{V \cdot x \cdot 10^{12}}{CF}$$
$$= \frac{0.0349 \cdot x \cdot 10^{12}}{456 \times 3} = 25.5117 \times 10^6 \text{ in}$$

When the severed tube is leaning against a neighboring tube, it will be assumed that the neighboring tube will vibrate at its first natural frequency while the severed tube maintains contact with it. Since the first bending frequency of the neighboring tube, which is roughly 52 inches long with fixed/partial restraint end conditions, is about 50 Hz, this frequency will be taken as the rubbing frequency between the two tubes. Based on the observed wear widths of 0 to 100 mils (circumferentially) on the tubes removed from Ginna, the mean amplitude of motion will be taken as 50 mils.

Defining T' as the rub velocity, then

$$T' = 2 \times \delta \times f$$
$$= 2 \times 0.050 \times 50 = 5 \text{ in/sec}$$

If " t " is the total time to rub the tube thickness down to the minimum wall before burst,

$$t = \frac{T}{T'} = \frac{25.5117 \cdot x \cdot 10^6}{5} = 5.1023 \times 10^6 \text{ sec}$$
$$= 59 \text{ days}$$

For an upper bound, " t " could be longer in proportion to the specific wear coefficient, or

$$t = 59 \times 456/58 = 1.27 \text{ years.}$$

The time periods calculated above reasonably envelope the observed wear range. For example, burst tube R42 C55 went from less than 40 percent to 84 percent wall thinning between May 1981 and January 25, 1982.

4.5.8.2 Wear by Severed Tube

The wear patterns seen in the Ginna B-Steam Generator point to rubbing the O.D. of a neighboring tube by a severed tube. In particular, the cut tube would lay against the next tube and then would fret transversely against it as a result of fluid-induced motion. In so doing, the severed tube would wear down the walls of the adjacent tube(s).

In contrast, an unsevered tube would not be able to inflict such wear damage on surrounding tubes for lack of contact. Mechanical, thermal

and hydraulic loads are insufficient to cause tube deflection sufficient for tubes restrained at both ends to interact, as evidenced by the lack of tube wear in regions mid-way between the tube sheet and first support plate. That is, wear by unsevered tube(s) does not represent the mechanism seen at Ginna.

4.5.8.3 Burst Strength of Tubes

The purpose of this section is to determine the minimum wall thickness to preclude bursting of an active tube and to correlate the analytical prediction with the actual wall measurements of the burst tube (R42 C55) from the Ginna B-Steam Generator.

The tube wall thickness for burst during normal operation is computed by assuming uniform thinning and using the pressure stress equation in NB-3324.1 of the ASME Code. In this case, however, the primary membrane stress intensity used will be the ultimate strength of the tube material.

For the Ginna tube:

$$\begin{array}{ll} P_m &= 89.7 \text{ ksi} & R_i &= 0.397 \text{ in} \\ P_i &= 2250 \text{ psia} & P_o &= 780 \text{ psia} \\ \Delta P &= 2250 - 780 = 1470 \text{ psi} \end{array}$$

$$t = \frac{1470 \times 0.397}{89700 - 0.5(2250 + 780)}$$
$$= 0.0066 \text{ in}$$

Measurements of the burst tube from Ginna showed that the thinnest wall was 0.008 inch. Thus, the thickness based on a rather simplistic calculation correlates well with the actual measured thickness.

References for Section 4.5

- 4.5.2-1 A. C. Spencer, "Method of Characteristics for Solving Two-Dimensional Reactor Core Flows", proceedings of the 1973 Conference on Mathematical Models and Computational Techniques for Analysis of Nuclear Systems", CONF-730414-P1(ANS), 1973, pp. III-3 to III-22.
- 4.5.2-2 WECAN: Westinghouse Electric Corporation ANalysis, User's Manual, Second Edition, March 1981.
- 4.5.4-1 J. C. Hunsaker and R. B. Rightmire, "Engineering Applications of Fluid Mechanics," McGraw-Hill Book Co., 1947, pp. 198-204.
- 4.5.6-1 M. J. Pettigrew and D. J. Gorman, "Experimental Studies in Flow-Induced Vibration to Support Steam Generator Design, Part III. Vibration of Small Tube Bundles in Liquid and Two Phase Cross Flow", AECL 5804, June 1977.
- 4.5.6-2 H. J. Connors, "Flow-Induced Vibration and Wear of Steam Generators", Nuclear Technology Volume 55, November, 1981.
- 4.5.6-3 R. E. D. Bishop and A. Y. Hassan, "The Lift and Drag Forces on a Circular Cylinder Oscillating in a Flowing Fluid", Proceedings of the Royal Society of London, Series A, Vol. 277, pp. 32-75, 1964.
- 4.5.6-4 M. J. Sox, "Fluctuating Pressure Field on a Yawed Rigid Cylinder", Ph. D. Thesis, University of Minnesota, December 1978.
- 4.5.8-1 DeWees, N. B., "Sliding-Wear Performance of 135 Material Couples in High Purity Water at 300°F and 500°F," Bettis Atomic Power Laboratory, WAPD-314 AEC Research and Development Report, Control AT-11-1-GEN-14, May 1967, Pittsburgh, PA.

TABLE 4.5.2-1

NOMINAL AND BETWEEN-TUBE CROSSFLOW VELOCITIES IN
AND NEAR THE PLUGGED TUBE REGION

<u>Location</u>	<u>Crossflow Velocity</u> <u>----(nominal)----</u>	<u>Crossflow Velocity</u> <u>(one cell of tubes plugged)</u>
Perimeter Cell (Face A)	8.2 ft/sec	8.91 ft/sec
Perimeter Cell (Face C)	8.2 ft/sec	8.91 ft/sec
Perimeter Cell (Face B)	9.01 ft/sec	9.11 ft/sec
One Cell in from Perimeter (Face B)	8.54 ft/sec	8.84 ft/sec
Two Cells in from Perimeter (Face B)	8.21 ft/sec	8.56 ft/sec

TABLE 4.5.3-1

SUMMARY OF WORST CASE AXIAL LOADS ON A PLUGGED TUBE

<u>Source</u>	<u>Type (no. of cycles)</u>	<u>Max. Value lb.....</u>	<u>Analysis Applicability*</u>
1. Secondary Pressure (maximum at no-load)	Constant	-604. (compression)	Flow Induced Vibration
2. Tube-to-Shell Interaction			
a. Hot standby with 70°F feed	Transient (200)	-1940.	Fatigue
b. Plant loading	Transient (14,500)	825.	Fatigue
c. Plant unloading	Transient (14,500)	-1375.	Fatigue
d. Full power steady-state	Constant	-550.	Flow Induced Vibration
3. Plugged-to-Active Tube Interaction (Full power steady-state)	Constant	1410	Collapse

* Pressure and thermal interaction loads cannot both occur on the same tube. However, tube-to-shell and plugged-to-active tube interaction loads can occur simultaneously on a tube. The actual load magnitude on a plugged tube would depend on the location of the tube and the number of active tubes around it. Assuming superposition of steady-state loads (Cases 2d and 3), tensile loads of the order of 1000 lbs can be expected in a plugged tube near a hot leg wedge location. Axial loads on tubing in cold-leg and/or regions away from the wedges would be lower due to smaller temperature differentials and support plate flexibility.

TABLE 4.5.4-1
FOREIGN OBJECT INDUCED LOADS

Case	$X_p(0)$ (inches)	U_{ss} (ft/sec)	U_A (ft/sec)	Model 1* Peak Load (lbs)	Model 2* Peak Load (lbs)
1	-5	2.3	0	26	107
2	0	.69	.69	.15	.28
3	0	.345	.69	.39	1.40

*Model 1: $K_{SG} = 3717 \text{ lb/inches}$
 $M_{SG} = .03767 \text{ lb} - \text{sec}^2/\text{inches}$

Model 2: $K_{SG} = 19439 \text{ lb/inches}$
 $M_{SG} = .01068 \text{ lb} - \text{sec}^2/\text{inches}$

TABLE 4.5.6-1
ANALYSIS PARAMETERS

Outside diameter	0.875 inch
Inside diameter	0.775 inch
Tube pitch	1.234 inches
Flexural moment of inertia	0.111 inch ⁴
Axial area	0.1290 inch ²
Tube density	0.304 lb/inch ³
Modulus of elasticity	29.2 x 10 ⁶ lb/inches ²
Secondary fluid density	50 lb/ft ³

TABLE 4.5.6-2

TUBE FUNDAMENTAL FREQUENCIES FOR
THE VARIOUS CASES ANALYZED

Cross Section	Fixed-Fixed	Fixed-Pinned	
	P=0	P=0	P= -1000 lbs
Cylinder	58.7 HZ	40.3 HZ	38.5 HZ
Flat	48.9 HZ	31.6 HZ	27.9 HZ
10 Ovalized	58.3 HZ	40.0 HZ	-----
Kidney	58.2 HZ	39.9 HZ	-----

TABLE 4.5.6-3

VORTEX-SHEDDING INDUCED LOADS ON PROTRUSIONS FOR A FLUID.
VELOCITY OF 10.0 FT/SEC

H/D	H (Inches)	Lift (lbs)	Torque (in-lbs)	Lift & Torque Frequency (HZ)	Drag (lbs)	Drag Frequency(Hz)
1.0	0.1	.28 (10 ⁻²)	.35 (10 ⁻⁴)	240	.28 (10 ⁻³)	480
1.0	0.20	.11 (10 ⁻¹)	.28 (10 ⁻³)	120	.11 (10 ⁻²)	240
1.0	0.30	.25 (10 ⁻¹)	.95 (10 ⁻³)	80	.25 (10 ⁻²)	160
1.0	0.40	.45 (10 ⁻¹)	.22 (10 ⁻²)	60	.45 (10 ⁻²)	120
1.0	0.50	.70 (10 ⁻¹)	.44 (10 ⁻²)	48	.70 (10 ⁻²)	96
5.0	0.50	.14 (10 ⁻¹)	.18 (10 ⁻³)	240	.14 (10 ⁻²)	480
5.0	1.00	.56 (10 ⁻¹)	.14 (10 ⁻²)	120	.56 (10 ⁻²)	240
5.0	1.50	0.13	.47 (10 ⁻²)	80	.13 (10 ⁻¹)	160
5.0	2.00	0.22	.11 (10 ⁻¹)	60	.22 (10 ⁻¹)	120
5.0	2.50	0.35	.22 (10 ⁻¹)	48	.35 (10 ⁻¹)	96

TABLE 4.5.7-1

CALCULATED STRESSES (KSI)
NOMINALLY PLUGGED TUBE

	a	a	a	b	c	d	e	f	g	h
Transient	σ_A	σ_H	σ_R	σ_B	σ_B	σ_B	σ_A	σ_B	σ_A	$\pm\sigma_{BH}$
Plant Heat Up	0.0	-9.77	-0.50	2.42	0.11	2.81	-4.96	3.02	0.0	22.0
Plant Cooldown	0.0	-9.77	-0.50	2.42	0.11	2.81	-4.96	3.02	0.0	22.0
Plant Loading	0.0	-7.74	-0.40	2.42	0.23	2.81	+4.54	2.85	+3.36	17.2
Plant Unloading	0.0	-7.74	-0.40	2.42	0.23	2.81	+4.54	2.85	+3.36	17.2
Step Load ± 10	0.0	-7.74	-0.40	2.42	0.23	2.81	+4.54	2.85	+3.36	17.2
Reactor Trip	0.0	-7.74	-0.40	2.42	0.23	2.81	+4.54	2.85	+3.36	17.2
50 Step Load Decrease	0.0	-7.74	-0.40	2.42	0.23	2.81	+4.54	2.85	+3.36	17.2
Hot Standby	0.0	-9.97	-0.50	2.42	0.11	2.81	+3.21	6.04	+9.94	22.0

.....
 *Largest axial stress is used to calculate this bending stress.

TABLE 4.5.7-2
PRINCIPAL STRESSES
NOMINALLY PLUGGED TUBE (KSI)

<u>Transient</u>	<u>Axial</u>	<u>Hoop</u>	<u>Radial</u>
Plant Heatup	-13.32	-31.77	-0.50
Plant Cooldown	-13.32	-31.77	-0.50
Plant Loading	12.85	-24.94	-0.40
Plant Unloading	12.85	-24.94	-0.40
Step Load \pm 10	12.85	-24.94	-0.40
Reactor Trip	12.85	-24.94	-0.40
50 Step Load Increase	12.85	-24.94	-0.40
Hot Standby	21.32	-31.77	-0.50

TABLE 4.5.7-3
USAGE FACTOR FOR A NOMINALLY PLUGGED TUBE

<u>Transient</u>	<u>Cycles</u>	<u>S_a*,ksi</u>	<u>Allowable Cycles</u>	<u>Usage Factor</u>
Plant Heatup	200	20.4	10 ⁶	0.0002
Plant Cooldown	200	20.4	10 ⁶	0.0002
Plant Loading	14,500	25.6	10 ⁶	0.0145
Plant Unloading	14,500	25.6	10 ⁶	0.0145
Step Load <u>±</u> 10	4,000	25.6	10 ⁶	0.004
Reactor Trip	400	25.6	10 ⁶	0.0004
50 Step Load Decrease	200	25.6	10 ⁶	0.0002
Hot Standby	200	36.9	10 ⁵	<u>0.002</u>
			TOTAL	0.036

* S_a is adjusted to E = 26 x 10³ ksi.

USAGE FACTOR FOR A NOMINALLY PLUGGED TUBE WITH NOTCH OR STRESS RISER

TransientPrincipal stresses, ksi.....			Cycle	S _a *,ksi	Allowable -Cycles--	Usage Factor
	Axial ^Δ	Hoop	Radial				
Plant Heatup	-39.96	-31.77	-0.50	200	29.0	300,000	0.0007
Plant Cooldown	-39.96	-31.77	-0.50	200	29.0	300,000	0.0007
Plant Loading	38.55	-24.94	-0.40	14,500	42.0	50,000	0.29
Plant Unloading	38.55	-24.94	-0.40	14,500	42.0	50,000	0.29
Step Load <u>±</u> 10	38.55	-24.94	-0.40	4,000	42.0	50,000	0.08
Reactor Trip	38.55	-24.94	-0.40	400	42.0	50,000	0.008
50 Step Load Decrease	38.55	-24.94	-0.40	200	42.0	50,000	0.004
Hot Standby	63.96	-31.77	-0.50	200	39.6	70,000	<u>0.003</u>
TOTAL =							0.6764

.....
^ΔStress concentration factor of 4.0 is applied for the notch or stress riser.

*S_a is adjusted to E = 26 x 10³ KSI

TABLE 4.5.7-5
STRESS AMPLITUDE AND ALLOWABLE CYCLES
WITH LATERAL IMPACT LOAD

<u>Impact Load, ksi</u>	<u>S_a*, ksi</u>	<u>No. of Cycles Allowed</u>
0.0	9.22	∞
10.0	14.15	10 ⁸
25.0	16.81	8.5 x 10 ⁶
50.0	22.14	2.4 x 10 ⁶

*S_a is adjusted to E = 26 x 10³ ksi

TABLE 4.5.7-6

POSTULATED FAILURE TIME WITH LATERAL IMPACT LOAD

<u>Impact Loads</u> <u>... (lbs) ...</u>	<u>Cycles/Day</u>	<u>Allowable</u> <u>... Cycles ...</u>	<u>Postulated Failure</u> <u>... Time** (days) ...</u>
0.0	3.33×10^6	∞	∞
10.0	3.33×10^6	10^8	30
25.0	3.33×10^6	8.5×10^6	2.5
50.0	3.33×10^6	2.4×10^6	0.7

** Failure is defined analytically when cumulative usage factor = 1.0.

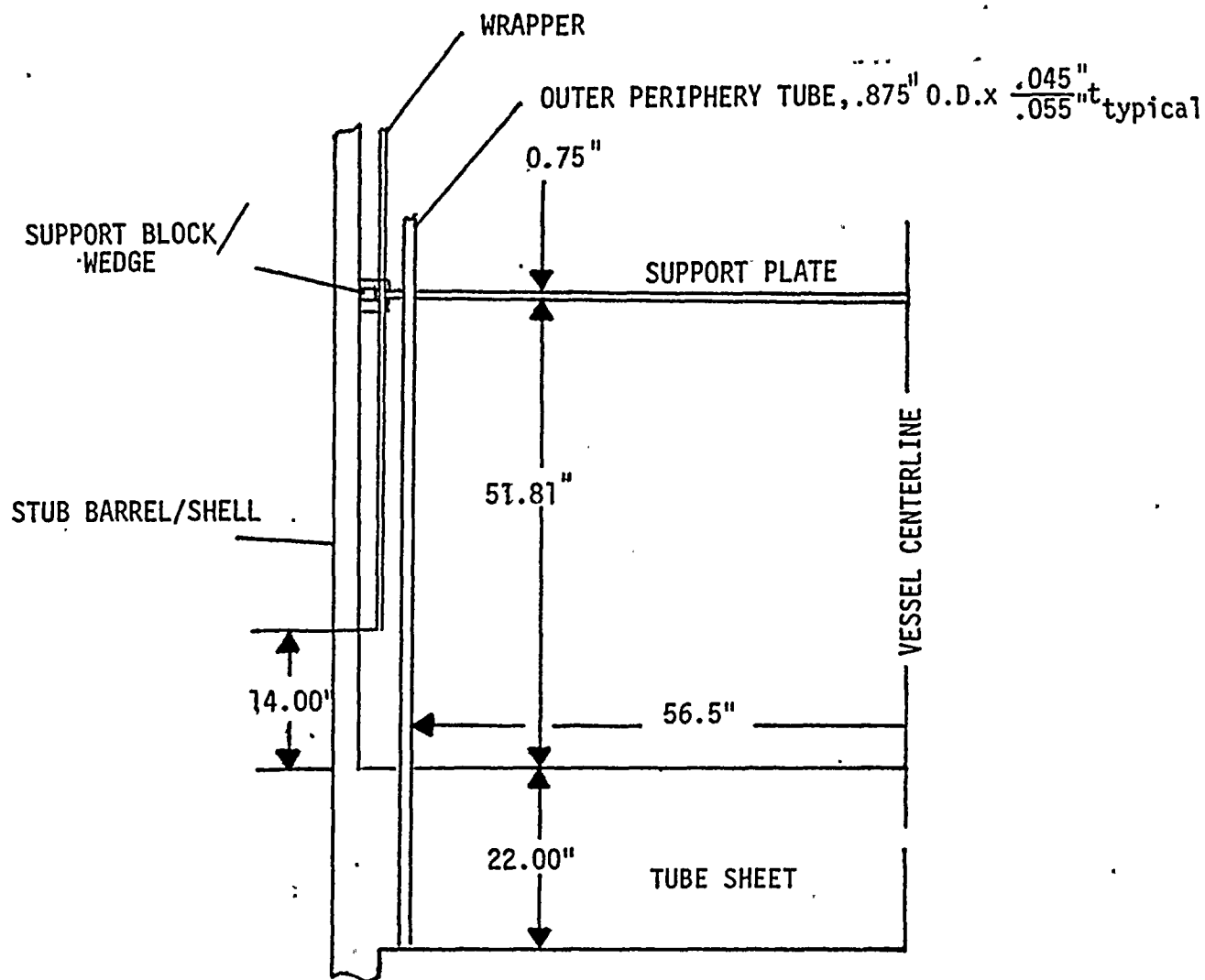


FIGURE 4.5.1-1 - SCHEMATIC SHOWING HOT LEG
SPAN GEOMETRY

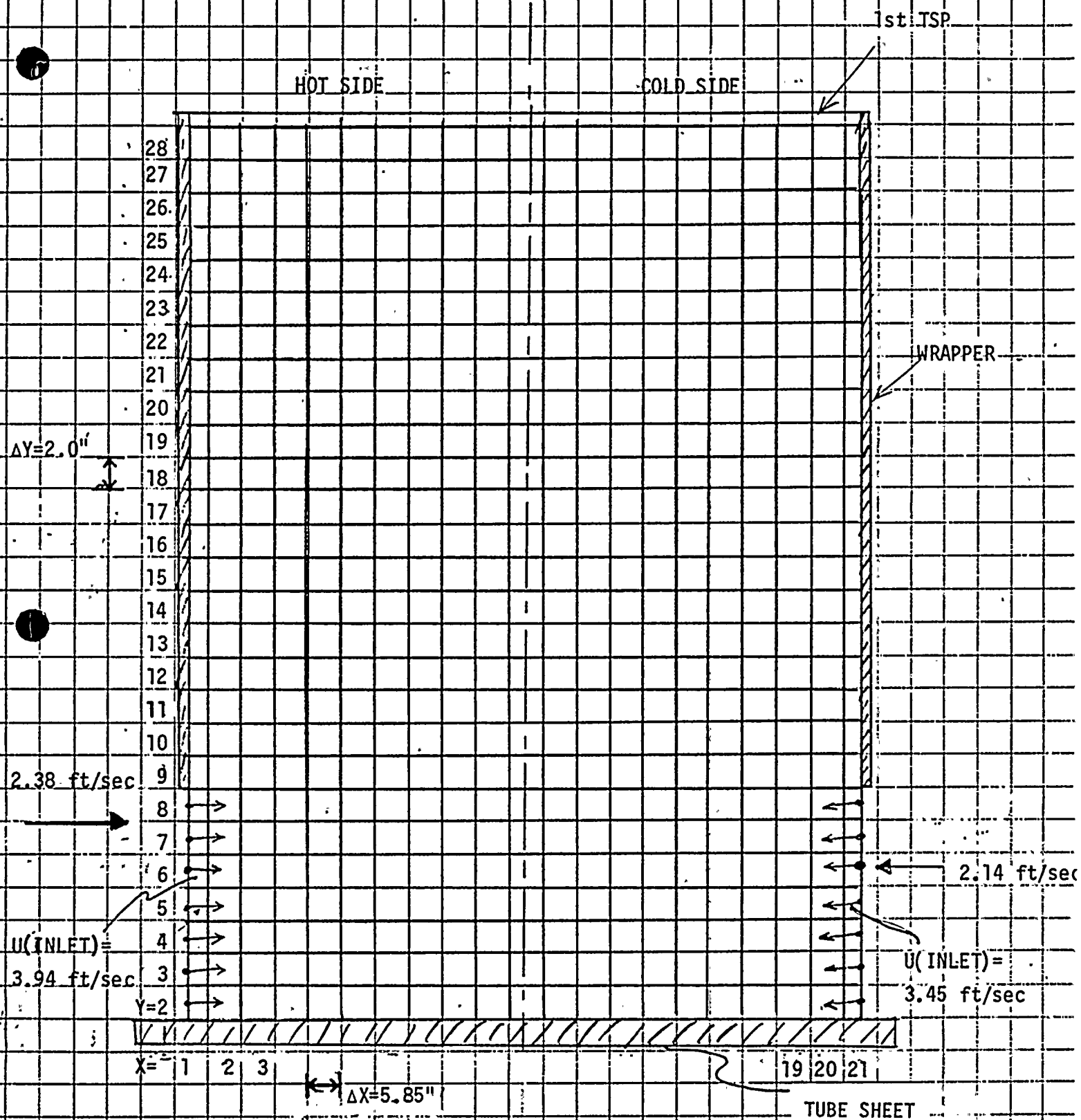


FIGURE 4.5.2-1

CHARM MODEL FOR RGE

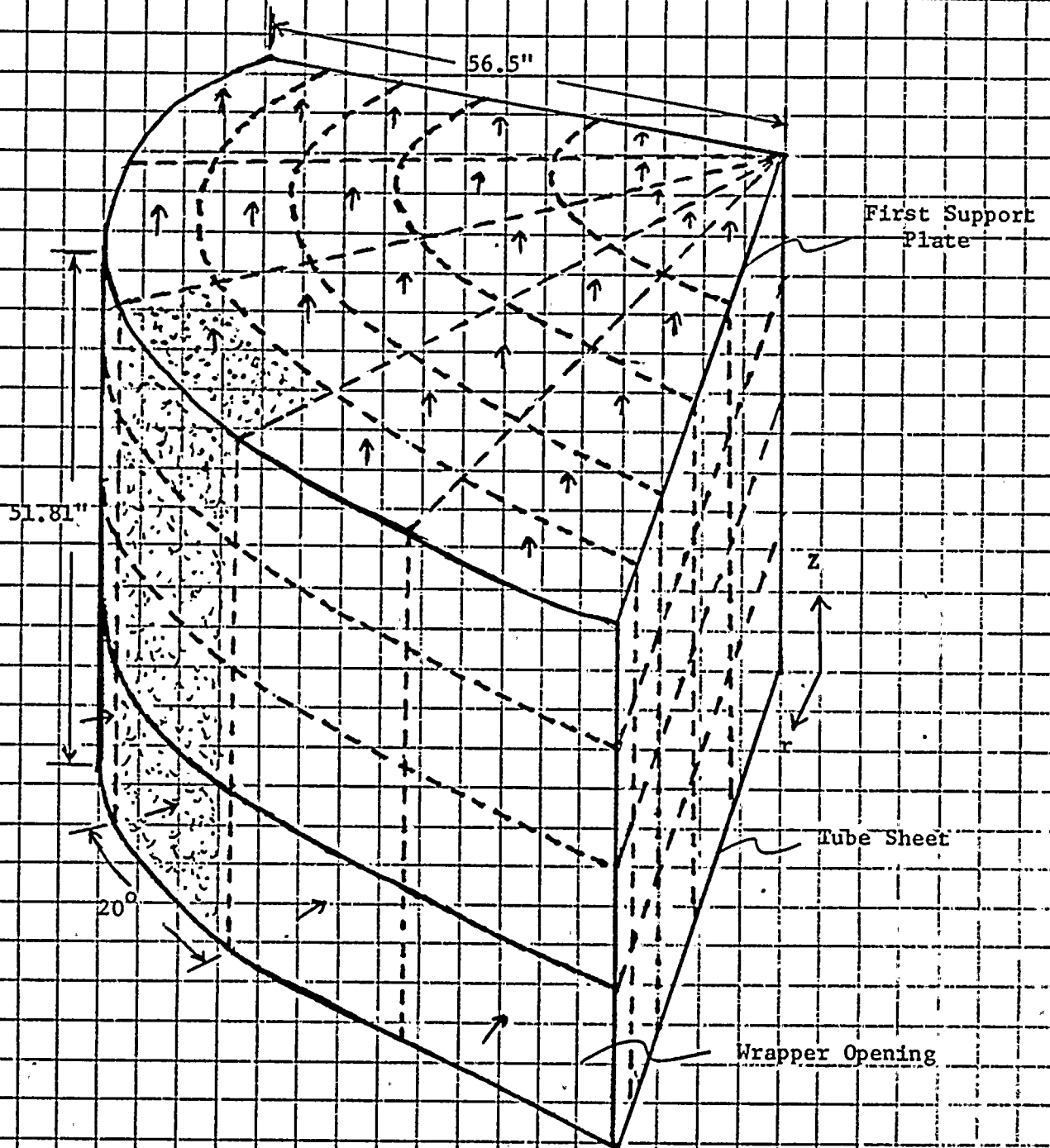
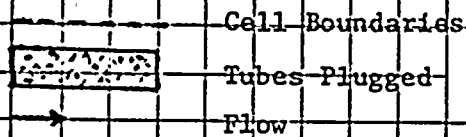
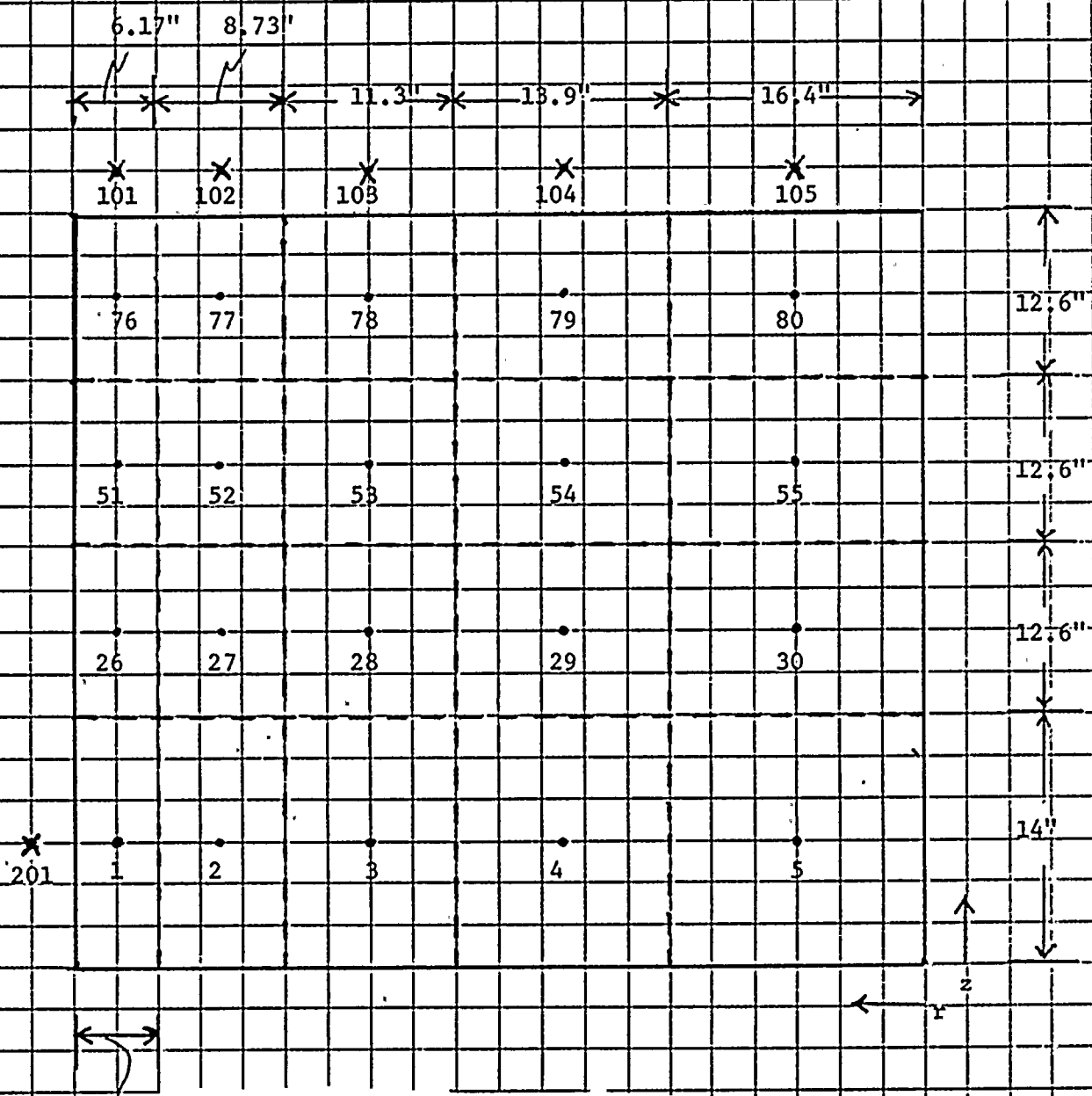


FIGURE 4.5.2-2 THREE-DIMENSIONAL (WECAN) HYDRAULIC MODEL OF TUBE SHEET TO FIRST SUPPORT PLATE REGION

* Boundary Node
 • Internal Node

Circumferential Node Spacing = 5



TUBES PLUGGED - 5 TUBE PITCHES

FIGURE 4.5.2-3 R - Z DISTRIBUTION OF NODES FOR 3-D
 HYDRAULIC ANALYSIS ($\theta = 10^\circ$ PLANE)

- ✕ Boundary Node
- Internal Node

Axial Node Spacing = 25

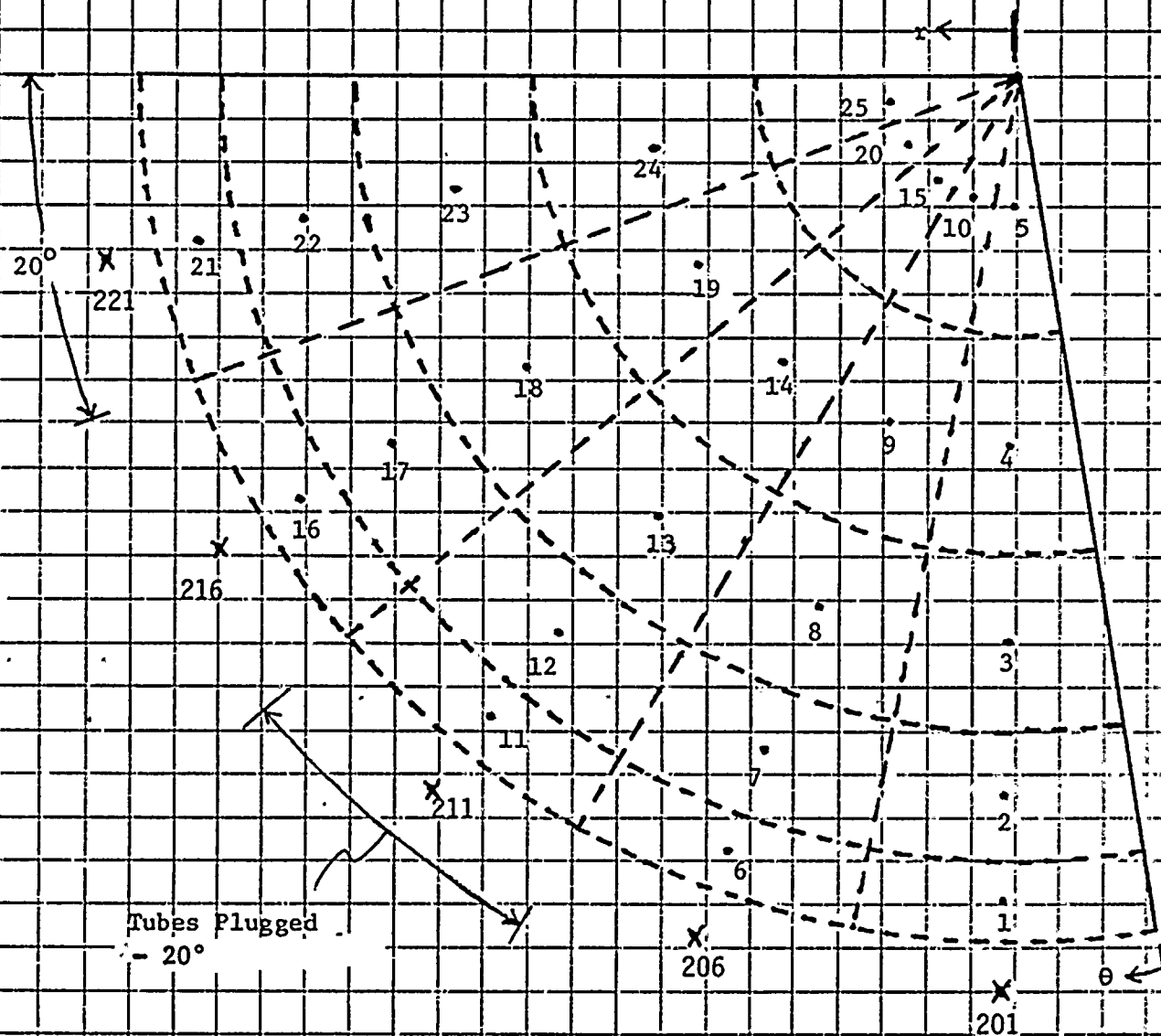


FIGURE 4.5.2-4 R- θ DISTRIBUTION OF NODES FOR 3-D
HYDRAULIC ANALYSIS (Z=7" PLANE)

AVERAGE VELOCITIES (LATERAL AND AXIAL)

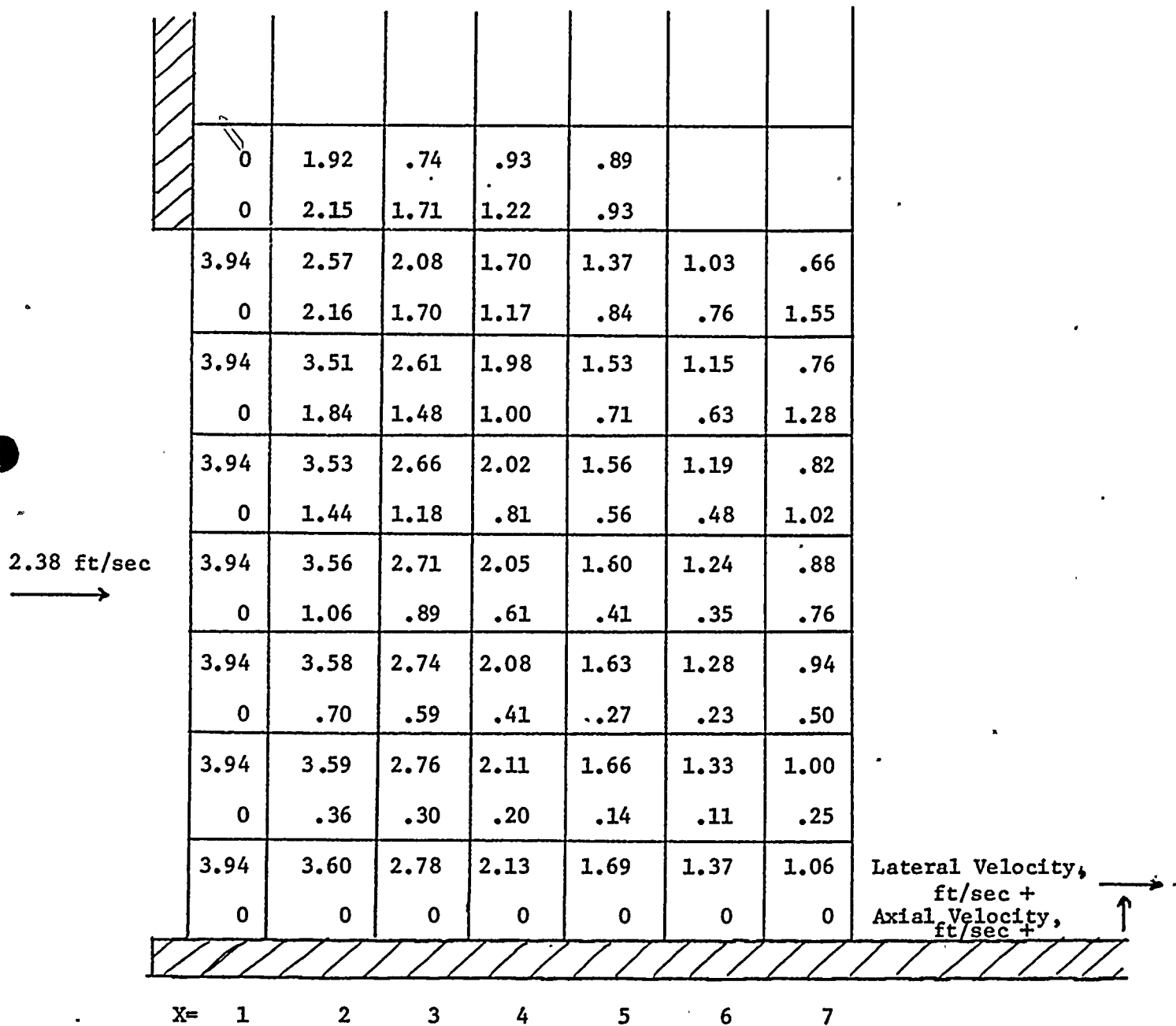


FIGURE 4.5.2-5: GINNA NOMINAL CASE .

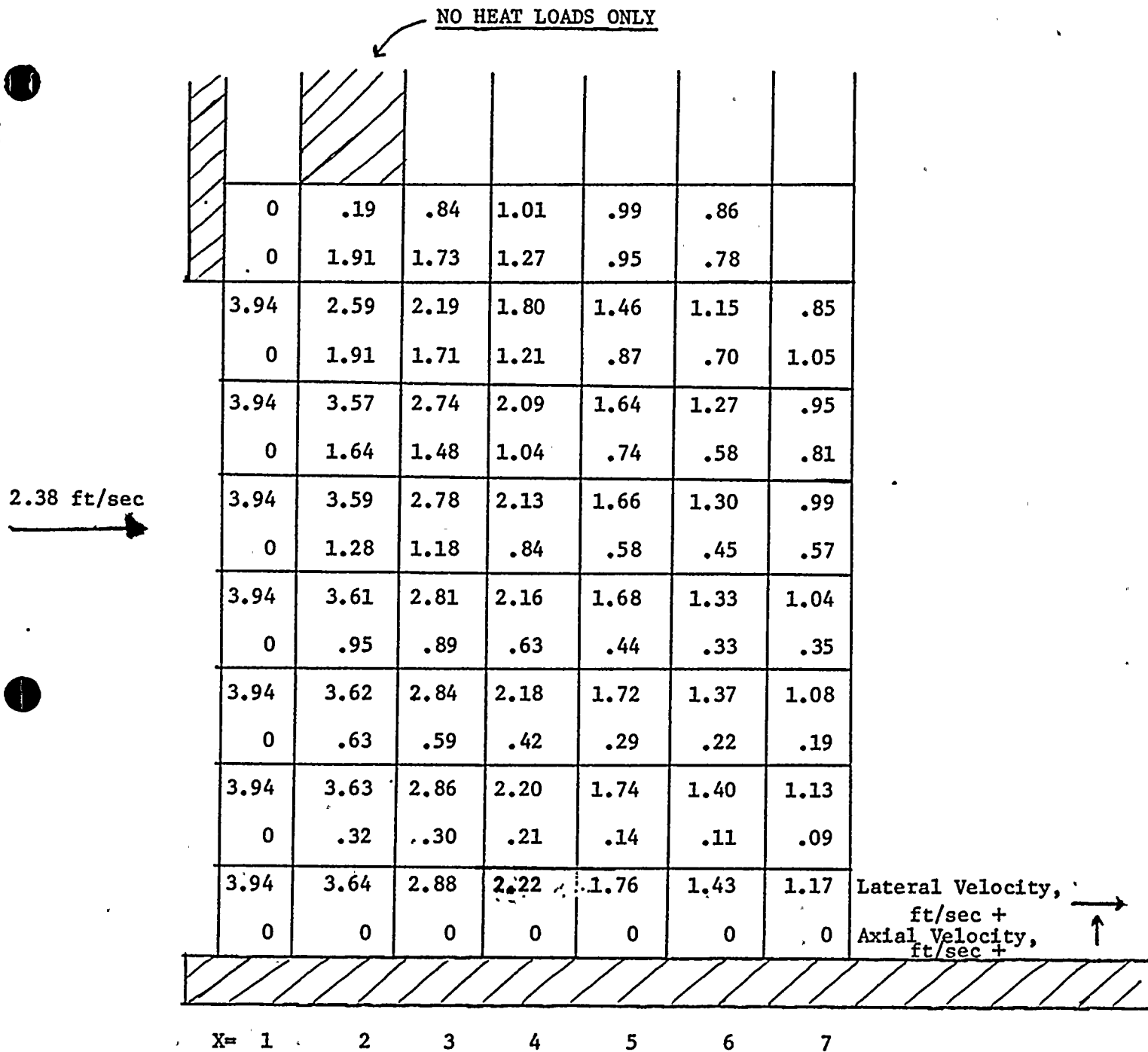


FIGURE 4.5.2-6: GINNA WITH TUBES PLUGGED

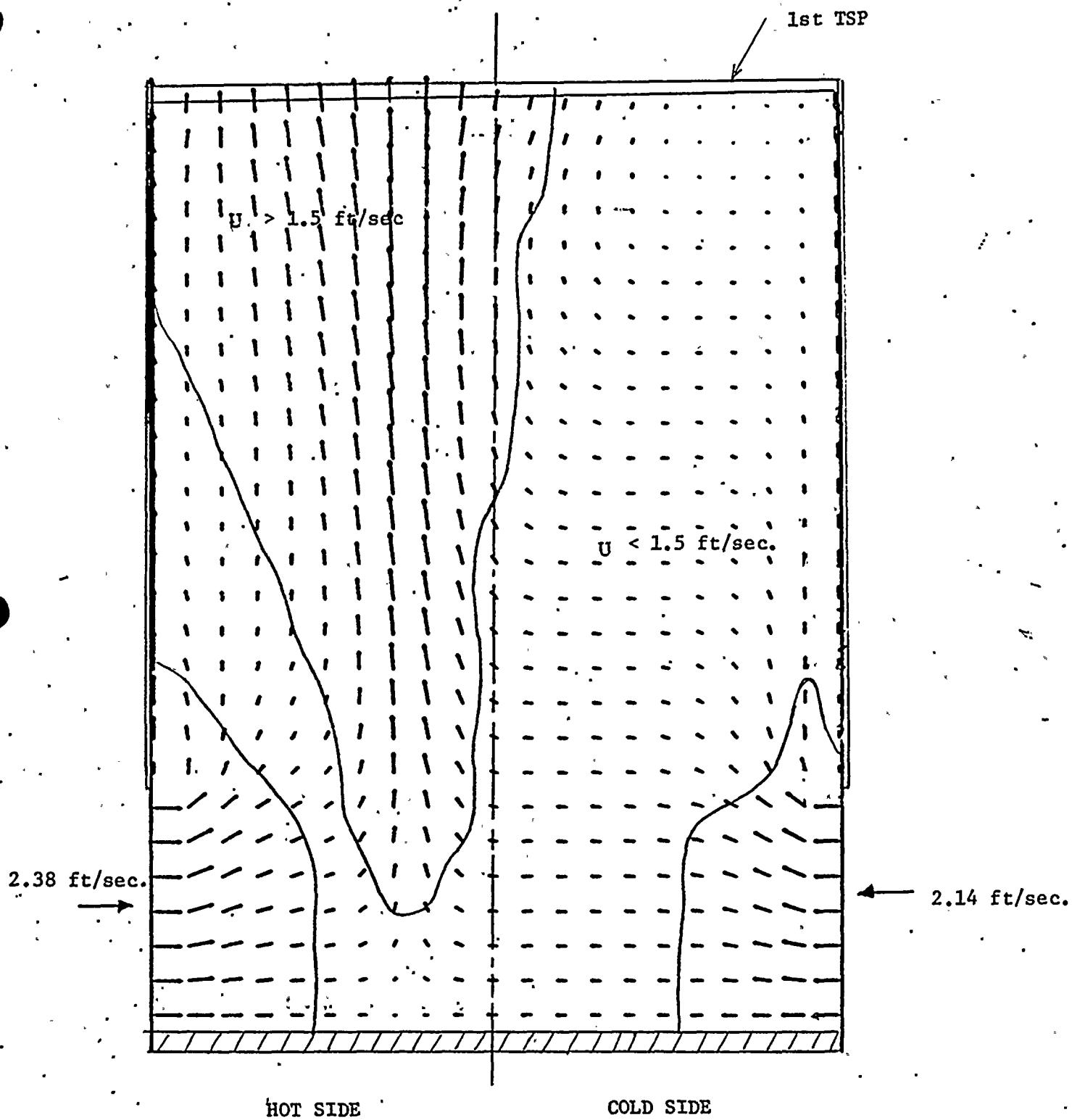


FIGURE 4.5.2-7

GINNA BASE CASE

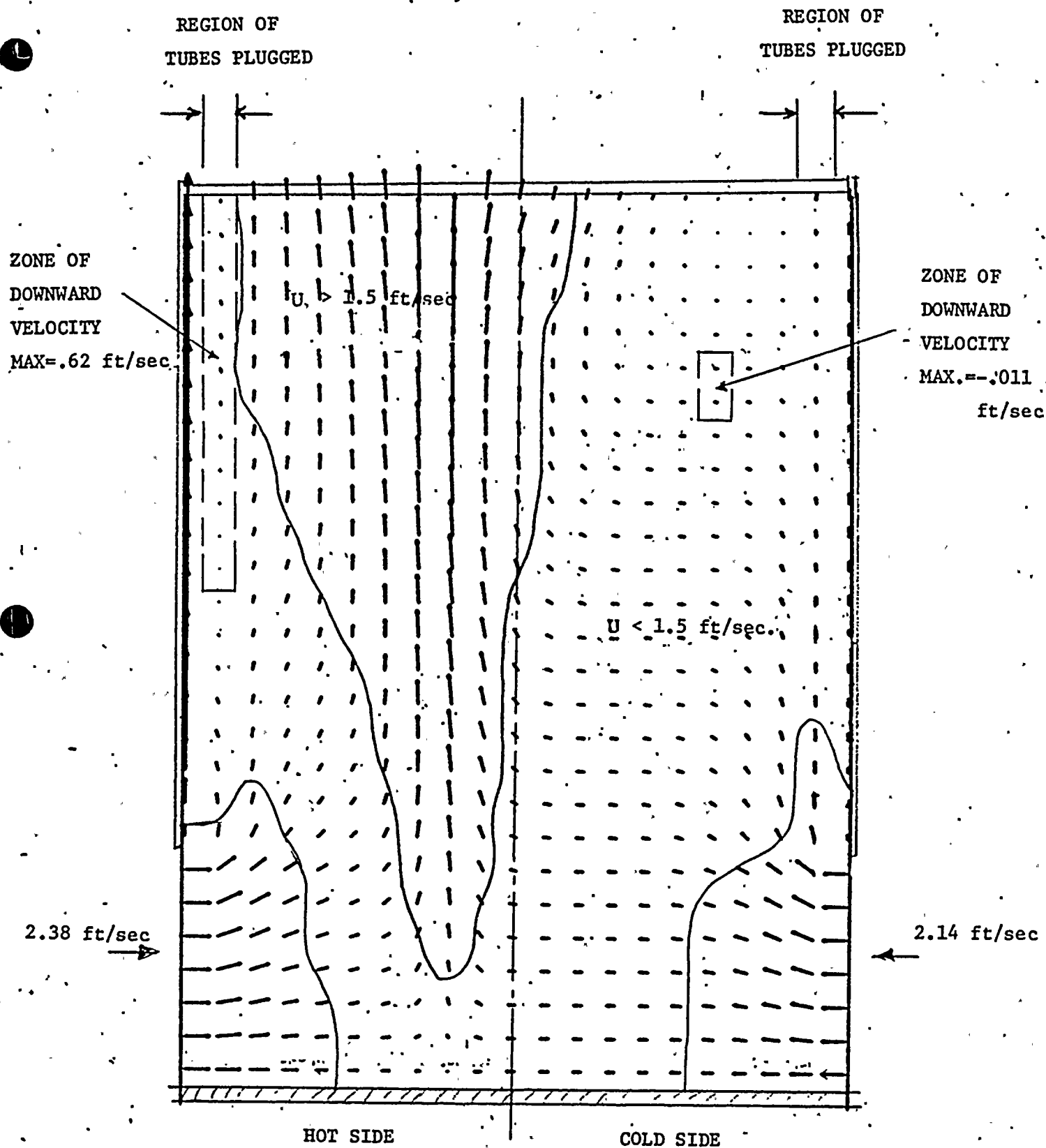


FIGURE 4.5.2-8
GINNA WITH TUBES PLUGGED

4.5-52

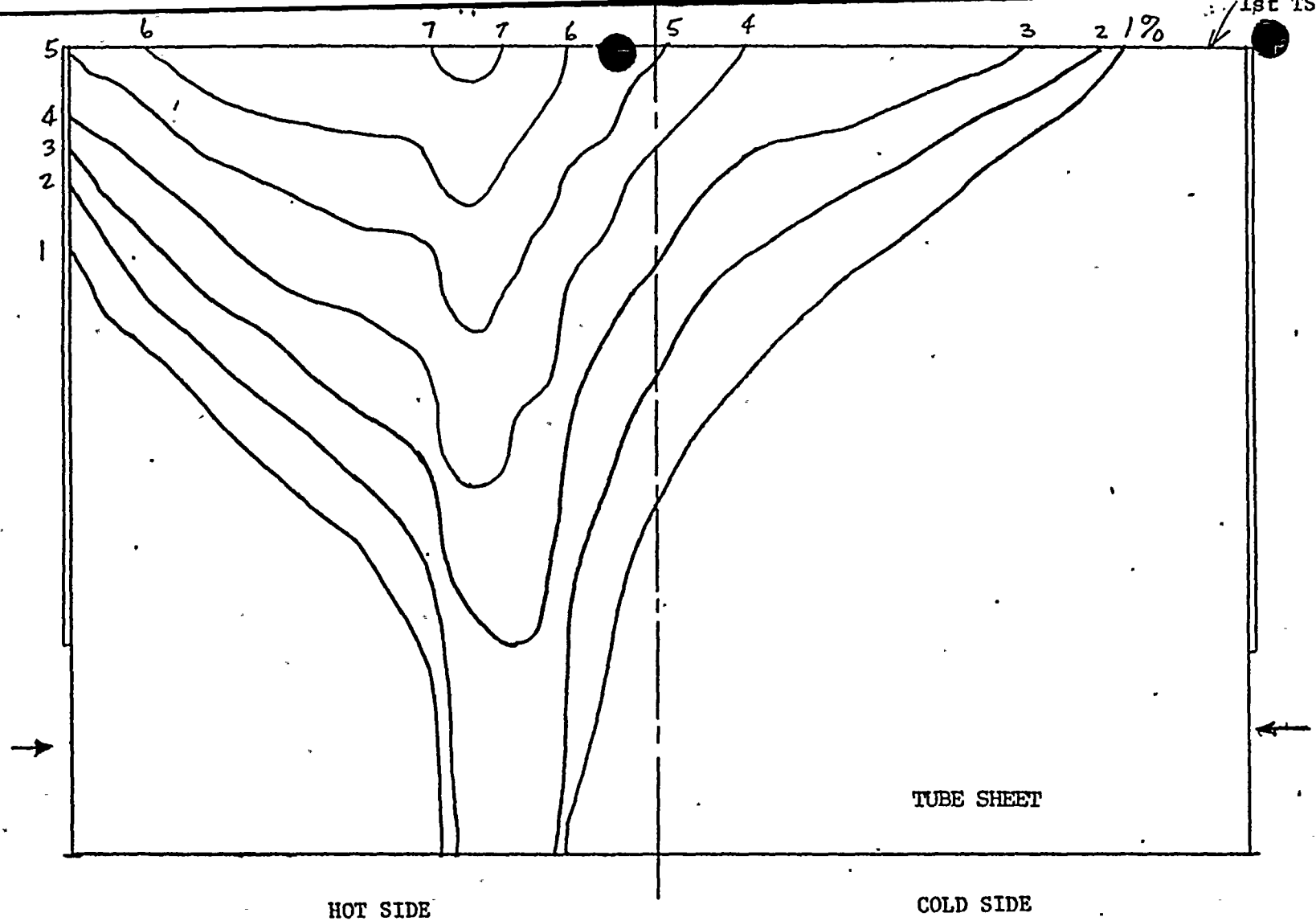


FIGURE 4.5.2-9
QUALITY DISTRIBUTION OF
GINNA BASE CASE

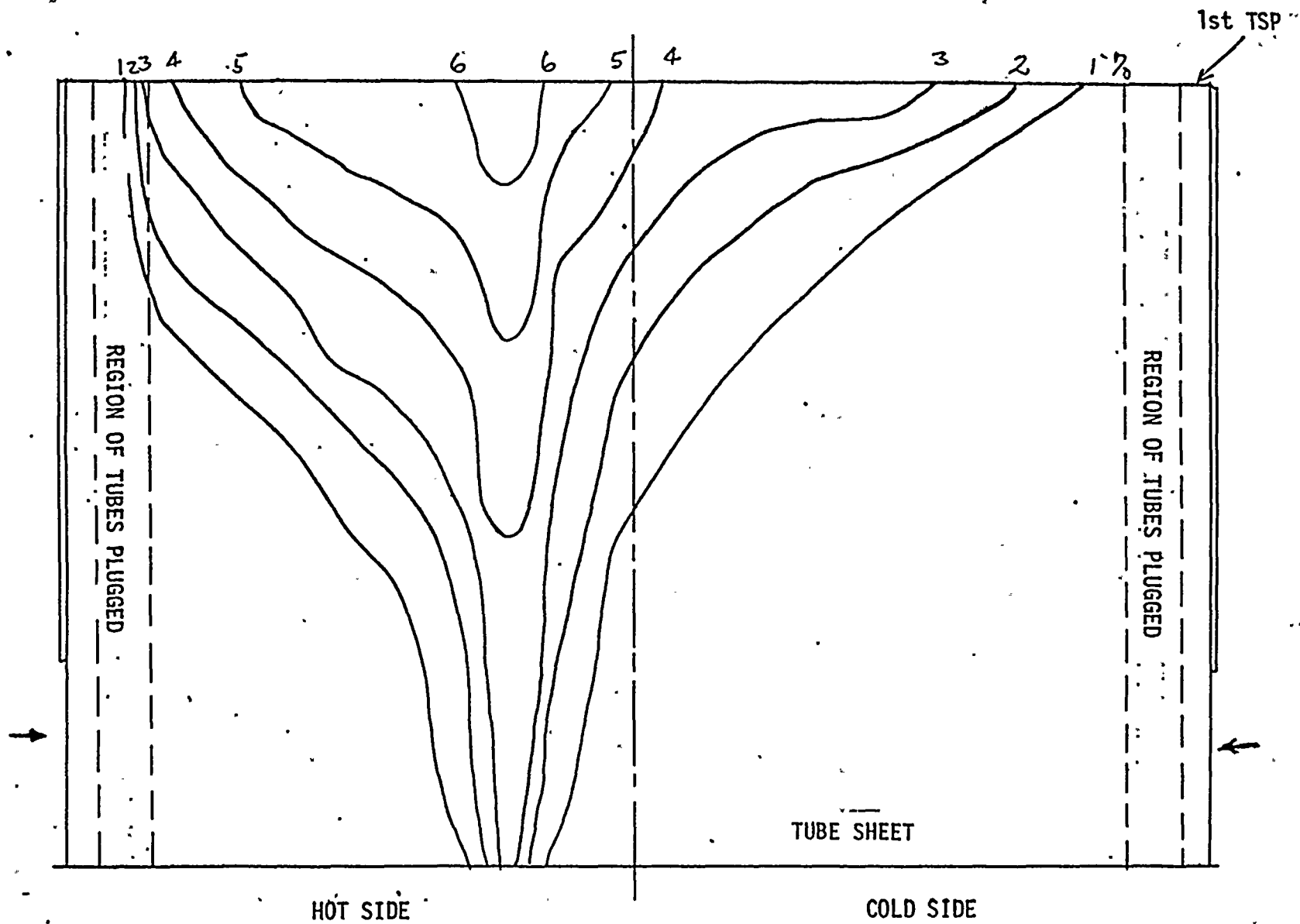


FIGURE 4.5.2-10 QUALITY DISTRIBUTION OF GINNA WITH TUBES PLUGGED

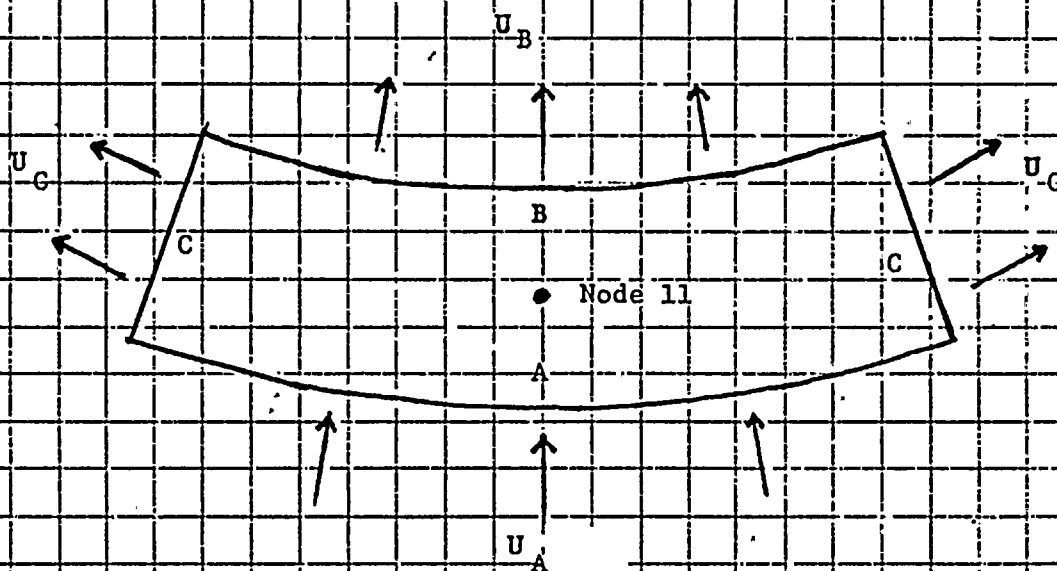
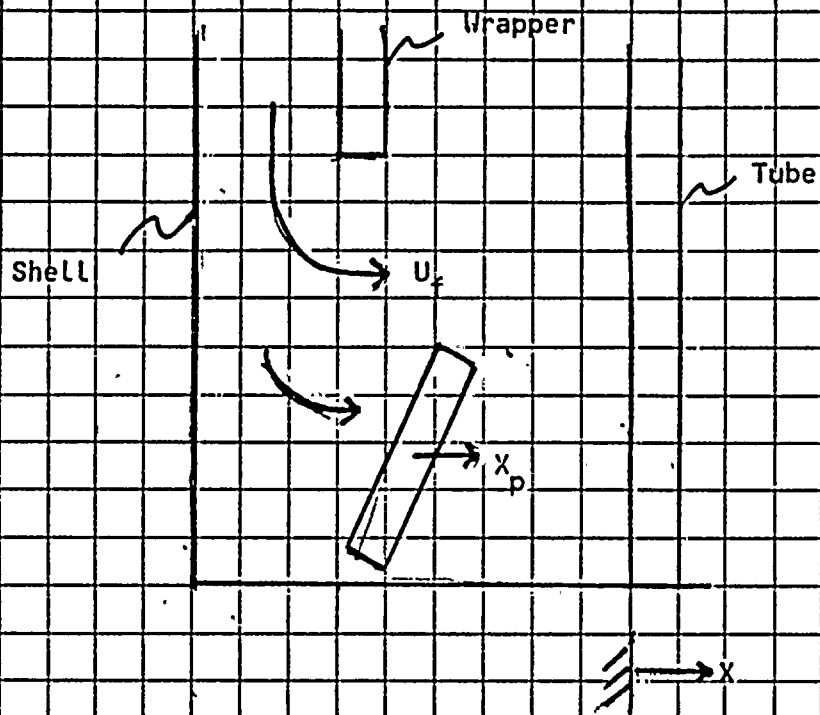
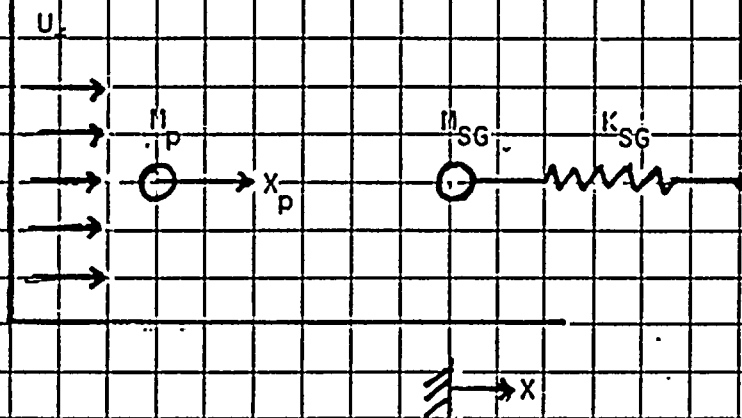


FIGURE 4.5.2-11 FLUID VELOCITIES IN THE NODE 11 Cell

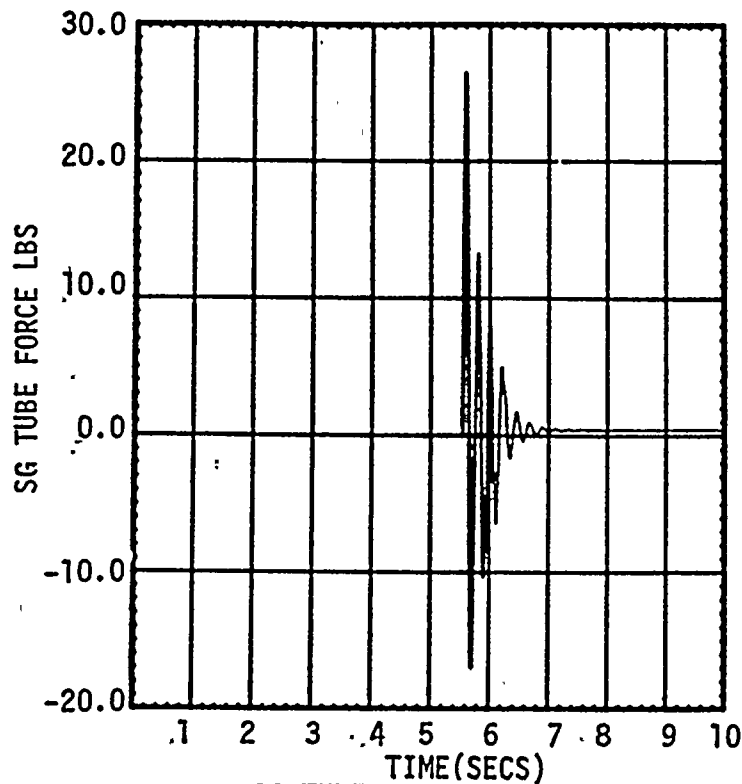


(a) TUBE BUNDLE ENTRANCE REGION WITH FOREIGN OBJECT



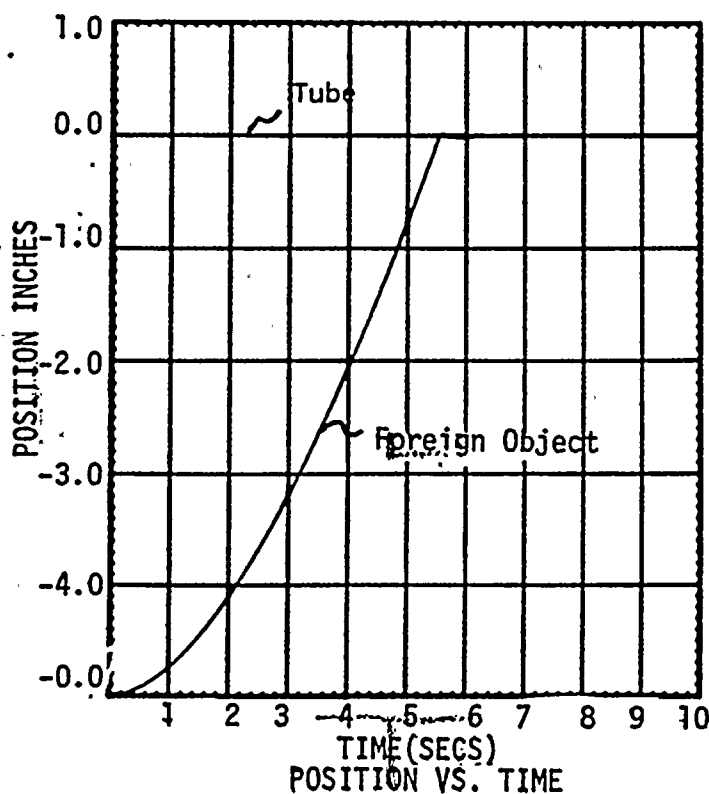
(b) Simulation

Figure 4.5.4-1 DYNAMIC MODEL OF FOREIGN OBJECT IMPACT



SG TUBE FORCE VS. TIME

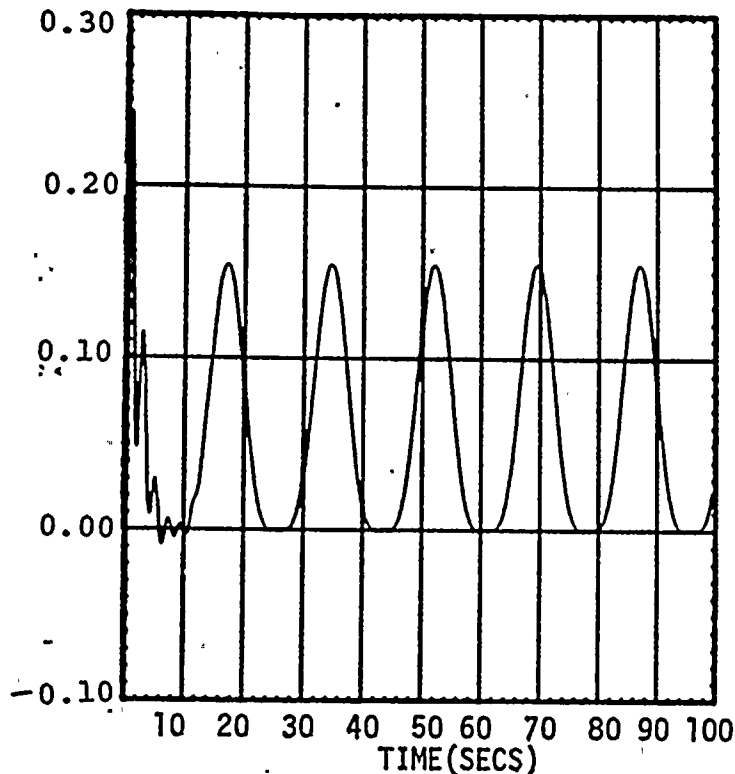
Figure 4.5.4-2 SG TUBE SPRING FORCE -TIME HISTORY (STEADY-
STATE FLUID VELOCITY = 2.3 ft/sec ALTERNATING
VELOCITY = 0)



POSITION VS. TIME

Figure 4.5.4-3 FOREIGN OBJECT AND SG TUBE DISPLACEMENT -TIME HISTORY
(STEADY-STATE FLUID VELOCITY = 2.3 ft/sec
ALTERNATING VELOCITY = 0)

S/G TUBE FORCE lbs.

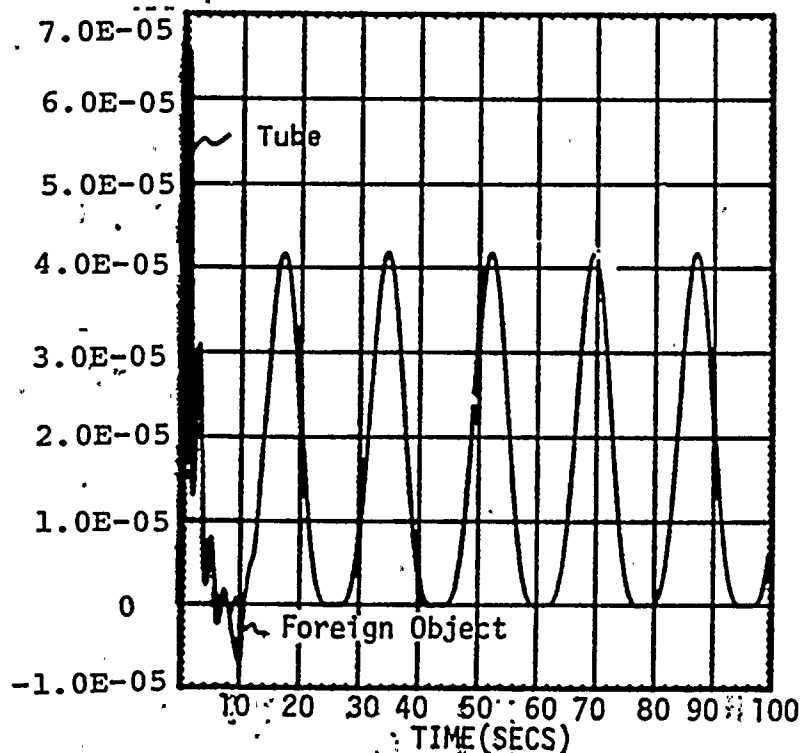


Model 1,
Case 2

Figure 4.5.4-4

S/G TUBE FORCE VS. TIME
S/G TUBE SPRING FORCE-TIME HISTORY (STEADY STATE
FLUID VELOCITY = .69 ft/sec. ALTERNATING VELOCITY=
.69 ft/sec.

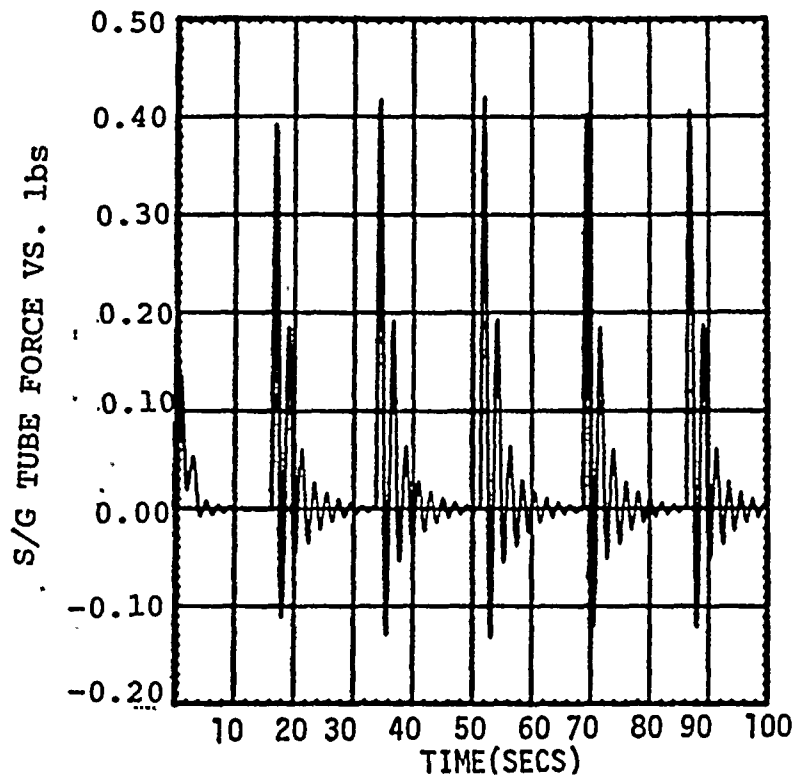
POSITION INCHES



Model 1,
Case 2

Figure 4.5.4-5

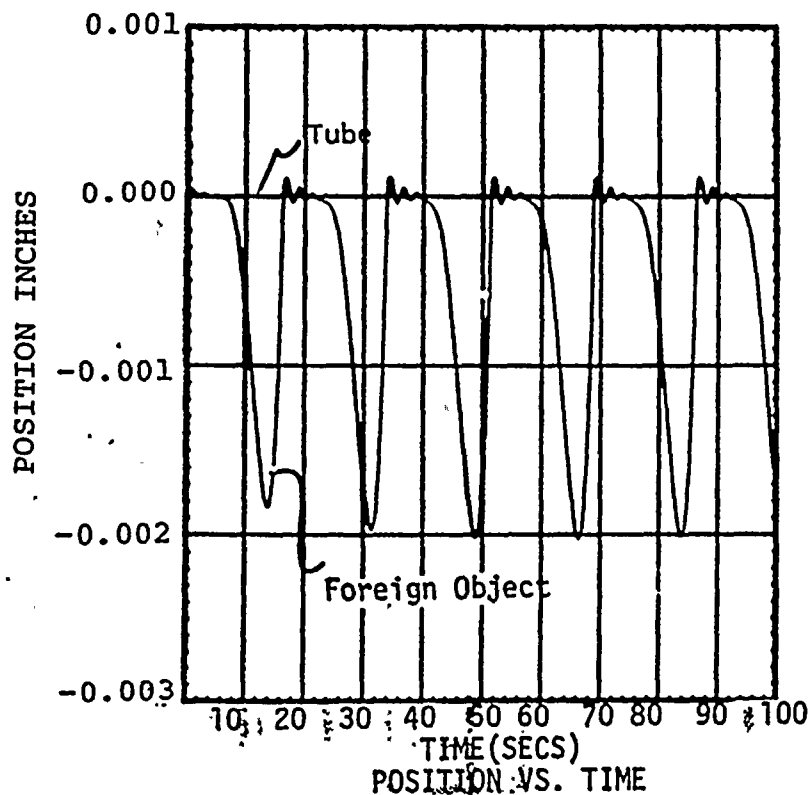
POSITION VS. TIME
FOREIGN OBJECT AND SG TUBE DISPLACEMENT
(STEADY STATE FLUID VELOCITY = .69 FT/SEC.
ALTERNATING VELOCITY= .69 FT/SEC.



Model 1,
Case 3

Figure 4.5.4-6

S/G TUBE FORCE VS. TIME
S.G. TUBE SPRING FORCE = TIME HISTORY
(STEADY STATE FLUID VELOCITY = .345 FT/SEC
ALTERNATING VELOCITY = .69 FT/SEC)



Model 1,
Case 3

Figure 4.5.4-7

FOREIGN OBJECT AND SG TUBE DISPLACEMENT-TIME HISTORY
(STEADY STATE FLUID VELOCITY = .345 FT/SEC
ALTERNATING VELOCITY = .69 FT/SEC)
4.5-58

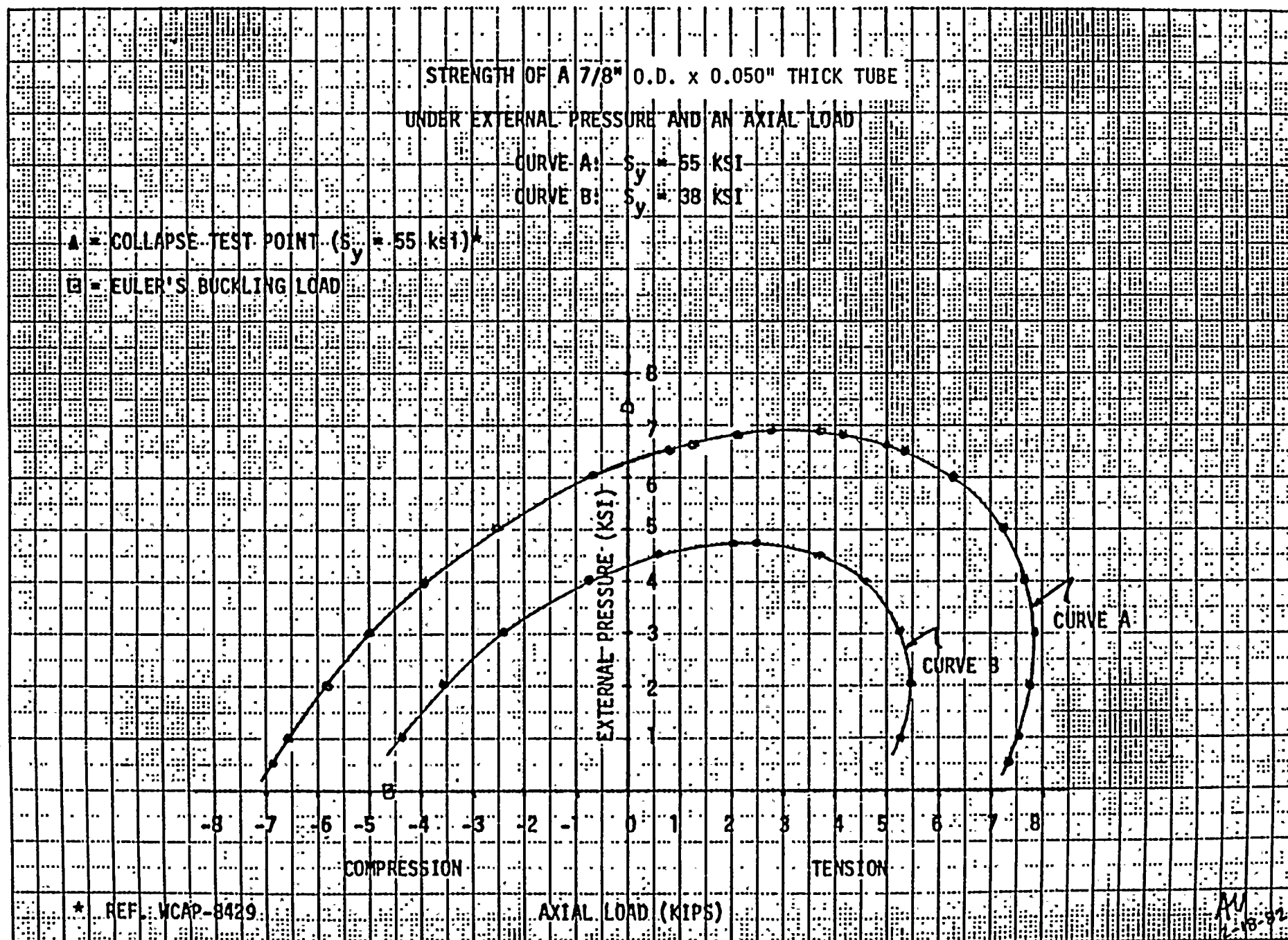
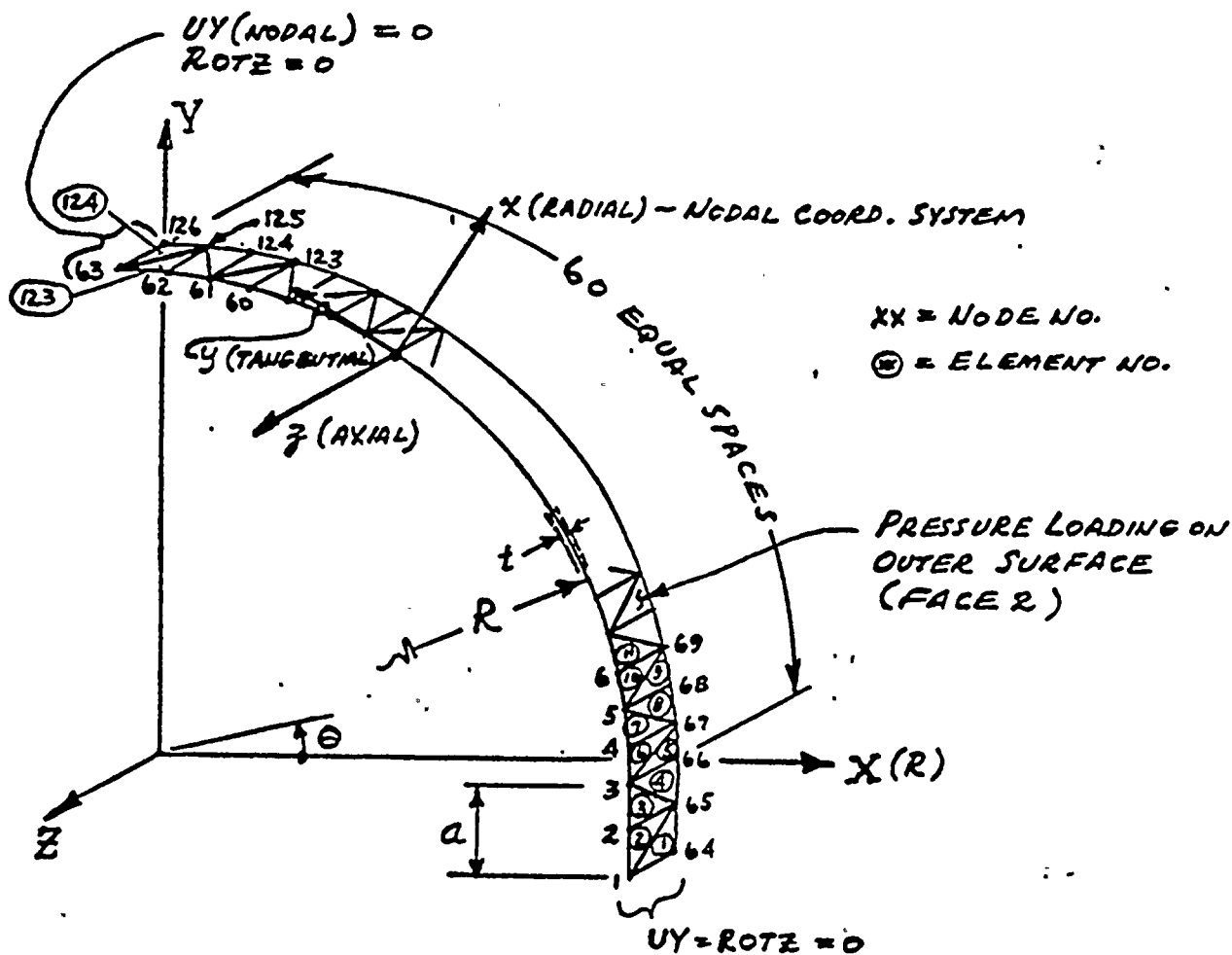


FIGURE 4.5.5-1 : EXTERNAL PRESSURE AND AXIAL LOAD REQUIRED FOR INCIPIENT YIELDING



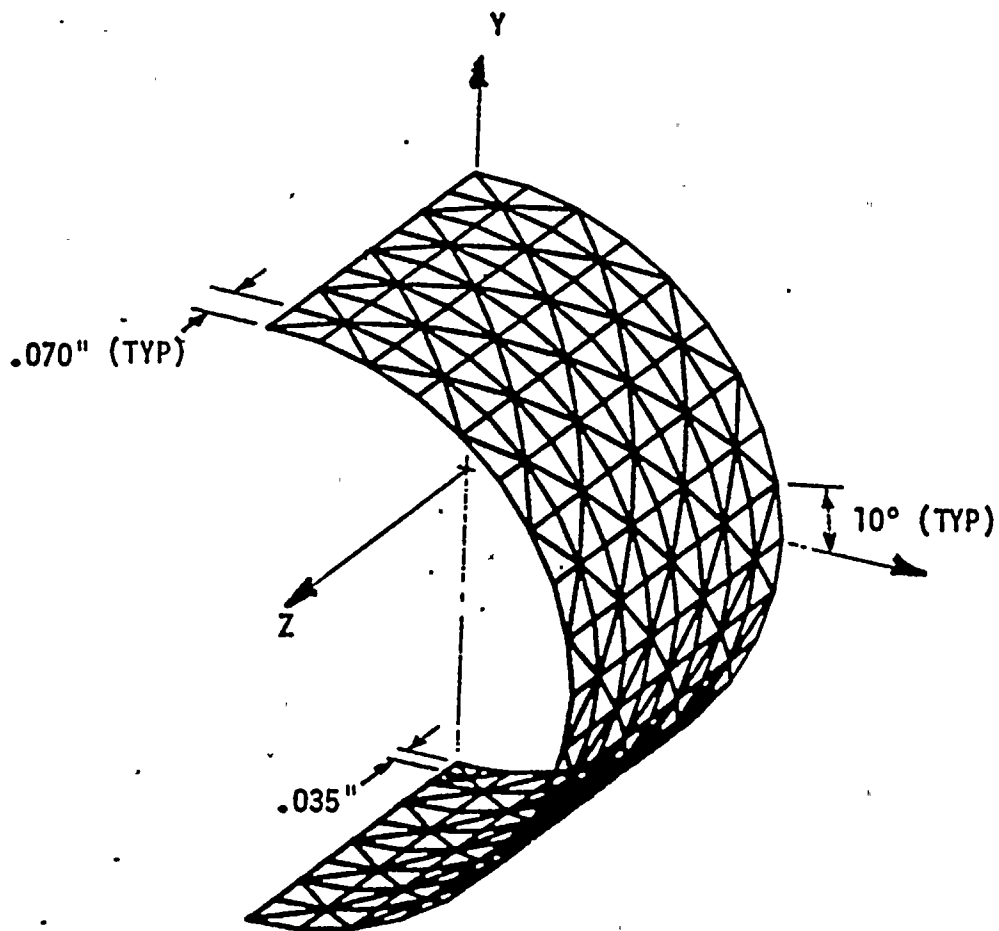
NODES 1 THRU 63: $UZ = 0$
 $NODAL ROTX = NODAL ROTY = 0$

NODES 64 THRU 126: COUPLED IN UZ
 $NODAL ROTX = NODAL ROTY = 0$

ALL ELEMENTS ANSYS STIF48

COMPUTER MODEL FOR UNIFORM PRESSURE LOADING

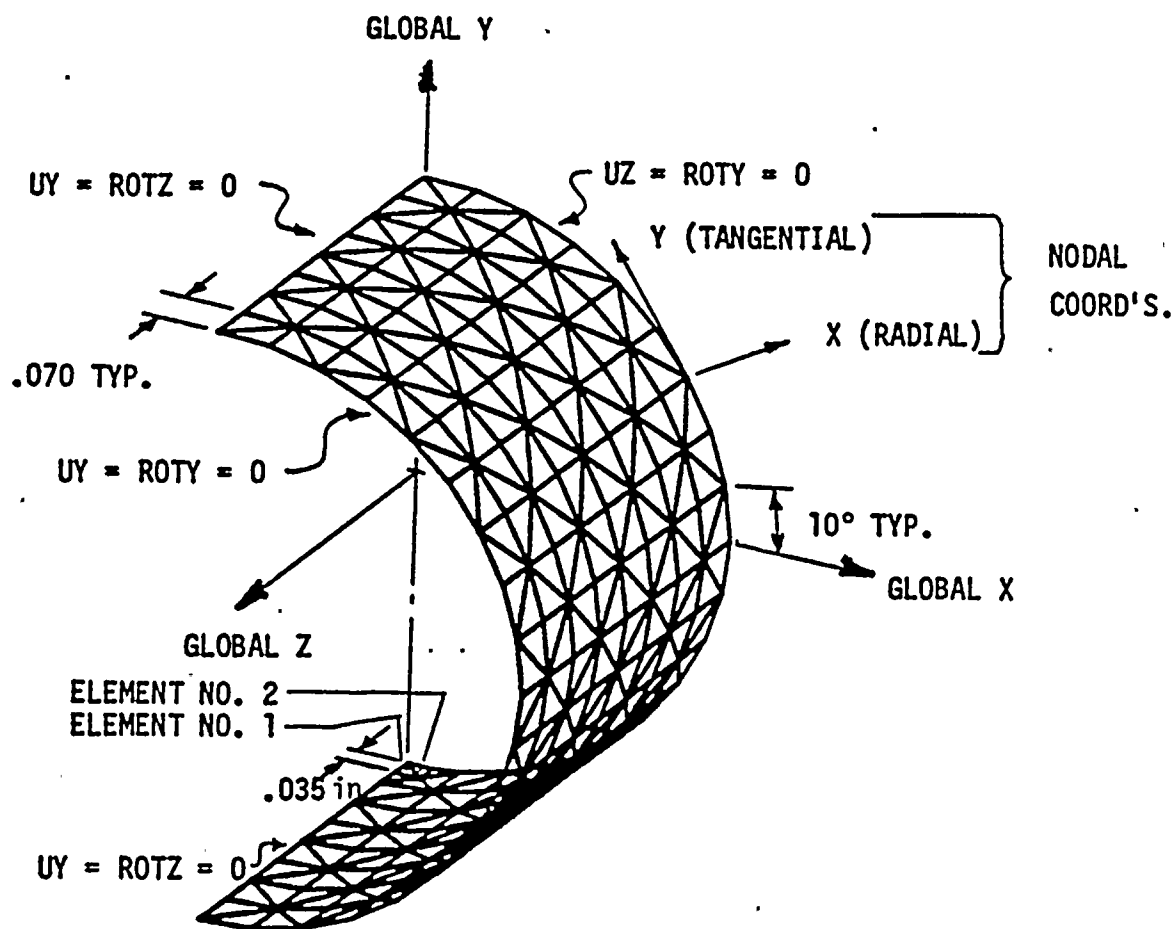
FIGURE 4.5.5-2



ALL ELEMENTS ANSYS STIF63

MODEL USED FOR CONCENTRATED LOADING

FIGURE 4.5.5-3



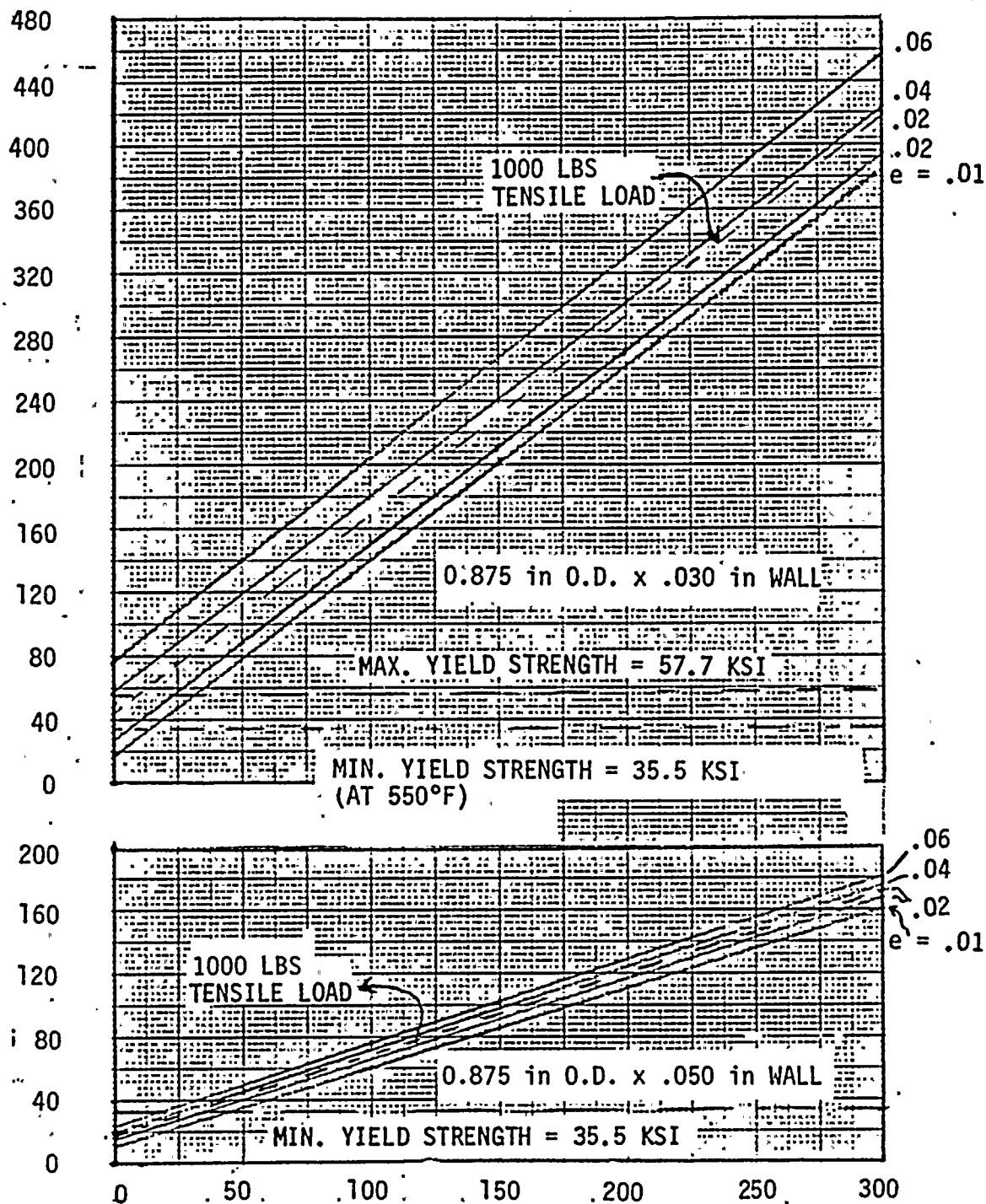
ELEMENT NO'S. 1 & 2 LOADED WITH INWARD ACTING RADIAL PRESSURE

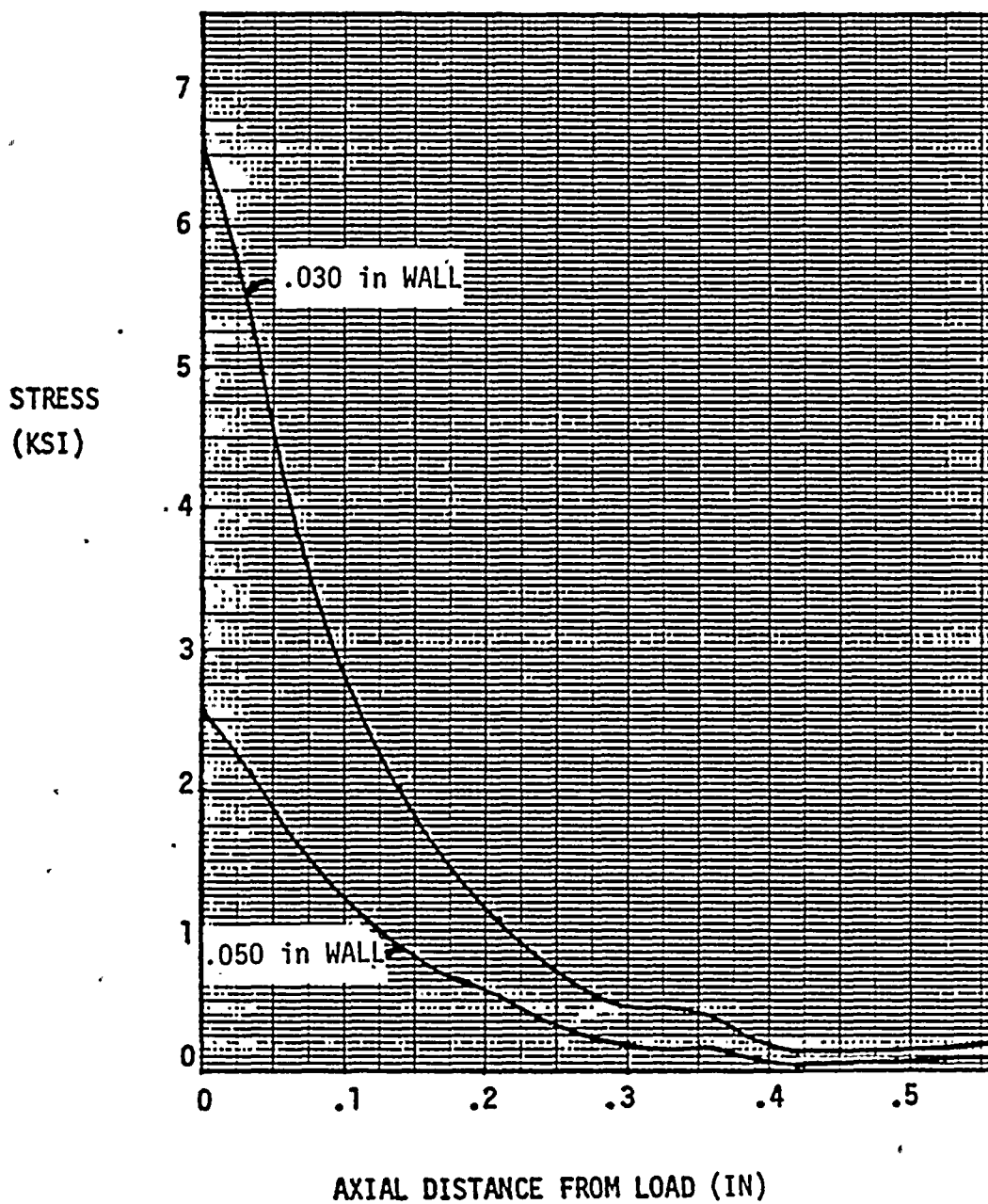
BOUNDARY DISPLACEMENTS IN NODAL COORDINATE SYSTEM

BOUNDARY CONDITIONS FOR CONCENTRATED LOAD MODEL

FIGURE 4.5.5-4

STRESS - (KSI)

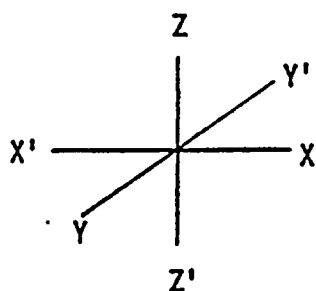




HOOP STRESS IN OUTER FIBER
DUE TO 5 POUND RADIAL LOAD

FIGURE 4.5.5-6

.875 IN O.D. .05 IN NOM. WALL
 LINEAR DIMENSIONS = IN
 VELOCITY Y = FPS



SECONDARY FLUID CROSS FLOW REGION

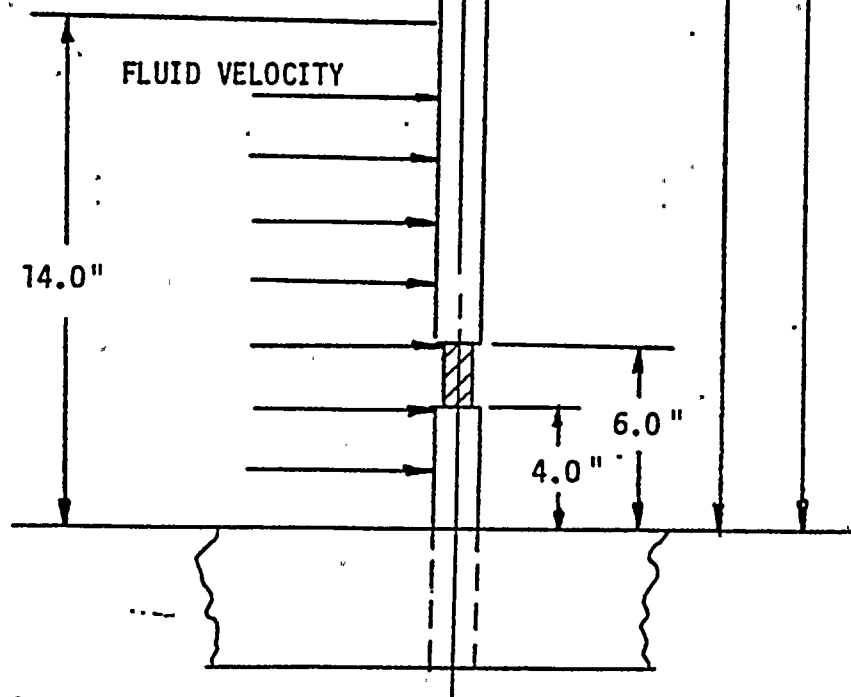


FIGURE 4.5.6-1 BASIC ANALYSIS MODEL GEOMETRY

FIXED-FIXED BOUNDARY CONDITIONS DAMPING RATIO = 0.01

<u>SYMBOL</u>	<u>CROSS SECTION</u>	<u>1ST MODE FREQ. - HZ</u>
○	CIRCULAR	58.7
□	FLAT	48.9
◇	10% OVALIZED	58.3
△	KIDNEY	58.2

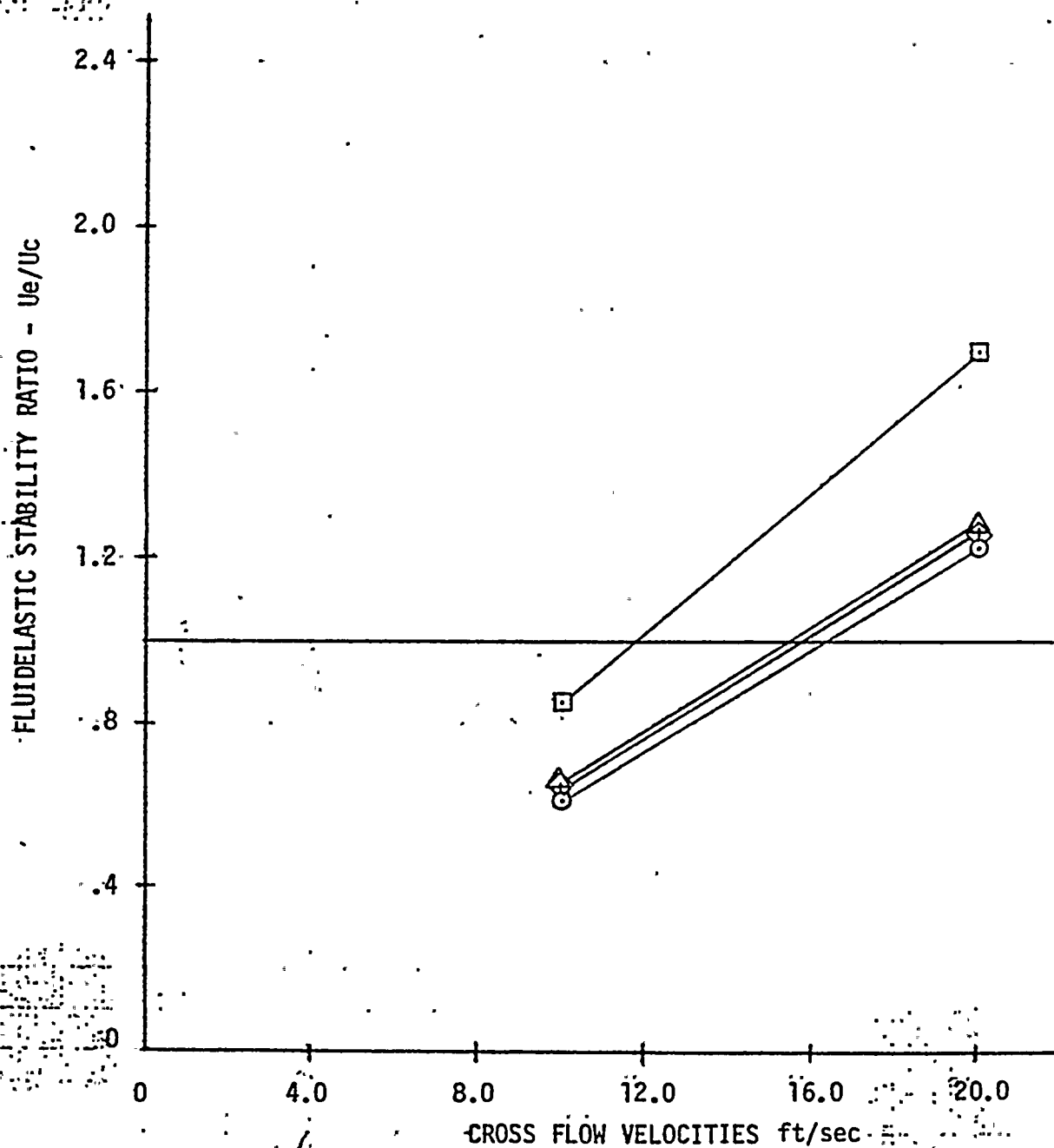


FIGURE 4.5,6-2: FLUIDELASTIC STABILITY RATIO OF TUBES AS A FUNCTION OF CROSS FLOW VELOCITY, FIXED-FIXED BOUNDARY CONDITIONS

FIXED-PINNED BOUNDARY CONDITIONS DAMPING RATIO = 0.01

<u>SYMBOL</u>	<u>CROSS SECTION</u>	<u>1ST MODE FREQ. - HZ</u>
○	CIRCULAR	40.3
□	FLAT	31.6
◇	10% OVALIZED	40.0
△	KIDNEY	39.9

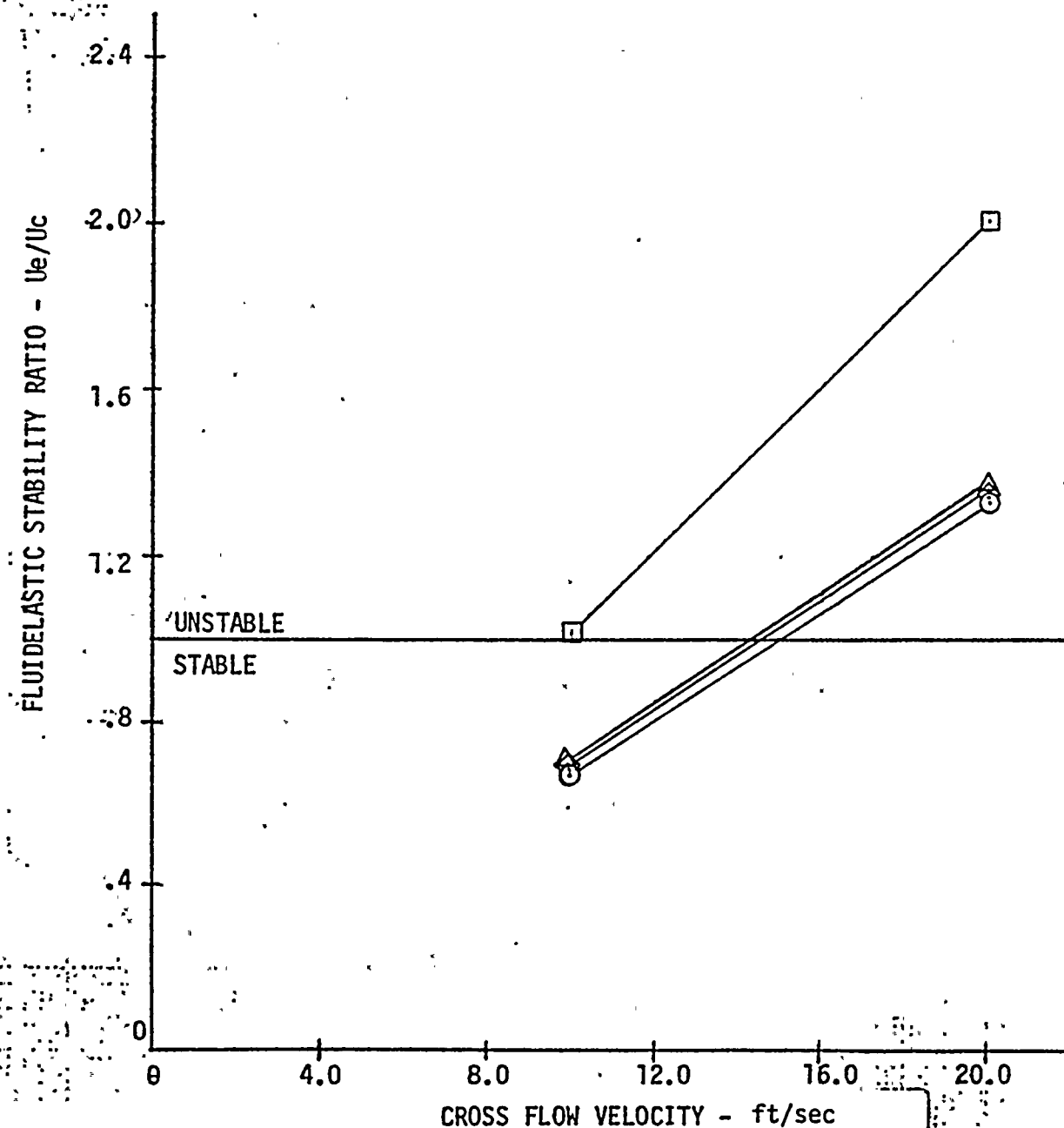


FIGURE 4.5.6-3: FLUIDELASTIC STABILITY RATIO OF TUBES AS A FUNCTION OF CROSS FLOW VELOCITY, FIXED-PINNED BOUNDARY CONDITIONS

FIXED-PINNED BOUNDARY CONDITIONS FOR FLAT CROSS SECTION

TUBE

SYMBOL



DAMPING RATIO

0.010

0.025

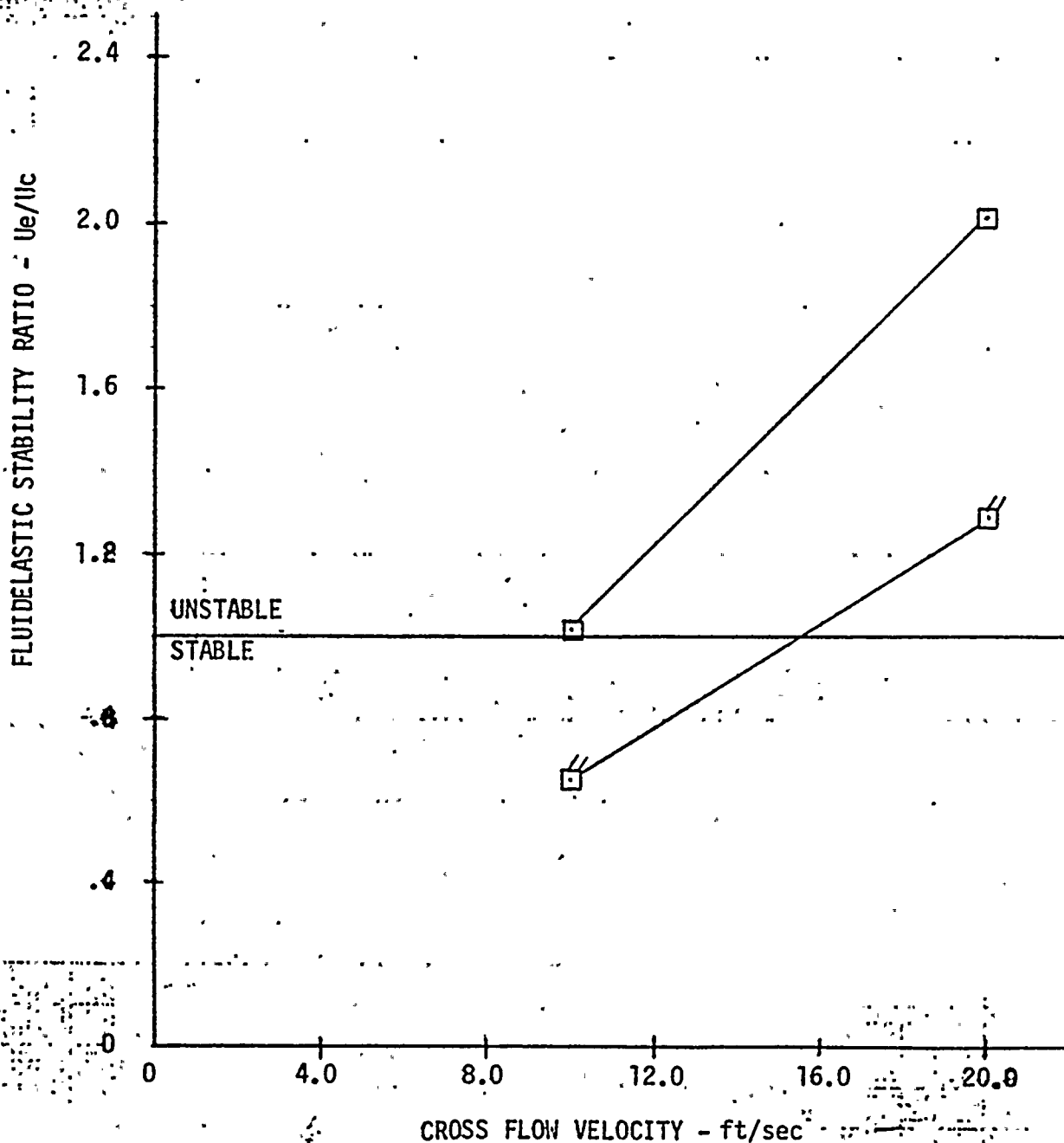


FIGURE 4.5.6-4: FLUIDELASTIC STABILITY RATIO COMPARISON FOR DAMPING RATIOS OF 0.01 AND 0.025 AS A FUNCTION OF CROSS FLOW VELOCITY, FIXED-PINNED FLAT DISTRESSED TUBE

CYLINDRICAL CROSS SECTION TUBE

SYMBOL AXIAL FORCE FIXITY

- ○ F-F
- ◇ ○ F-P
- △ 1000 lbs COMP F-P

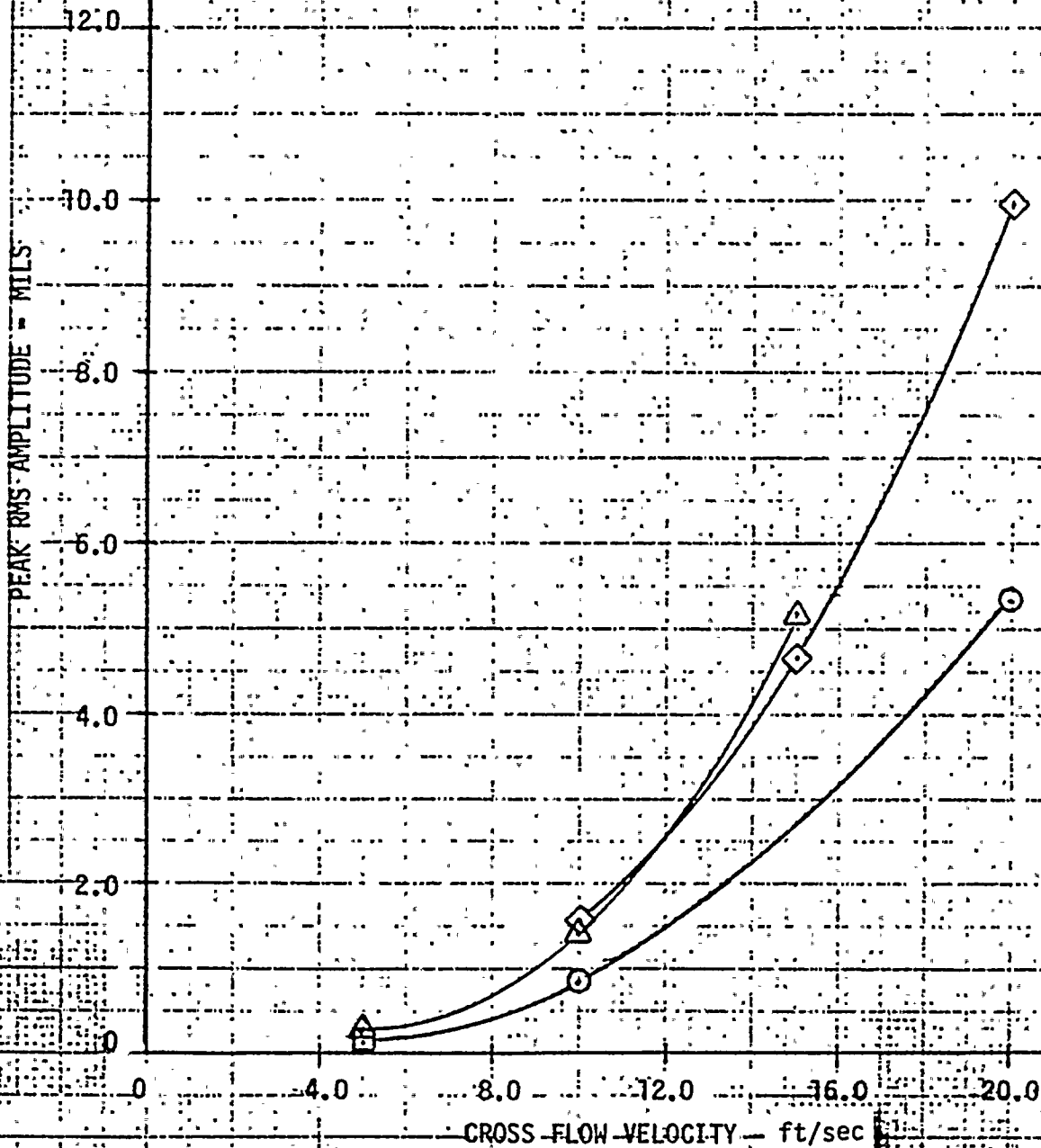


FIGURE 4.5.6-5: PEAK RMS AMPLITUDE DUE TO TURBULENCE AS A FUNCTION OF CROSS FLOW VELOCITY

FLAT CROSS SECTION TUBE

SYMBOL AXIAL FORCE FIXITY

- ○ F-F
- ◇ ○ F-P
- △ 1000 LBS COMP F-P

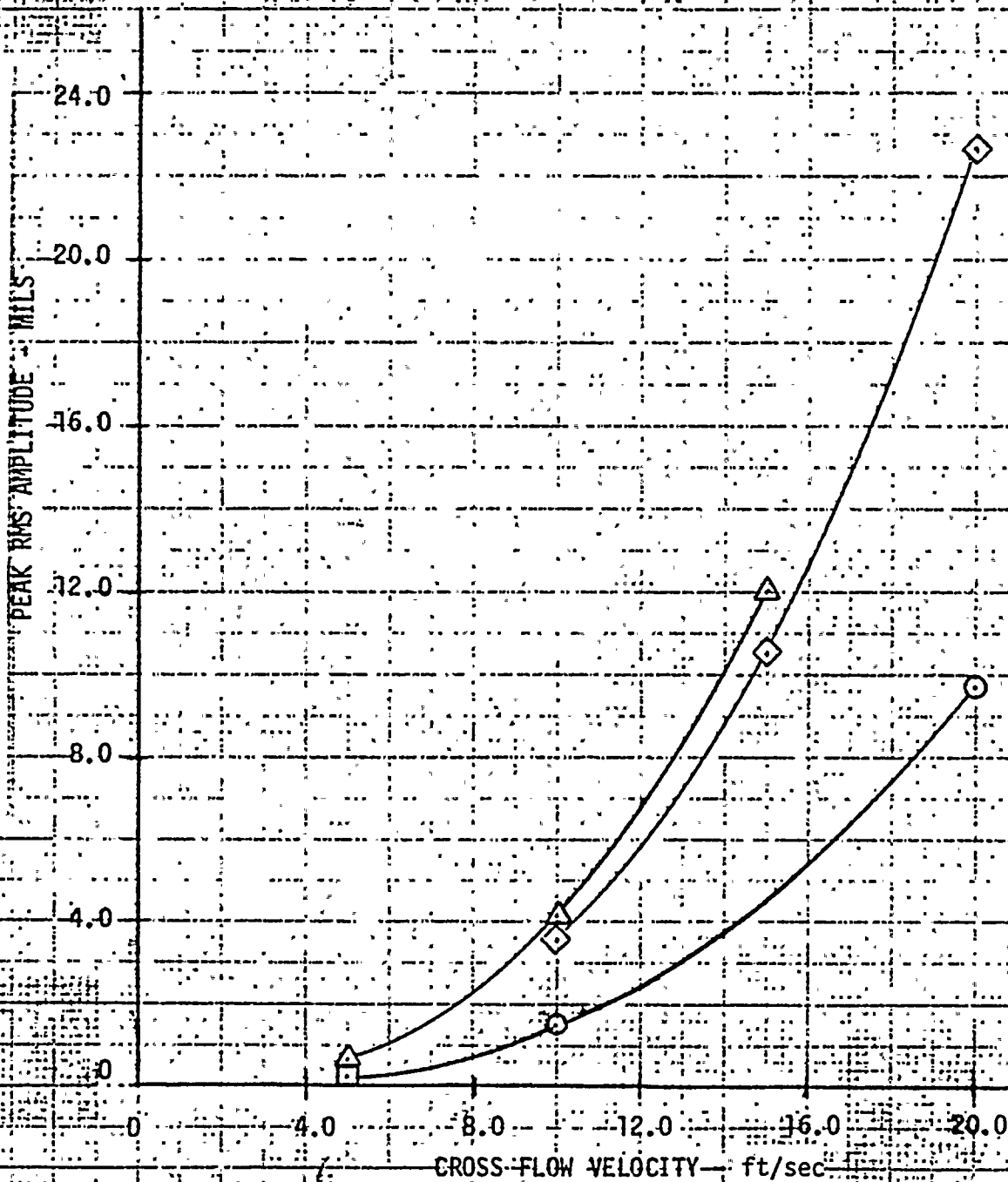


FIGURE 4.5.6-6: PEAK RMS AMPLITUDE DUE TO TURBULENCE AS A FUNCTION OF CROSS FLOW VELOCITY

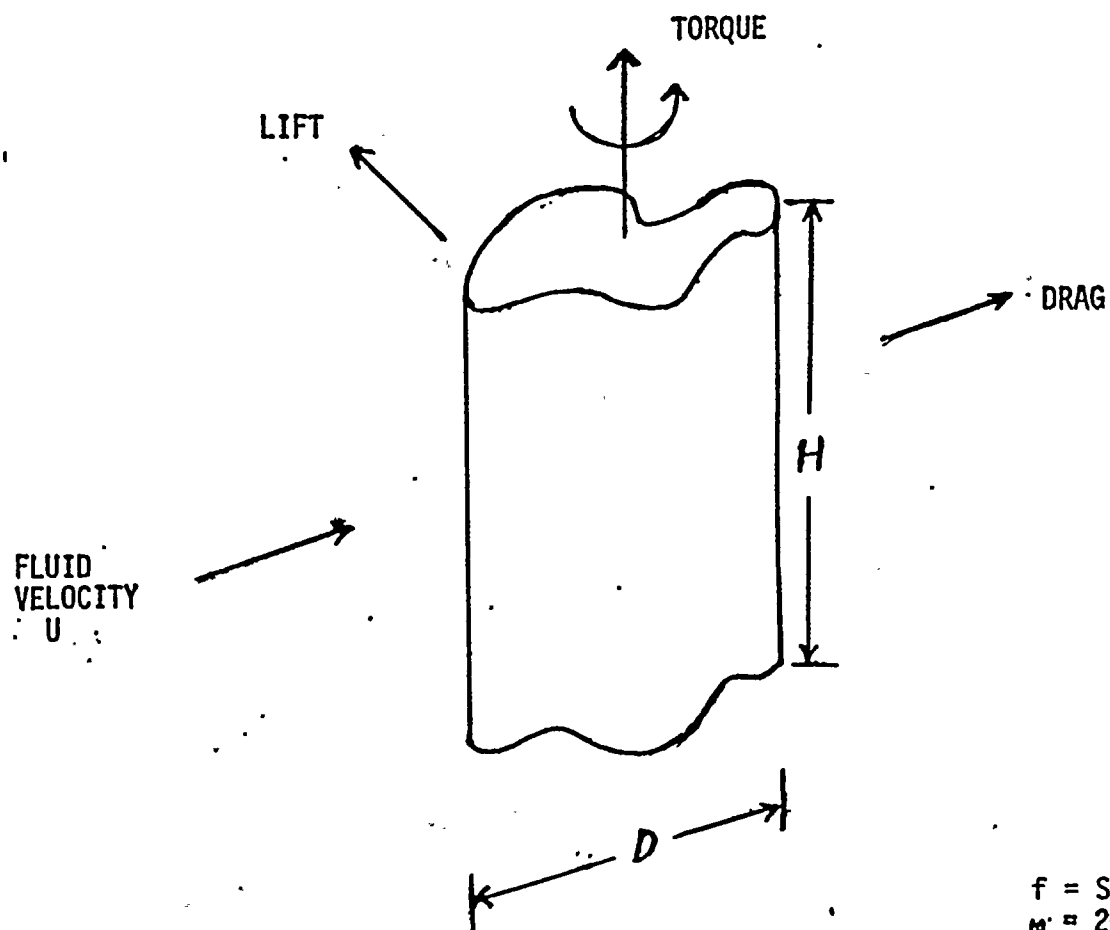


FIGURE 4.5.6-7: Kármán Model for Calculating Vortex-Shedding Loads

$$f = S U/D$$

$$\omega = 2\pi f$$

$$\text{LIFT} = C_L (\rho_f U^2/2) H D \exp(i\omega t)$$

$$\text{DRAG} = C_D (\rho_f U^2/2) H D \exp(i\omega t)$$

$$\text{TORQUE} = C_L (\rho_f U^2/2) (H D^2/8) \exp(i\omega t)$$

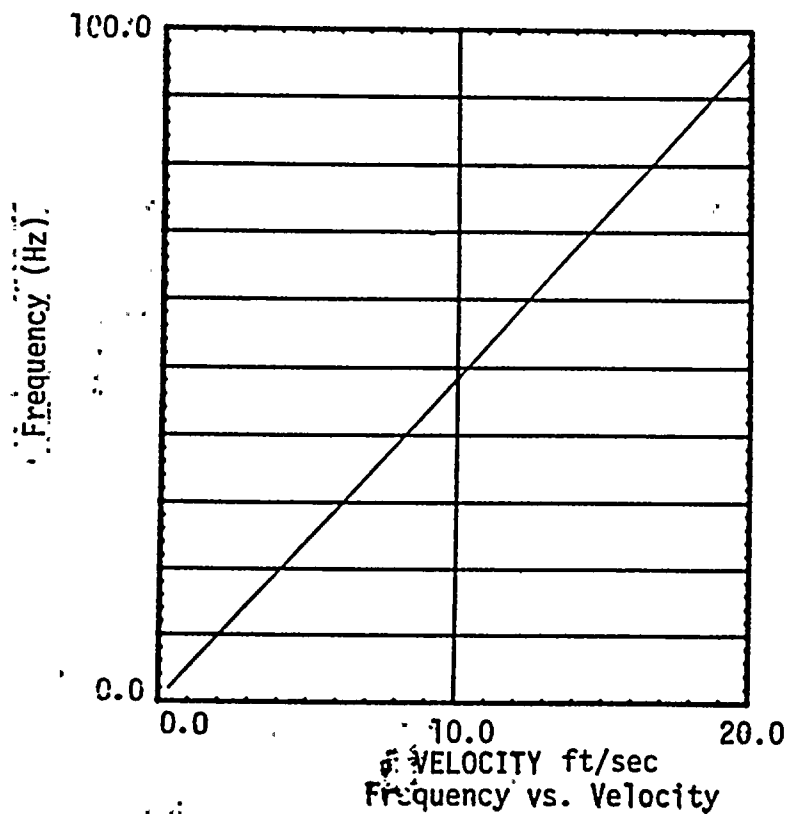
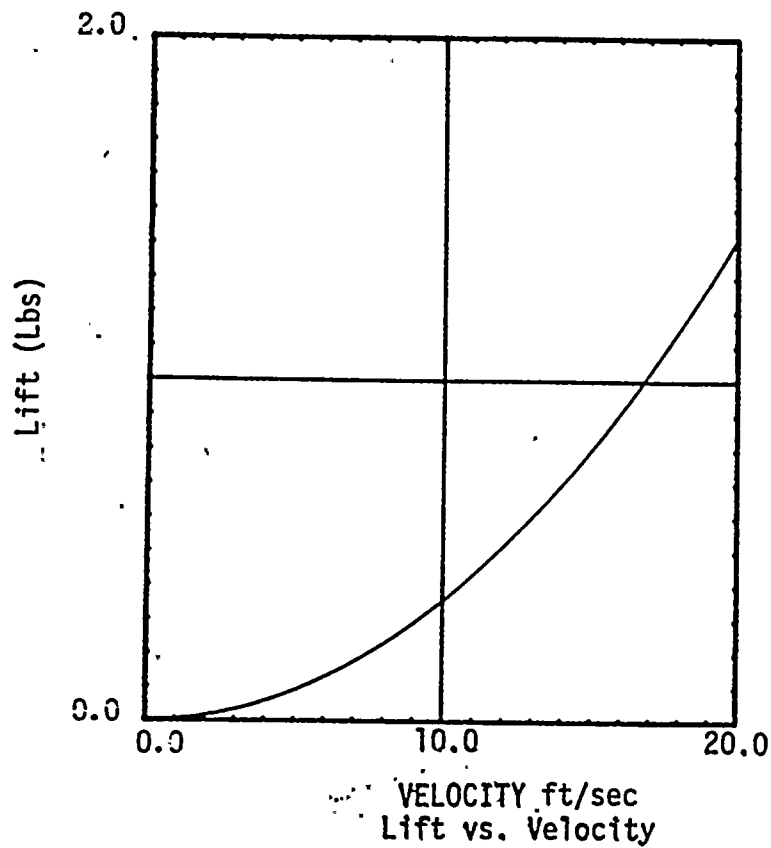


FIGURE 4.5.6-8: Alternating Lift (lbs) and Frequency (HZ) vs. Fluid Velocity for a Tear 0.5 Inch Wide by 2.5 Inches High

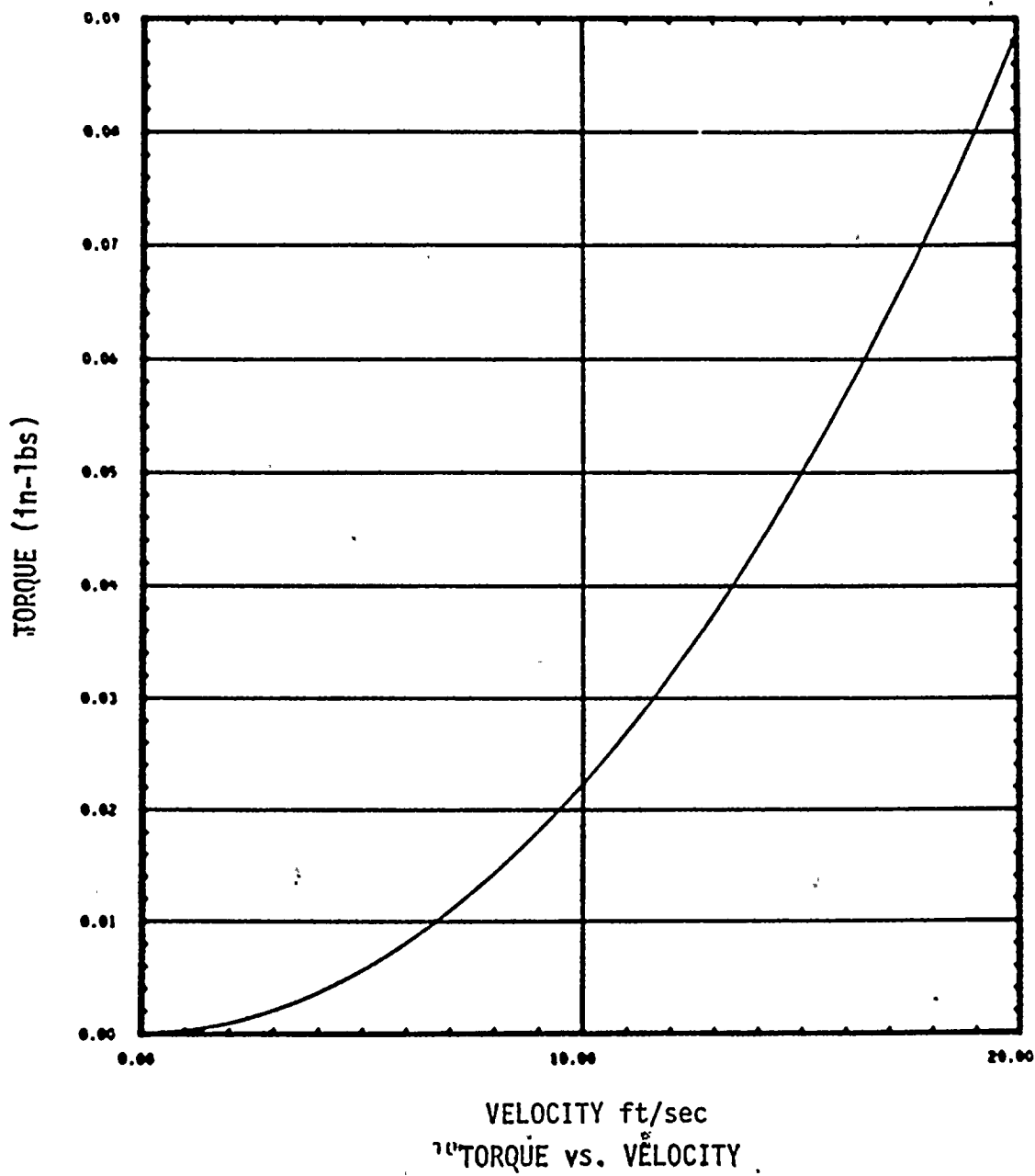


FIGURE 4.5, 6-9

Alternating Torque (in-lbs) vs. Fluid Velocity For
a Tear 0.5 Inch Wide by 2.5 Inches High

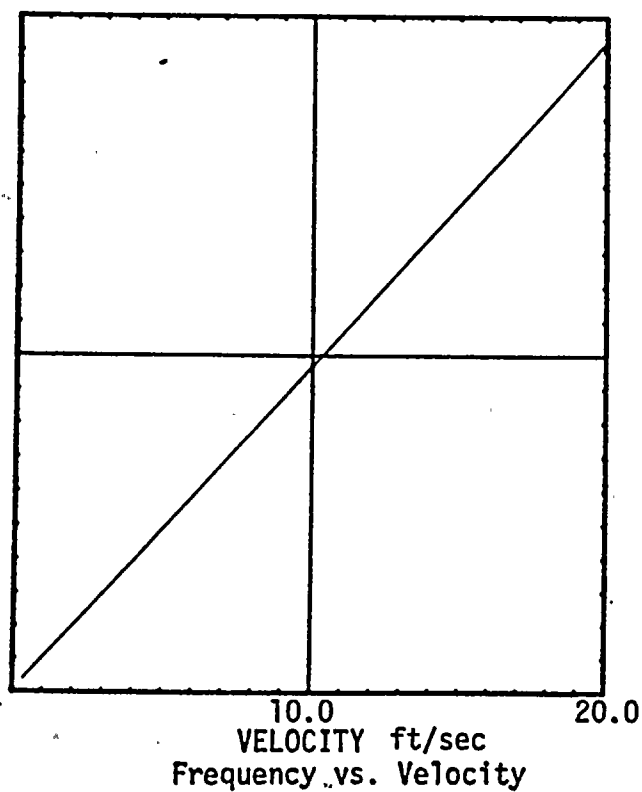
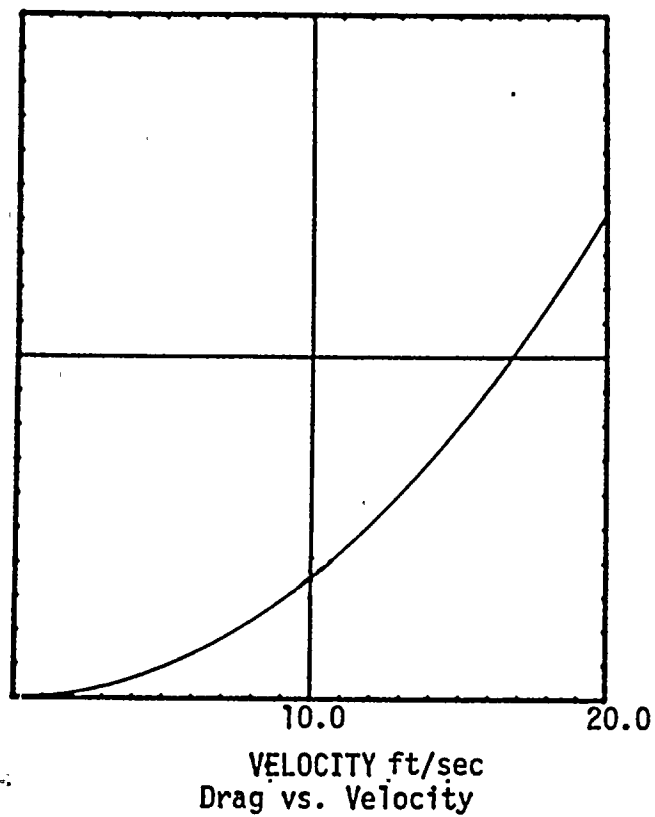


FIGURE 4.5.6-10: Alternating Drag (lbs) and Frequency (HZ) vs. Fluid Velocity for a Tear 0.5 Inch Wide By 2.5 Inches High

4.6 Model Test

4.6.1 Test Objectives

A partial full scale flow model of the downcomer and tube bundle entrance region of the Ginna steam generator Number 4 wedge region was constructed and used for testing at the Westinghouse Engineering Test Facility in Tampa, Florida. The purpose of the test was to investigate the following elements associated with the postulated failure mechanism.

- a) The nature and extent of foreign object mobility in the downcomer annulus.
- b) The magnitude of foreign object impact loads on tubes.
- c) The stability characteristics of degraded tubes near the tube bundle entrance region when subjected to various flow conditions.
- d) The nature and extent of tube-to-tube interaction once a tube becomes severed near the top of the tube sheet.

4.6.2 Test Apparatus

The tube bundle at the flow inlet region of the Ginna steam generator was represented using forty-eight (48) tubes (.875 inch O.D.) extending from the tube sheet to the first tube support plate. The flow model is illustrated in Figures 4.6.2-1 through 4.6.2-4. The orientation of the test model with respect to the overall steam generator geometry is shown in Figures 4.6.2-5 and 4.6.2-6.

The tests were run at ambient pressure and temperature using the cold flow loop illustrated in Figure 4.6.2-7. Water flow to the test model was controlled by a flow measuring venturi. The maximum downcomer velocity was 14 ft/sec during flow testing.

The flow field between the tube sheet and the first support plate consists of approximately 75 percent cross flow and 25 percent parallel flow for the region modeled. Therefore, the perforated rear boundary plate (Figure 4.6.2-3) contains three times the flow area as the first tube support plate.

A ENDEVCO Model M42A Biaxial Piezoelectric Accelerometer was placed inside selected tubes (R44 C58 and R45 C54) to sense tube motions resulting from impact forces and fluid flow. Refer to Figure 4.6.2-8 for accelerometer orientation details. The accelerometer was located in the tube midway between the simulated support plate and tube sheet and was connected, through a low noise cable and pre-amplifier to Unholtz-Dickie Model 1112H charge amplifiers/signal conditioners. Output from these conditioners was recorded on a Tektronix Series 5000, 8 channel, storage oscilloscope with a Polaroid camera attachment. Displayed data were in units of "g's" per division.

PCB Pieotronics impact force transducers were also mounted on perpendicular axes in the tube support plate for selected tubes in the test vessel (R44 C58 and R45 C54). Refer to Figures 4.6.2-9 and 4.6.2-10 for orientation details.

These sensors provided an output of 50 millivolts per pound force. Data acquisition was by the Tektronix oscilloscope with the Polaroid attachment. Displayed data were in units of pounds force per division.

During calibration testing, an instrumented impact hammer was used to generate tube accelerometer and force transducer time histories. The signatures derived from these known impact forces were compared with signals obtained as a result of the foreign object impacting with an instrumented tube during flow testing.

4.6.3 Test Procedure and Results

A foreign object, with similar dimensions to the largest object removed from the Ginna B-Steam Generator, was positioned in the downcomer annulus of the test model. The object is illustrated in Figure 4.6.3-1. The orientation and position of the object within the wrapper annulus region was varied to determine its relative stability and susceptibility to flow induced vibration. At each position, the object motion was observed through windows in the side of the test vessel and accelerometer and force transducer time histories were obtained.

4.6.3.1 Object Mobility

Object motion was random in nature and occurred for virtually all orientations and positions. The object demonstrated the ability to assume various positions within the downcomer annulus as well as the ability to provide a relatively uniform cyclic loading on the tubes.

4.6.3.2 Impact Magnitude

Foreign object impact forces were estimated by comparing accelerometer time histories recorded during flow testing with those obtained by striking the same tube with an instrumented impact hammer. Typical accelerometer and force transducer time histories recorded from foreign object impact during flow testing are shown in Figures 4.6.3-2 and 4.6.3-3. Acceleration and force envelopes are shown in Figure 4.6.3-4. The maximum recorded tube acceleration was approximately 200 g and the maximum force transducer response was 30 lb. It should be noted that the force transducer load will only be a small fraction of the impact load since the major portion of the impact load will be reacted at the tube sheet end of the tube and only a minor part of the impact load will be reacted at the support plate end where the force transducer is located.

Typical accelerometer and force transducer signals recorded from impact with the instrumented metal hammer are given in Figures 4.6.3-5 and 4.6.3-6. Reasonable agreement with tube response signatures from foreign object impact during flow testing can be observed by comparing Figures 4.6.3-5 and 4.6.3-6 with 4.6.3-2 and 4.6.3-3. Data relating

hammer force, tube acceleration and force transducer response are plotted in Figures 4.6.3-7 and 4.6.3-8. Based on accelerometer calibration data, maximum foreign object impact forces measured during flow testing ranged between 120-180 lbs. Using the force transducer calibration data, maximum measured impact forces ranged between 200-350 lbs. The duration of the impact force was short, approximately one millisecond.

In order to investigate tube degradation from the foreign object during flow testing, an extended flow test was performed in which the object was allowed to remain in the test vessel for eight (8) hours, while the downcomer flow was maintained at 14 ft/sec. Visual examination of the tubes indicated degradation at several locations, with the most significant degradation occurring on the R45 C54 tube. A photograph of the resulting degradation is provided in Figure 4.6.3-9.

4.6.3.3 Stability Characteristics

Tubes with locally degraded, structurally degraded, and/or severed cross-sections could experience flow induced vibrations leading to fatigue failure. In order to investigate the flow induced vibration characteristic of degraded tubes, the tube in R44 C58 was locally degraded by progressively machining away the cross-section at the location of maximum foreign object scars approximately four inches above the tube sheet face.

Tubes with undegraded and locally degraded cross-sections were stable with respect to flow induced vibration during all flow testing. Figure 4.6.3-10 illustrates the tube in R44 C58 with only 40 percent of the circumference remaining. Accelerometer response envelopes are illustrated in Figure 4.6.3-11 for 40 percent remaining circumference and 10 percent remaining circumference at 14 ft/sec downcomer flow without a foreign object being present. Tube accelerations were higher with only 10 percent of the circumference remaining, which is indicative of higher tube vibration amplitudes as expected. Accelerations became more erratic when the foreign object was introduced in the vicinity of the tube with only 10 percent of the circumference remaining, as shown in Figure 4.6.3-12.

4.6.3.4 Tube-to-Tube Interaction

Severed tubes could degrade adjacent tubes through tube-to-tube impact and/or sliding which results in wear. To investigate the behavior of severed tubes at the periphery of the tube bundle, the tube located in R44 C58 was severed at the location of maximum foreign object impact scars, approximately four inches above the tube sheet surface. The resulting accelerometer response curves for an accelerometer located within the severed tube, Figure 4.6.3-13, indicated intermittent impacts with adjacent tubes. The severed tube did tend to nestle between the R43 C57 and R43 C58 tubes. The observed amplitude of tube motion in this position was small, less than one-tenth of an inch.

4.6.4 Conclusions

The following overall conclusions were drawn from the flow model testing, and support the proposed mechanism:

- a) Foreign object movement in the downcomer annulus was random in nature. The foreign object demonstrated the ability to assume a variety of positions in the annulus region.
- b) Based on accelerometer readings, foreign object impact forces between 120-180 lbs are possible. Using force transducer data, impact forces between 200-350 lbs are possible.
- c) Tubes with undegraded and locally degraded cross-section were stable with respect to flow induced vibration during all flow testing.
- d) The tubing accelerometer response envelope increased in magnitude as the tubing cross-section was progressively degraded by machining it away.
- e) Tube acceleration increases for a degraded tube were more erratic when the foreign object was permitted to interact with the tube.
- f) A tube severed near the tube sheet interacted intermittently with adjacent tubes. The severed tube tended to nestle between neighboring tubes and in such a position the tube motion was small, less than one-tenth of an inch.

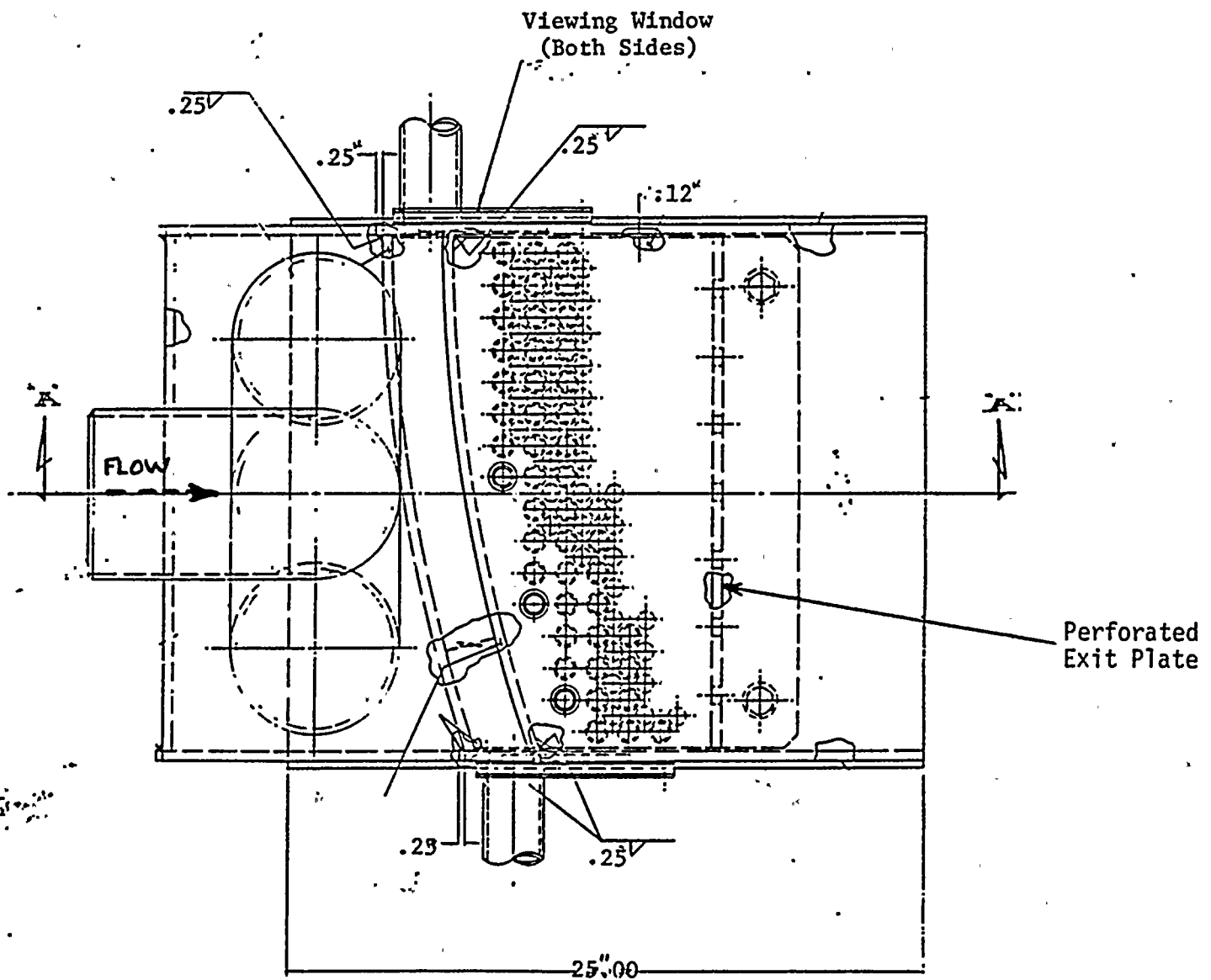
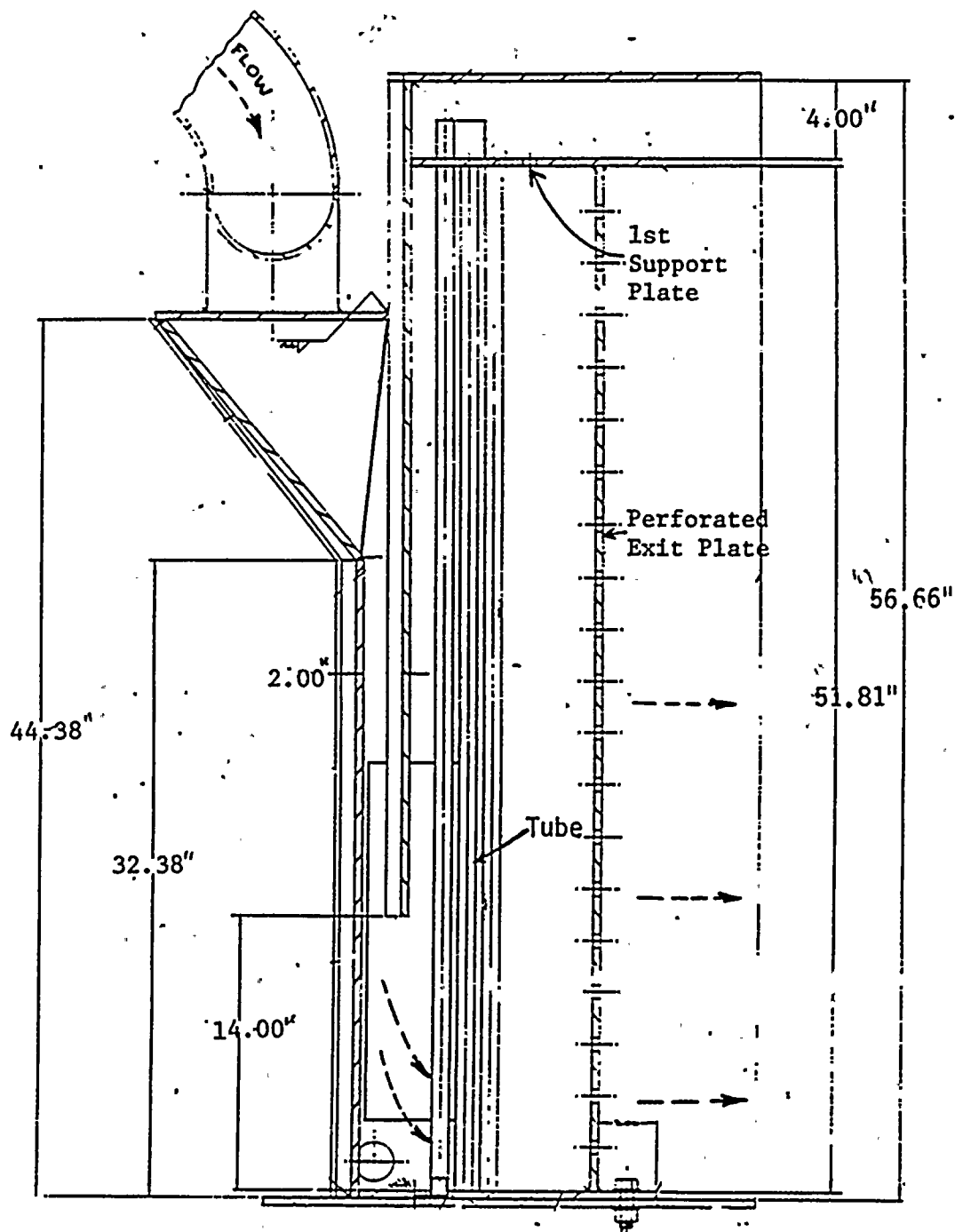


Figure 4.6.2-1. Plan View of Flow Test Model



SECTION A-A

Figure 4.6.2-2 Section View of Flow Test Model

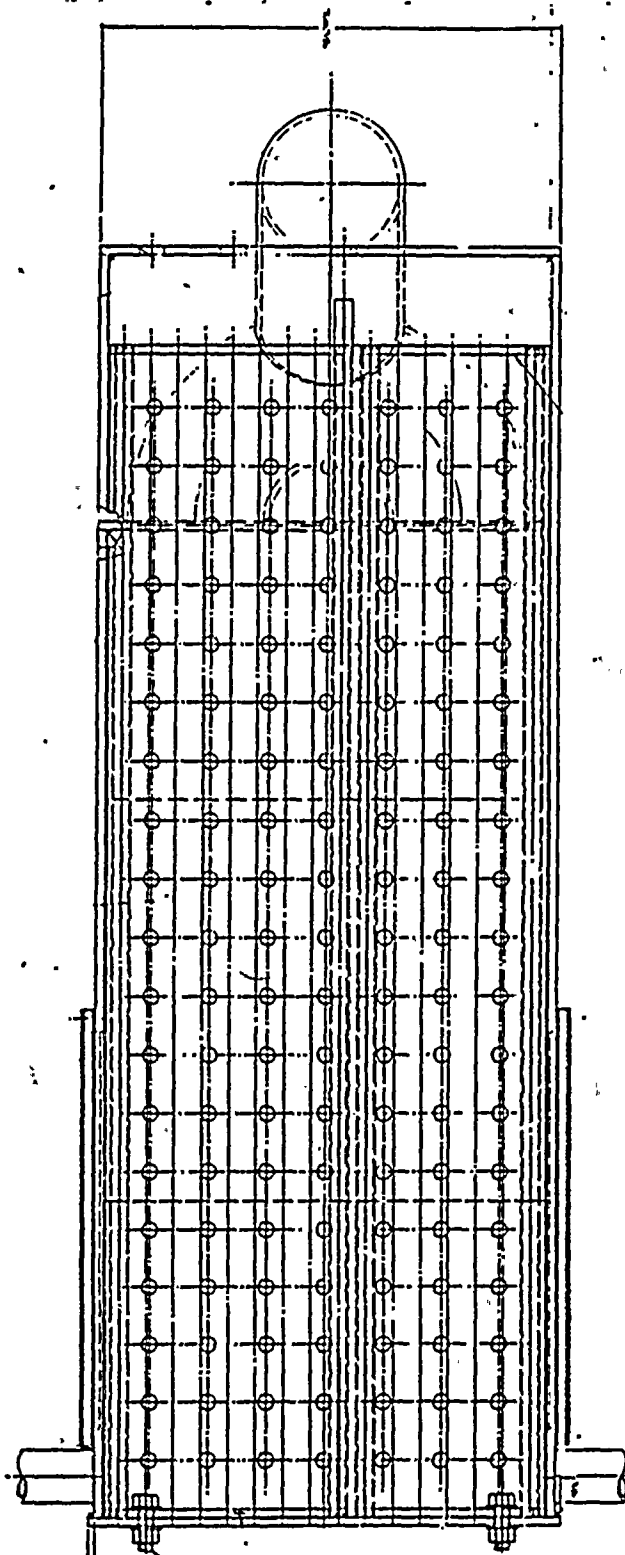


Figure 4.6.2-3 Rear Elevation View of Flow Test Model Showing Perforated Exit Plate.

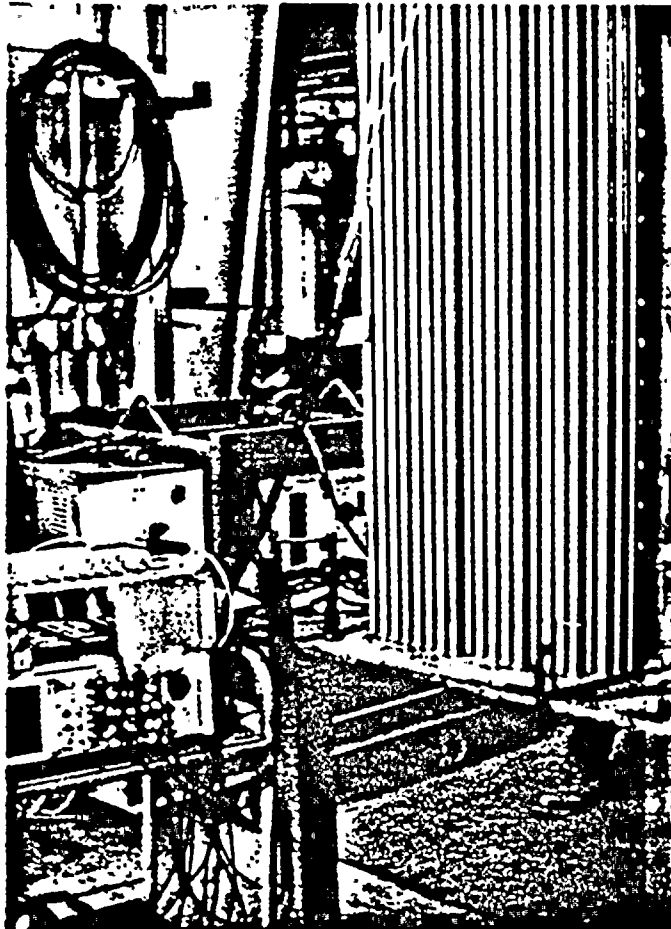


Figure 4.6.2-4 Photograph of Tube Bundle Used in Flow Test Model

REGION OF TEST SIMULATION

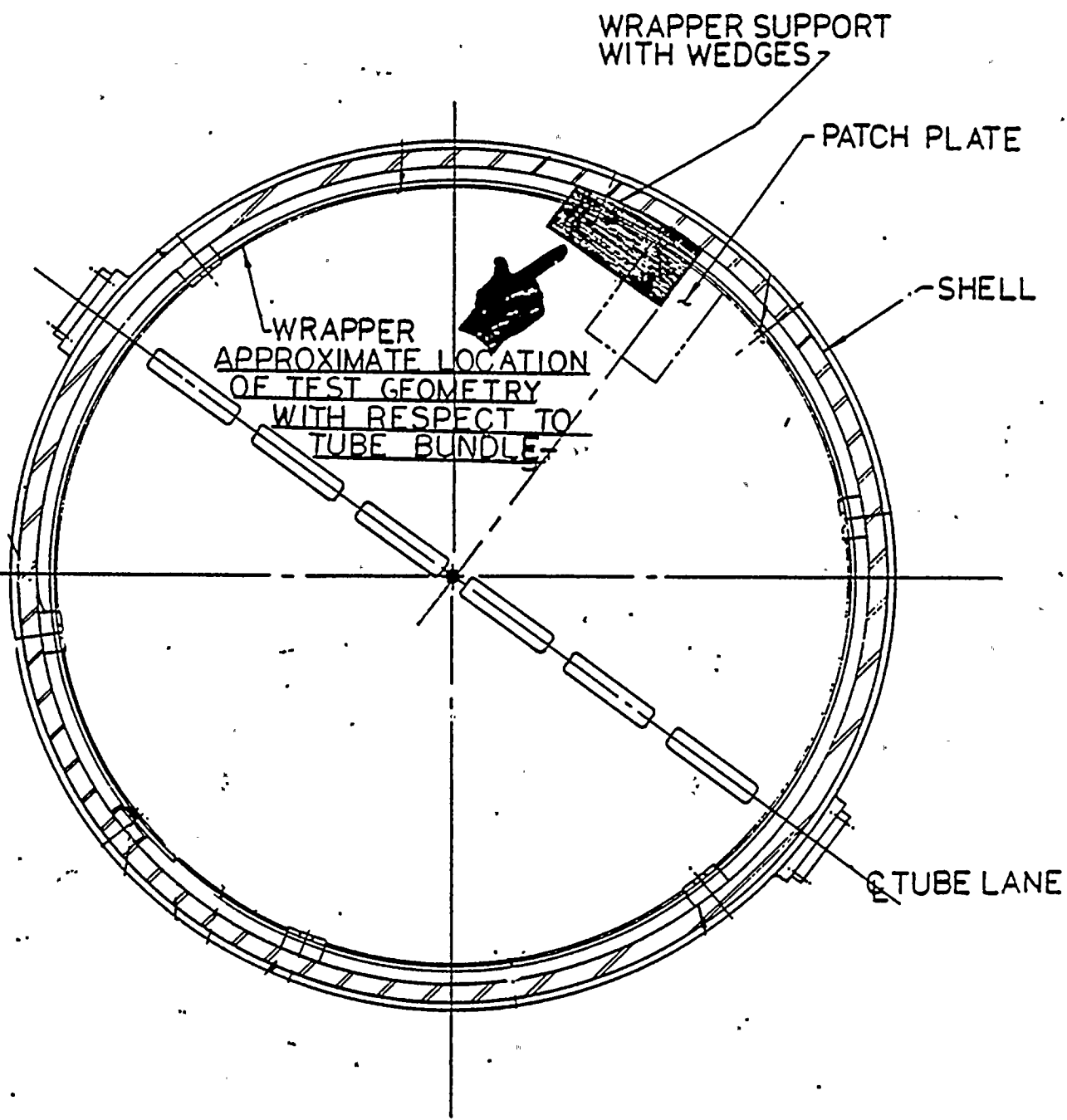
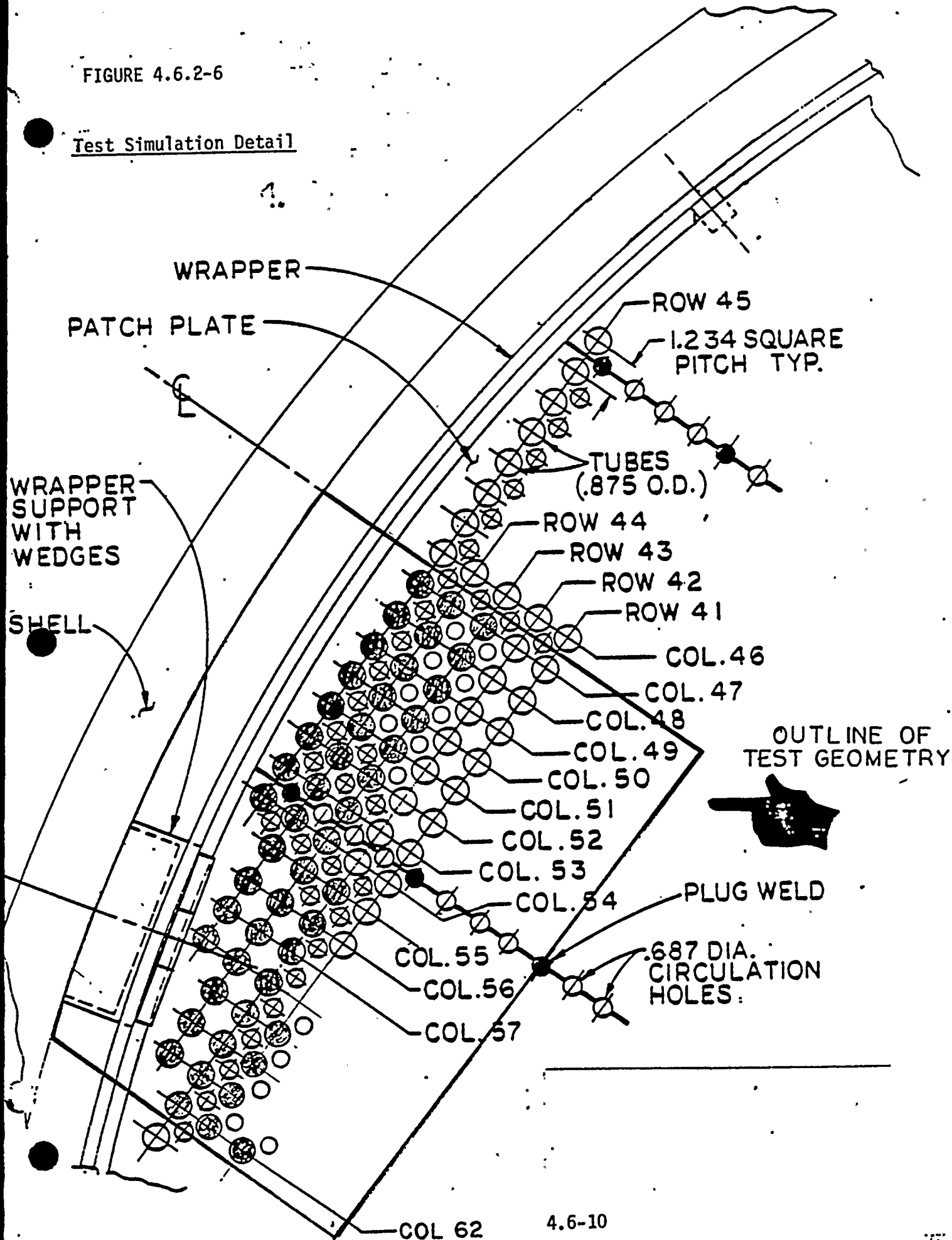


Figure 4.6.2-5

FIGURE 4.6.2-6

Test Simulation Detail



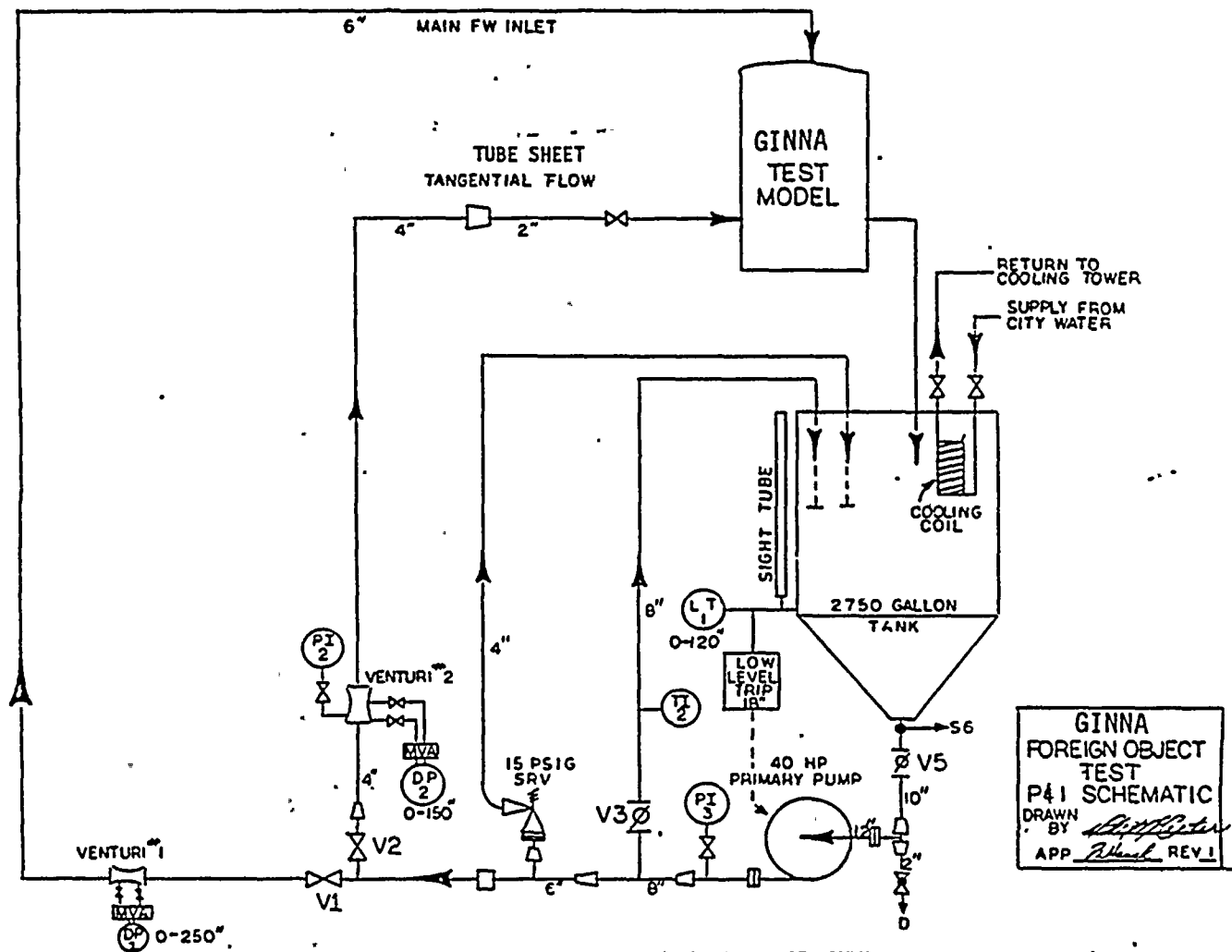


Figure -4.6.2-7 Cold Flow Loop

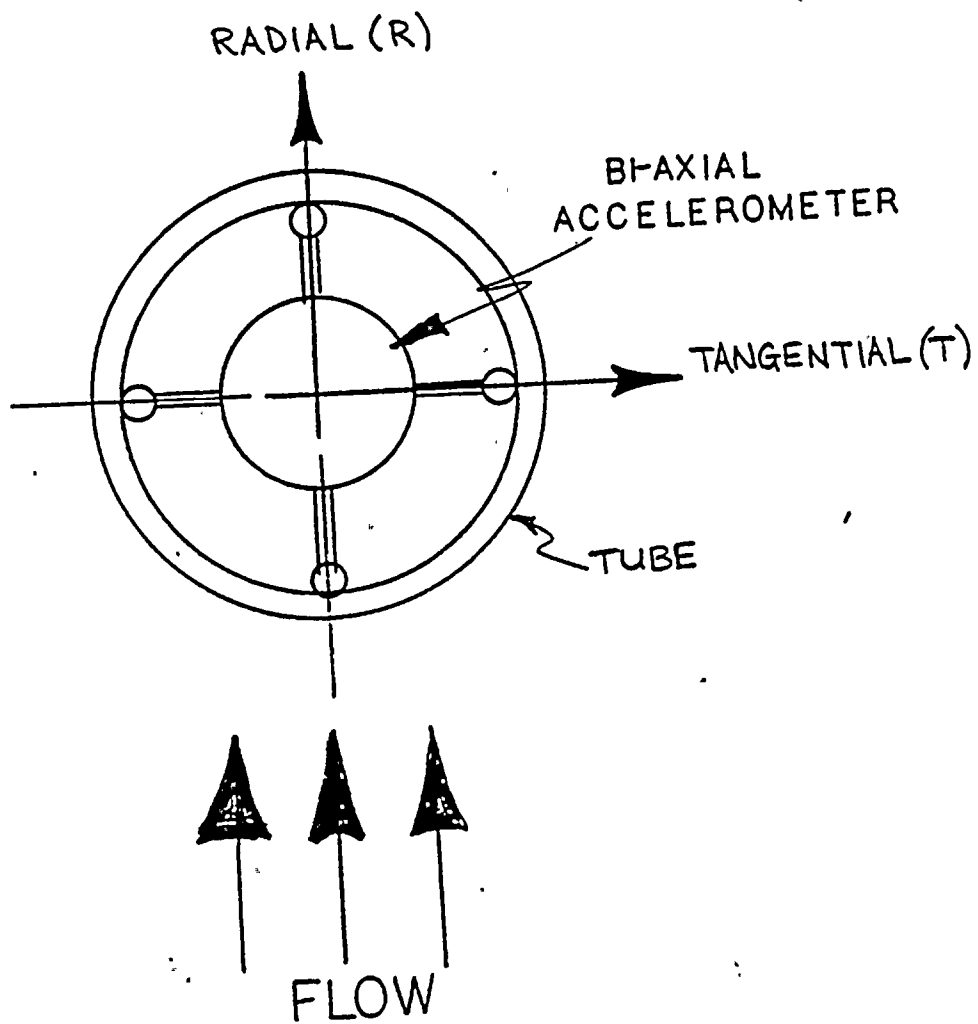


Figure 4.6.2-8 Bi-axial Accelerometer Orientation

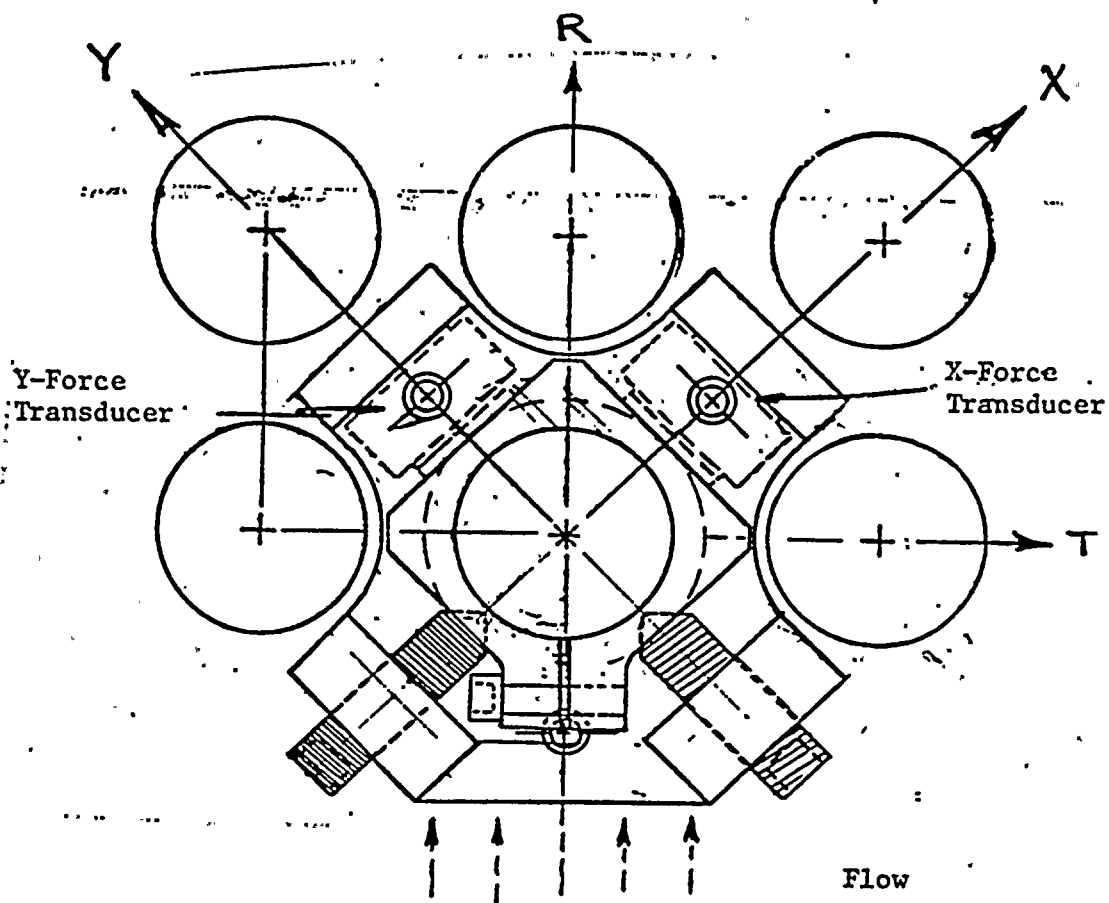
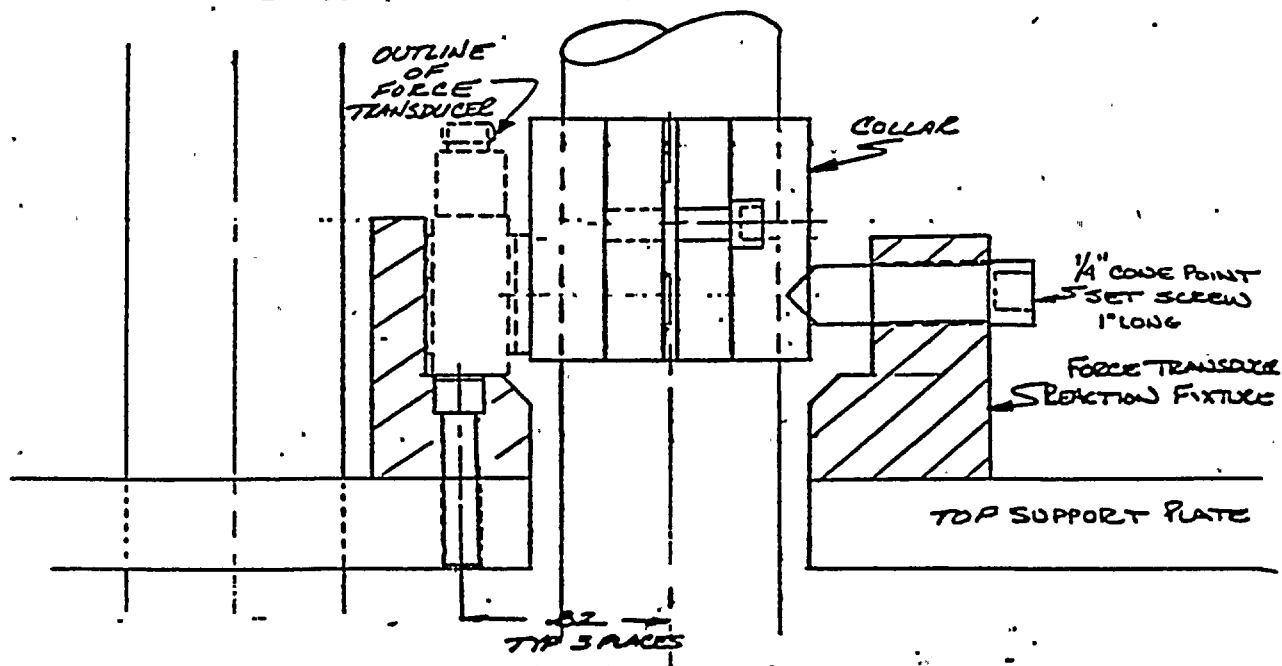


Figure 4.6.2-9 Force Transducer Orientation and Installation Assembly

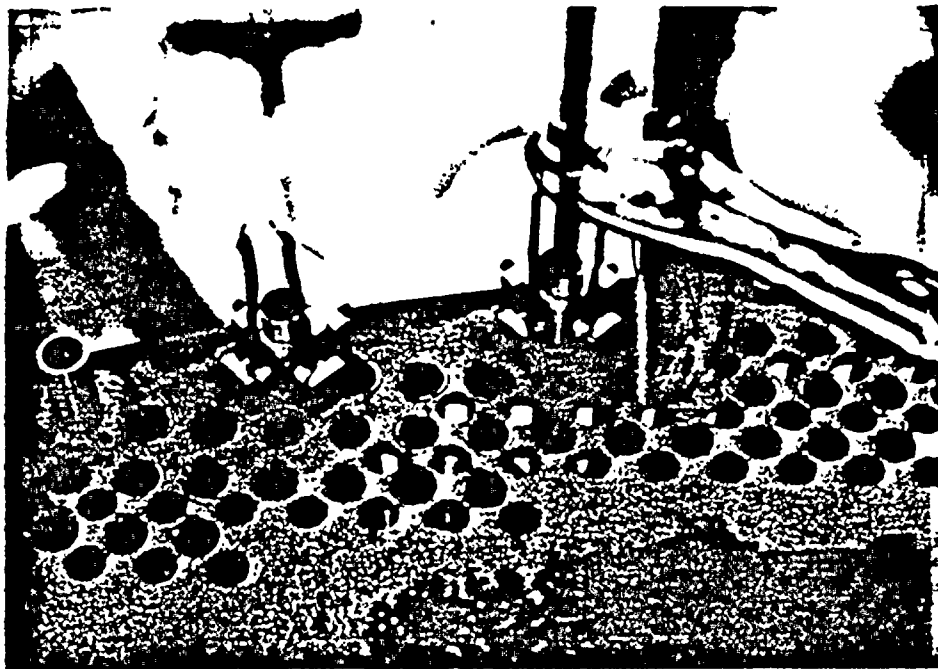


Figure 4.6.2-10 Force Transducers Mounted in Tube Support Plate

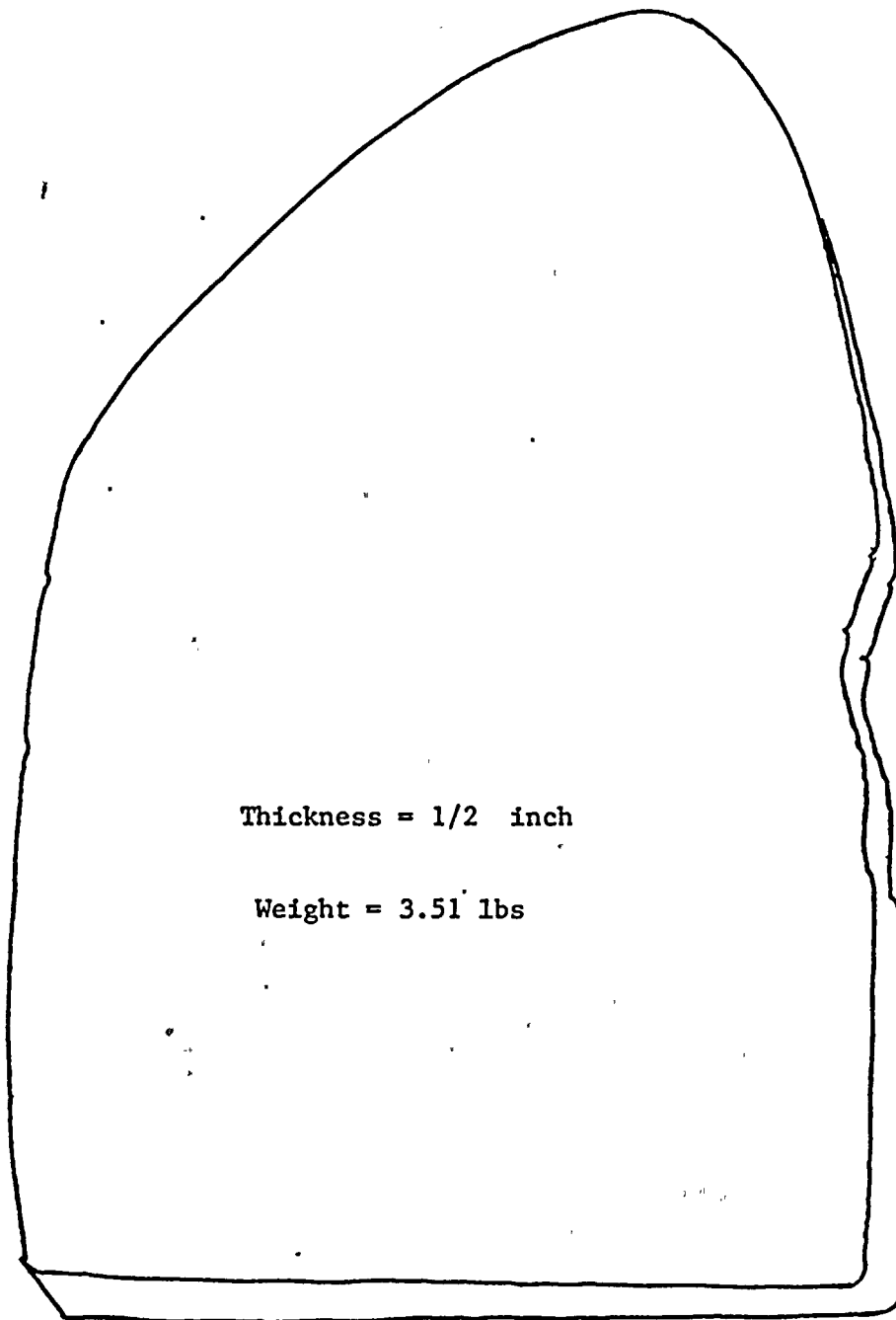
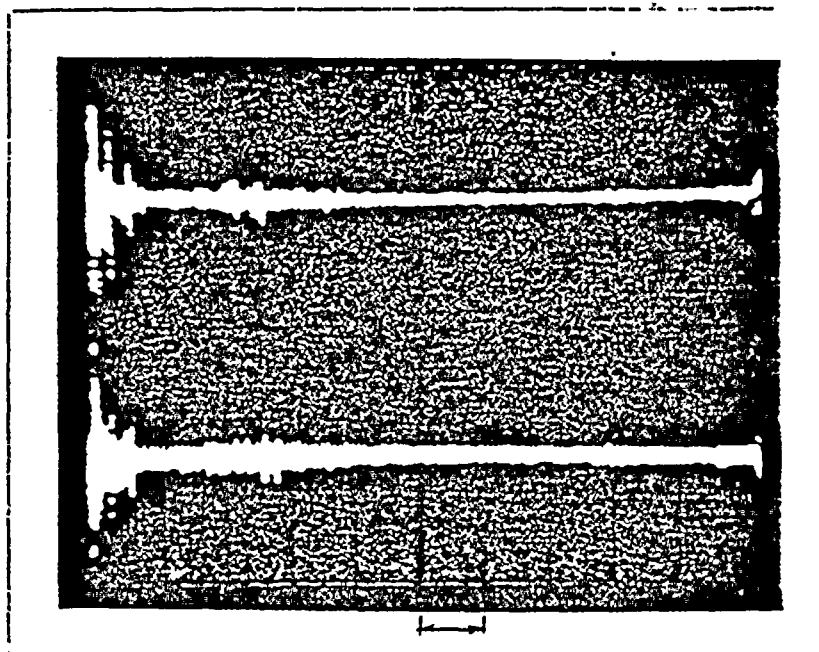


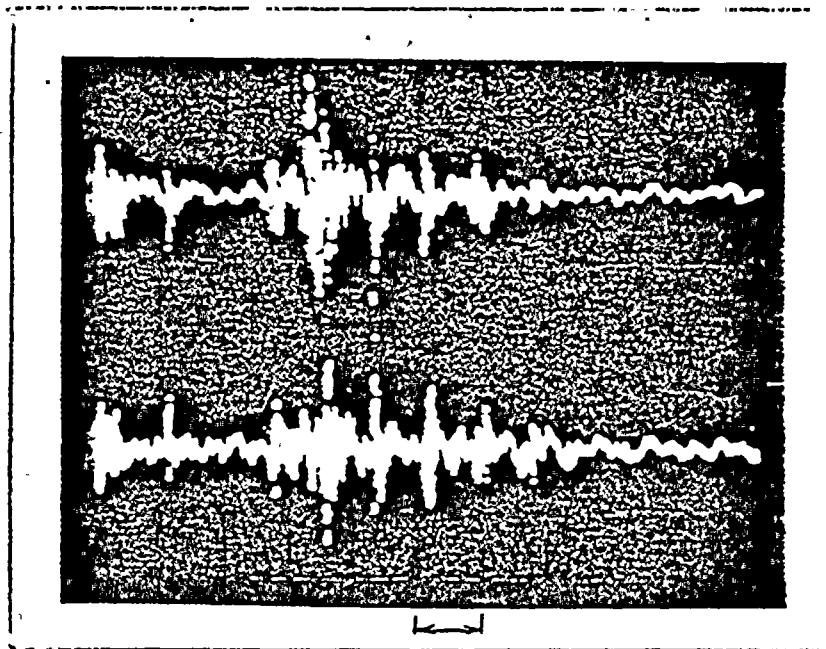
Figure 4.6.3-1 Foreign Object (Full Scale)



R Acceleration
(100 g/div)

T Acceleration

50 MSec/Div

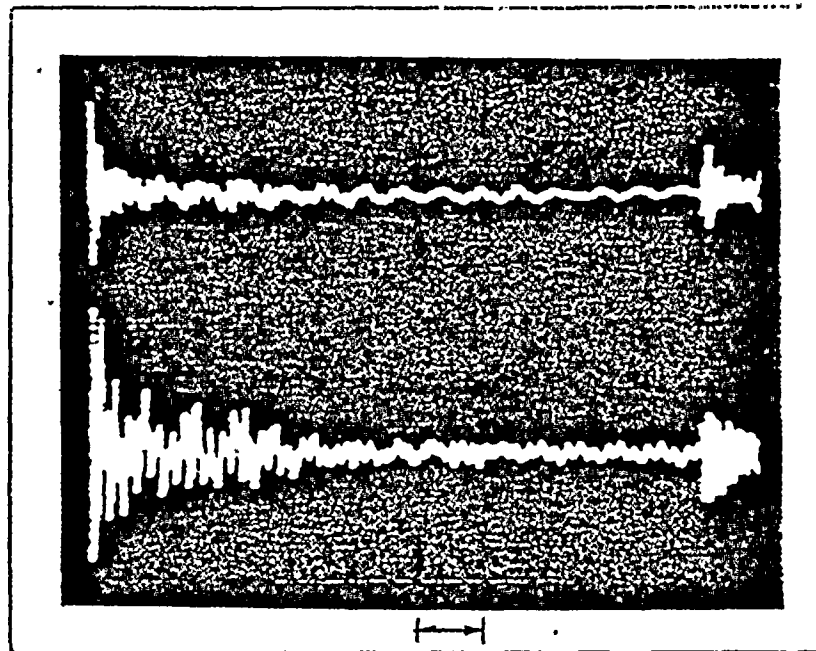


R Acceleration
(100 g/div)

T Acceleration

5 MSec/Div

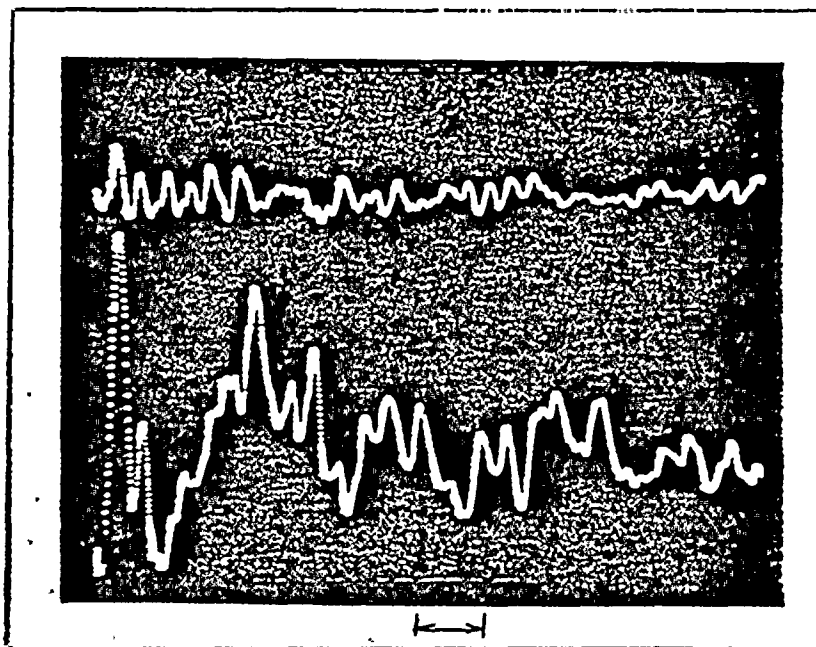
Figure 4.6.3-2 Tube (R45 C54) accelerometer response time-histories for foreign object impact. Downcomer flow = 14 ft/sec



X Force
(10 lb/div)

Y Force

50 MSec/Div

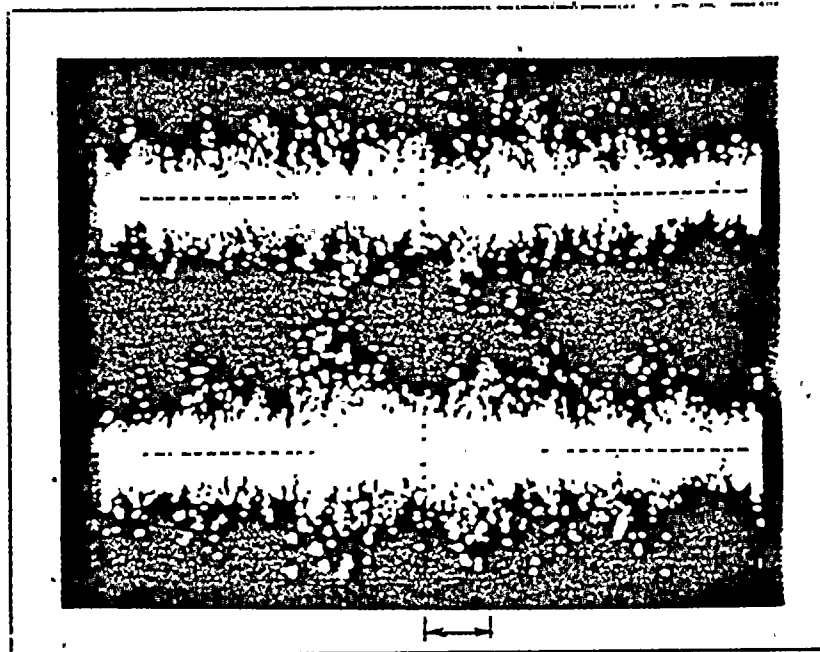


X Force
(10 lb/div)

Y Force

2 MSec/Div

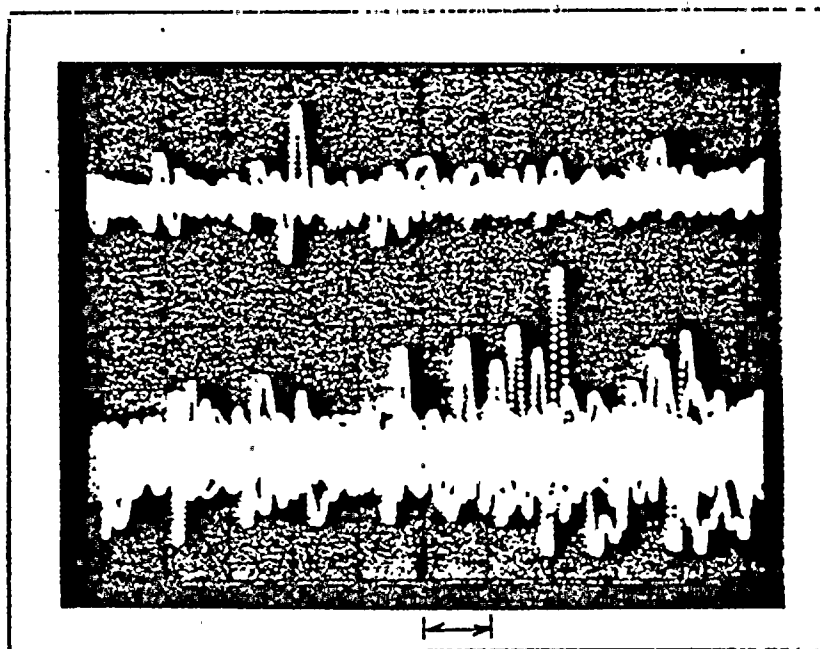
Figure 4.6.3-3 Tube (R45 C54) force transducer time histories for foreign object impact. Downcomer flow = 14 ft/sec



R Acceleration
(100 g/div)

T Acceleration

2 MSec/Div

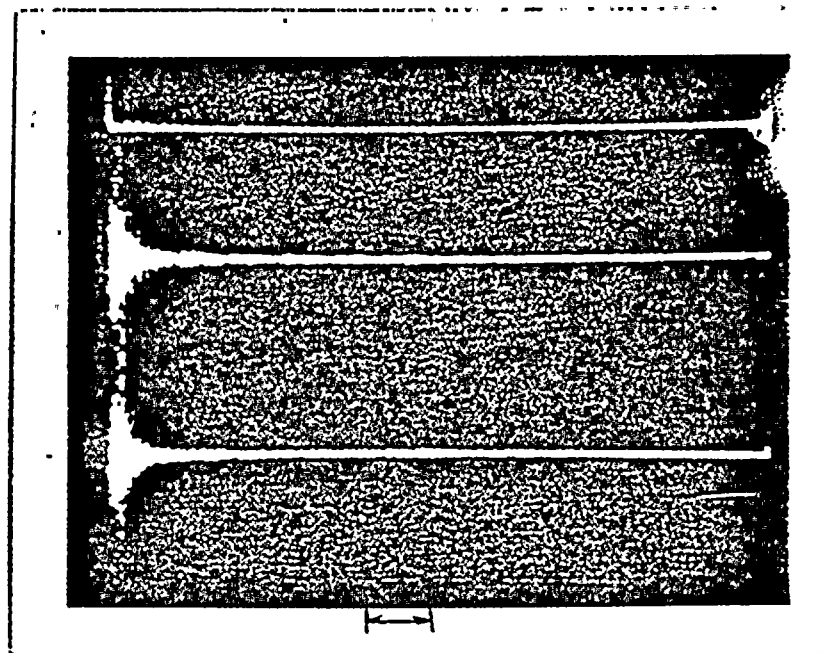


X Force
(10 lb/div)

Y Force

2 MSec/Div

Figure 4.6.3-4 Tube (R45.C54) response envelopes for foreign object impact.
14 ft/sec downcomer flow.

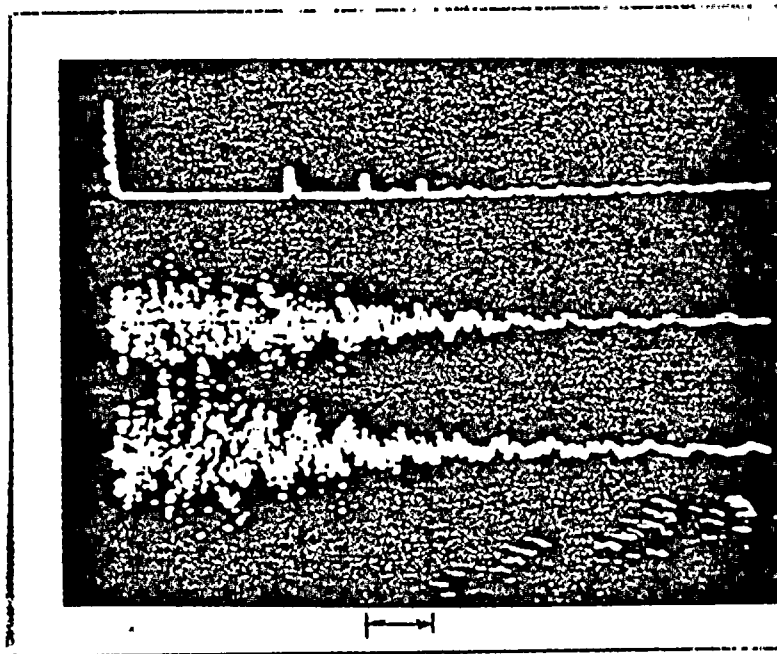


Impact Force
(200 lb/div)

R Acceleration
(100 g/div)

T Acceleration

50 MSec/Div



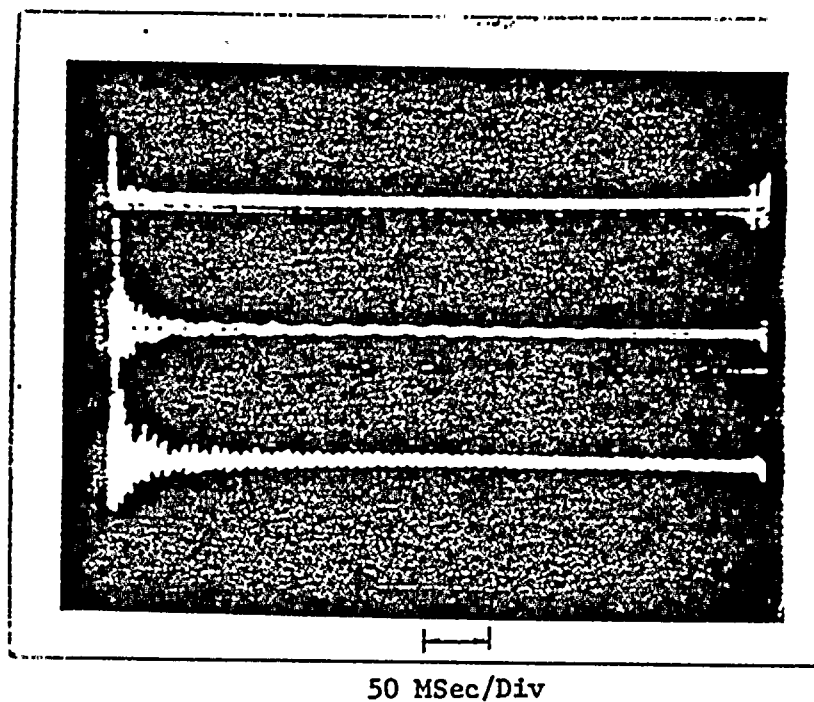
Impact Force
(100 lb/div)

R Acceleration
(100 g/div)

T Acceleration

5 MSec/Div

Figure 4.6.3-5 Tube (R45 C54) accelerometer response time histories for instrumented impact hammer.

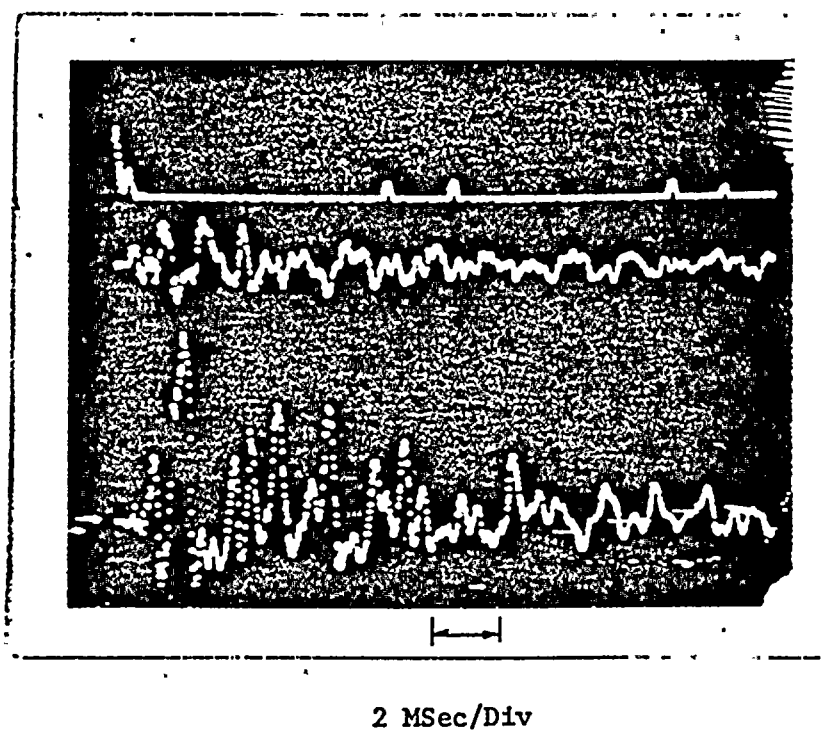


Impact Force
(200 lb/div)

X Force
(10 lb/div)

Y Force

50 MSec/Div



Impact Force
(200 lb/div)

X Force
(10 lb/div)

Y Force

2 MSec/Div

Figure 4.6.3-6. Tube (R45 C54) force transducer response for instrumented impact hammer

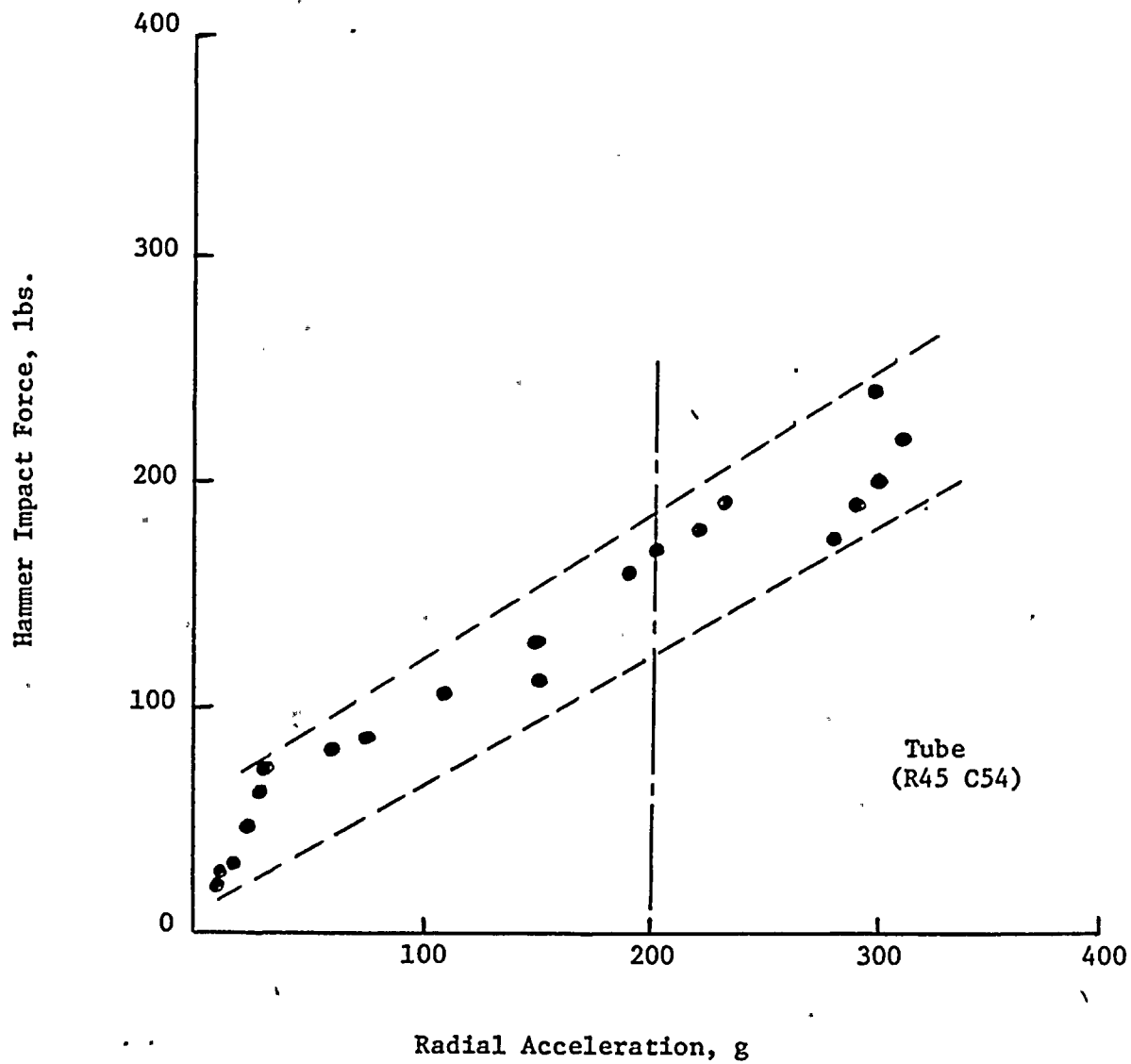


Figure 4.6.3-7 Accelerometer Calibration Data.

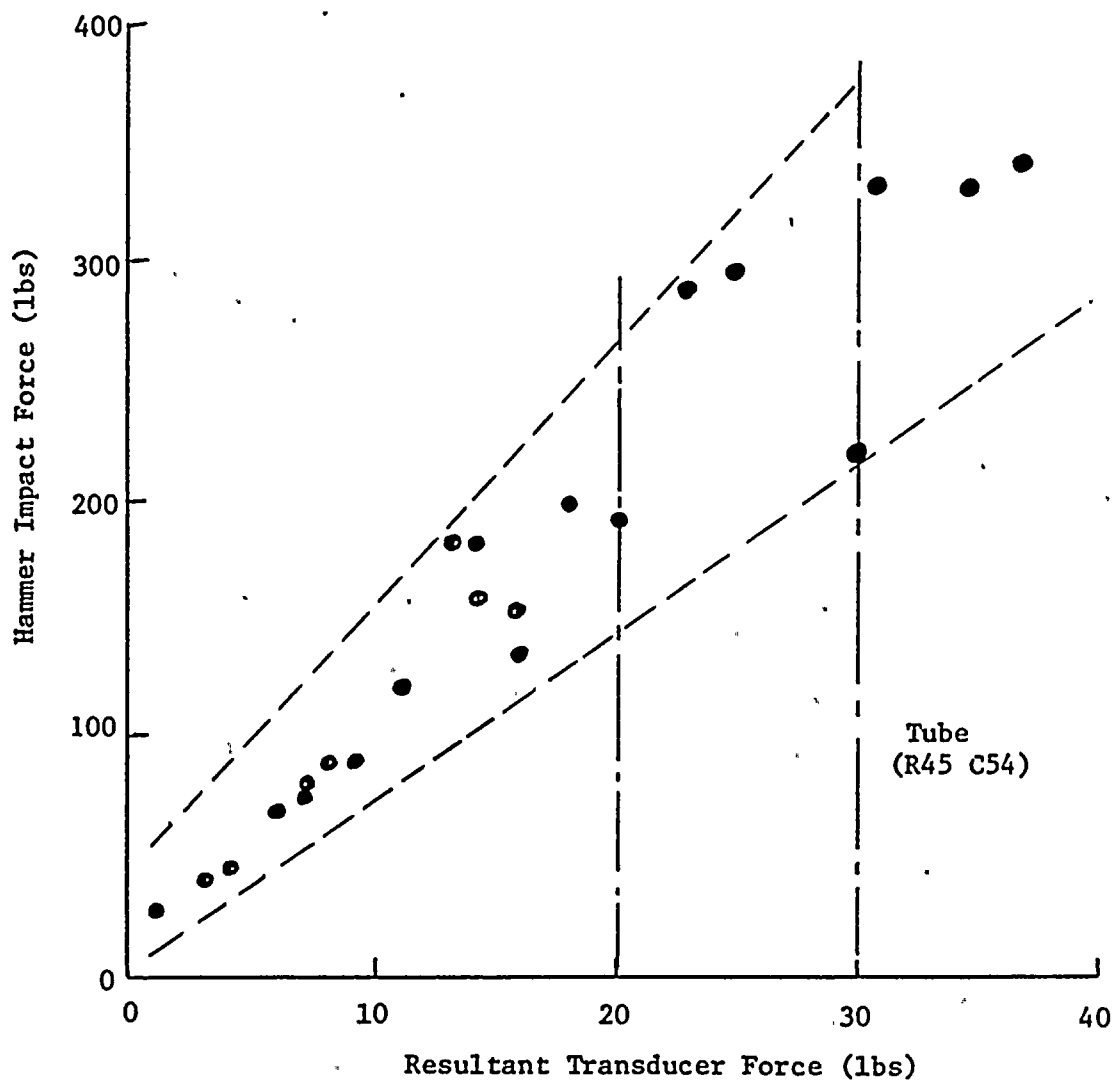


Figure 4.6.3-8 Force Transducer Calibration Data.

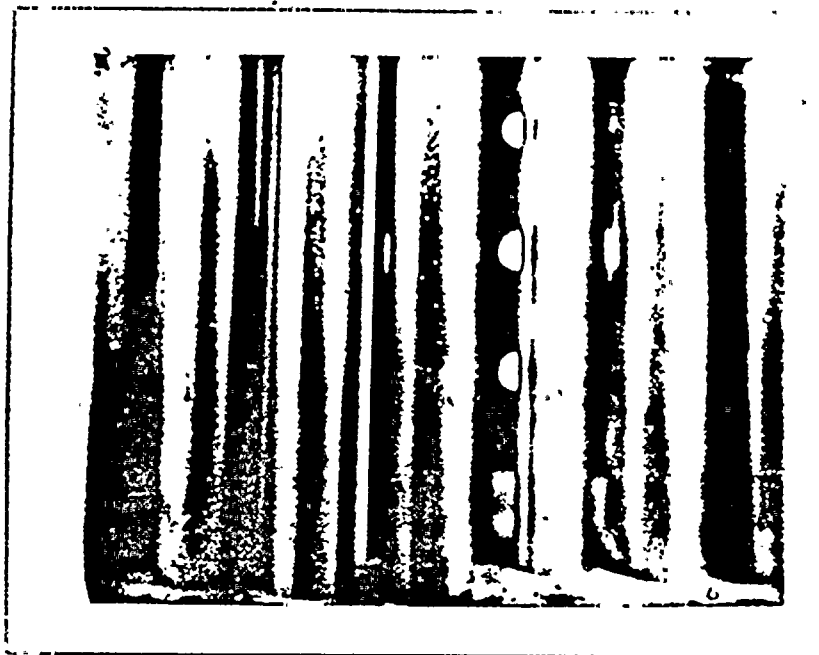
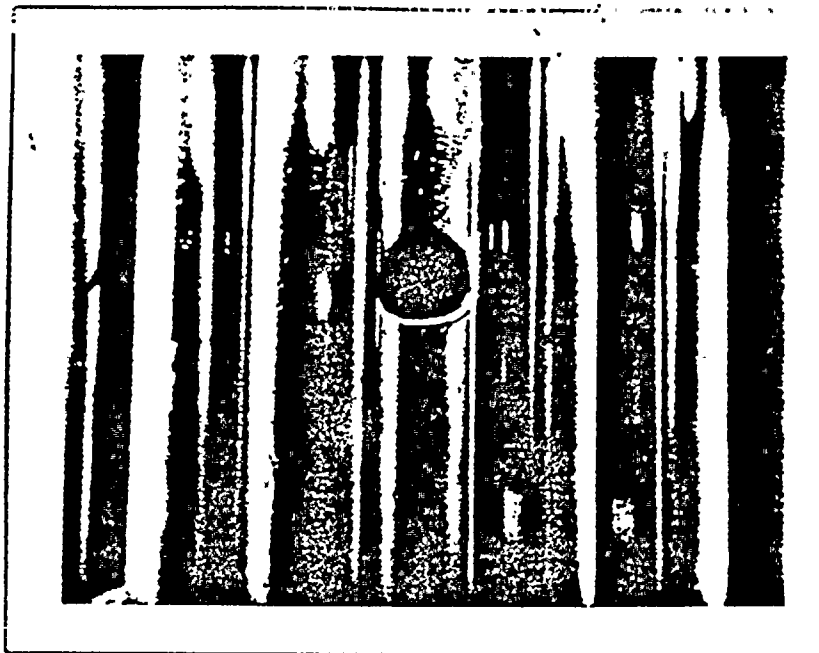


Figure 4.6.3-9 . Tube degradation after 8 hours of flow testing with foreign object in downcomer annulus. Maximum degradation occurred at R45 C54 tube.

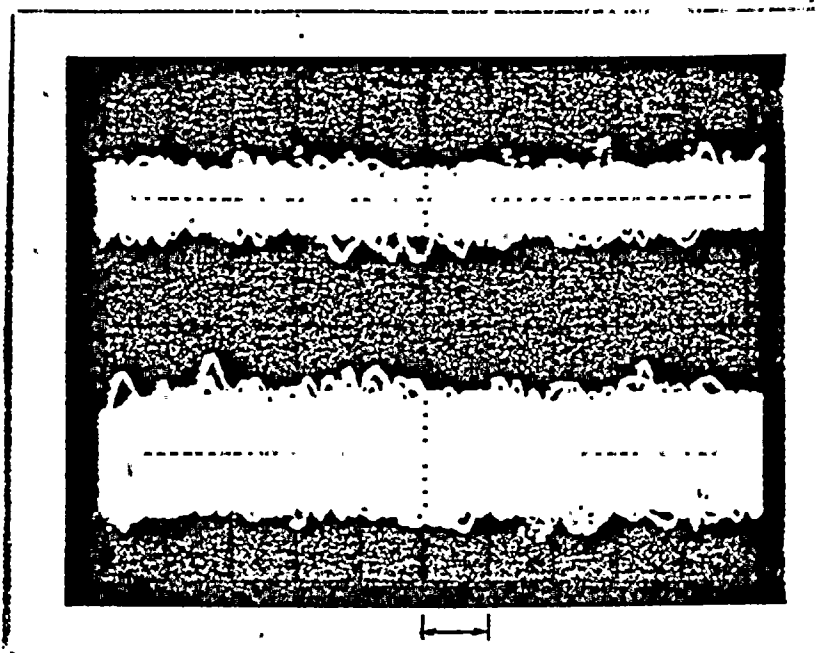


Front View



Side View

Figure 4.6.3-10 Tube(R44 C58) with machined opening. 40% remaining circumference.

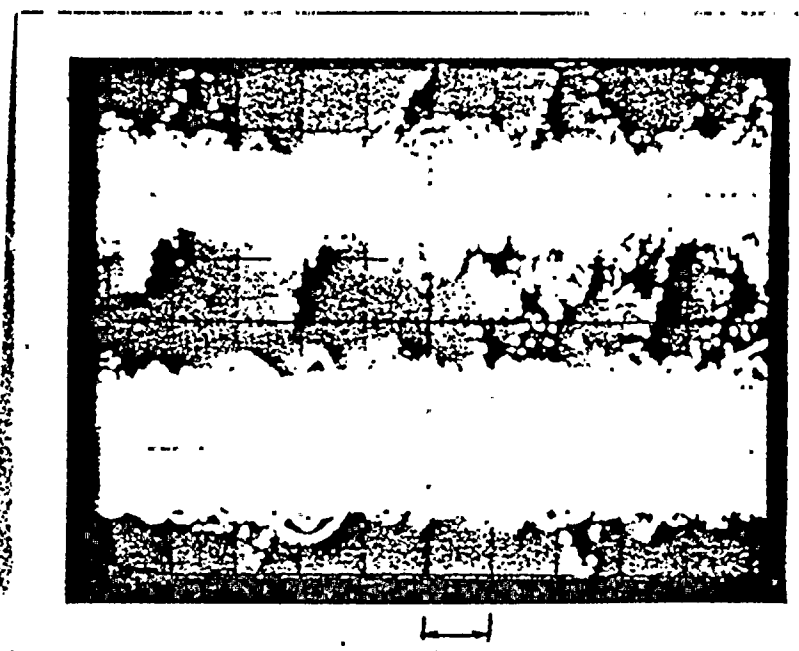


R Acceleration
(1 g/div)

T Acceleration

2 MSec/Div

40% Remaining Circumference



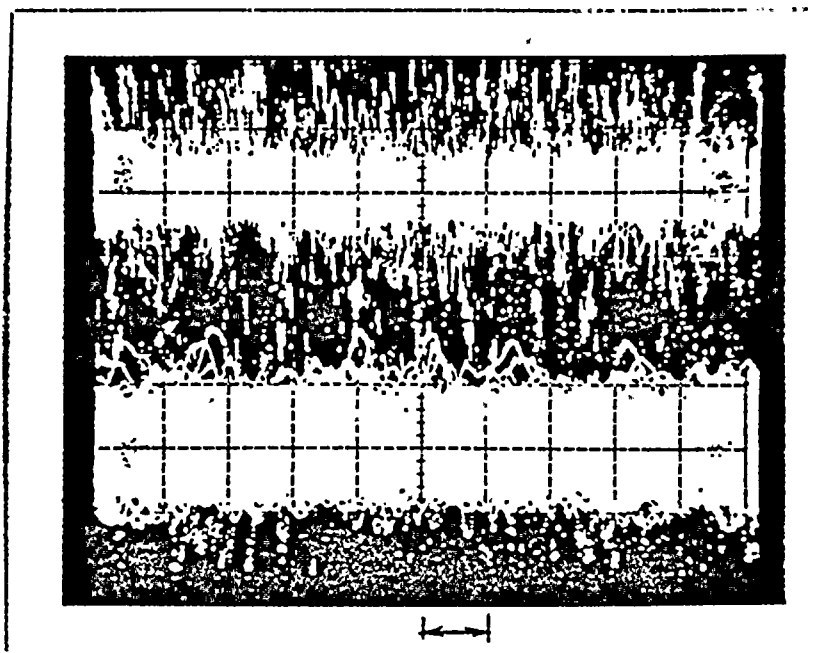
R Acceleration
(1 g/div)

T Acceleration

2 MSec/Div

10% Remaining Circumference

Figure 4.6.3-11 Tube (R44 C58) accelerometer response envelopes for 14 ft/sec downcomer flow with tube degradation. No foreign object.

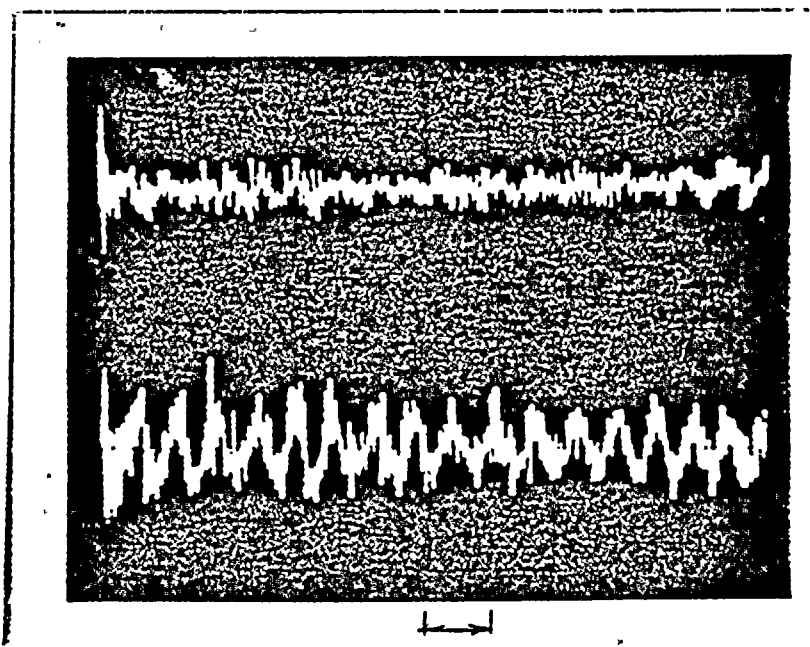


R Acceleration
(1 g/div)

T Acceleration

2 MSec/Div

Envelope



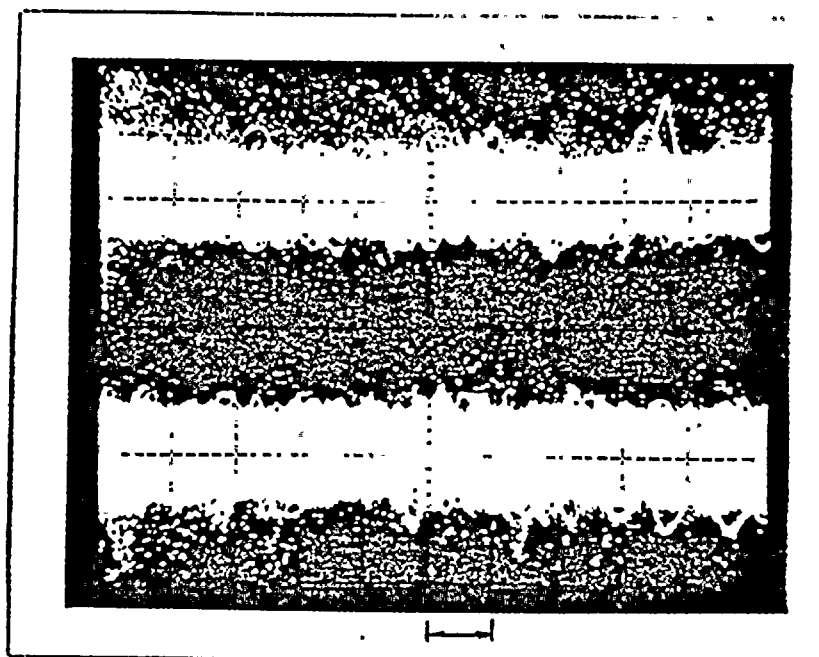
R Acceleration
(1 g/div)

T Acceleration

50 MSec/Div

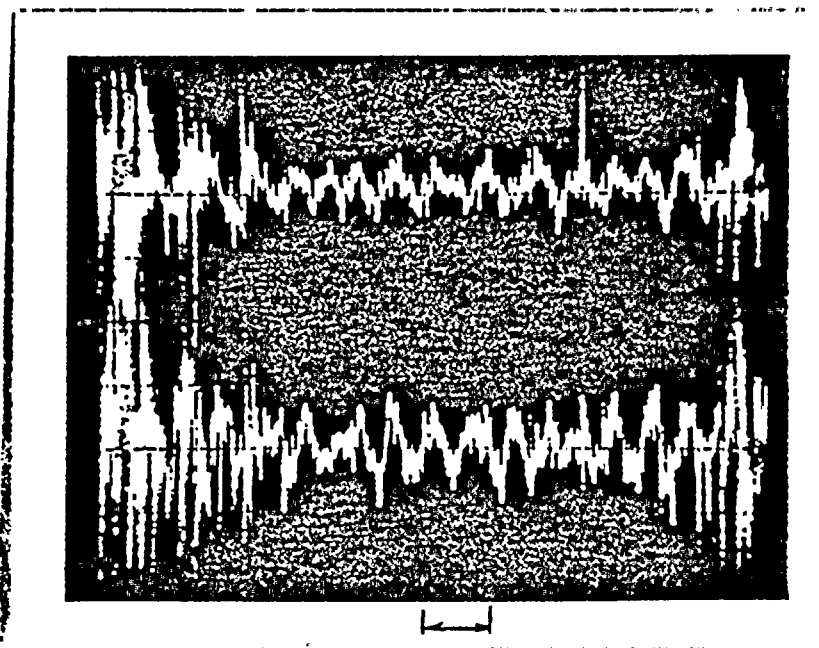
Single Sweep

Figure 4.6/3-12 _ Tube (R44, C58) accelerometer response for 14 ft/sec downcomer flow with tube degradation (10% remaining circumference). Foreign object is present.



2 MSec/Div

Envelope



50 MSec/Div

Single Sweep .

Figure 4.6.3-13 Severed tube (R44 C58) accelerometer response for 14 ft/sec downcomer flow. No foreign object.

4.7 Laboratory Tests

4.7.1 Collapse Testing

This test was designed to verify that repeated lateral load impacts on a 0.875 inch outside diameter (0.050 inch wall) steam generator tube subject to a 1000 psig external pressure could ultimately result in collapse. The lateral loads are applied by an impact rod driven by a hydraulic cylinder.

4.7.1.1 Specimens

The specimens are Inconel 600 steam generator tube with 0.875 inch O.D. and 0.050 inch nominal wall. The test lengths are either 19.2 inches or 52.0 inches. Some specimens were machined to provide a 0.030-inch wall over the 4.00-inch test section being impacted.

4.7.1.2 Test Equipment

The test fixture schematic and photographs of the test setup are shown in Figures 4.7.1-1 through 4.7.1-3. The photograph in Figure 4.7.1-3 shows the instrumentation details.

The tube specimen is mounted inside a 2.00-inch diameter tube with associated end caps, tees, seals, etc. A hydraulic cylinder applies the impact force through a rod and a hydraulic controller and function generator control the servovalve which controls the fluid supplied to the hydraulic cylinder.

The force, deflection, and acceleration are measured by the load cell, LVDT and accelerometer respectively. The LVDT and accelerometer can be seen in Figure 4.7.1-2. The transducer signals are monitored and recorded on the Nicolet storage scope.

The cyclic frequency and deflection are set to give the specified test load. At high frequencies, the hydraulic system cannot react fast enough to provide a large load. Therefore the frequency and/or deflection must be adjusted appropriately.

4.7.1.3 Test Procedure

The following procedure is used to perform the loading tests on the steam generator tubes. Prior to each test the specific test parameters are determined and are used where the test procedure calls for "as specified" test requirement.

- a) Cut tube to the "as specified" length.

- b) Measure and record I.D., O.D., and ovality of the tube in the test section. Mark the end of the tube to indicate the smallest diameter if there is ovality.
- c) Install the tube in the test fixture ensuring the smallest diameter is in line with the impact rod.
- d) Install end cap seals and other test fixture hardware.
- e) Turn set screws to provide a hand tight contact with the tube.
- f) Align the impact rod to meet the test requirements.
- g) Apply 1000 psig water or gas (as specified) pressure. Check for leaks and eliminate if they exist.
- h) Apply a 1000 lb axial load if specified.
- i) Apply the lateral load, as specified, at various locations on the tube surface over an area centered four inches from the simulated tube sheet support, and approximately two inches long in the axial direction and roughly forty degrees in the circumferential direction.

4.7.1.4 Test Results and Conclusions

The testing program is currently in progress and the results and conclusions will be reported in an addendum to this report.

4.7.2 Fatigue Testing

The purpose of this test is to determine the fatigue characteristics of tubes structurally degraded such as seen in the Ginna steam generator.

4.7.2.1 Test Approach

Nominal 0.875 inch O.D. x 0.50 inch thick tubes will be mechanically degraded locally near one end and set in a tube sheet simulation (collar) at that end and a tube support plate simulation at the other. The end conditions of the specimens will approach approximately a "fixed-pinned" situation. The structurally degraded section will be 2 inches long with its center 4 inches from the tube sheet simulated end. Three damaged configurations will be considered: flattened (to simulate a full collapse), kidney-shaped (to simulate a partial collapse) and impacted (to simulate degradation as a result of interaction with a foreign object). The flattened shape is achieved by clamping the 2-inch section of the tube in a vise, and squeezing the tube. The kidney-shaped section is one in which half of the tube circumference is made to nestle into the other half. This is done by means of a specially-designed set of dies. The impacted cases will be one in which the tube will be degraded in a region centered 4 inches from the tube sheet to simulate impacting by a foreign object.

4.7.2.2 Test Equipment

Figures 4.7.2-1 through 4.7.2-4 show the test setup being used.

The vibration exciter is attached to the tube with a small hose clamp approximately 10 inches from the pinned end of the tube. Deflections are monitored with a linear variable differential transformer. The deflection is set by adjusting a micrometer to the specified (single amplitude) deflection. The tube is then vibrated until it just touches the micrometer. The LVDT output is then observed and maintained at that amplitude for the duration of the test.

An instrumentation block diagram is shown in Figure 4.7.2-5.

4.7.2.3 Test Procedure

- a). Find fundamental bending resonance of tube.
- b) Map mode shape of resonance. While monitoring response at one location on the tube to make sure the response level remains constant measure the response at approximately six increments along the tube. Use two miniature accelerometers for this purpose.
- c). Fatigue Test - Adjust the maximum response amplitude to that specified in the table below. Run at this condition for 200,000 cycles. Failure will be detected as a drop in frequency. If failure does not occur proceed to the next step. Repeat until failure occurs.

<u>Step</u>	<u>Amplitude</u>	<u>Step</u>	<u>Amplitude</u>
1	.050 DA*	6	.200 DA
2	.070 DA	7	.250 DA
3	.090 DA	8	.300 DA
4	.120 DA	9	.400 DA
5	.160 DA	10	.500 DA

- d). Install a new specimen and run at next amplitude (or slightly lower amplitude) until failure.
- e) Test 2 additional samples at 2 different amplitudes to attempt to get 3 well spaced failures.

4.7.2.4 Test Results

Two tests were performed using the above procedures and are discussed below.

.....
*Dynamic or peak-to-peak amplitudes in inches.

A fixed/pinned beam with a 2-inch flat degradation was tested with no axial load. The natural frequency was 39.29 Hz. The fatigue testing was performed with 240,000 cycles for Step 1; 283,000 cycles for step 9 and 361,000 cycles for step 10 or a total of 2.87×10^6 cycles. There was no failure.

A fixed/fixed beam with a 2-inch flat deformation was also tested with a 1000 lb axial load. The natural frequency was 64.72 Hz. The fatigue test was run with 202,000 cycles for Step 1 and 2.08×10^6 cycles for step 8. The amplitudes in the other steps were not used. No failure of the specimen was observed.

4.7.2.5 Additional Tests

The following identifies additional planned testing.

- a) Flat collapse: fixed-fixed, 1000 lb axial load and .005 inch deep by 1/4 inch long notches at 2 locations near the collapsed section.

The test will be run for a minimum of 10^6 cycles at .300" DA.*

- b) Kidney shaped collapse (1 inch long)

a. Fixed-fixed: 0 lb axial load and 1000 lb axial load

b. Fixed-pinned: 0 lb axial load

1) Run strain gage response survey.

2) Run fatigue tests if strain measurements warrant it.

- c) Kidney shaped collapse - 2 inch long

same as 2. above

- d) Impact fatigue

Vibrate tube such that it will impact against a hard edge measuring load at impact.

Run fatigue tests in one or more of the above three configurations as appropriate.

4.7.2.6 Test Results and Conclusions

Testing is still in progress and specific test results and conclusions will be reported later in an addendum to this report.

.....
*Dynamic or peak-to-peak amplitude in inches.

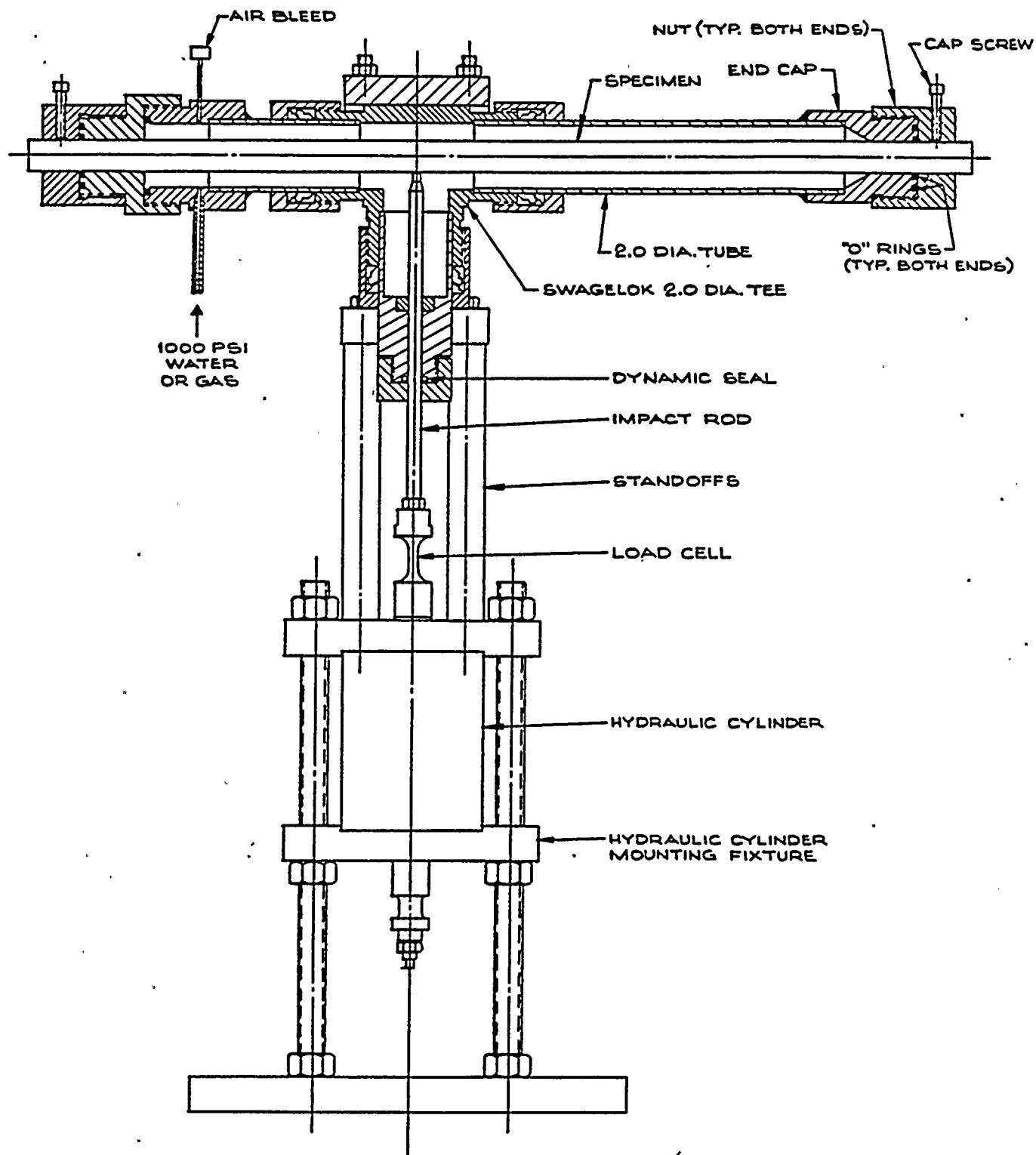


FIGURE 4.7.1-1: Test Fixture for Collapse of Steam Generator Tubes

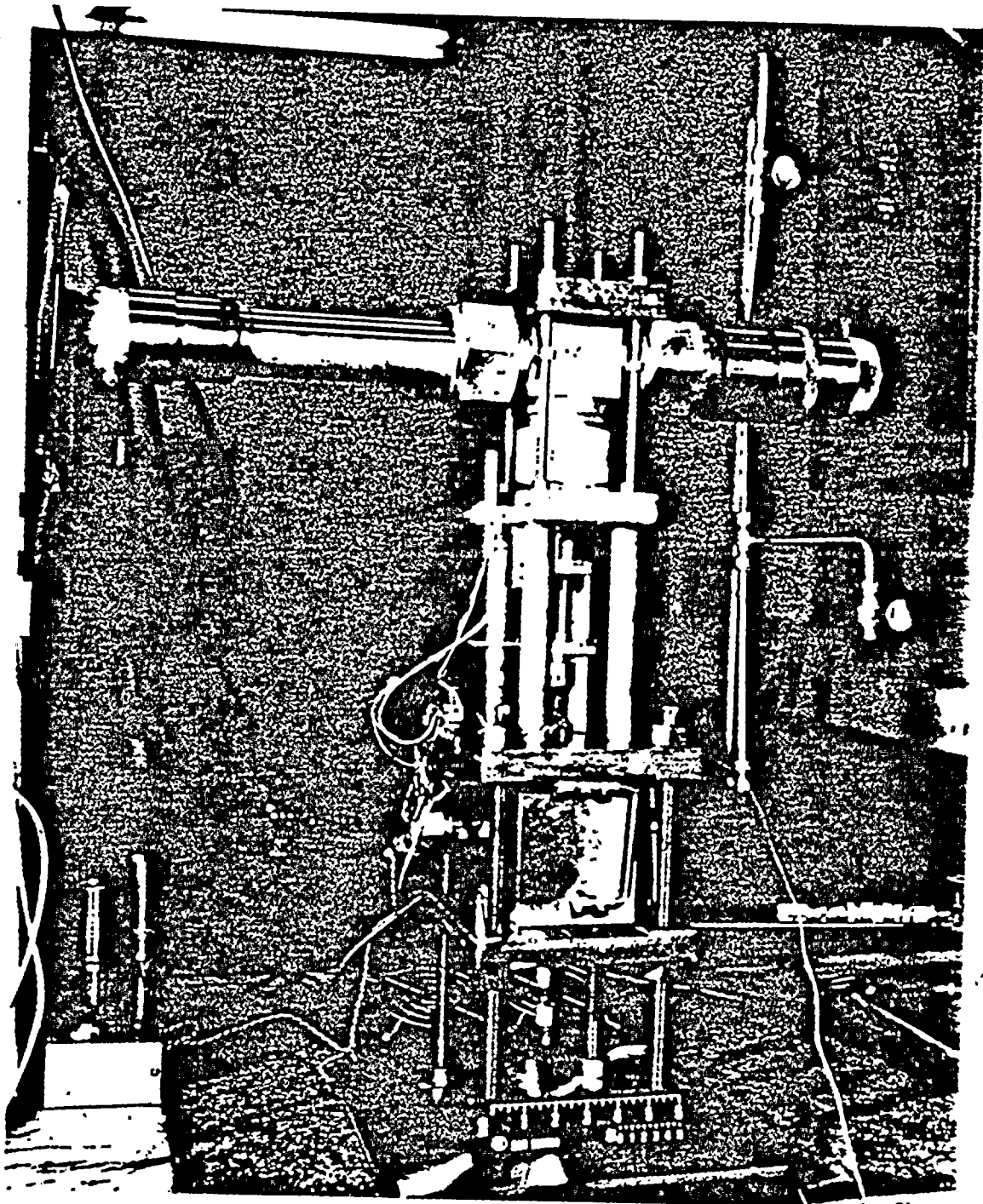
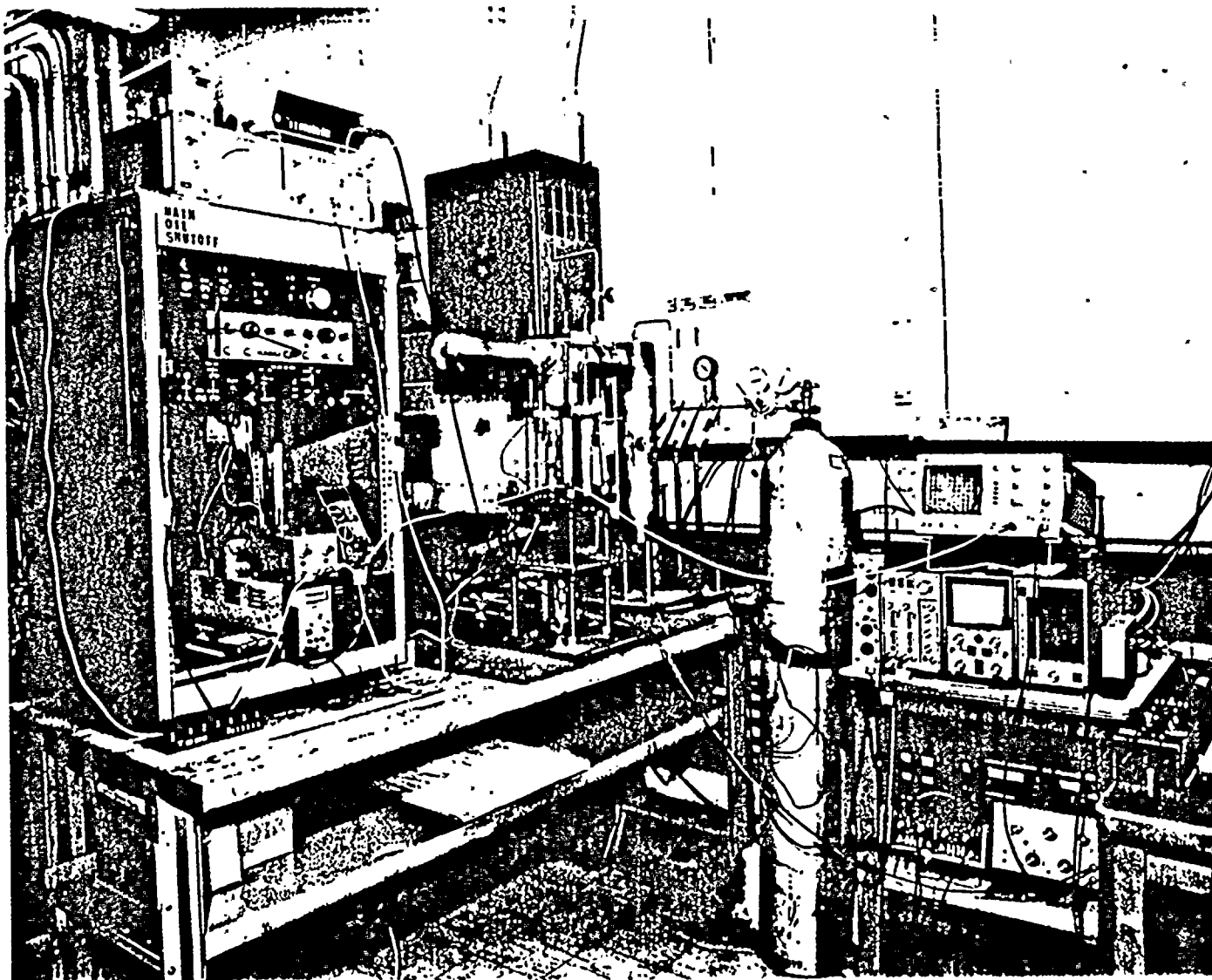


FIGURE 4.7.1-2: PHOTOGRAPH SHOWING THE TEST SET-UP FOR TUBE
COLLAPSE TEST



4-7-7

FIGURE 4.7(1-3) PHOTOGRAPH SHOWING INSTRUMENTATION DETAILS FOR THE TUBE COLLAPSE TEST

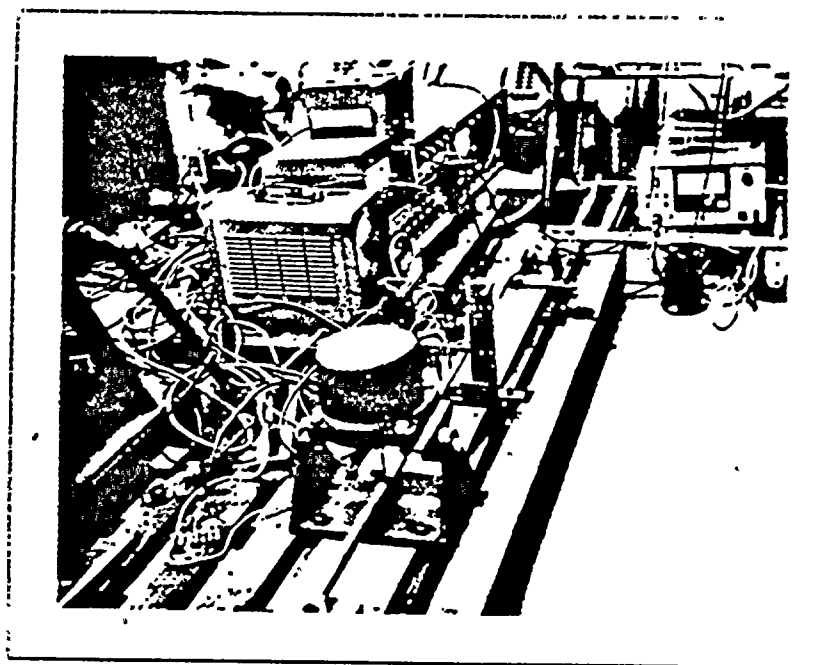


FIGURE 4.7.2-1 VIEW OF FATIGUE TEST SETUP

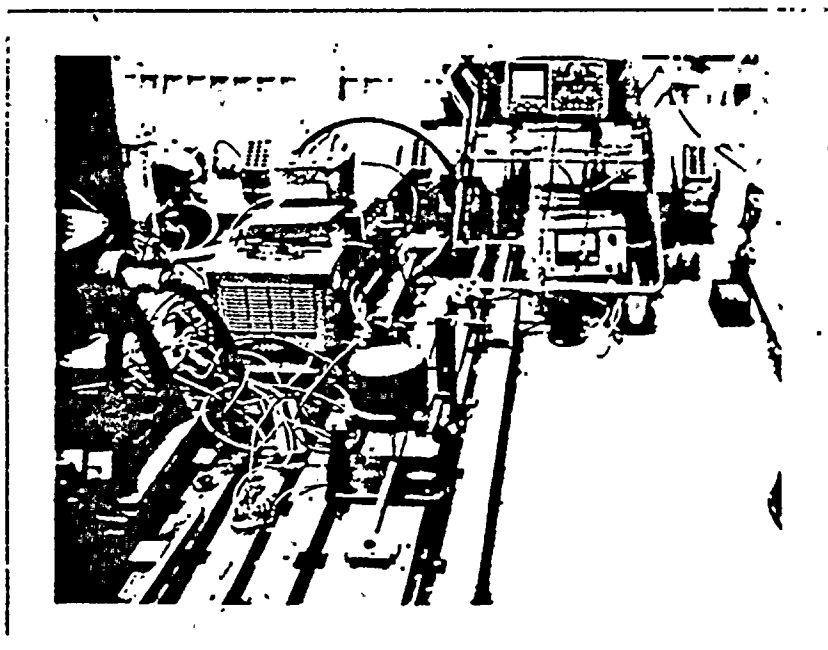


FIGURE 4.7.2-2 ANOTHER VIEW OF FATIGUE TEST SETUP

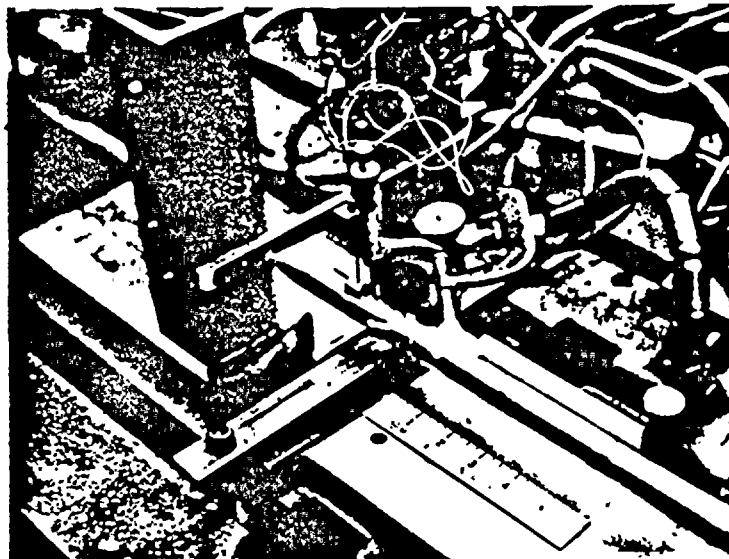


FIGURE 4.7.2-3 CLOSE VIEW OF FATIGUE TEST SETUP

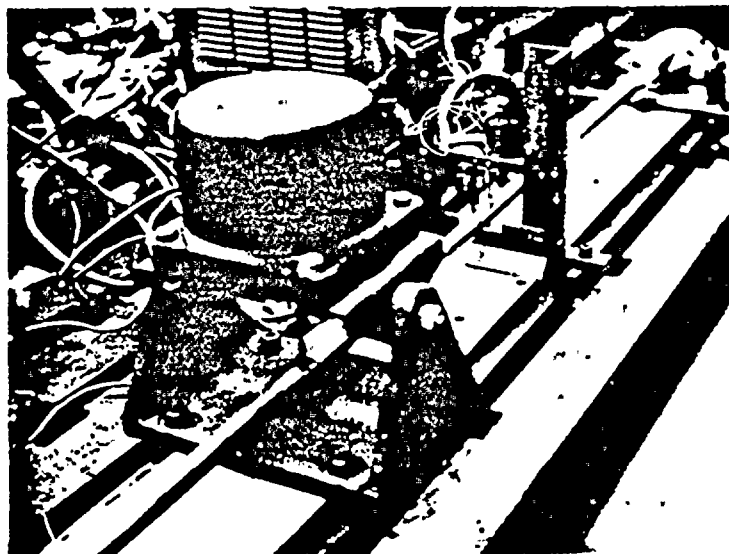


FIGURE 4.7.2-4 ANOTHER CLOSE UP OF FATIGUE TEST SETUP

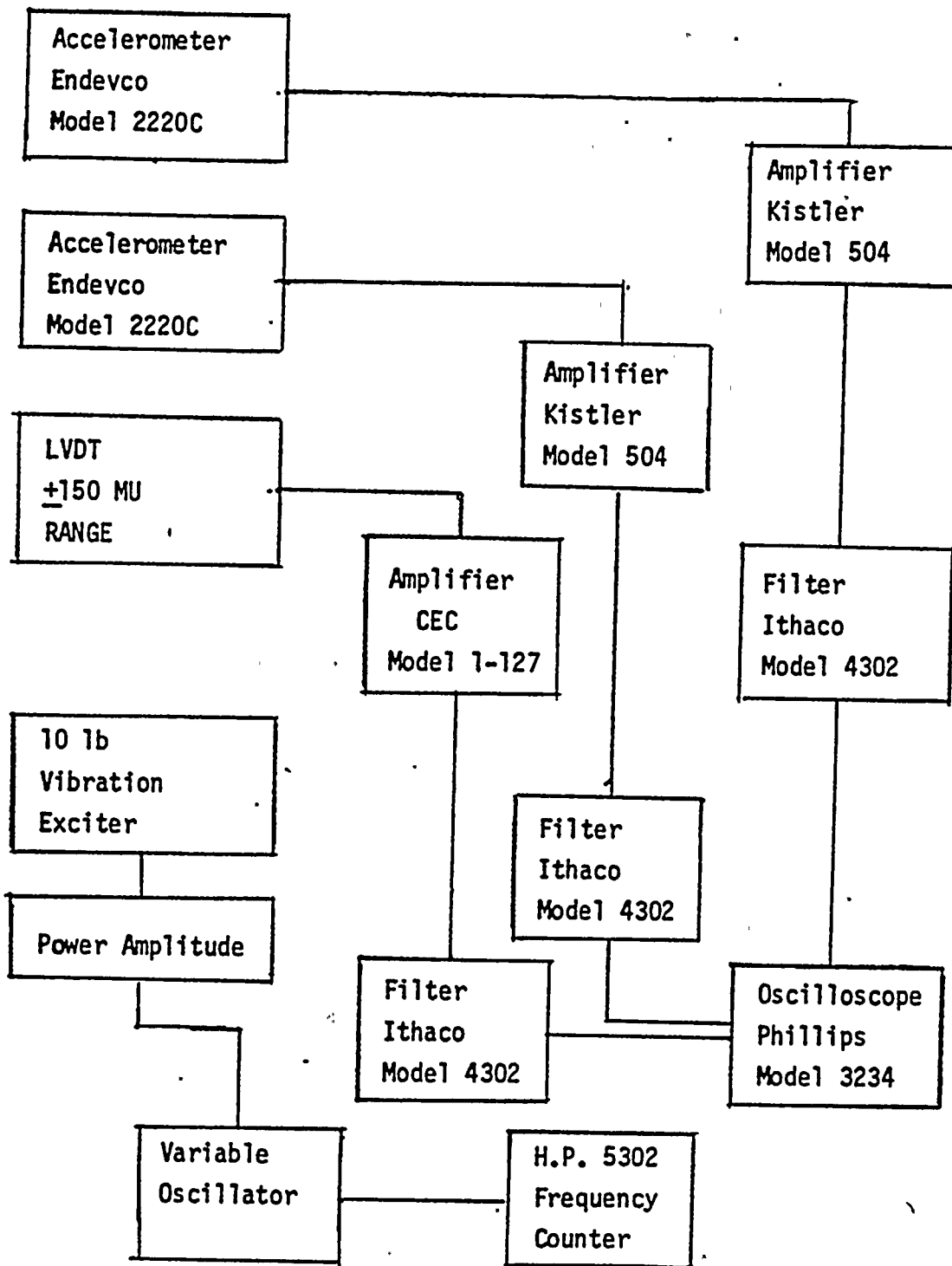


FIGURE 4.7.2-5 INSTRUMENTATION BLOCK DIAGRAM

4.8 Conclusions

This section summarizes the major results of the various testing and analytical programs described in Section 4 of the report and based on these results, provides conclusions regarding specific elements of the overall failure mechanism which led to a rupture of tube Row 42 Column 55 of the B-Steam Generator.

The approach that will be taken in presenting the conclusions resulting from the steam generator tube failure analysis program will be to assimilate available information on the following specific elements of the overall failure mechanism:

Collapse
Fatigue
Wear
Burst

Pertinent information associated with collapse is summarized in Table 4.8-1. This information indicates that collapse of a plugged tube can occur as a result of pressure, axial, and lateral impact loads. It is concluded that plastic deformation due to normal operating loads, axial restraint loads, and lateral impact loads resulted in sufficient tube ovalization to cause collapse.

Pertinent information associated with fatigue is summarized in Table 4.8-2. This information indicates that severing of a collapsed or degraded tube with a notch on stress riser can occur as a result of a continual lateral impact load. Once a tube has been severed it can interact with neighboring tubes and through wear sufficiently degrade these tubes such that they could also fail in fatigue or by burst if internally pressurized.

Pertinent information associated with wear is summarized in Table 4.8-3. This information indicates that wear played a significant role in propagation of the initial peripheral tube degradation toward the center of the tube bundle. Wear primarily seemed to be associated with a severed or free tube rubbing against another tube.

Pertinent information associated with tube bursting is summarized in Table 4.8-4. This information indicates that sufficient wear to result in bursting of an active tube can occur in a relatively short period of time and that the actual failure is consistent with analytical predictions.

Based on the above, it is concluded that the failure mechanism shown in Figure 4.8-1 was responsible for the January 1982 Ginna burst tube incident. The basic ingredients for initiation of the mechanism are plugged peripheral tubes and a foreign object. The foreign object, it is felt, interacted in an impacting manner with plugged peripheral tubes on the hot leg side of the generator and this ultimately resulted in extensive tube degradation and severance of a tube near the top of the tube sheet enabling the tube to pivot about a point of fixity at the first support plate. Such a severed tube could then interact with

neighboring tubes causing extensive tube degradation via wear and could ultimately experience a fatigue type severance at the first support plate.

Extensive tube degradation of neighboring tubes would result in their total failure and enable them to interact with other tubes.

In summary, it is concluded that the failure mechanism shown in Figure 4.8-1 resulted in the January 1982 Ginna burst tube incident.

TABLE 4.8-1

COLLAPSE

The conditions for tube collapse could be established by an external source wearing against the tube and thinning the tube over a portion of its surface and/or impacting a tube with sufficient magnitude to cause plastic deformation and tube ovalization.

- Laboratory examination of a collapsed tubing surface identified significant cold work that could have been caused by a foreign object impacting against the tube.
- Analytical calculations and model testing indicate that a foreign object similar to that removed from the steam generator is capable of impacting the tube with sufficient magnitude to cause plastic deformation.

Accelerometer readings taken during model flow testing indicate that the foreign object could exert impact forces in the range of 120 to 180 lbs. Force transducer data also taken during model flow testing indicated maximum impact forces in the range of 200 to 350 lbs. Analytical calculations indicate that impact forces in excess of 100 lbs are obtainable.

Analytical calculations for a 7/8 inch O.D. tube subjected to an external pressure of 1000 psi and a concentrated lateral load indicated that plastic deformation leading to tube ovalization will occur with lateral loads in the range of 50 to 75 lbs. The actual load required will depend upon tube ovality, wall thickness, and yield strength. An axial load could reduce the required lateral load for incipient yielding by approximately 10 lb.

TABLE 4.8-2

FATIGUE

Fatigue failure of a tube can be caused by a significant reduction in its load carrying capability as a result of wear and/or by continuous impact by a foreign object.

- Analytical calculations indicate that a nominal plugged tube with or without a notch or stress riser will not fail in fatigue considering worst case operating thermal and mechanical loads.
- Structurally degraded tubes will not fail due to fluid induced vibrations alone.

Fluid elastic instability would not be predicted analytically for a mechanically or structurally degraded tube. However, for a structurally degraded tube, the margin to instability is minimal.

During model flow testing tubes with degraded and structurally degraded cross section were stable with respect to flow induced vibration.

- A structurally degraded tube continuously impacted by a foreign object can fail due to high cycle fatigue. Calculated failure times range from a few hours to a few weeks depending on the magnitude and frequency of the impact load.
- Laboratory scanning electron microscope fractographs revealed fatigue type striations at failed tubing surfaces.
- Oscillating lift, drag and torque fluid loads are not large enough to cause tearing of tubing protrusions, consequently tube shredding must be related to another process, such as wear.

TABLE 4.8-3

WEAR

Extensive wear was instrumental in the propagation of initial peripheral tube degradation toward the center of the tube bundle and seemed to be associated with a severed or free tube rubbing against another tube.

- Metallographic examination of removed tube sections identified wear zones as having cold work surface layers indicating the presence of an external source such as a loose tube. Tube wear patterns were primarily circumferential in nature extending over a fairly large length in the axial direction and were compatible with one tube rubbing against another.
- During model flow testing, a tube severed near the top of the tube sheet was observed to interact intermittently with adjacent tubes.
- Analytical calculations indicate that sufficient degradation of a tube, due to wear of one Inconel tube on another can occur such that bursting of an active tube could result consistent with the actual Ginna data.
- Eddy current indications in the B-Steam Generator hot leg periphery appear to be primarily of an I.D. type prior to February, 1979. Starting in February 1979, the pattern of O.D. indications identified by eddy current inspections is consistent with the development of O.D. degradation by a foreign object in the most peripheral tubes followed by the propagation of degradation to neighboring tubes by a wear process, which could be caused by a neighboring tube severed near the top of the tube sheet and free to rotate about a point of fixity at the first support plate or a piece of free tubing which had been severed at the tube sheet and first support plate.

TABLE 4.8-4

BURST

Tube bursting occurred as a result of wear and is consistent with analytical predictions.

- Calculations indicated that the minimum tube wall required to preclude bursting of a tube under normal operating conditions is 6.6 mils assuming a material ultimate strength of approximately 90 ksi. This compares well with the 8 mils remaining wall measured in the laboratory for the burst tube.
- Laboratory examinations indicated that the failure of tube R42 C55 was a purely ductile failure in the region of the tube wall that had been worn to a thickness of approximately .008 inches over a length of approximately 4.0 inches.
- Analytical calculations indicated that sufficient degradation of a tube due to wear of one Inconel tube on another can occur such that bursting of an active tube could result consistent with the actual Ginna data.

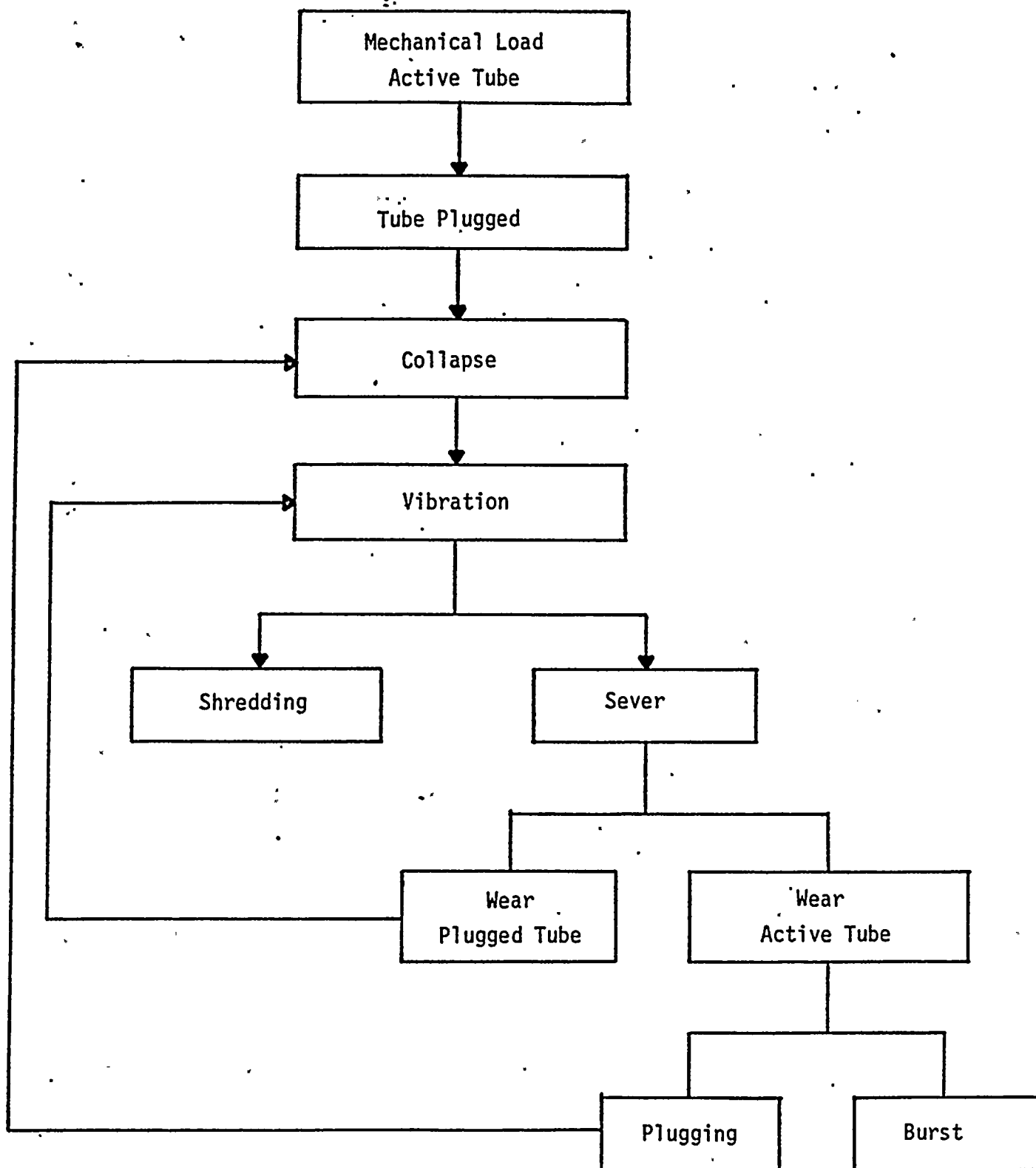


Figure 4.8-1
Postulated Failure Mechanism Sequence

5.0 STEAM GENERATOR REPAIR PROGRAM

5.1 Access Holes

5.1.1 Description

To provide access for detailed inspection and tube removal, two, 3 inch diameter access holes were drilled in the stub barrel on the secondary side of the B-Steam Generator. These holes were centered approximately 6 inches above the tube sheet on the hot leg side at the Number 4 and 6 wedge areas. Fig. 5.1 is a cross sectional view of the steam generator showing the vertical position of the access holes relative to the area of repairs. Fig. 5.2 and Fig. 5.3 are detailed plan views of the Number 4 and 6 wedge areas showing the location of the access holes relative to the tubes removed.

5.1.2 Installation

The access holes were mechanically machined starting with a small pilot hole and enlarged with successively larger drills until the final, finished hole diameter was achieved. The holes were sized to preclude the necessity for weld reinforcement. Following repairs, the holes are sealed with a cover plate and gasket. The cover plate is attached to the steam generator by bolts threaded into holes drilled and tapped into the stub barrel. Fig. 5.4 shows the details of the cover plate assembly.

5.1.3 Design

The access holes are designed in accordance with the requirements of the ASME Code. A description of the structural analysis for the holes is contained in Section 6.2.1 of this report.

5.2 Tube Removal

5.2.1 Summary

In order to determine the extent of repairs required to the B-Steam Generator, the defects in periphery plugged tubes were categorized as follows:

- a) structurally degraded - tubes that are collapsed, severed, or have visible through wall defects; the size of the defect is large enough to cause a significant reduction in section modulus.
- b) video O.D. indication - tubes that were observed by video inspection to have minor dings, wear marks, or similar small defects on the outside; the defects do not involve any significant loss of volume or reduction in section modulus.
- c) eddy current signal - tubes that were observed by video inspection to have no defects on the outside; the tubes have no defect beyond that for which they were originally plugged.
- d) preventatively plugged - 3 tubes surrounding R42 C55 preventatively plugged prior to performing the secondary video inspections; these tubes showed no defect either by eddy current or video inspection.
- e) pulled tube - one tube (R45 C52) was pulled for metallurgical examination in 1978.

All of the defects categorized as structurally degraded or video O.D. indication were in the section of tube between the tube sheet and first support plate in the hot leg side.

5.2.2 Categorization of Tubes

Figure 5.5 is a listing of all the plugged tubes by category and area on the B-Steam Generator periphery. There are a total of 56 tubes including R45 C52. Of these, 24 are categorized as structurally degraded (including R42 C55), 11 as having video O.D. indications, 17 as being plugged for eddy current indications, and 3 preventatively plugged. The number in each category by area is shown in the figure.

5.2.3 Tube Removal

All tube sections categorized as structurally degraded have been removed from the steam generator. This included 6 from the Number 6 wedge area, and 19 from the Number 4 wedge area. The basic removal procedure (except for the pulled tube) involved cutting the lower 8 to 12 inches above the tube sheet of each tube using an electrode discharge machining (EDM) procedure. The

remaining 38 to 44 inch section below the first support plate was cut using a mechanical cutter. The cutting operations were performed entirely through the access holes at the Number 4 and 6 wedge areas. The tubing sections were manually removed from the steam generator either through the access holes or the existing 6 inch handhole at the end of the tube lane.

5.2.4 Severed Tube Removal

As indicated in Section 3.4, 2 tubes (R45 C54 and R44 C56) were found already severed at the tube sheet and first support plate. These were simply cut into smaller sections and manually removed through the access hole at the Number 4 wedge area. The severance at the upper end, in one case, was just below the support plate and, in the other case, just into it. An analysis of this configuration is provided in Section 6.2.3.3 of this report.

5.2.5 Tube Pull

One tube (R45 C47) with an eddy current indication approximately 24 inches above the tube sheet was removed for metallurgical examination. This tube was pulled from the secondary side of the steam generator. This operation involved cutting out a section of the tube in the U-bend region above the upper support plate; mechanically cutting the tube just above the tube sheet; hydraulically pulling the tube from above; and cutting it into sections as it was removed. The final step was installation of a restraining device on the cut tube end at the first anti-vibration bar. Access to the U-bend region for this tube removal operation was provided by a manhole cut in the wrapper. This hole was sealed following completion of the pulling operation.

5.2.6 U-Bend Restraint

During a similar pull of another tube (R45 C52) in 1978, U-bend and sections of 2 adjacent tubes (R45 C53 and R45 C51) were also removed. Since the lower section of R45 C53 was removed during the present repairs, it was restrained at the upper end by expansion on either side of the support plate. This restraint is designed to preclude any possibility of this tube moving during operation.

5.2.7 Remaining Tubes

Other than the removal of R45 C47 for metallurgical examination, no sections of tubes categorized in Figure 5.5 as having only video O.D. indications or eddy current signals were removed from the steam generator. A structural evaluation of tubes with minor O.D. defects is provided in Section 6.2.3 of this report. The tubes with eddy current indications were plugged in accordance with the requirements of the plant Technical Specifications.

5.3 Loose Parts Removal

As indicated in Section 3.5, several loose parts and pieces of tubing were found in the steam generators. The few, small loose parts in the A-Steam Generator were simply removed manually or with the aid of remotely operated mechanical grippers. A more extensive program of inspection and removal was necessary in the B-Steam Generator. Where loose parts or pieces of tubing were accessible from the tube lane handholes, or periphery access holes, they have been removed manually. Where size allowed, they were removed with remote mechanical devices using grippers or magnets. Pieces too small to remove by these means have been removed by vacuuming or water lancing. These operations were designed to remove all loose parts and pieces of tubing, regardless of size, from the steam generators.

5.4 Mechanical Plug Removal

Since the damaged section of R42 C55 was removed from the B-Steam Generator, the 3 adjacent good tubes (R41 C55, R42 C54, and R42 C56) have been restored to service. The 6 mechanical plugs installed in the tube sheet ends of these tubes have been removed. The removal was accomplished by hydraulically stretching and pulling the plug from each tube end. Subsequent eddy current examination will be performed to assure that there are no unacceptable indications in any of these tubes.

5.5 Material Control

Several material control procedures were used during repair and modifications of the steam generators. A Material Control Log was used to verify that all material and tools entering the steam generator were either removed or installed. Openings around work areas on the secondary side were sealed to prevent material or tools from entering other areas of the steam generators. Lanyards were attached to parts being cut out to assure their retrieval. In addition, parts removed during modifications were reconstructed outside the steam generator. Finally, Quality Control surveillance, hold points, and cleanliness inspections were used to verify that no tools or loose parts had been left in the steam generators.

5.6 Post Repair Inspections/Tests

Following completion of the repairs in the B-Steam Generator, a series of inspections and tests will be performed to assure that it is ready for return to service. Sections of tubes adjacent to areas involved in the repair operations will be eddy current examined to assure that no unacceptable defects are present. A final series of video inspections will be performed to assure that no loose parts or tubing fragments remain and to verify that no unacceptable O.D. defects were caused by the repairs. A secondary side hydrostatic test will be performed to verify integrity of the access hole covers. A primary side hydrostatic test will be performed to assure that no measurable primary to secondary leakage is present.

5.7 Radiation Exposure

5.7.1 Planning

Ginna Station's ALARA program was applied to all of the steam generator inspection, repair, and modification activities. All inspection, repair, and modification activities were reviewed technically and radiologically before implementation. Procedures and equipment were tested, and personnel trained, in full scale mockups prior to use in the steam generators. The secondary video inspection system was developed at Ginna Station using Rochester Gas and Electric's steam generator mockup. Special mockups were built to check out the equipment for machining the 3 inch access holes.

5.7.2 Tube Removal

Due to the potential exposure associated with removal of the tube sections, a significant effort went into exploring various alternatives. Several different types of tube removal methods and equipment were evaluated. The process finally selected provided a technically acceptable means of tube removal with the lowest radiation exposure. The process incorporated equipment from several sources. A Westinghouse-developed electrode discharge machining procedure (EDM) procedure was used for cutting the lower section of each tube. Equipment furnished by Babcock & Wilcox, NUS, and Alliance Tool and Die was used for the mechanical cutting and removal of the remaining tube sections. Development of this I.D. mechanical cutting and removal system eliminated the need for additional access holes or U-bend removal. This saved several hundred man-rem.

5.7.3 Exposure

The radiation exposure associated with inspection and repair of the B-Steam Generator will be approximately 310 man-rem. This includes approximately 200 man-rem for the initial inspections and Phase I repairs; 80 man-rem for tube removal; and 30 man-rem for the post repair inspections and tests. These numbers include the exposure associated with the inspections and repairs resulting from the tube rupture. They do not include the exposure received during the normal inspections and modifications performed, as previously planned, as part of the refueling outage. Table 5.1 summarizes the exposure experienced during this outage.

TABLE 5.1

1982 B-STEAM GENERATOR RECOVERY EXPOSURE

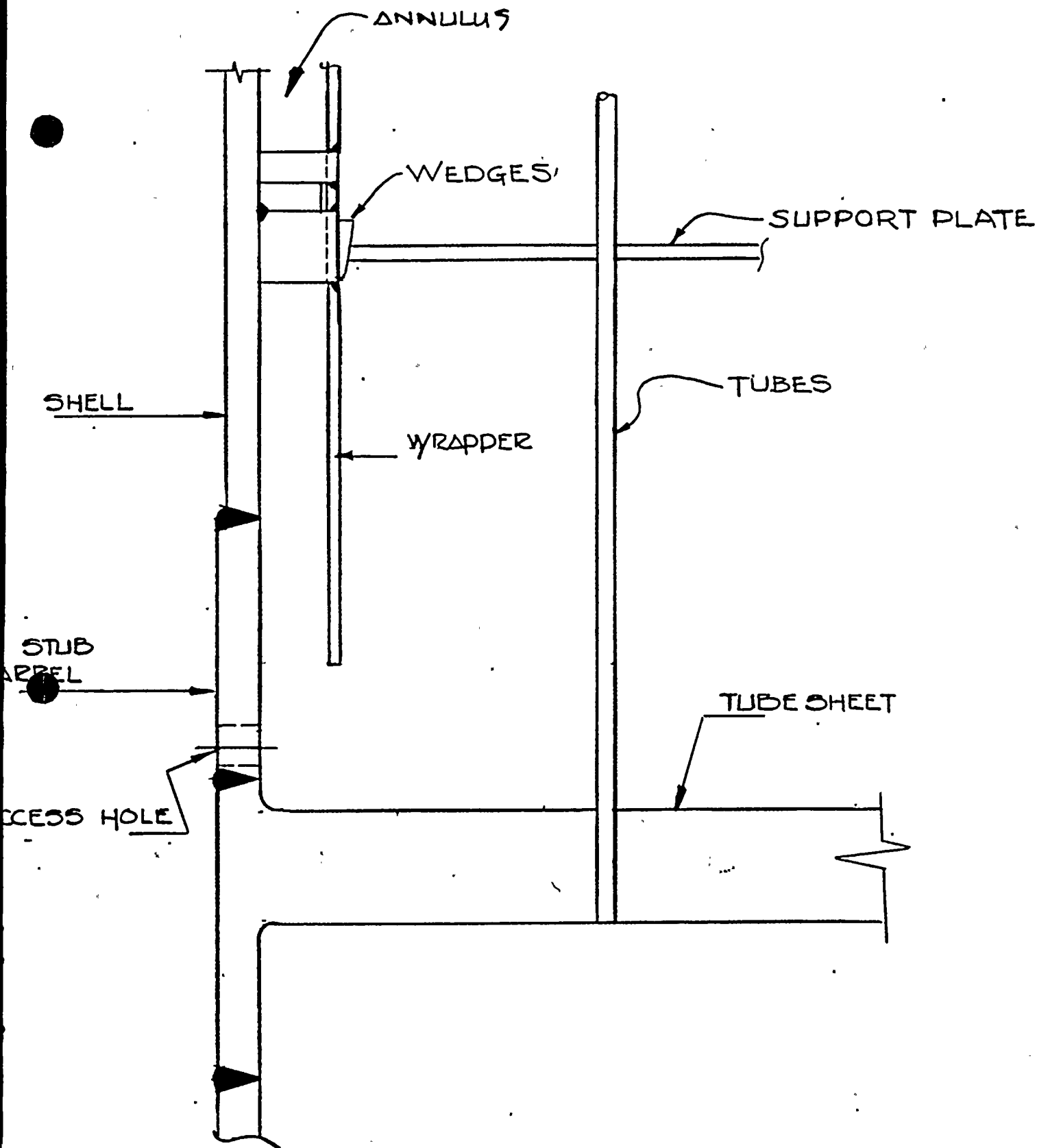
Activity	Man-rem
1) Initial investigation of B-Steam Generator. This involved opening both primary and secondary sides of the generator, ECT of hot and cold legs, plugging 21 tubes, sludge lancing and closing the primary side.	53.668 (a)
2) Fiber optic and video-camera examination of the secondary side of the generator.	32.209 (a)
3) Procedure EM-306. This involved second sludge lancing, opening and hydro-lasing the steam spaces, cutting the wrapper, third sludge lancing, and setting up the platform and water shielding on the handhole area.	37.628 (a)
4) Drilling the first 3 inch port, in the Number 4 wedge area.	14.533 (a)
5) Cut and remove tube samples through the 3 inch port (EDM cuts).	8.841 (a)
6) Shield the U-tube bundle, cut and remove 1 tube from the top.	21.645 (a)
7) Drilling the second 3 inch port, in the Number 6 wedge area.	13.097 (a)
8) Fiber optics and video-camera evaluation of generator prior to closing.	2.923 (a)
9) Close out for generator fill. Involves removing lead from the U-tube bundle, modifying the seal scaffold, putting the wrapper cut-out in place, and closing the secondary side.	11.340 (a)
10) Following partial completion of secondary modifications, set up for lower removal of damaged tubes between the tube sheet and the first support plate.	.800 (a)
11) EDM and router cuts and removal of damaged tubes in the Number 4 and Number 6 wedge areas.	23.000 (a)
12) Machining of a radius on the inside of the Number 4 and Number 6 wedge holes.	1.470 (a)
13) Vacuuming, fiber optics and camera inspection of the B-Steam Generator tube sheet.	1.500 (a)

TABLE 5.1 (Continued)

Activity	Man-rem
14) Mechanical plug removal set up.	3.835 (a)
15) Mechanical plug removal.	15.650 (a)
16) Stabilization of U-Bends and unsupported tube.	12 (e)
17) Eddy current test periphery area.	12 (e)
18) Alignment check - laser.	2 (e)
19) Reinstall wrapper patch.	15 (e)
20) Water lance.	7.5 (e)
21) Final video camera inspection.	6 (e)
22) Final closeout. Includes removal of scaffolding from steam space, and closure of all channel head and secondary openings, dismantling platforms and removal of water shields and lead.	10 (e)
Total	306.7 (e)

(a) - actual

(e) - estimated



O	ORIGINAL	INITIAL DATE			
NUMBER	REVISION	DRAWN BY	CHECKED BY	RESP. ENG.	ENG. MANG'R.
ROCHESTER GAS & ELECTRIC CORP. ROCHESTER, NEW YORK		"B" STEAM GENERATOR 3" ACCESS HOLE		SCALE NO.	

GINN STATION
B-STEAM GENERATOR
NO. 4 WEDGE AREA

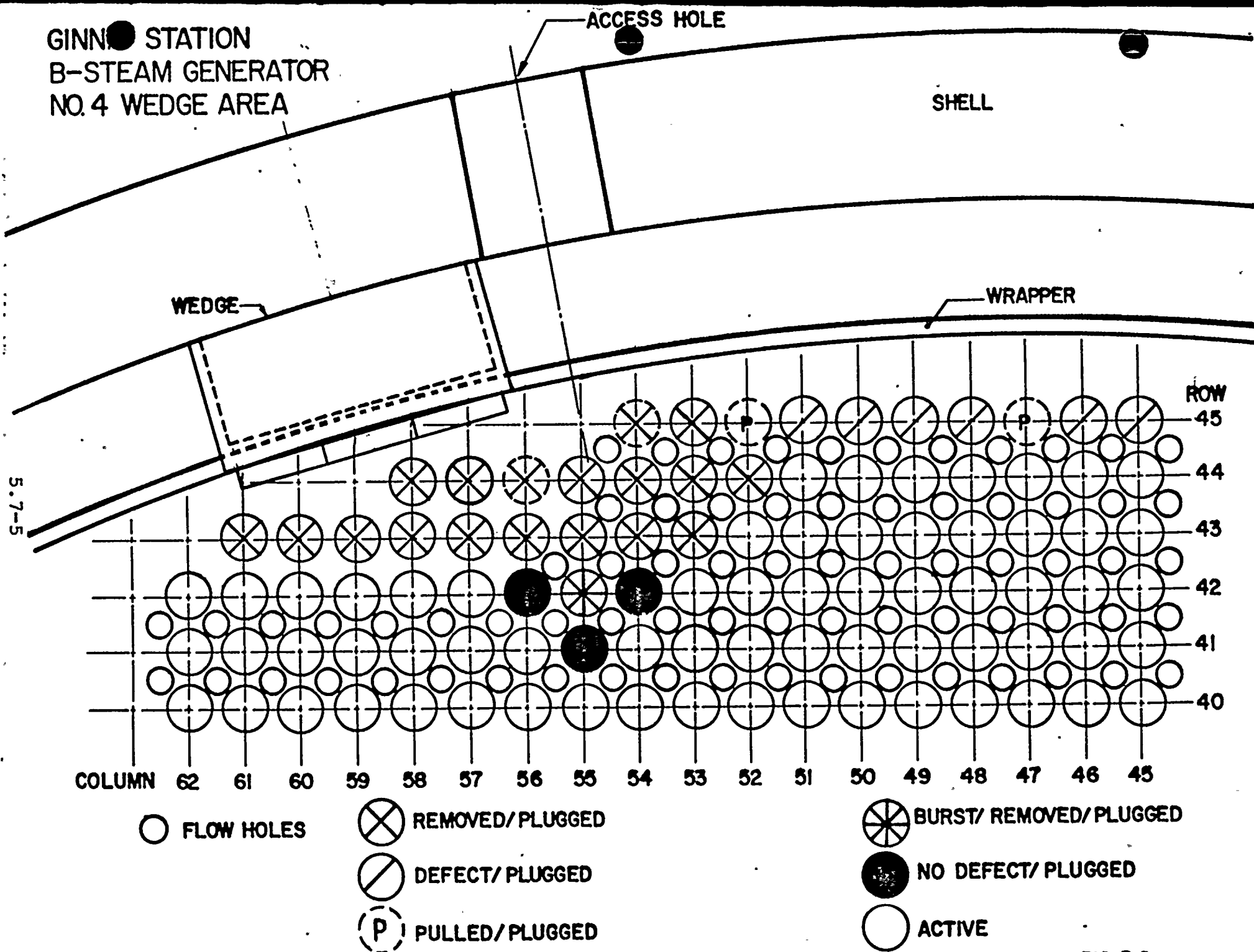


FIG. 5.2

INNA STATION -STEAM GENERATOR O. 6 WEDGE AREA

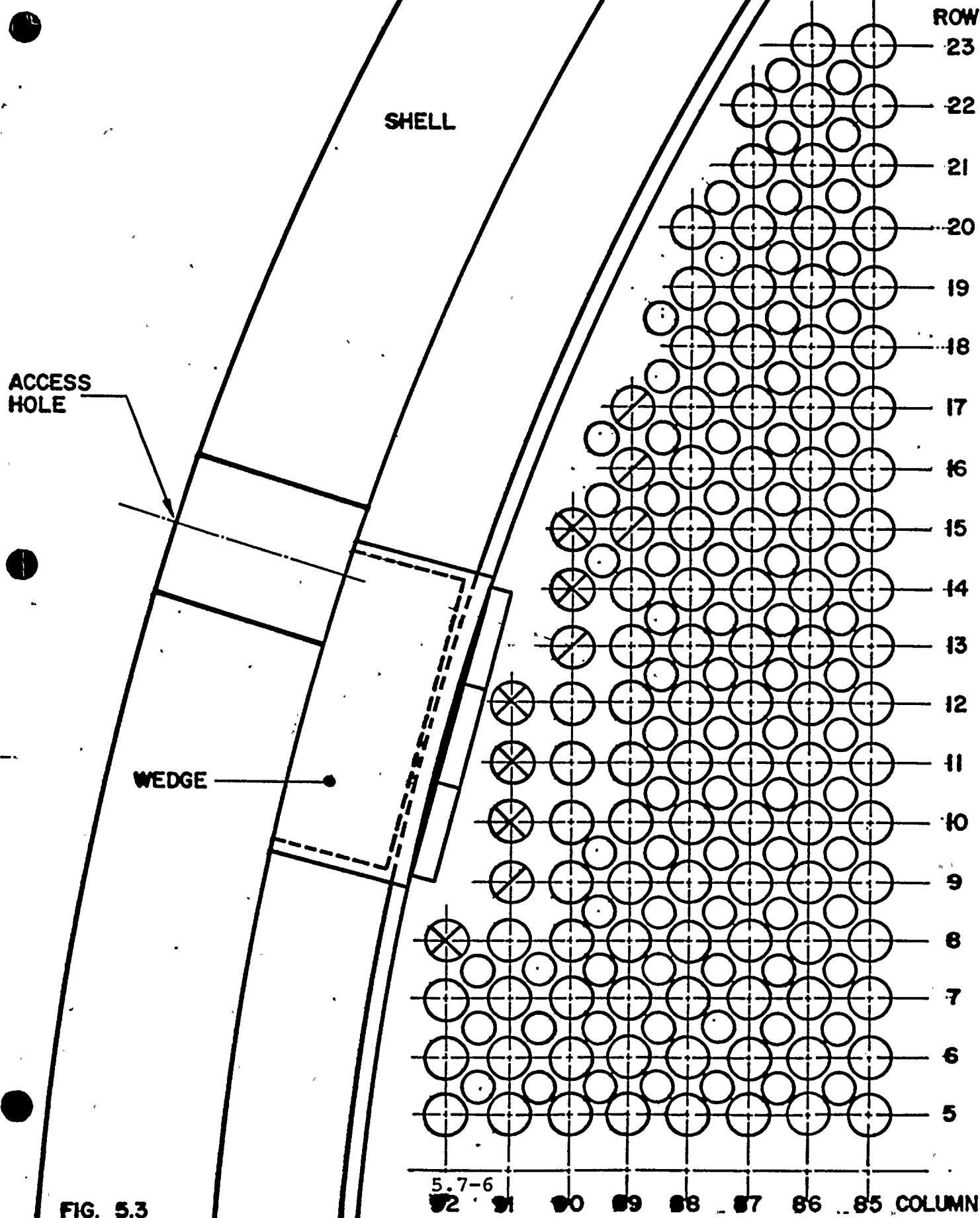
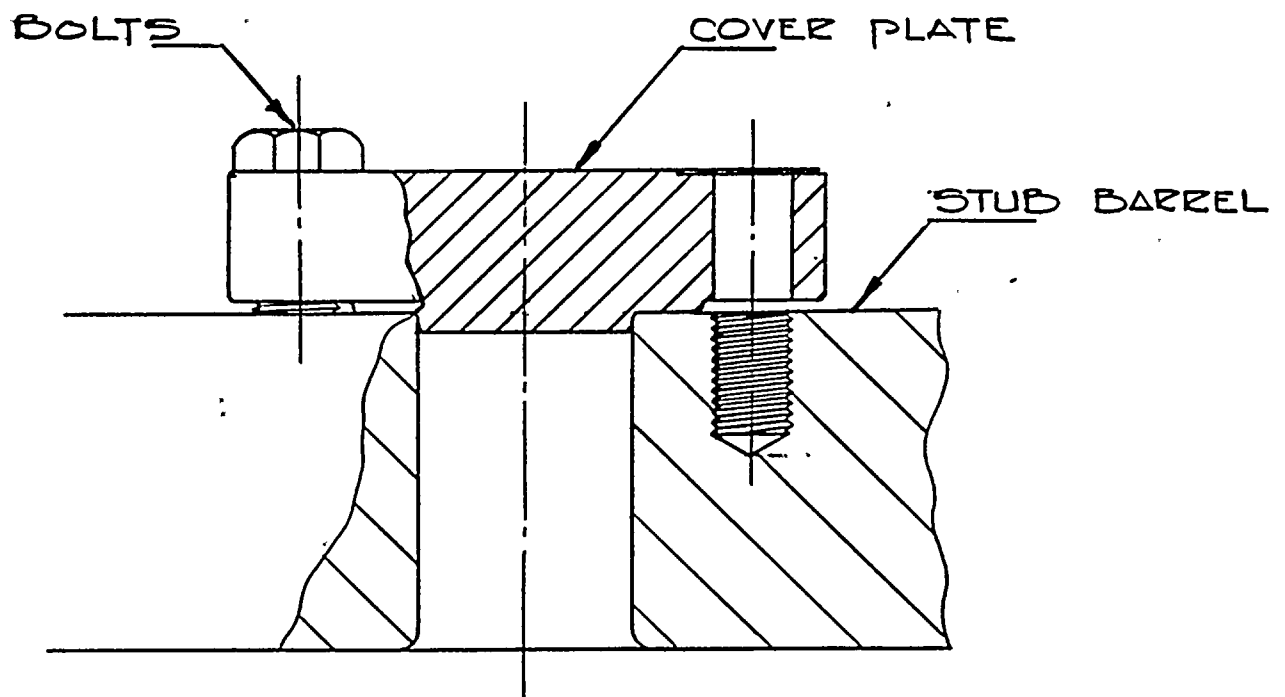
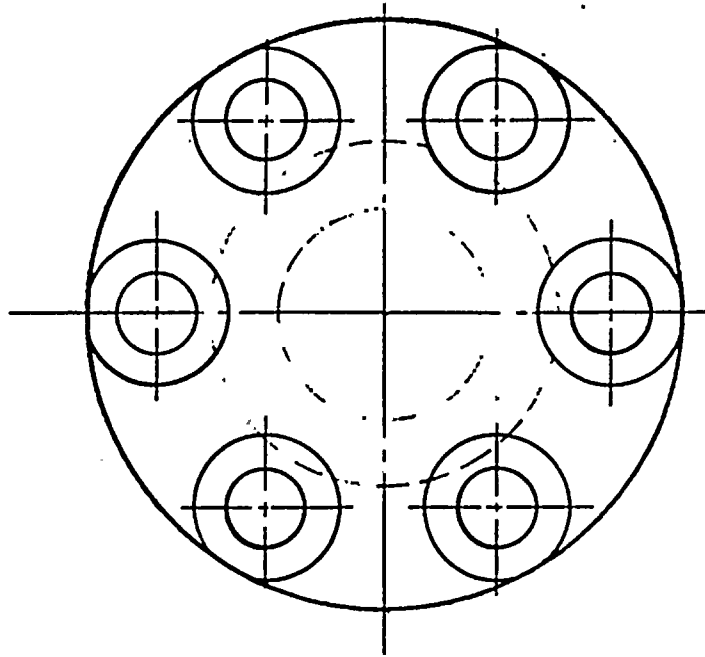


FIG. 5.3



ORIGINAL	INITIAL DATE				
NUMBER	REVISION	DRAWN BY	CHECKED BY	RESP. ENG.	ENG. MANG'R.
ROCHESTER GAS & ELECTRIC CORP. ROCHESTER, NEW YORK		B STEAM GENERATOR ACCESS HOLE COVER		SCALE NO.	

N.H.S. 70 1183

FIGURE 5.4
5.7-7

FIGURE 5.5

GINNA STATION
B-STEAM GENERATOR
CATEGORIZATION OF DEFECTS

CATEGORY.	NO. 6 WEDGE AREA	R40C70 AREA	NO. 4 WEDGE AREA			NO. 2 WEDGE AREA
1. Structurally Degraded	R8C92 R10C91 R11C91 R12C91 R14C90 R15C90		R42C55M R43C53 R43C54M R43C55M R43C56M R43C57 R43C58	R43C59 R43C60 R43C61 R44C52 R44C53M R44C54	R44C55M R44C56 R44C57 R44C58 R45C53 R45C54	
2. Video OD Indication	R9C91 R13C90 R16C89 R17C89	R38C71 R38C72 R39C68 R39C69 R39C70	R45C51			
3. Eddy Current Signal	R15C89	R35C75 R40C67 R40C68 R41C66	R45C46 R45C47M R45C48 R45C49 R45C50			R12C2 R28C12 R30C15 R31C15 R32C15 R32C16 R33C15
4. Preventatively Plugged			R41C55 R42C54 R42C56			
TOTALS	11	9	28			7

M Metallurgical Samples

R45C52 pulled April 1978.

6.0 Technical Basis for Repairs

6.1 Introduction

This section provides details of an analytical evaluation to verify the acceptability (and compliance to the ASME Code requirements) of the Ginna B-Steam Generator. The pertinent analyses and evaluations are described in the following sections.

6.2 Analyses

The following analyses were performed in support of the repair program:

- a) Access holes: Structural analyses of the secondary shell for the two 3-inch diameter access ports were performed to verify the Code acceptance of the shell subject to the applicable loading requirements in the Equipment Specifications. Based on these analyses, the access ports are structurally acceptable.
- b) Thermal/Hydraulic evaluation: Thermal/hydraulic analyses were performed to determine the type of flow redistribution due to the removal of structurally degraded tube spans on the hot leg periphery and to examine the effect of the flow redistribution on the fluid induced vibration characteristics of the remaining tubes. Based on detailed analyses, it is shown that the maximum tube gap velocity is increased by approximately 12 percent; however, the modification is structurally acceptable since significant margin exists for both the fluid-elastic stability ratio and vibrational stresses due to cross-flow turbulence.
- c) Structural evaluation: An evaluation was performed to address the structural acceptability of plugged tubes with visual surface irregularities such as small scars or stress risers. The evaluation considers both the fatigue margin under operating transients and collapse integrity of such a tube. Additionally, the geometric stability of tube(s) severed just below the first tube support plate is also examined. Results of the evaluations indicate that plugged tubes with minor surface irregularities and tubes severed just below the first support plate are structurally acceptable and can be left in the tube bundle.

Details of the above three analyses are given separately in the following subsections.

6.2.1 Access Ports

A structural analysis of the 3-inch diameter access ports was performed. The ports are located on the secondary side of the steam generator just above the tube sheet secondary surface. The location of the two ports is shown in Figure 6.2.1-1.

The geometry of the access port was modeled using the WECAN computer code, Reference 6.2-1. Three-dimensional isoparametric elements were used for the shell and cover and beam elements were used for the bolts. Plots of the finite element model are shown in Figure 6.2.1-2.

The loadings and loading conditions were obtained from the Ginna Equipment Specification. The specific loadings applied to the finite element model include internal pressure, thermal transients, tube sheet interaction with the stub barrel, and bolt preload. The stresses from these loads were combined per the E-Spec requirements and compared to the ASME Code Section III allowable values.

The results of the analysis are summarized in Table 6.2.1-1. As shown in the table, all of the ASME Code requirements are met. The design of the 3-inch diameter access ports is therefore structurally acceptable.

6.2.2 Thermal-Hydraulic Evaluation

6.2.2.1 Purpose

The removal of tubes from the periphery of the hot leg tube bundle between the tube sheet and the first support plate will lead to flow redistribution. The flow velocities resulting from this flow redistribution must be evaluated to determine if flow induced loads on the tubes around the tube removed region are significantly affected.

The CHARM computer program (Reference 6.2-2) was used to perform a thermal-hydraulic analysis in the region of the tube bundle between the tube sheet and the first support plate. Three cases were considered: a) nominal, which will be the same as previously presented in Section 4.5.2, b) one block of tubes removed from the periphery of the bundle, and c) two blocks of tubes removed in the periphery of the bundle. Case b is most representative of the proposed tube removal (≈ 80 tubes); Case c may be considered a very conservative upper bound. The CHARM analysis was performed in the plane of symmetry perpendicular to the tube lane which divides the hot and cold legs into equal halves. At nominal conditions, there is no flow across this plane.

Because the CHARM analysis was two-dimensional (axial and radial), a separate three-dimensional hydraulic analysis was performed of the tube sheet-to-first support plate region with the WECAN hydraulic conductance element (Reference 6.2-1). The purpose of this analysis was to determine the effect of tube removal on the three-dimensional aspects of the flow distribution. This analysis used a pressure-forced boundary condition.

6.2.2.2 Analysis

The CHARM model used in the present analysis is basically the same as that described in Section 4.5.2 (see Figure 4.5.2-1). The only difference is that, to simulate tube removal, the flow resistances in the tubes-removed region were set equal to zero as well as setting the heat loads to zero. Thus, in columns two (and three for Case c) both the heat input and flow resistances were set equal to zero, whereas in columns 20 (and 19 for Case c), only the heat load was set equal to zero. (See Figure 4.5.2-1.)

The WECAN hydraulic conductance is basically the same as that discussed in Section 4.5.2. For those flow paths which connect the tube-removed region to the other parts of the model, the hydraulic conductances were altered to reflect the fact that the removal of tubes effectively decreases the flow resistance to zero over that part of the flow path. As in the plugged tube case of Section 4.5.2, the deadwater region above the wrapper opening was simulated by setting the axial hydraulic conductances in this region to very small numbers.

6.2.2.3 Results

Figures 6.2.2-1 through 6.2.2-4 show the CHARM lateral and axial velocity values and velocity vector plots for the one block of tubes removed and two blocks of tubes removed cases, respectively. As discussed in Section 4.5.2, the axial velocities shown in these figures are between tube axial velocities and need no correction. To convert the lateral or crossflow velocities to between-tube maximum velocities it is necessary to multiply the values shown on the figure by a factor of 2.08 to remove the porosity correction and account for the crossflow blockage presented by the tubes. For conservatism, an additional area ratio factor can be applied to account for the flow area convergence of the radially inward flow.

The 3-D WECAN analysis indicates behavior in the tube-removed region similar to that of the plugged tube region of Section 4.5.2. However, increased hydraulic conductances in the tube-removed region results in a slight increase in the radial flow velocities entering that region, unlike the plugged tube case, where the entering radial velocities decreased slightly below nominal values. Estimates of maximum crossflow velocities therefore included this effect as well as the effects discussed in Section 4.5.2. Otherwise the methodologies are the same. Table 6.2.2-1 gives a summary of the maximum between-tube crossflow velocities for tubes on the periphery of the tube-removed region as well as the face b crossflow velocities of several regions downstream (radially inward).

Figures 6.2.2-5 and 6.2.2-6 show the quality distributions predicted by CHARM for Case b and c. As in the plugged tube case, the main effect here is a shift of the vaporization boundary radially inward and away from the low velocity zone. Conditions just above the tube sheet are quite similar for the nominal, plugged tube and both tube-removed cases.

In summary, the removal of tubes from the periphery of the tube bundle has the following effects:

The major effect of tube removal is the appearance of a reduced fluid velocity field and a low quality region between the wrapper opening and the first support plate in the region where the tubes are removed. This behavior is similar to the plugged tube case in Section 4.5.2. This low velocity region tends to increase fluid crossflow velocities in the region near the wrapper entrance.

The highest between-tube crossflow velocity increases from 9.01 ft/sec in the nominal case to 10.12 ft/sec in the one block of tubes removed case and 10.95 ft/sec in the two blocks of tubes removed case. These are increases of 12.3 percent and 21.5 percent, respectively. Based on analyses presented in Section 4.5, these increases have practically negligible effect on tube loadings and resonances.

6.2.3 Structural Evaluation

The basis of steam generator repair has been to remove all structurally-degraded tubes. This includes tubes with significant reduction in stiffness and frequency due to the loss of cross sectional moment of inertia resulting from collapse, large structural discontinuities in the form of visual notches and cuts, and large holes. On the other hand, tubes with visual surface irregularities due to small ovality and distortion were not removed.

This section addresses the structural acceptability of the tube bundle following the repair effort. Specifically, the following two considerations are examined for a plugged tube with surface irregularities:

- a) Fatigue margin under operating transients, and
- b) Collapse integrity

Additionally, the geometric stability of a tube severed and/or cut just below the first tube support plate (TSP) is also verified. As far as surface damage on an active tube is concerned, it is to be noted that safe operation for an active tube is assured by eddy-current testing in accordance with the applicable tube plugging margin per the Technical Specification limits.

6.2.3.1 Fatigue Margin

Consistent with the repair program objective, it is assumed that all structurally damaged tube spans between the tube sheet and the first TSP are removed as well as all foreign objects. For fatigue evaluation, therefore, only tubing with surface irregularities in the form of cross section distortions and/or surface irregularities need be considered.

As far as thermal mechanical loading on such a tube is concerned, the loads are the same as in the case of a nominally plugged tube described in Section 4.5. Effect of small distortion/ovality would be to increase the hoop bending stress due to the external pressure loading. For example, the maximum hoop stress for a nominally plugged 0.050-inch wall tube under 1000 psi pressure increases from 15.0 ksi at two percent ovality to 25.0 ksi at six percent ovality. This increase in the hoop stress has a relatively insignificant impact on the usage factor. Assuming a 30-year remaining plant life for a six percent oval tube with a design minimum wall of 0.045 inch, a significant fatigue margin exists based on the code calculations in Section 4.5.7 for a notched, plugged tube. Thus, from the view-point of fatigue due to operating plant transients, plugged tubes with surface irregularities are acceptable.

From the viewpoint of hydraulic loading, the effect of tube removal on the maximum tube gap velocity was considered in order to determine the acceptance of such tubing subject to the mechanisms of fluid-elastic stability, turbulence and vortex shedding. Details of thermal-hydraulic

analyses to determine the maximum gap velocities for the before and after tube removal cases were given in the previous section. Table 6.2.3-1 summarizes the results of these analyses. The one block of tube removed case corresponds closest to the post-repair steam generator tube bundle geometry. The expected maximum gap velocity is 10.12 ft/sec, or approximately 12 percent greater than the calculated velocity prior to the tube removal condition.

Based on the results of flow-induced vibration analyses in Section 4.5.6, it is seen that the calculated velocity change has a rather insignificant impact on the fluid-elastic stability, turbulence and vortex shedding responses of a tube with given cross section and under a given boundary condition. The results also indicate that response of a tube with small ovality and/or distortions are essentially the same as those of a nominally round tube. The actual vortex shedding and cross-flow turbulence amplitude of a fixed-fixed tube span with various degrees of localized distortion and subjected to a 10.0 ft/sec cross-flow velocity over the 14.0-inch wrapper opening are summarized in Table 6.2.3-2. Again, the comparison indicates that with the exception of the case of significant tube distortion or collapse, the vibration amplitudes are relatively stable, that is, about the same as the nominal round tube.

6.2.3.2 Collapse Integrity

Inconel-600 tubing typical of PWR steam generators has been extensively tested to determine the effect of local degradation on the external collapse pressure strength of the tubing. Figures 6.2.3-1 through 6.2.3-3 show the results of an NRC-sponsored test program, Reference 6.2-3. These tests were performed on mill-annealed Inconel-600 straight length tubing with nominal 7/8 inch O.D. x 0.050-inch wall placed in a 600 F autoclave, and pressurized externally by water simulating the secondary side steam generator fluid. Local degradations considered in this testing include: (1) elliptical wastage typical of local wear due to tube-to-tube or tube-to-a-foreign object contact, (2) uniform thinning typical of chemical wastage, and (3) EDM slots to simulate axial cracking.

The following is to be noted, based on these test results:

- a) Expected collapse strength of a nominal tube is approximately 5000 psi.
- b) Collapse strength is relatively unaffected by short (length less than or equal to the tube diameter) through-wall cracks.
- c) For tube collapse corresponding to the external pressure of 1020 psi (maximum expected secondary side pressure for the Ginna steam generators) required tube wall degradation is approximately 80 percent for uniform thinning, and greater than approximately 90 percent for localized thinning.

Thus tubes with small surface scars and localized wear have significant margin to collapse. As far as the effect of local tube distortion/

ovality is concerned, it is to be noted that 1) the collapse mode of tube failure results from plastic instability of the tube shell and thus, represents an instantaneous failure mode, 2) of all the design-basis loading conditions for the Ginna steam generator tubing, the maximum secondary side pressure of 1020 psi occurs during normal operation at the hot standby condition.* In other words, plant operation (at hot standby) in itself represents a proof collapse test. Therefore, tubes with local distortions have ovality below the threshold of plastic instability and consequent collapse. In the absence of any external mechanism, these tubes are expected to remain stable during subsequent operation.

6.2.3.3 Geometric Stability of Cut/Severed Tubes

The degraded tube sections between the tube sheet and the first TSP are removed by cutting the tube spans near the top of the tube sheet and 2 to 4 inches below the first TSP. Additionally, a small number of tubes had their lower spans severed (due to fatigue) just below the first TSP. It is imperative that the geometric stability of the remaining partial tubes, as schematically shown in Figure 6.2.3-4, be assured by verifying that the broken legs will be confined within the TSP.

The broken leg of the tube can move axially with respect to the confining TSP as a result of both the mechanical pressure loads in the tubing as well as thermal growth mismatches. The following summarizes the worst case loadings and relative motions.

o Worst Case Pressure Loading

Subject to the 2560 psi maximum primary pressure differential during a postulated feedline break condition, the maximum broken leg motion, δ , is calculated assuming the broken tube is coupled rigidly to the tube bundle at the U-bend. Using the largest radius tube bend,

$$\delta = p A_f L / A_m E = 0.14 \text{ in}$$

where p = inside pressure differential
 A_f = flow area inside the tube
 A_m = tube metal area
 L = length of largest tube
 E = Young's modulus

The maximum calculated stretch of 0.14 inch is significantly less than the TSP thickness of 0.75 inch. Hence, the broken tube end will remain confined within the TSP.

* Secondary side hydro test, although at a pressure somewhat higher than the hot standby pressure of 1020 psi is not critical due to the offsetting effect of higher yield strength at the lower temperature of secondary hydro.

o Thermal Growth Mismatches

Thermal growth mismatches due to tube-to-tube and tube-to-shell interactions during various thermal transients can result in motion of the broken tube leg relative to the TSP.

For a total pull-out through a 0.75-inch thick TSP, a required thermal differential of $T = 1900^{\circ}\text{F}$ is calculated assuming a constant expansion coefficient at 600°F . Compared to the required $T = 1900^{\circ}\text{F}$ for the pull-out, the maximum expected ΔT during normal operating and postulated LOCA transients are less than 100°F and 400°F , respectively. Thus, a significant margin to pull-out exists due to thermal growth mismatches.

In addition to the above direct axial movements, the broken tube end can move axially also due to lateral tube deflection resulting from seismic and flow-induced vibrations. However, for the tube span between the first and second tube support plates, the vibration amplitudes are very small. Consequently, no significant axial movement of the broken tube will result.

6.2.3.4 Conclusions

Based on the discussions above and the results of analyses presented in Section 4.5, the following conclusions are applicable to the post-repair structural integrity of plugged tubes with slight surface irregularities in the form of small scars, local wear and distortion.

Fluid-elastic stability, vortex shedding and turbulence responses are practically unaffected by small distortions and surface irregularities. Removal of tubes has no adverse impact on remaining tube stability due to fluid interactions. For surface degraded tubes, acceptable fatigue margin exists for subsequent operation. Plant operation being a proof collapse test, structurally stable tubes will remain stable during subsequent operations. Tubes severed at the first TSP are geometrically stable and cannot pull out of the plate due to operating and faulted transients.

The safety and integrity requirements of active tubes are satisfied by existing Technical Specification limits for steam generator tubing.

References for Section 6.2

- 6.2-1 WECAN - Westinghouse Electric Computer Analysis User's Manual, Second Edition, March 1981.
- 6.2-2 A. C. Spencer, "Method of Characteristics for Solving Two-Dimensional Reactor Core Flows," Proceedings of the 1973 Conference on Mathematical Models and Computational Techniques for Analysis of Nuclear Systems, CONF-730414-PI(ANS), 1973, pp. III-3 to III-22.
- 6.2-3 Vagins, M., et.al., "Steam Generator Tube Integrity Program - Phase I Report," NUREG/CR-0718, September 1978.

TABLE 6.2.1-1

STRESS SUMMARY FOR 3 INCH DIAMETER ACCESS PORT

<u>Load Condition</u>	<u>Ratio of Maximum Stress to Allowable Stress</u>		
	<u>Bolt</u>	<u>Cover</u>	<u>Shell</u>
Design	0.63(1)	0.29(3)	-- (6)
Normal and Abnormal	0.65(1)	<1.0	1.01(5)
	0.98(2)		
Test	0.65(1)	0.29(3)	-- (6)
	0.62(2)		
Fatigue Usage Factor	0.85(4)	0.00	0.16
Bolt Replacement Interval	8 years	--	--

Notes: (1) Average Service Stress

(2) Maximum Service Stress

(3) Primary Membrane Plus Bending

(4) Fatigue usage factor based on specified replacement interval

(5) Acceptable per Code. A simplified elastic - plastic analysis was invoked for the fatigue evaluation.

(6) Primary stress limits are satisfied by Code rules for opening not requiring reinforcement.

TABLE 6.2.2-1
BETWEEN-TUBE CROSSFLOW VELOCITIES IN AND NEAR
THE TUBES REMOVED REGION

<u>Location</u>	<u>Crossflow Velocity (nominal)</u>	<u>Crossflow Velocity (1 block of .. tubes removed)* ..</u>	<u>Crossflow Velocity 2 blocks of .. tubes removed) ..</u>
Perimeter Cell (Face A)	8.2 ft/sec	9.13 ft/sec	9.13 ft/sec
Perimeter Cell (Face C)	8.2 ft/sec	9.13 ft/sec	9.13 ft/sec
Perimeter Cell (Face B)	9.01 ft/sec	10.12 ft/sec	10.33 ft/sec
One Cell in from Perimeter (Face B)	8.54 ft/sec	9.48 ft/sec	10.95 ft/sec
Two Cells in from Perimeter (Face B)	8.21 ft/sec	9.16 ft/sec	10.46 ft/sec

* This case is most representative of the actual tube removal.

TABLE 6.2.3-1

SUMMARY OF MAXIMUM TUBE GAP VELOCITIES
WITH AND WITHOUT TUBE REMOVAL

<u>.....Case.....</u>	<u>Maximum Gap Velocity, ft/sec</u>
Nominal	9.01
One block of tubes removed (6.0 inches on periphery)	10.12
Two block of tubes removed (12.0 inches on periphery)	10.95

TABLE 6.2.3-2

SUMMARY OF VORTEX SHEDDING AND TURBULENCE ANALYSES

- FIXED-FIXED BOUNDARIES
- CROSS-FLOW VELOCITY, 10.0 FT/SEC
- DAMPING RATIO, 0.01

<u>Cross Section of Distorted Zone</u>	<u>Vibration Amplitudes, Mils</u>	
	<u>Vortex Shedding</u>	<u>Turbulence</u>
Cylinder (nominal)	0.77	0.81
10 percent ovality	0.79	0.83
Kidney	0.79	0.83
Flat	2.13	1.53

Vibration amplitude due to vortex shedding and cross-flow turbulence are relatively unaffected by small distortions and surface irregularity.

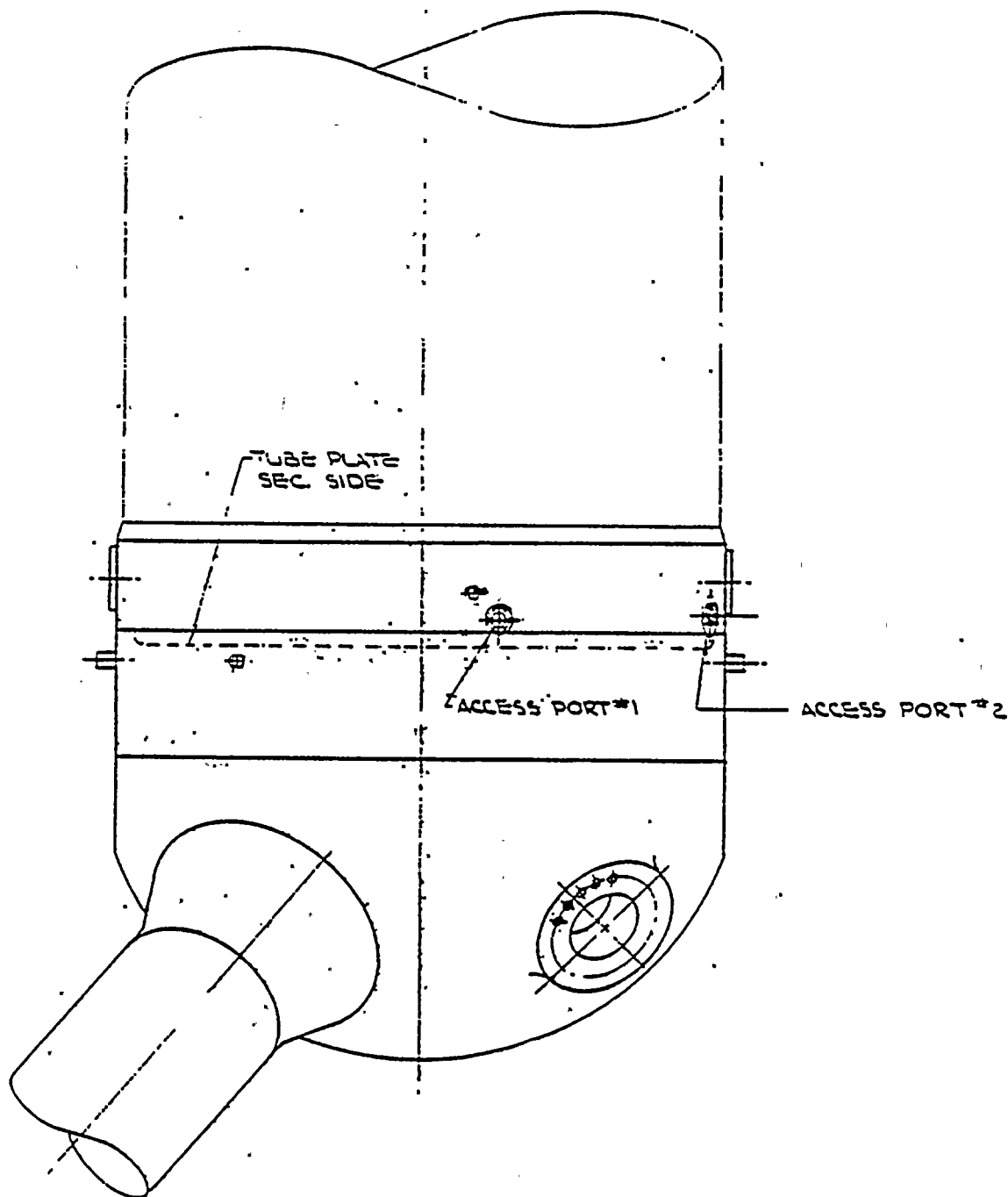
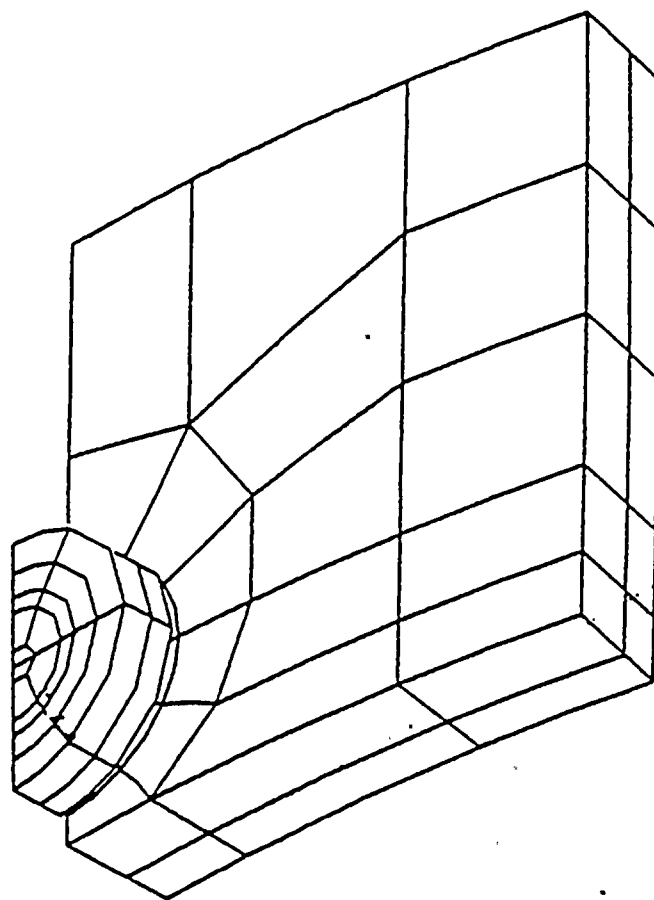
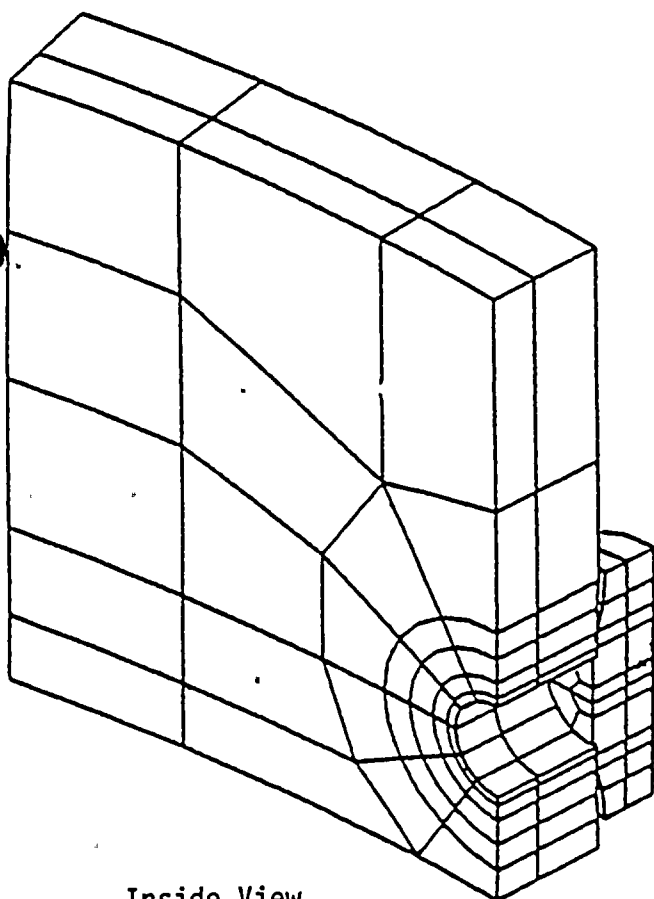


Figure 6.2.1-1: Location of Access Ports





Outside View



Inside View

Figure 6.2.1-2: Finite Element Model

Lateral Velocity
ft/sec + 
Axial Velocity
ft/sec + 

6.2-15

X=	1	2	3	4	5	6	7	8	9
----	---	---	---	---	---	---	---	---	---

Lateral Velocity, $\frac{\text{ft}}{\text{sec}} + \rightarrow$
Axial Velocity, $\frac{\text{ft}}{\text{sec}} + \uparrow$

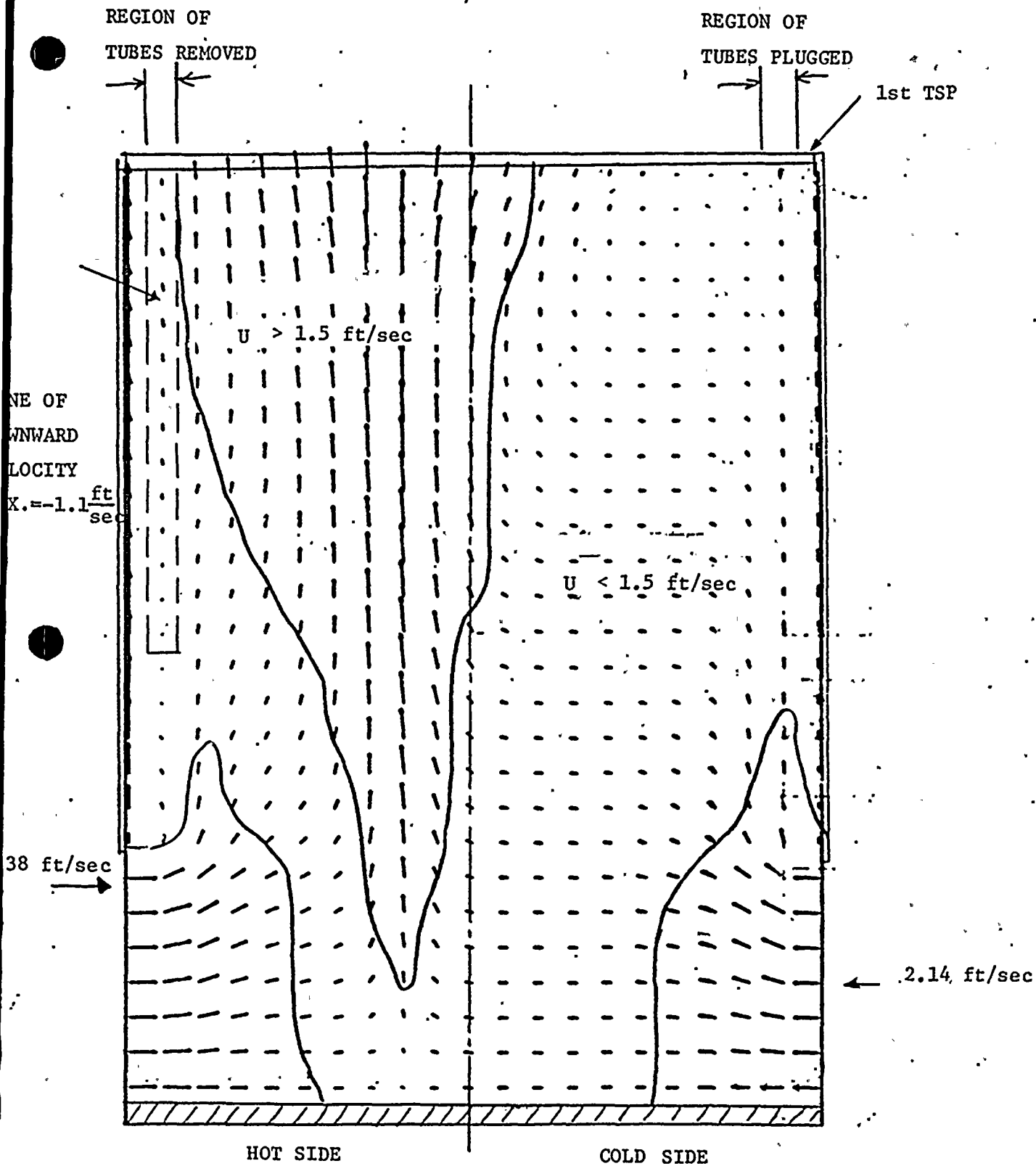


Figure 6.2.2-3. RGE WITH TUBES REMOVED IN COLUMN 2
AND PLUGGED IN COLUMN 20

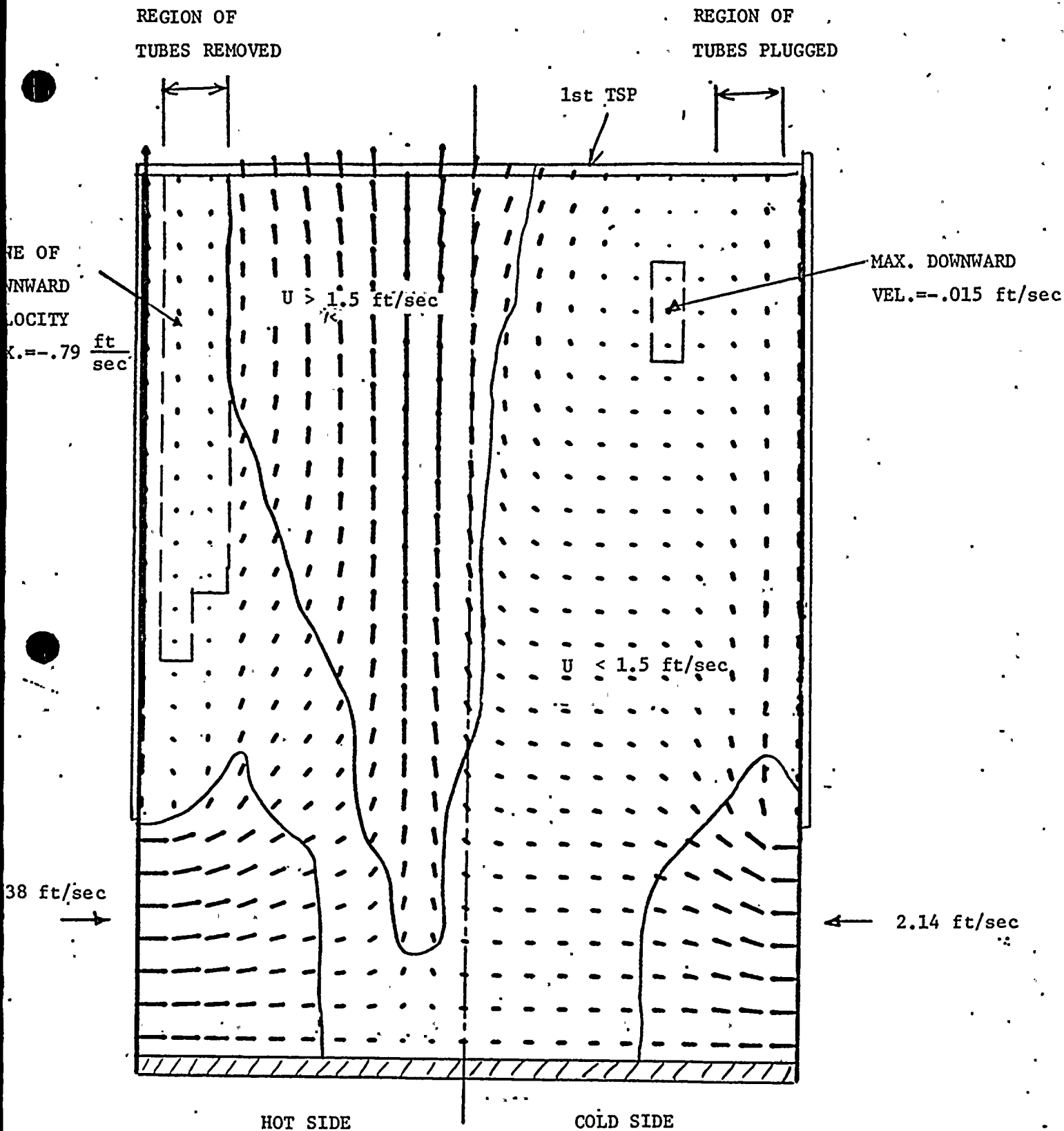


Figure 6.2.2-4. RGE WITH TUBES REMOVED
IN COLUMNS 2 and 3 AND PLUGGED IN COLUMNS 19 and 20

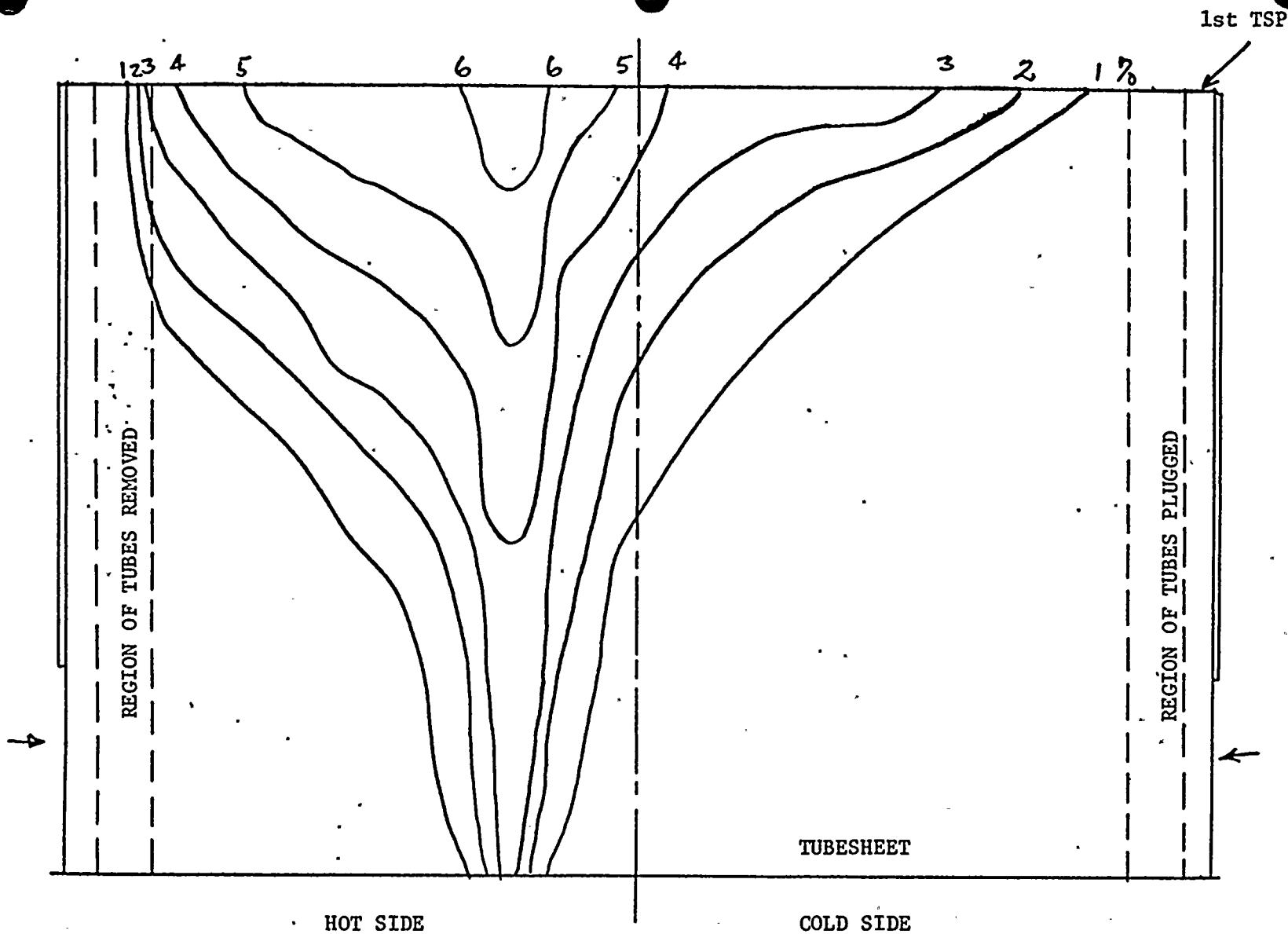


FIGURE 6.2.2-5

QUALITY DISTRIBUTION WITH TUBES REMOVED IN
COLUMN 2 AND PLUGGED IN COLUMN 20

6.2-20

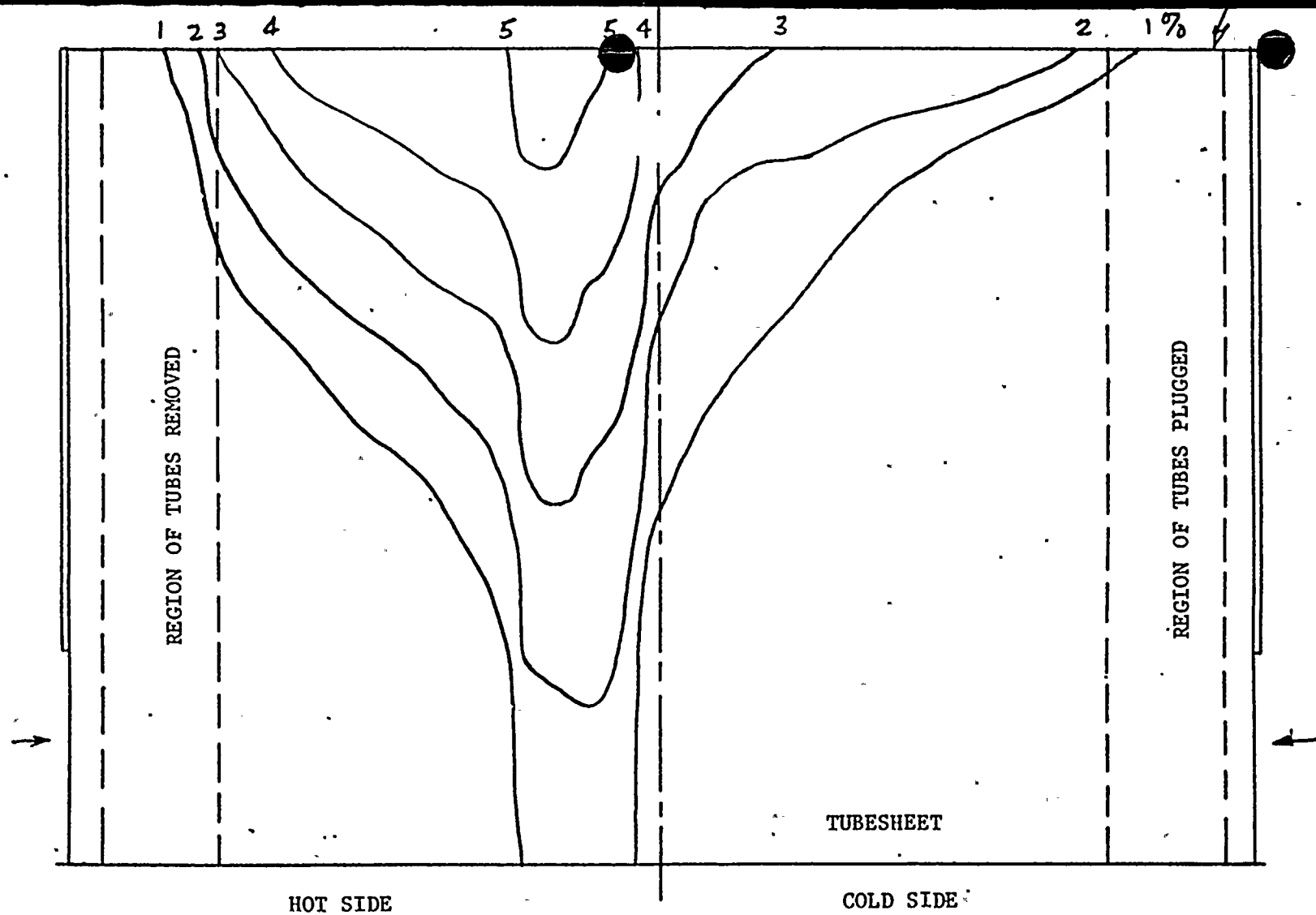


FIGURE 6.2.2-6.

QUALITY DISTRIBUTION WITH TUBES REMOVED IN COLUMNS
2 AND 3 AND PLUGGED IN COLUMNS 19 AND 20

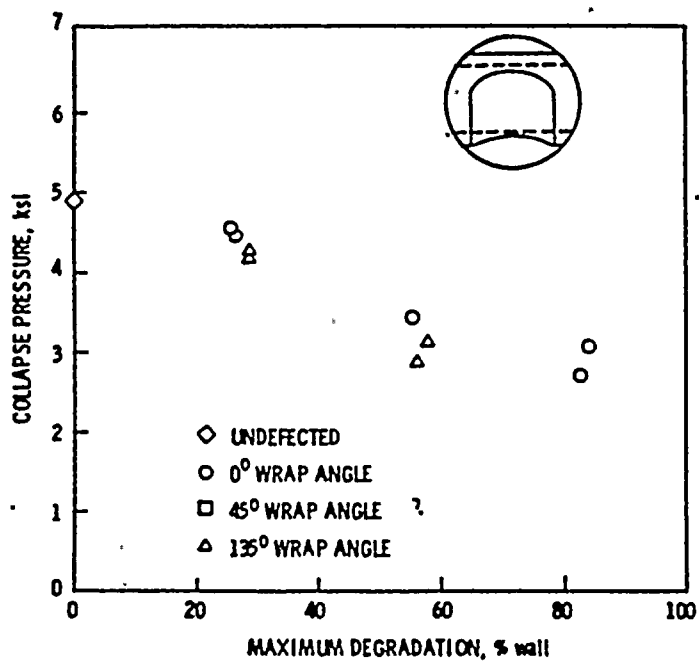


FIGURE 6.2.3-1 Collapse Pressure of Tubing with Elliptical Wastage (from Reference 6.2-3)

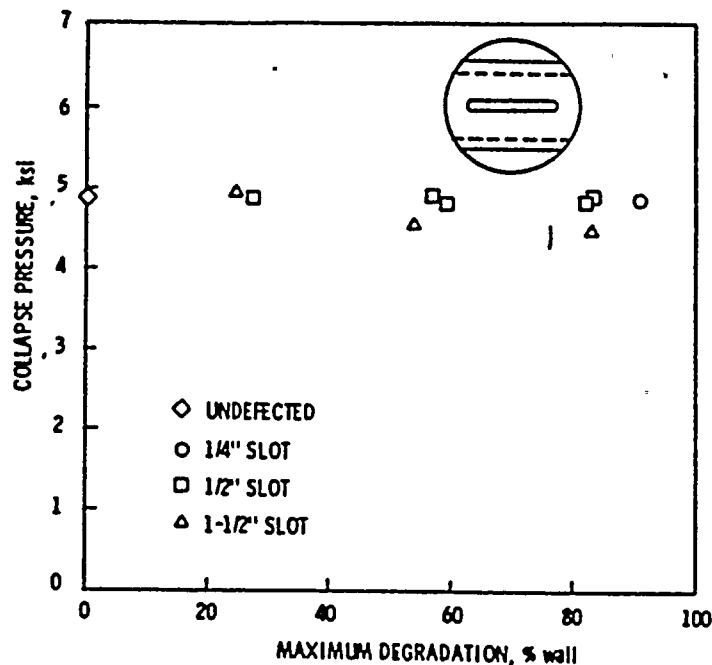


FIGURE 6.2.3-2 Collapse Pressure of Axially (EDM) Slotted Tubing (from Reference 6.2-3)

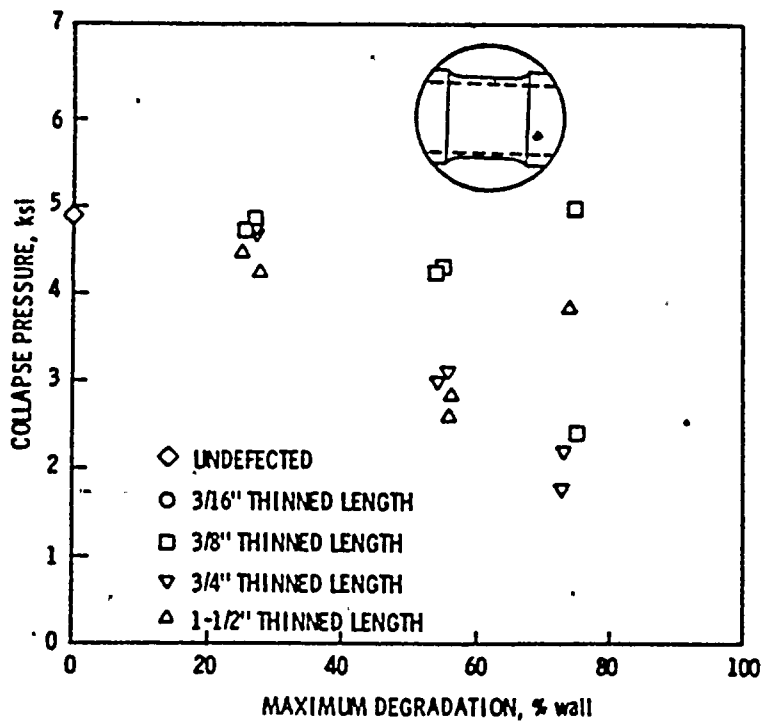


FIGURE 6.2.3-3 Collapse Pressure of Uniformly Thinned Tubing (from Reference 6.2-3)

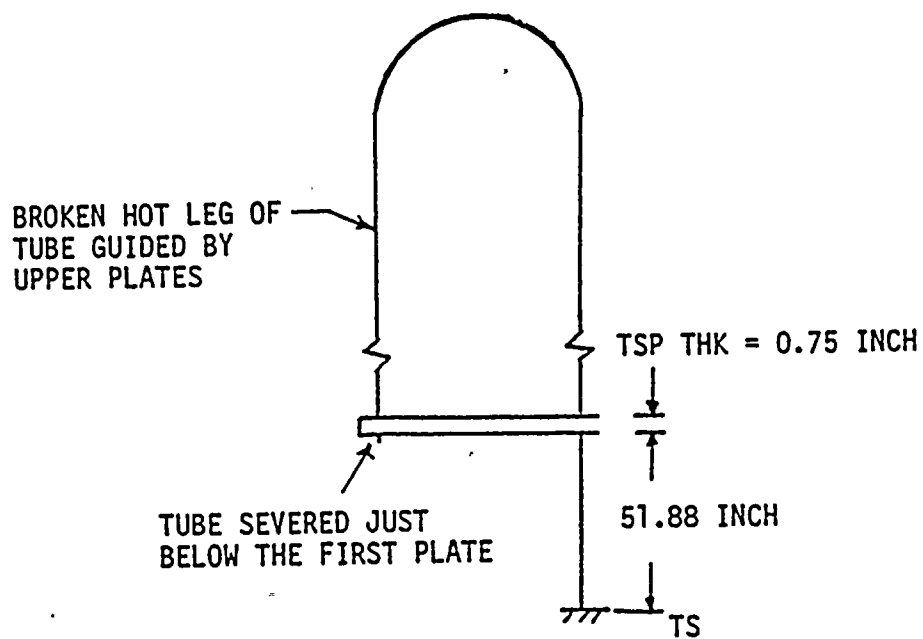


Figure 6.2.3-4 Schematic of a Partial Tube

7.0 FUTURE ACTIVITIES

7.1 Metallurgical Examination

As described in Section 5.2.3, additional tube sections were removed from the B-Steam Generator during the Phase II repairs. Many of these tube sections have been selected for metallurgical examination. This work is presently in progress at Westinghouse and Battelle Columbus. The results of these examinations are scheduled for completion about May 1, 1982. These results will be submitted in an addendum to this report in early May.

7.2 Testing

7.2.1 Westinghouse

As stated in Section 4.7, collapse and fatigue testing is presently in progress at Westinghouse. This testing is scheduled for completion about May 1, 1982. The test results and conclusions will be submitted in an addendum to this report in early May.

7.2.2 Combustion Engineering

Combustion Engineering is presently conducting testing relative to the effects of axial load and loose part impacting on a steam generator tube's propensity for local buckling. The testing is being performed using a model which simulates a single steam generator tube between the tube sheet and first support plate. The test model is capable of applying axial load, peening, and external pressure to the tube. Tube specimens will be eddy current and metallurgically examined following each test cycle. The tests are scheduled for completion in early May.

7.3 Loose Parts Monitoring System

7.3.1 Summary

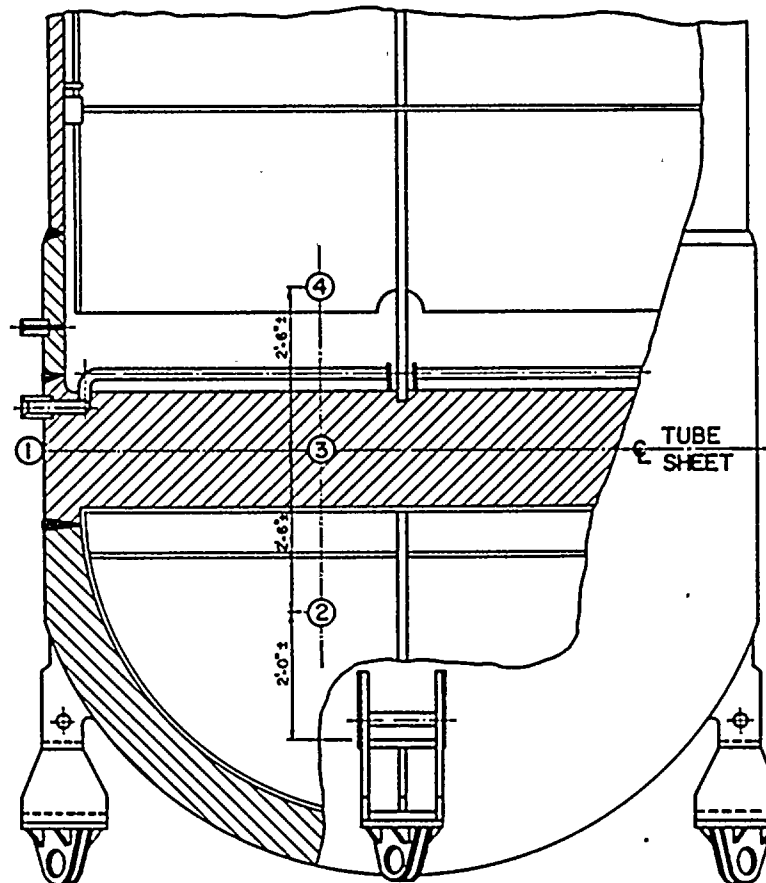
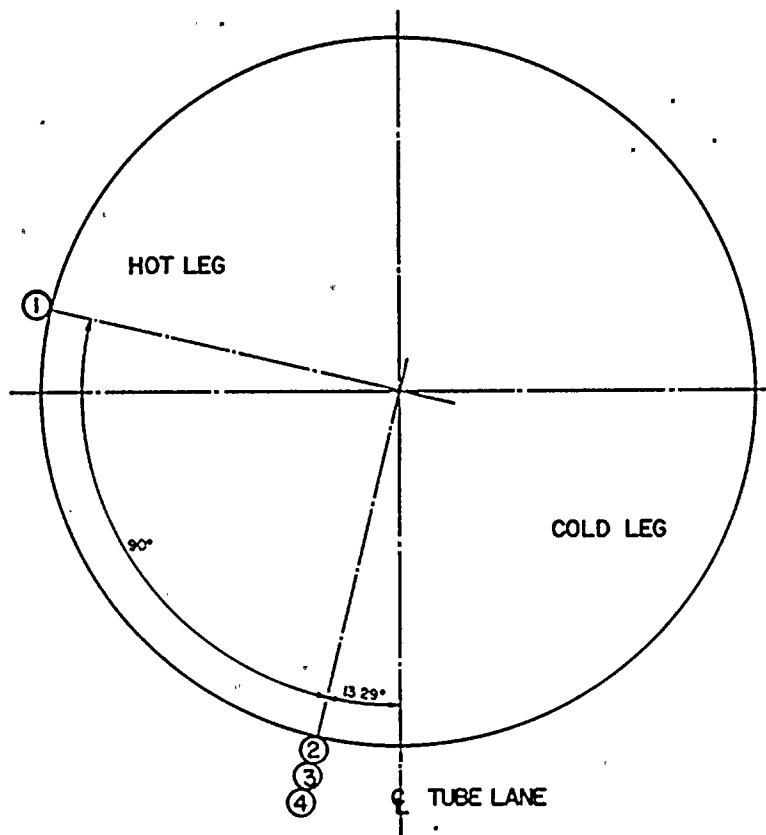
A loose parts monitoring system will be installed on both steam generators at Ginna prior to returning the plant to power operation. The system is intended to provide, within the sensitivity of the instrumentation, indication of foreign objects in either the primary channel heads or secondary side of the tube sheet. The system will be a Westinghouse metal impact monitoring system. The system will include sensors (accelerometers) located on the exterior surface of both the primary and secondary sides of the steam generators. The sensors will be located to allow detection of a loose part in either the primary channel head or on the secondary side of the tube sheet. Figure 7.1 shows the specific location of the sensors. The sensors are capable of detecting acoustic disturbances in the steam generators. The system will be capable of detecting a metallic loose part that weighs from 0.25 lb. to 30 lb. and impacts with a kinetic energy of 0.5 ft-lb on the inside surface of the steam generator within 3 feet of a sensor.

7.3.2 Description

Sensor signals are transmitted to a preamplifier mounted near each sensor. The preamplifiers transmit a signal by shielded cable to a signal processing/data output panel located outside the containment building. The signal processing/data output panel will provide audio and recorder outputs, alarm outputs, and data processing. The alarm output will interface with the plant computer which alarms in the control room. An electrical one line drawing of the system is shown in Figure 7.2. The system will provide automatic, continuous, on line monitoring of the steam generators for loose parts. The system will be tested prior to being placed in service to determine background noise and system frequency signatures as well as the frequency spectrum and on-line sensitivity for metal impacts.

7.4 Intermediate Outage

An intermediate steam generator inspection outage is planned at no more than 120 effective full power days (EFPD) after return to power. During this outage eddy current, fiber optics and video, and visual inspections will be performed. The purpose of these inspections is to assure that the corrective actions taken to preclude further periphery tube O.D. defects have been successful.

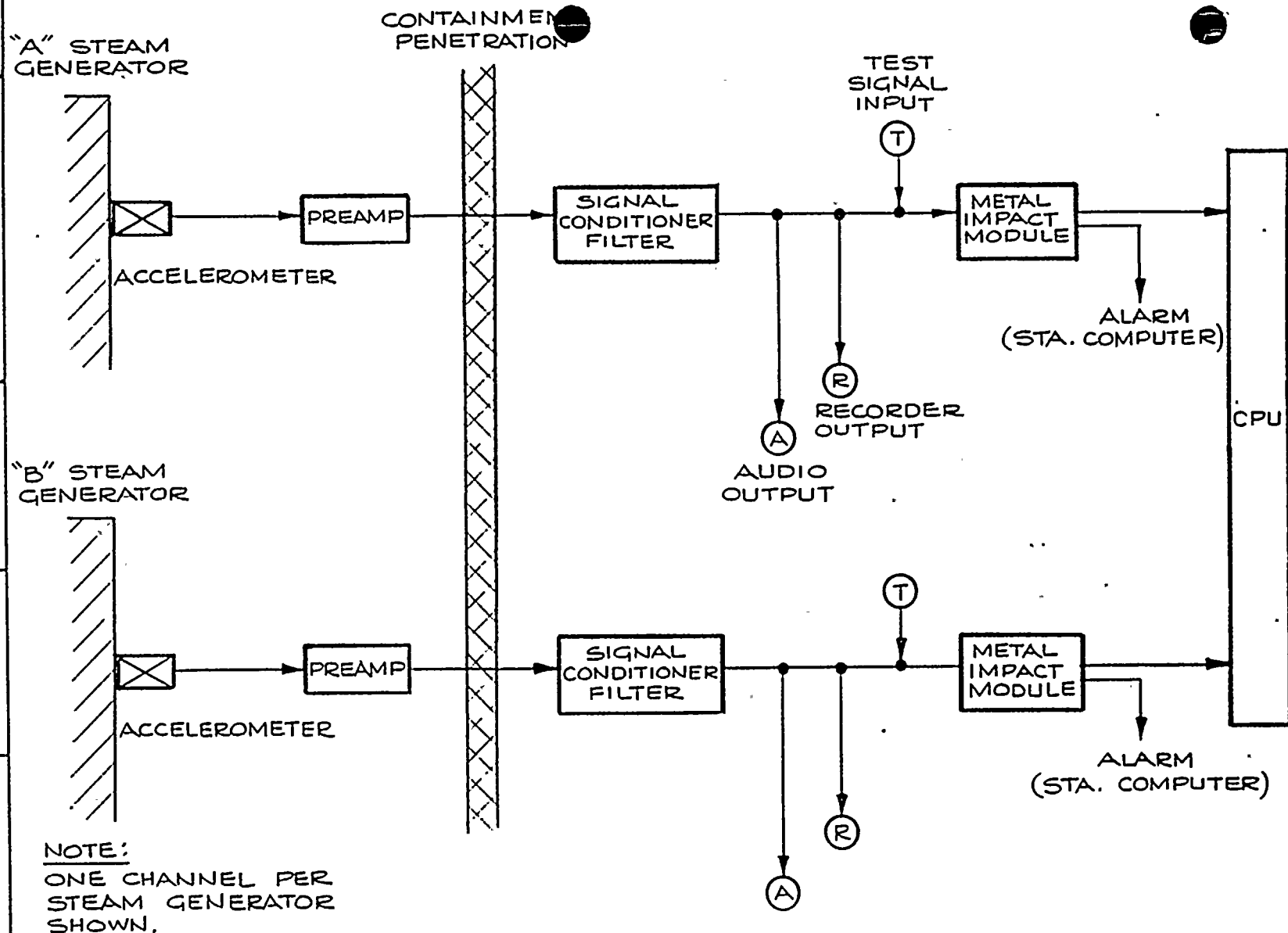


S/G LOOSE PART
MONITOR SENSOR
LOCATIONS

FIGURE 7.1

REV. 4/14/82

	ORIGINAL	INITIAL DATE	EJD 3-12-82		
	REVISION			CHECKED BY	
NUMBER					RESP. ENG.
ROCHESTER GAS & ELECTRIC CORP. ROCHESTER, NEW YORK			ELECTRICAL ONE LINE STEAM GEN/LOOSE-PART DETEC SYSTEM		
			GINNA STATION NO.		
			ENG. MANC'R.		



ELECTRICAL ONE LINE

STEAM GENERATOR LOOSE-PART DETECTION SYSTEM

FIGURE 7.2

APPENDIX A

Metallurgical Examination of Ginna Steam Generator Tubes*

* This report was also submitted
to the NRC by letter dated
April 23, 1982.

Abstract

Detailed microscopic examinations were performed on a section of Row 42 - Column 55 (R42-C55) tubing taken from the hot leg side of the R. E. Ginna "B" steam generator in the region where the tube burst. Five neighboring previously plugged tubes were also examined. All of these Inconel 600 tubes displayed on their O.D. surfaces one or more axially oriented flat zones which contained circumferential striations. Thirty-eight of the forty flat zones that were examined exhibited cold work (O.D.) surface layers, a feature which is consistent with a wear process. The burst in R42-C55 occurred at one of these flats where the wall thickness had been reduced from the nominal 0.050 in. to 0.008 in. Cold work was not identified on the flat that burst. Fractography revealed a normal ductile tensile overload failure at the burst. Fatigue cracking was identified as one mode of breakage of previously plugged tubes. Normal metallurgical properties were identified for the burst tube and for one plugged tube.

1.0 Introduction

On January 25, 1982, a tube ruptured in the "B" nuclear steam generator of the Rochester Gas and Electric Corporation (RGE) R. E. Ginna Power Plant.

The burst tube was determined to be three tube-rows in from the periphery on the hot leg side at Row 42 - Column 55 (R42 C55).

The leak was due to an axially oriented "fish-mouth" opening just above the top of the tubesheet. In addition, some of the previously plugged neighboring peripheral tubes exhibited collapse, deformation, or fracture conditions which were not present at the time these tubes were plugged.

A hole was cut in the shell at Column 55 and nine-inch lengths of the leaking and neighboring tubes were removed. Sections of six tubes were sent to the Westinghouse R&D Center, Pittsburgh, Pennsylvania for metallurgical characterization. These consisted of the leaking tube (R42 C55) and five neighboring and previously plugged tubes (R44 C54, R43 C54, R44 C55, R43 C55 and R43 C56).

2.0 Nondestructive Examinations

Prior to removal of each section from the steam generator, a yellow dot was placed on each section to define the tube surface closest to the perimeter of the generator. In the current examination this dot was taken as the 0° position. Each tube length was received in one or two sections, originally extending from near the top of the tubesheet to ten in. above the top of the tubesheet.

Photographs of the leaking tube from Row 42 - Column 55 (R42 C55) show a "fish-mouth" opening at 0° and axially oriented flats at 0, 60 and 315°. These flats had circumferential striations, Figures 2-1 and 2-2. Photographs in Figures 2-3 to 2-8 are of the neighboring previously plugged tubes: R43 C55, R44 C55, R43 C54, R44 C54 and R43 C56. Similar flats were observed on all tubes at various angular positions. There is extensive metal loss and apparent deformation on all tube sections. Tubes from R44 C55 and R44 C54 arrived in two sections.

Wall thickness measurements were consistent with a nominal 50 mil wall away from the flats and a wall thickness reduction at the flats, Figure 2-9, Table 2-1.

Double wall x-ray radiographs were made of all tube sections at 0, 45, 90 and 315°. A Seifert Industrial X-ray unit was used with the following settings: 5 min. exposure time, 110 to 70 kV, 10 milliamperes, 60 in. source-to-film distance, large focal spot, and Kodak M-8 lead pack film. Wall thickness reductions were easily seen; however, there was no evidence of intergranular attack or stress corrosion cracking.

On tube R44-C55, an EDS analysis on a flat was rich in Al, Si, Cr, Fe, Cu and Zn as compared to Inconel 600, Figure 4-5. The fracture surfaces near the bottom of the tube were not well defined and contained deposits, Figures 4-6 to 4-9.

Other fractographs on R44-C54 indicated that fatigue contributed to the fracture, Figures 4-10 and 4-11.

5.0 Composition and Mechanical Properties of Tubes

An EDS analysis of Section 1A of tube R44-C55 indicated that the principal elements were within specification. The mechanical properties of the Inconel 600 tubing were estimated and tabulated in Table 5-1. Knoop (500 g) hardness readings were made mid-wall on the metallographic mounts 4 inches down on Tubes R42-C55 and R44-C55. These were converted to Rockwell "B", R_B, readings which were then used to estimate yield strength by two methods. One was a correlation established previously on Inconel 600 tubing, Figure 5-2, and the other was an International Nickel Company correlation on Inconel 600 sheet and strip. Reasonable agreement existed between the two conversions: all estimates of yield strength were between 45,000 and 62,000 psi. An estimate of ductility of the Inconel tubing was obtained with bends. Rings 7A, 7B and 7C from Tube R44-C55 and 7A and 7B from tube R42-C55 were used. Each ring was positioned such that a location free of flats between 145° and 225° would be at the apex of a U-bend. The bend was made by placing the ring over a 3/32 in. diameter mandrel with a line of contact at the designated position and deforming the ring at this location around the bar. This strained the O.D. circumference in tension. No fissures were observed on the O.D. surface at the apex and the calculated outer fiber strain was twenty-eight percent.

6.0 Conclusions

1. The microstructure and mechanical properties of the burst tube and a neighboring plugged tube were determined and were normal for the mill annealed Inconel 600 tubing material.
2. There was no evidence of stress-corrosion cracking or intergranular attack on I.D. or O.D. surfaces of any tube.
3. All tubes displayed flat zones of O.D. wall reduction with circumferential striations within the flats.
4. Thirty-eight of the forty flats that were studied showed cold work on the O.D. surface, indicating that a wear process produced the flats.
5. The "fish-mouth" burst occurred at a flat where the wall thickness had been worn to 0.008 in. from the nominal 0.050 in. original wall; cold work was not identified on this flat.

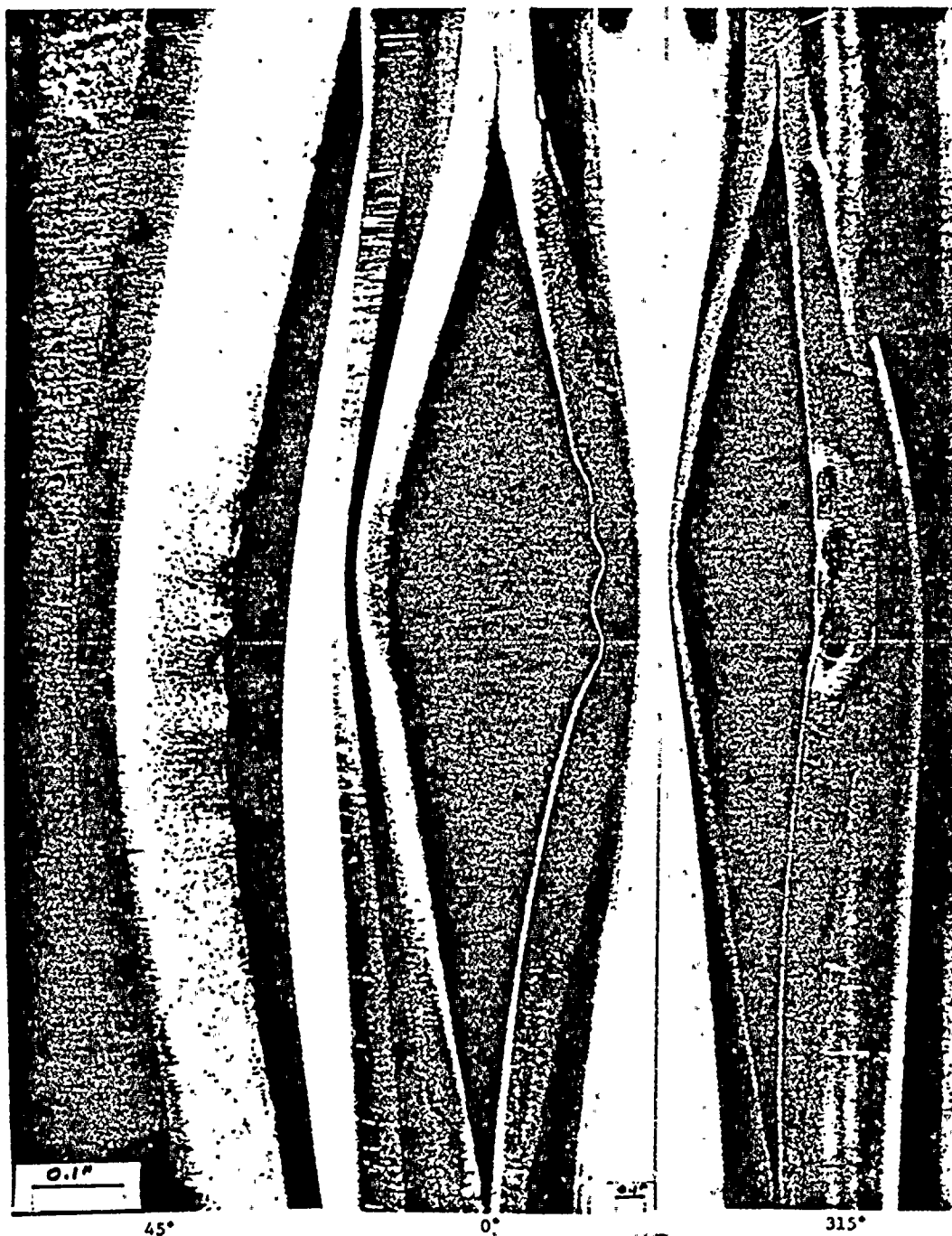


Fig. 2-1. Fish mouth crack at near 0° on Tube R42-C55 from RGE (GINNA), SGB, hot leg

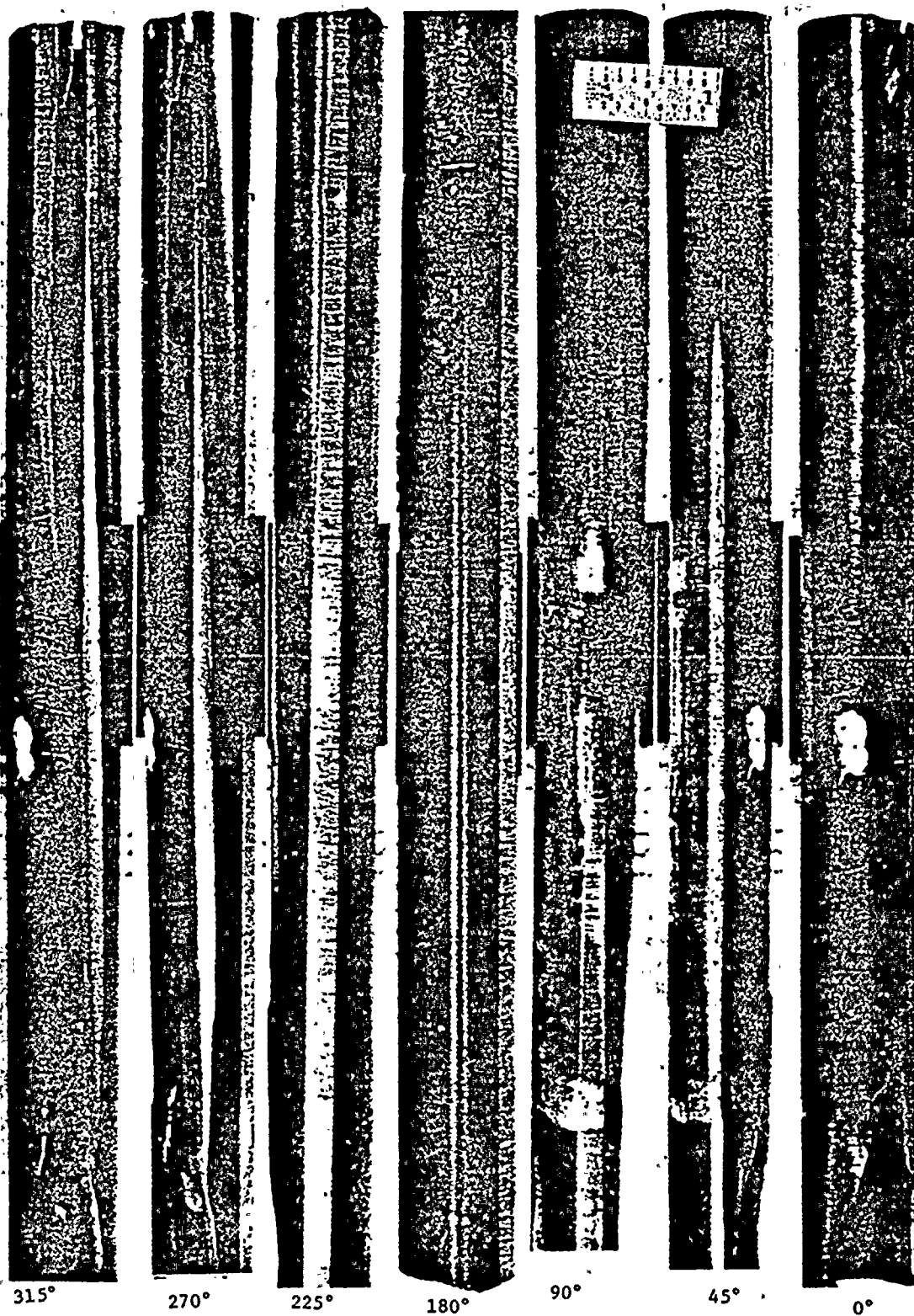


Fig. 2-3. Tube R43-C55 from RGE (GINNA), SGB, hot leg

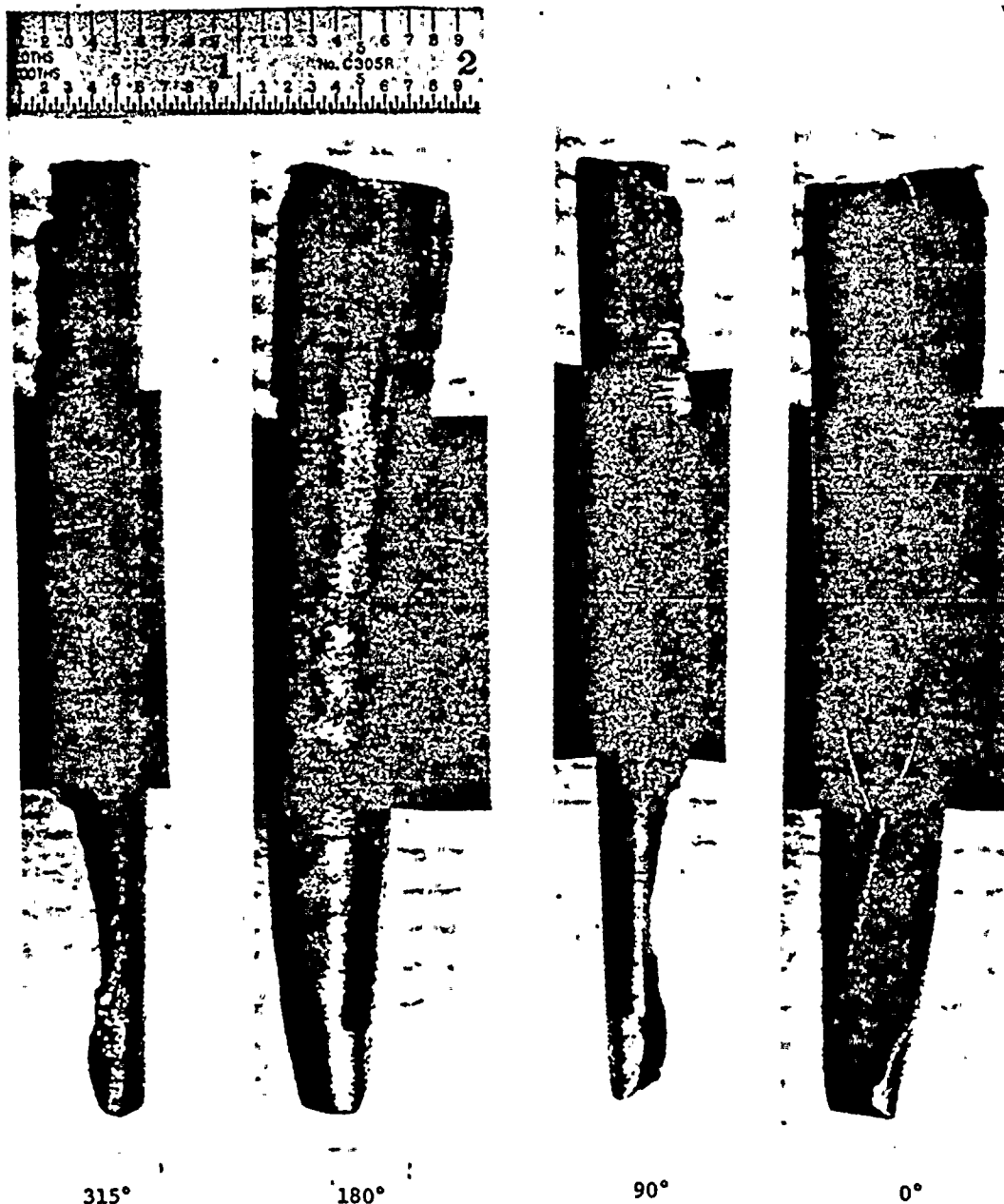


Fig. 2-5. Tube R44-C55 from RGE (GINNA), SGB, hot leg

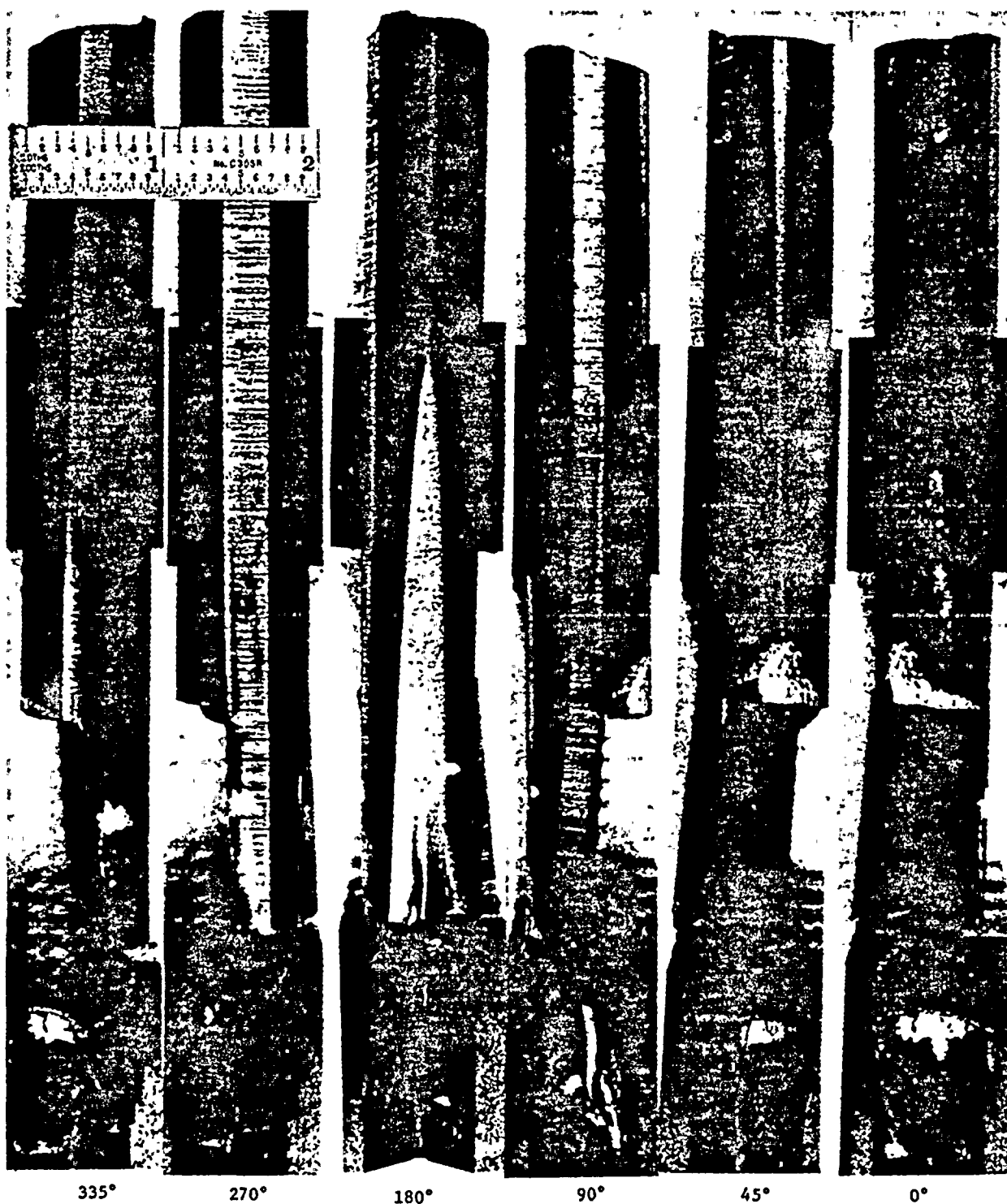


Fig. 2-7. Tube R44-C54 from RGE (GINNA), SGB, hot leg

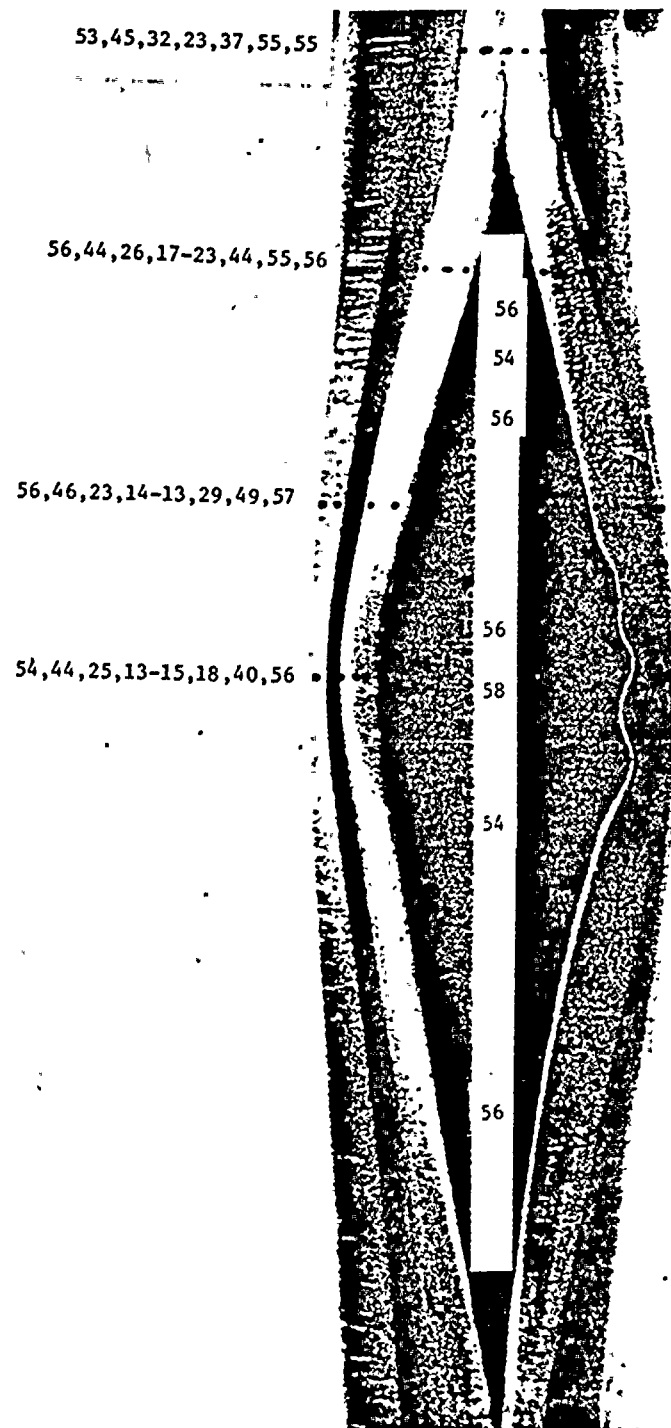


Fig. 2-9. Wall thickness measurements (mils) superimposed on 0° photograph of R42-C55

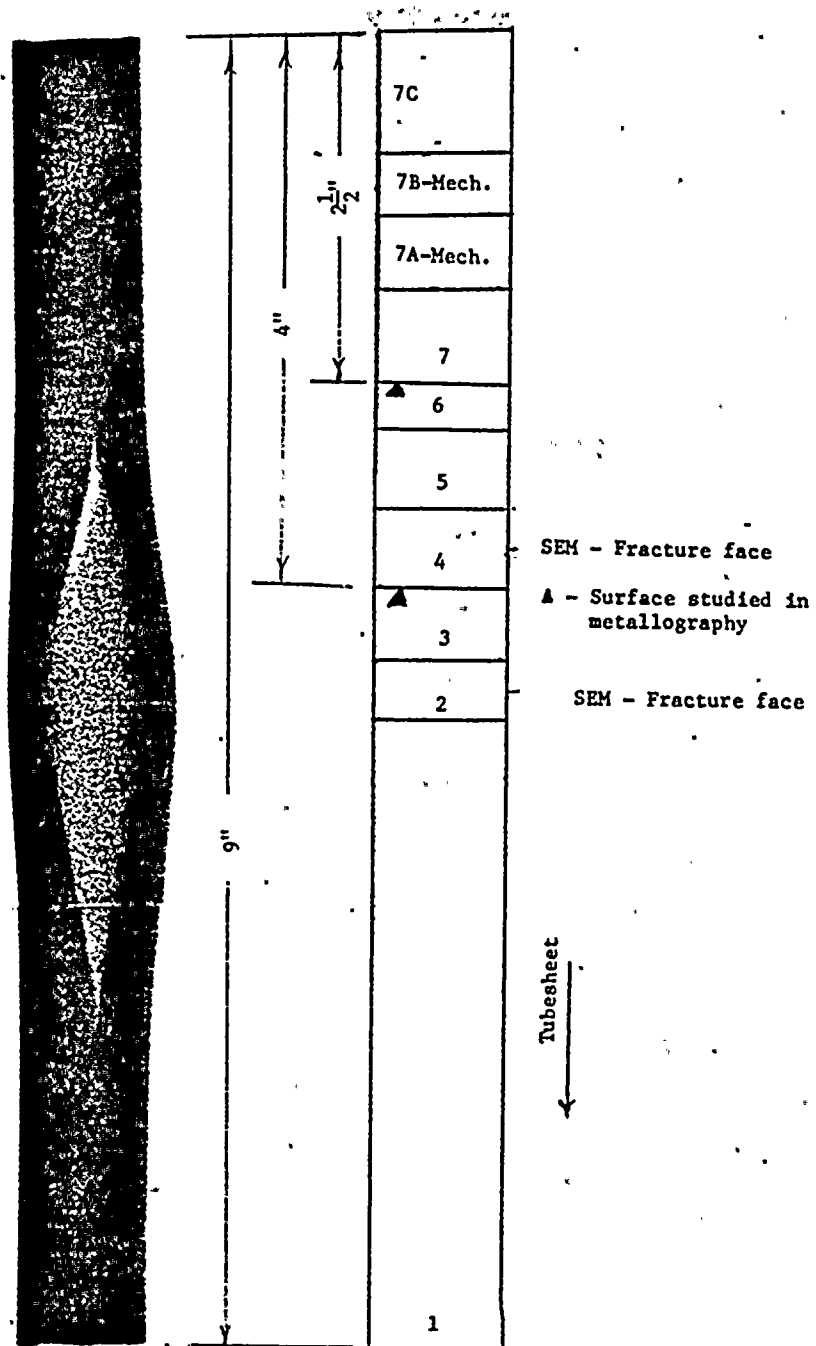


Fig. 2-10. Print of double wall X-ray radiograph at 0° for Tube R42-C55 and diagram showing cuts, section identification, and sample use.

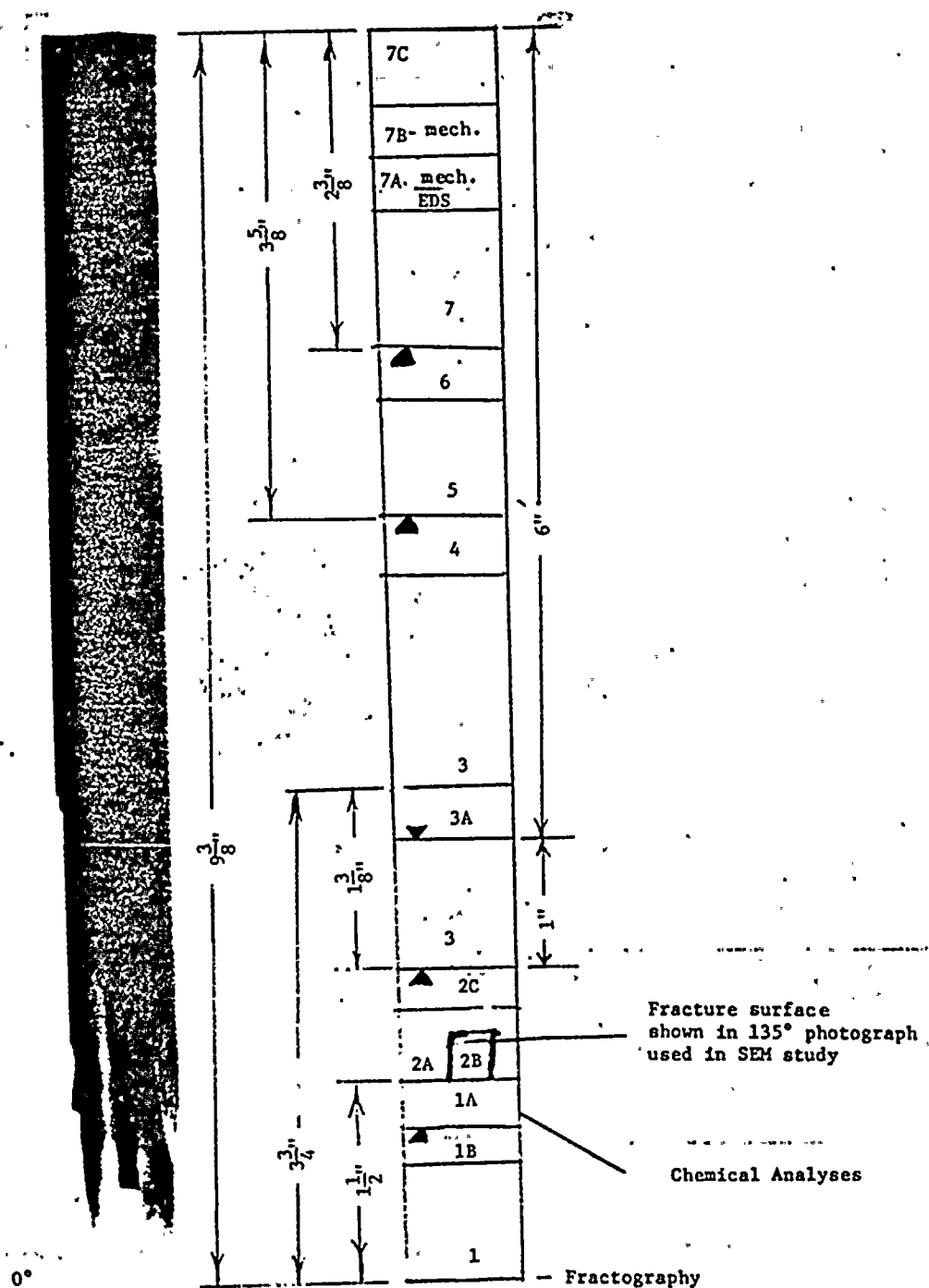


Fig. 2-12. Print of double wall X-ray radiograph at 0° for top portion of Tube R44-C55 and cutting diagram

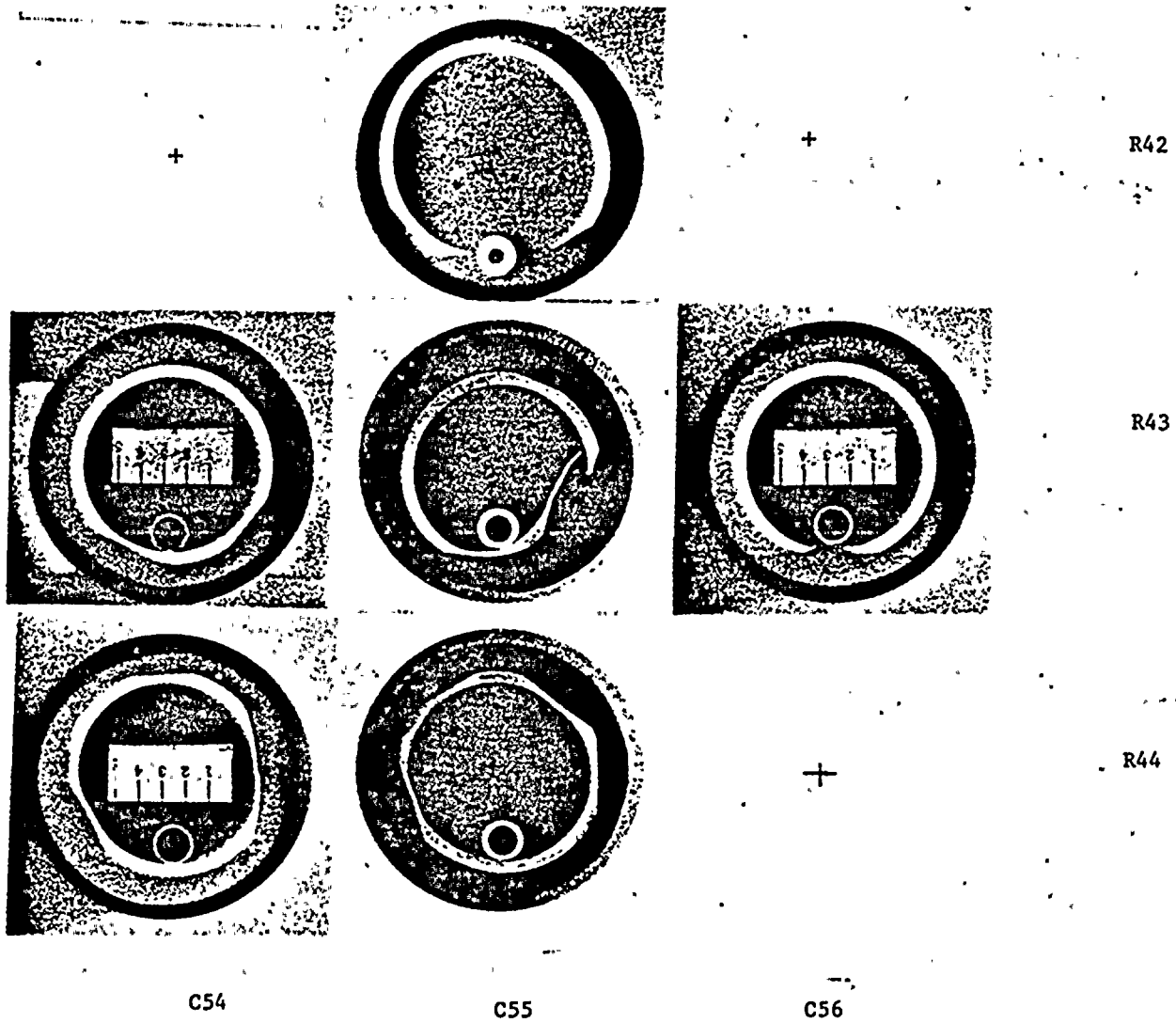


Fig. 3-2. Transverse cross-sections at $\sim 4''$ from the tops of the sections

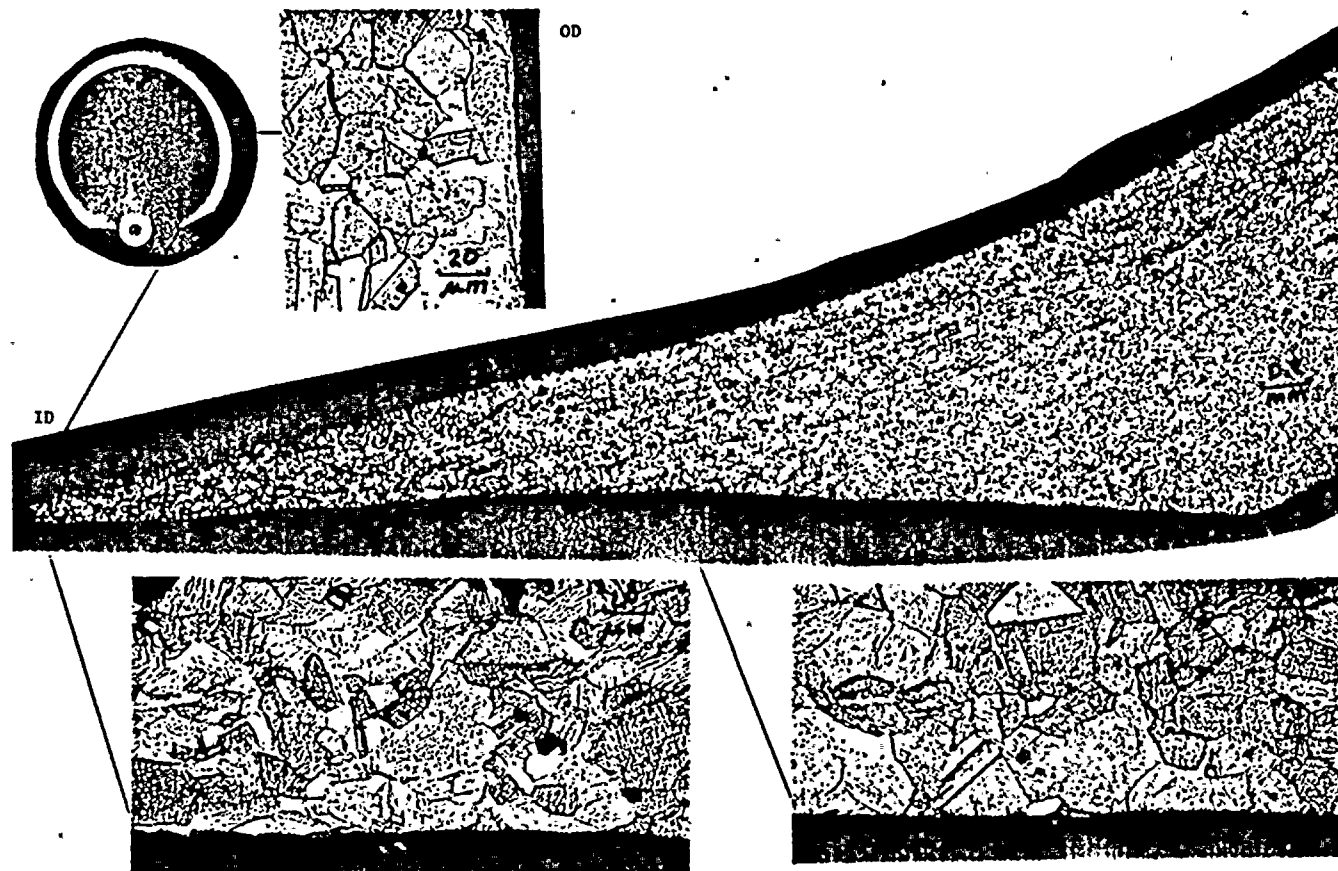


Fig. 3-4. Metallography on transverse cross-section ~4" towards tubesheet
on section from Tube R42-C55

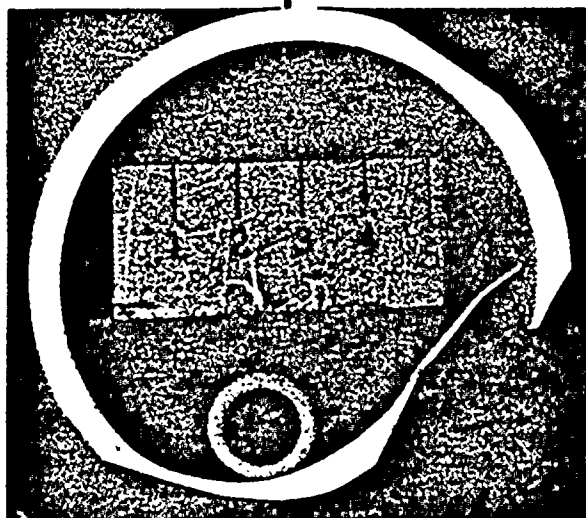


Fig. 3-6. OD surfaces 4" down from the top of the section from Tube R43-C55

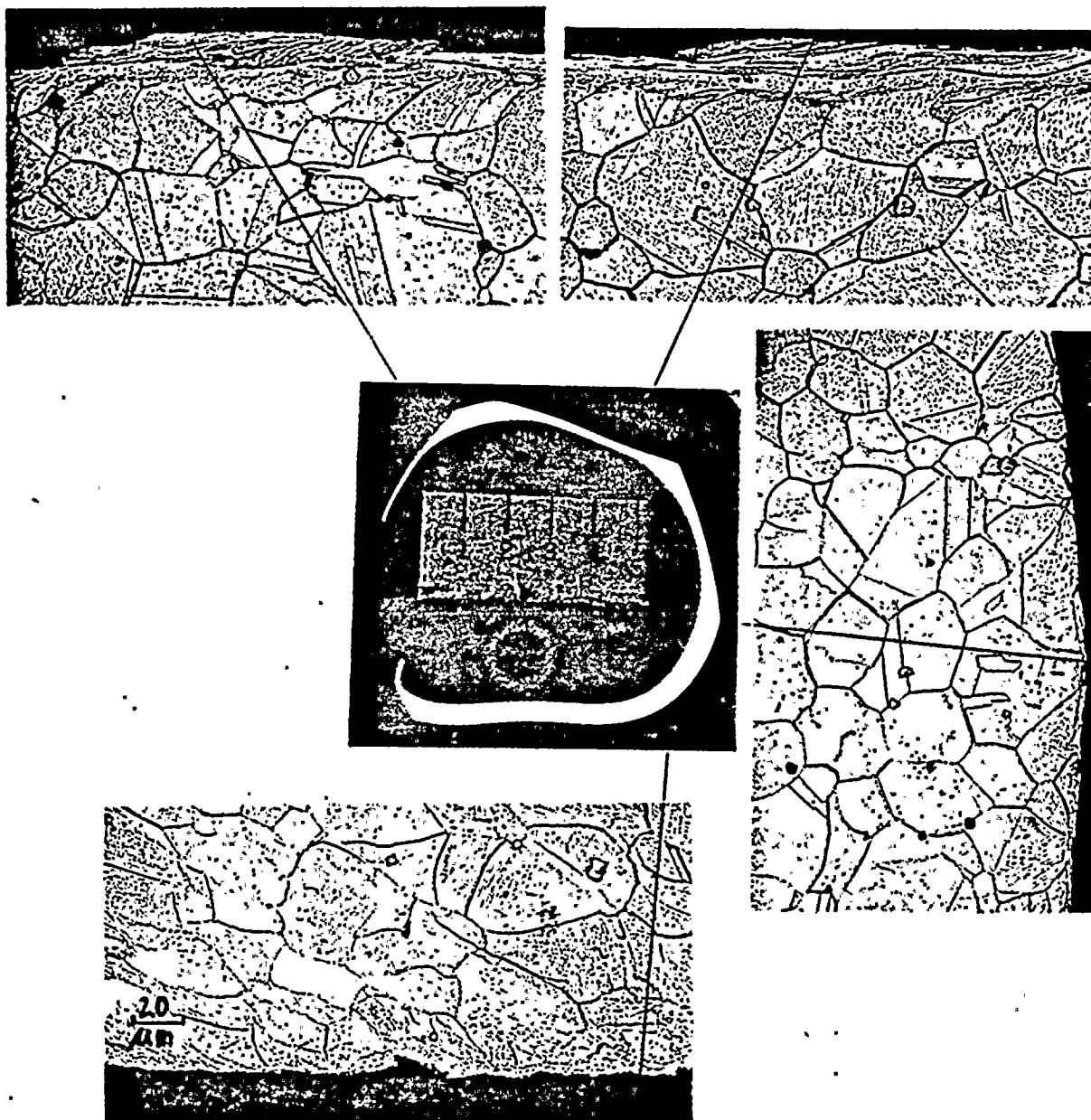


Fig. 3-8. Metallography on transverse cross-section down 6" from top of top portion of Tube R44-C55. Similar results were observed after polishing an additional 24 mils.

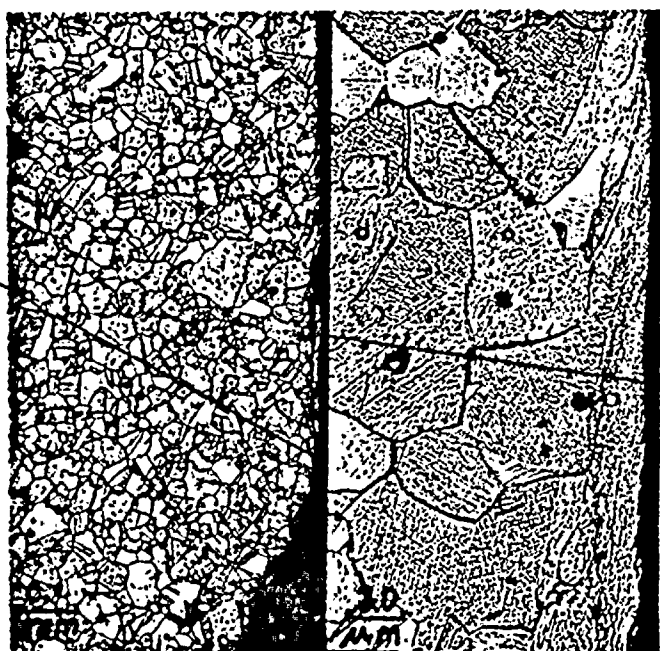
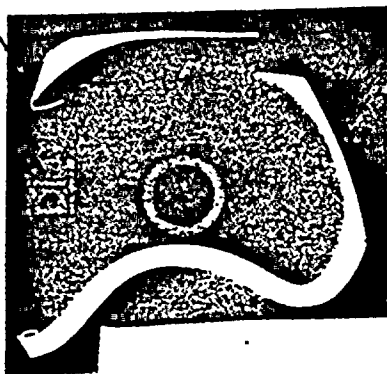
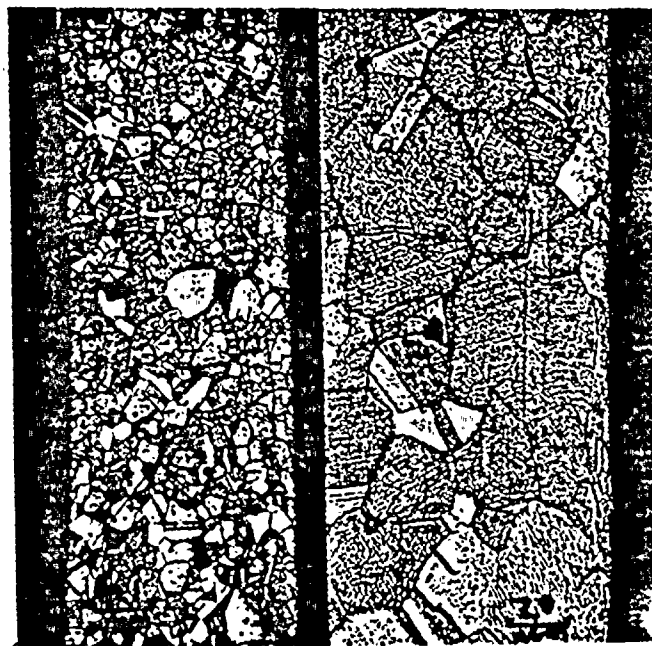


Fig. 3-10. Continuation of metallography 7" from top of top portion of Tube R44-C55

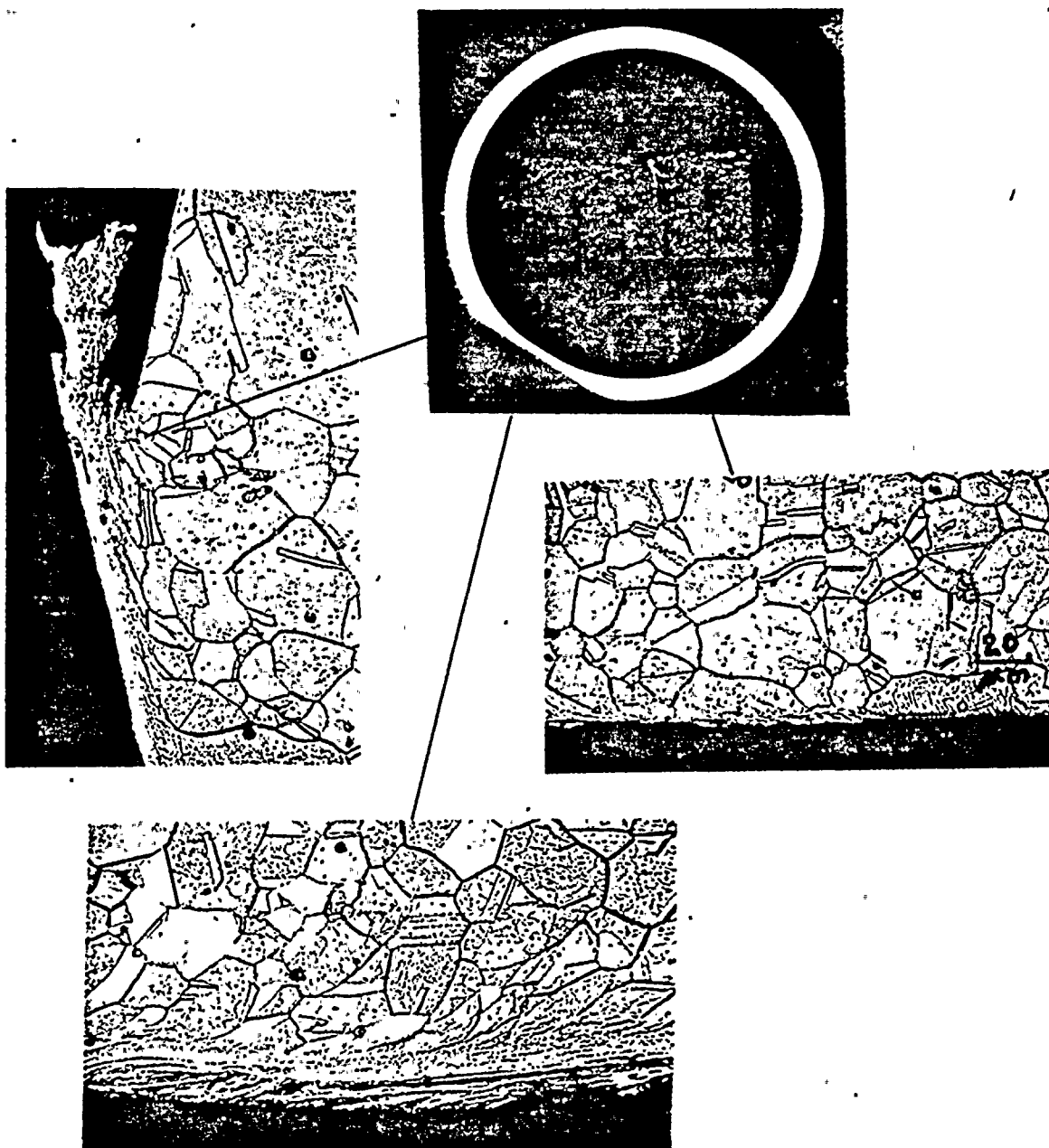


Fig. 3-12. Metallography $2\frac{1}{2}$ " down from the top of section from Tube R43-C54

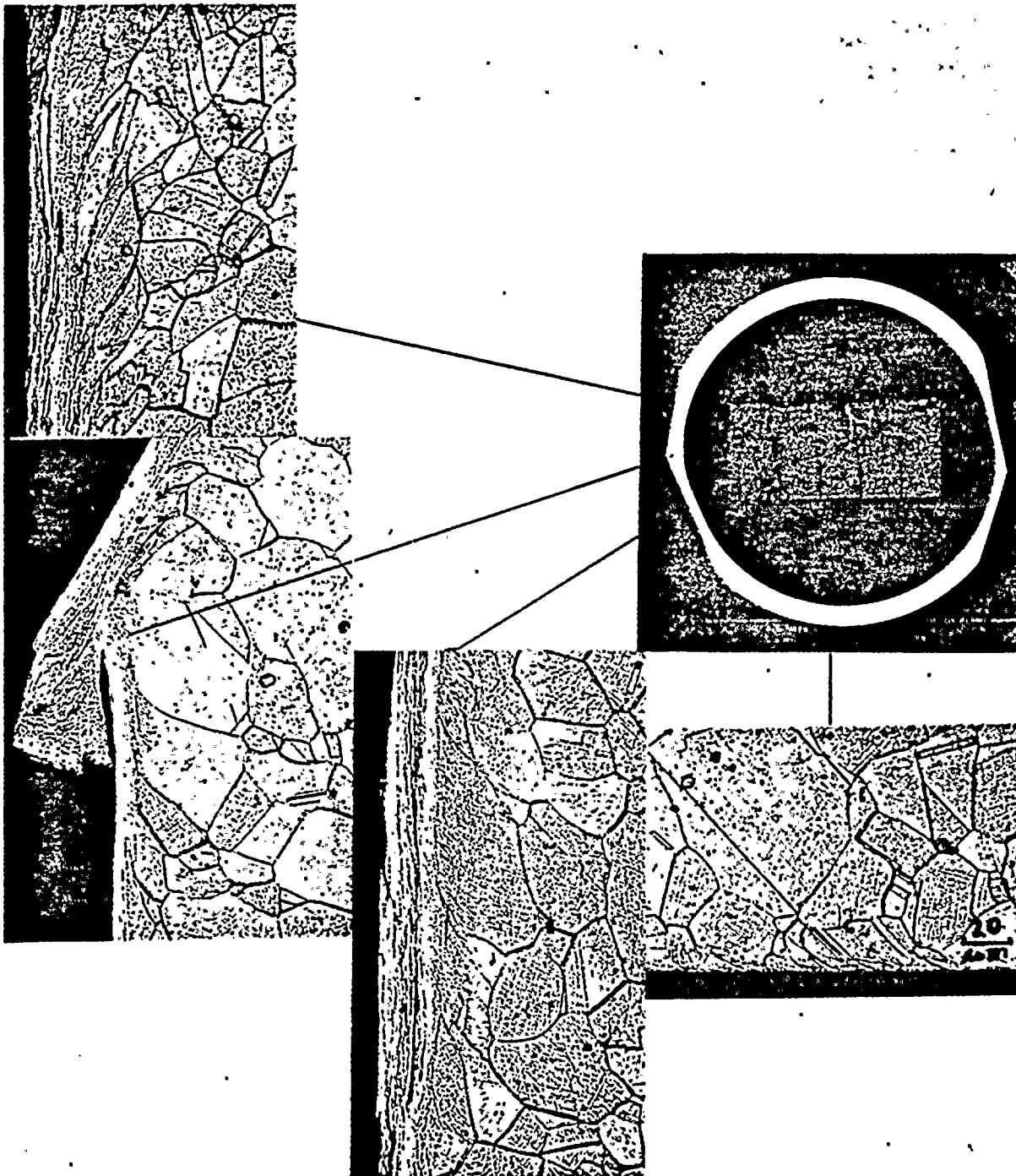


Fig. 3-14. Transverse cross-section $2\frac{1}{2}$ " down from the top of the top portion of Tube R44-C54

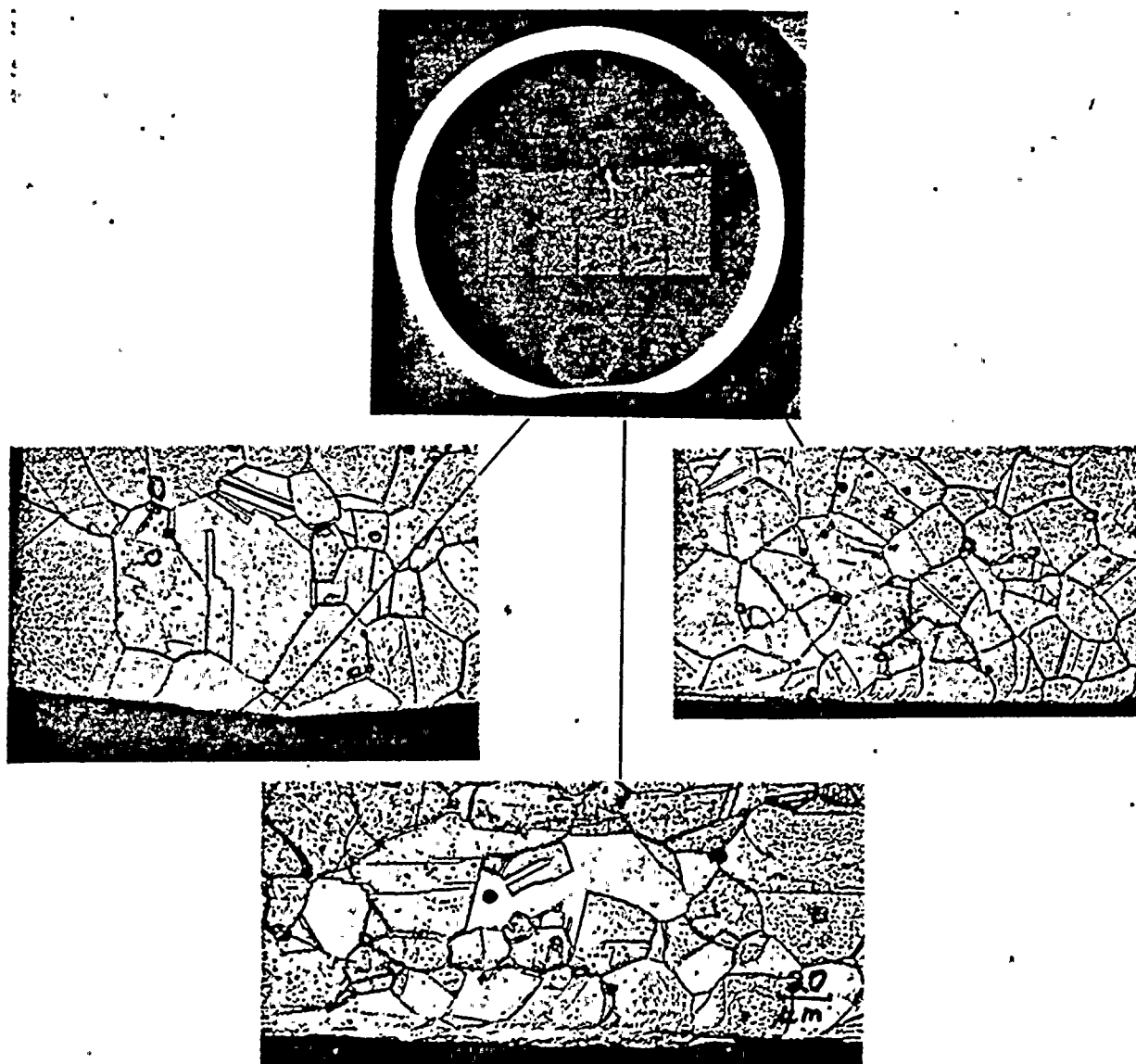


Fig. 3-16. OD surfaces $2\frac{1}{2}$ " down from the top of the section from Tube R43-C56

Table 3-1

Depth of cold work to the nearest 0.1 mil on wall reduced areas (Tabulated values are angular position-max. depth in mils)

Tube No.
(Approximate
Axial Position
From Top of
Tube Section)

R42-C55

2-1/2" (0° - 0.0)* (60° - 0.4)*
4" (0° - 0.0)* (60° - 0.4)

R43-C55

2-1/2" (30°-1.3) (225°-0.5) (270°-0.4) (330°-0.2)
4" (30°-0.3) (45°-0.5) (225°-0.5) (300°-0.4)

R44-C55

2-1/2" (60°-0.5) (225°-0.6) (270°-0.3)
4" (75°-0.2)* (105°-0.2) *(150°-1.0) (200°-0.6) (270°-0.4)
6" (105°-0.5) (150°-0.8)* (270°-0.6)*
7" (90°-0.0)* (180°-0.5) (240°-0.6)*

R43-C54

2-1/2" (30-0.9)*
4" (30°0.9)*(195°-0.5) (315°-0.5)

R44-C54

2-1/2" (60°-0.9)*(90-1.0)*(270°-0.6) (300°-0.9)
4" (60°-1.1)*(105°-1.0)*(180°-0.6) (270°-0.7)

R43-C56

2-1/2" (0°-0.3)*
4" (0°-0.5)*

*Shown in photomicrographs on transverse cross-sections

Table 3-2
Knoop (100g) microhardness traverses at
various locations on Tubes R42-C55 and R44-C55

Tube	Position No.	Remarks	~ Depth from OD surface in mils					
			1	2	4	9	14	19
R42-C55	1	Flat	224	228	231	237	--	--
	2	Flat	180	194	195	192	--	--
	3	No Flat	258	224	229	213	--	--
R44-C55	4	Flat	321	300	223	224	254	--
	5	No Flat	364	261	312	289	261	209
	6	Flat	321	312	248	214	226	194

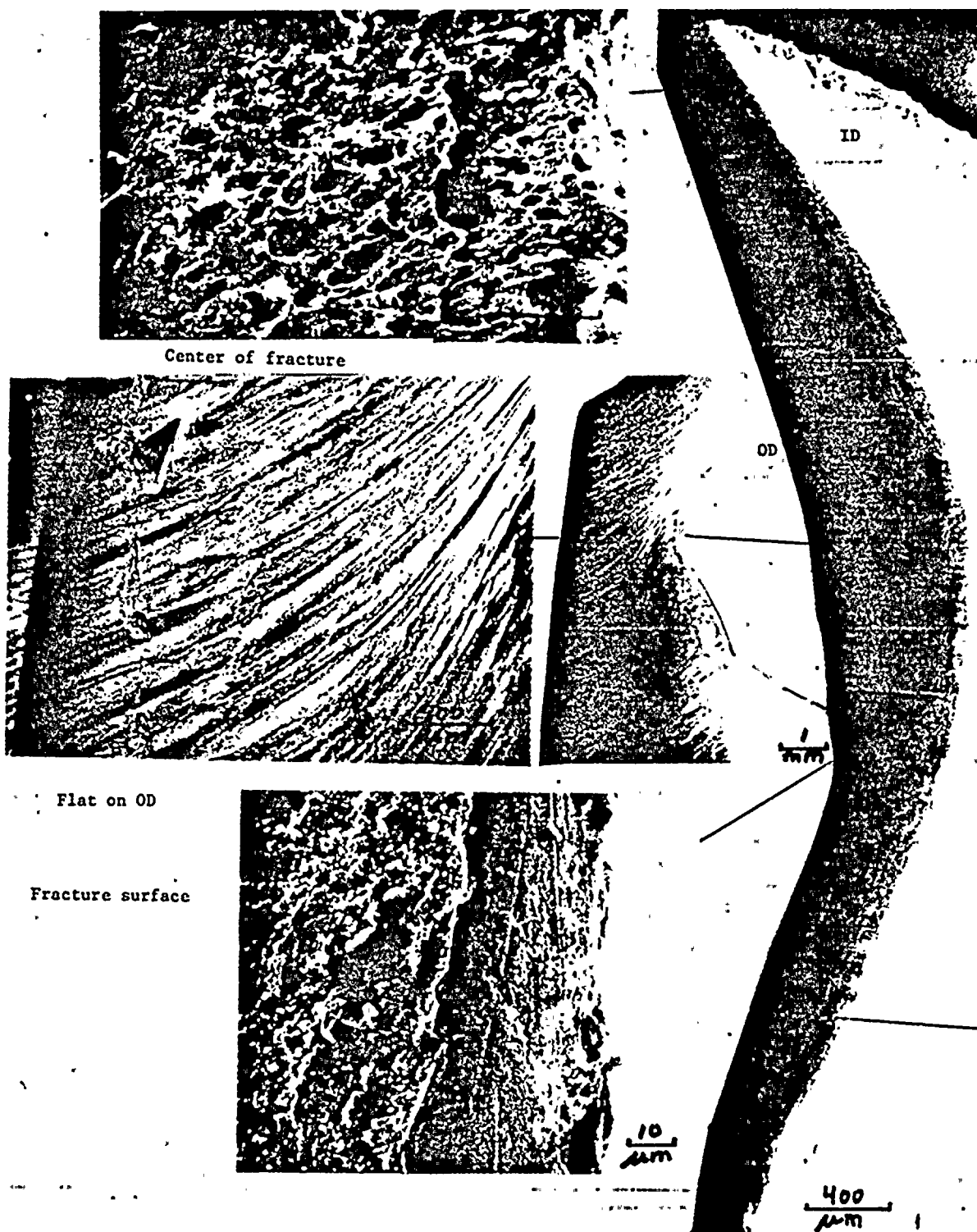
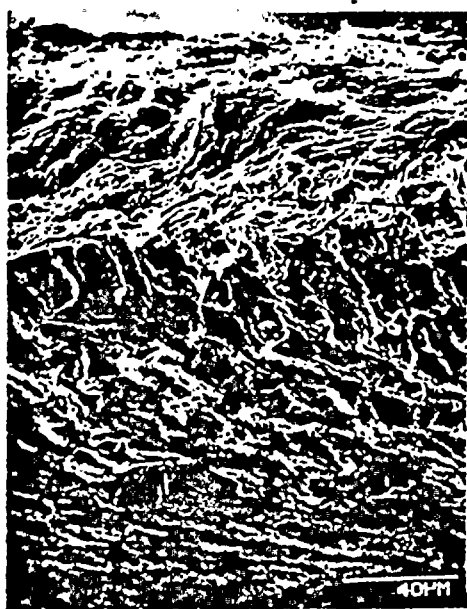


Fig. 4-2 SEM's of flat and fracture surface at center of fish mouth crack on Tube R42-C55



OD surface near peak in prior figure



Fig. 4-4. SEM's near peak in prior figure and on fracture face.

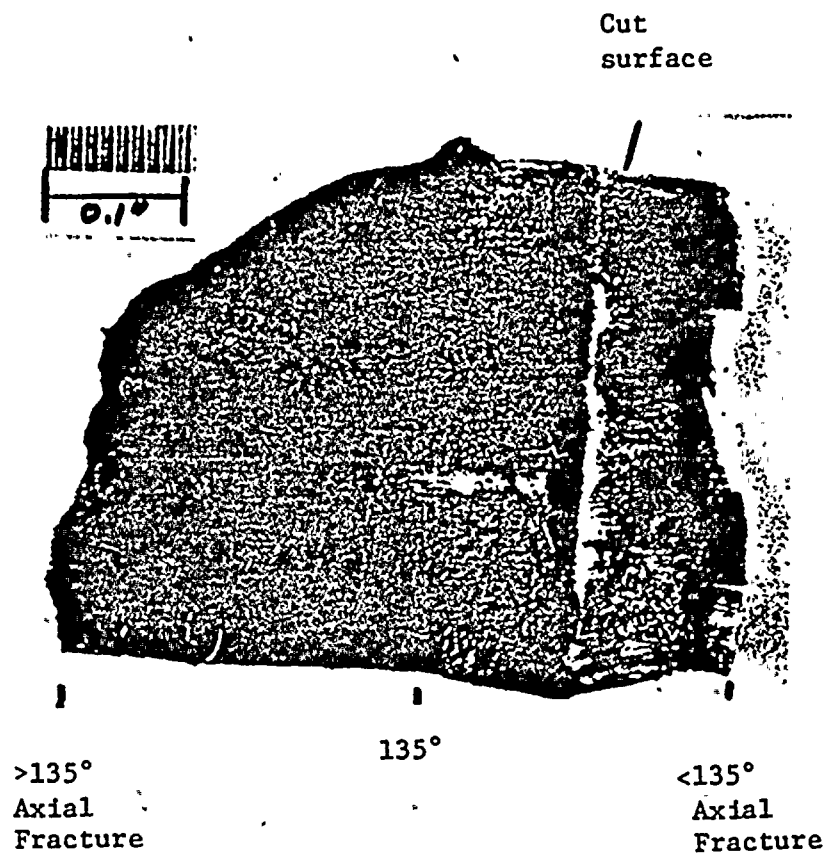


Fig. 4-6. Fractography was performed on two axial fracture surfaces 1-1/2" from the bottom of the top portion of Tube R44-C55

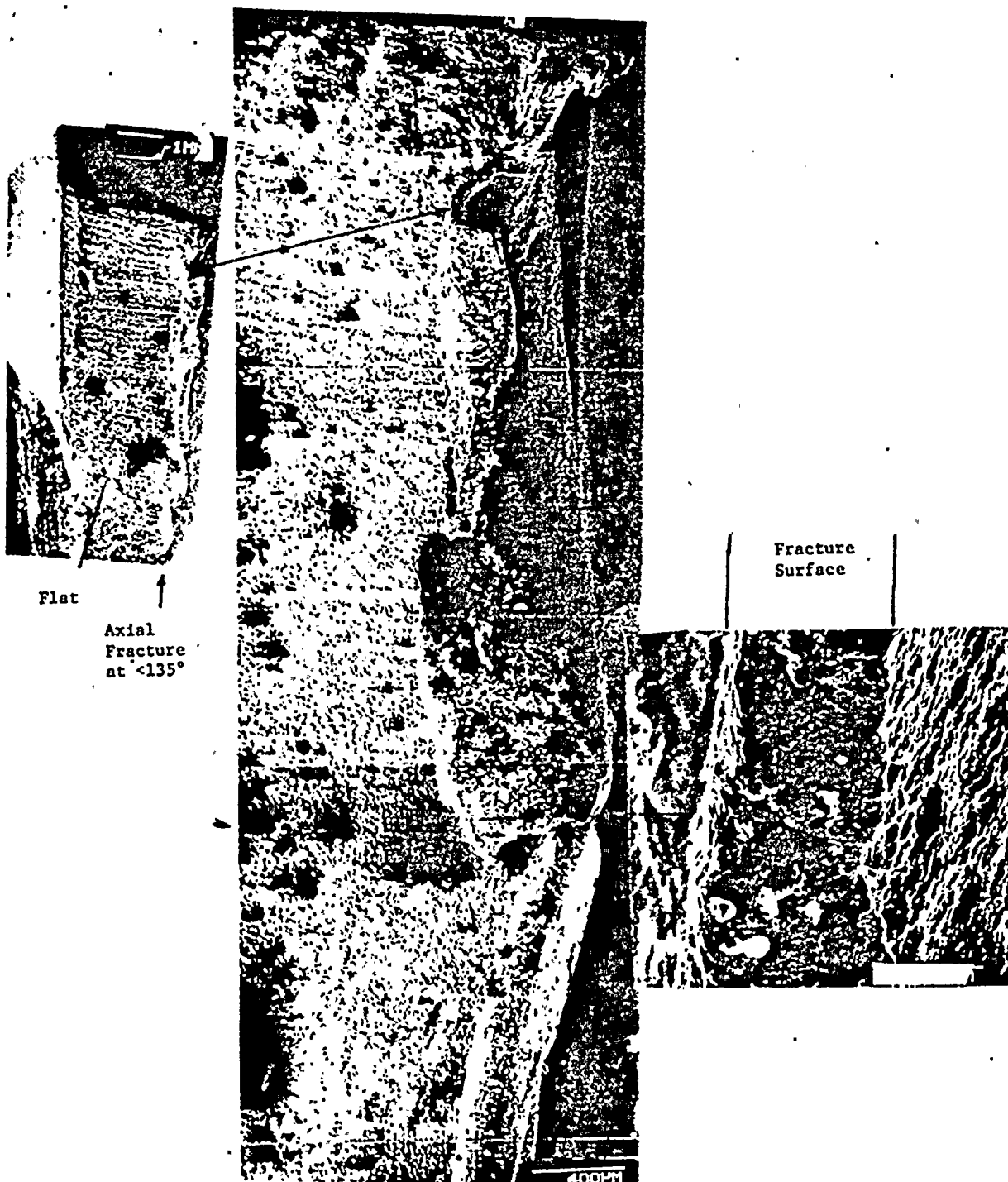
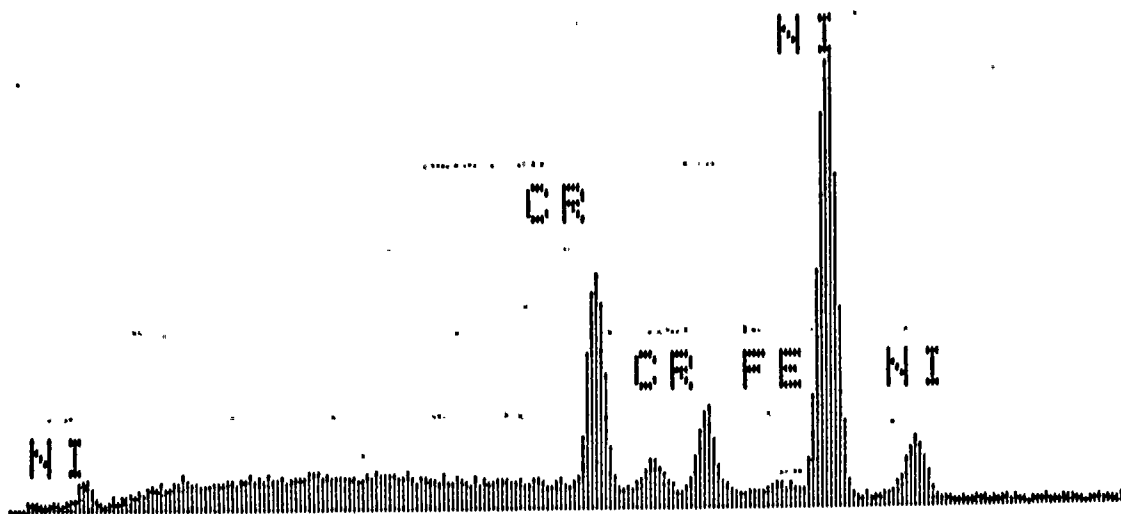


Fig. 4-8 Fractography on $<135^\circ$ axial fracture



Fig. 4-10. 180° view of ring at bottom of Tube R44-C54 (Top) and fractography on bottom fracture surface showing areas studied in more detail



EDS Analysis		ASTM Spec.
Element & Line	w/o	SB-163 w/o
Cr K α	17.0	14.0 to 17.0
Fe K α	8.5	6.0 to 10.0
Ni K α	74.4	72.0 (min)

Fig. 5-1. EDS spectrum and analysis for principal elements on Section 1A from Tube R44-C55 (Included are ASTM specifications).

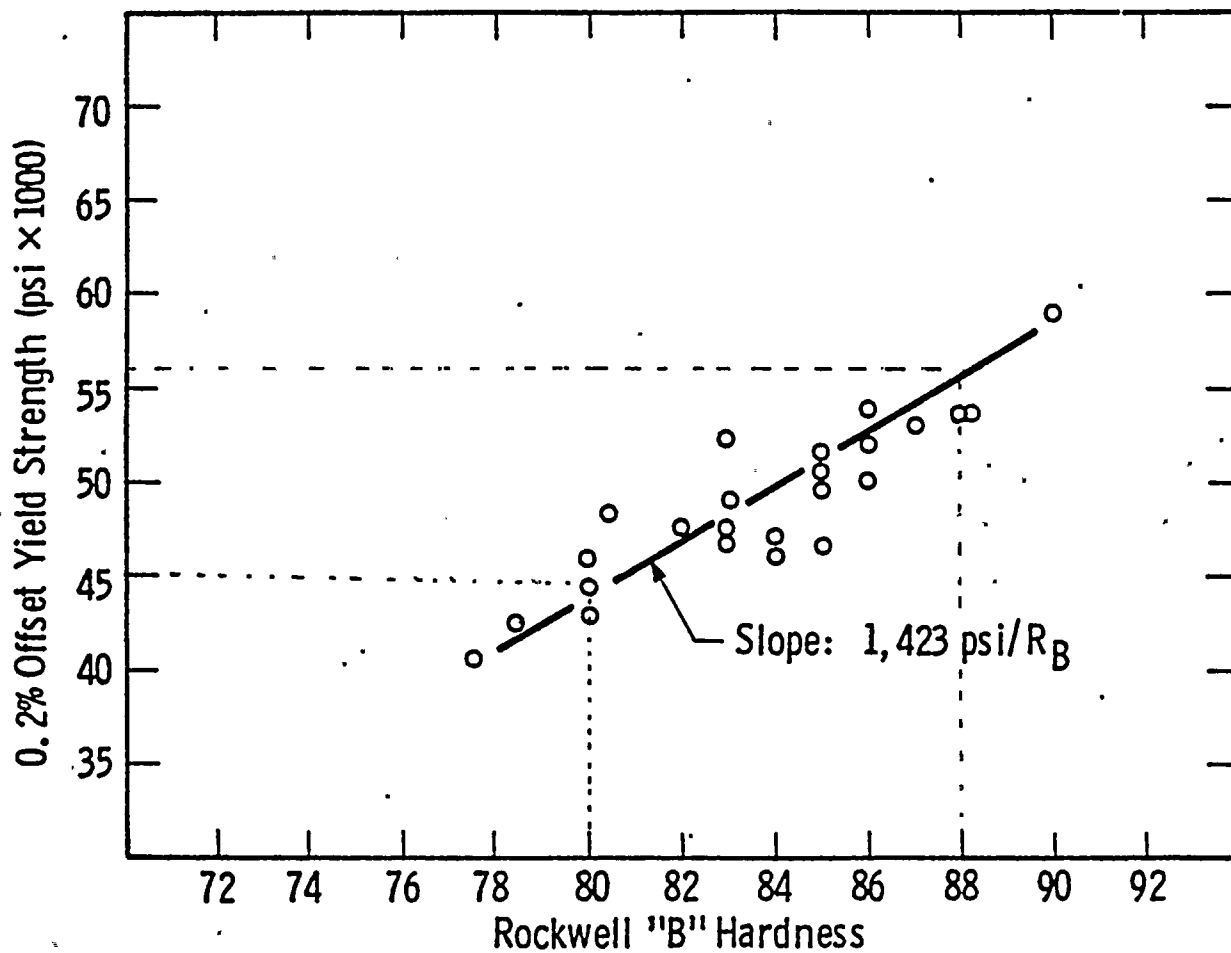


Fig. 5-2. Correlation of Rockwell "B" hardness and yield strength on 24 heats of Inconel 600 tubing and estimated strengths of two Ginna tubes (dashed lines).

APPENDIX B

EPRI/CE ANALYSES AND TESTS STEAM GENERATOR TUBING STRUCTURAL ANALYSIS

B.1. Summary

The initial analytical efforts in evaluating the Ginna tube damage have been concerned with identifying potential sources of tube stresses. Emphasis in this work phase has been on flow induced vibrations and those factors affecting tube vibrations. This work was performed to provide general information and trends. Analysis assumptions do not, in all cases, conform exactly to Ginna conditions.

A multiple span single tube was developed to assess tube vibration due to flow conditions. The model specifically addresses the influence of a compressive axial load on the tube frequency and the associated critical flow velocity. Results of the initial investigation confirm that compressive tube loadings produce a reduction in the tube frequency, and consequently, a reduction in the critical velocity to initiate fluid elastic coupling.

A multiple tube/support plate model was developed to define the variation in tube loads in the vicinity of a "hard spot" wedge location. Tube loads were developed as a function of the thermal expansion mismatch between the shell and tubes. The initial analysis was performed assuming all active (no plugged) tubes and demonstrated that the tubes nearest the "hard spot" experienced the highest axial loads. Tube loads diminished rapidly with increasing distance from the wedge location because of the flexibility of the support plate.

The effect of tube plugging was also considered in the multiple tube model assuming that tubes were plugged subsequent to "locking-in" all of the tubes at 100% full power conditions. The results, after the unit is returned to full power, indicate tensile loads in the plugged tubes and compressive loads in the adjacent active tubes.

Considerably higher compressive tube loads can be predicted for the hot standby steady state condition; however, the associated flow is not sufficient to be of concern. The large compressive loads are not particularly damaging for only an infrequent occurrence of this condition.

The results of the work performed indicate that the plugged peripheral tubes at the "hard spot" experience a predominately tensile load during power operation (assuming that the tubes were "locked-in" at full power and subsequently plugged). The absence of a significant compressive load in the tubes suggests that flow induced vibration is not the prime initiator of the initial

damage in the plugged tubes. Some other initiating mechanism appears likely. However, once the initial failure is established, flow induced vibration can certainly contribute in the progressive damage.

B.2 Failure Sequence Hypothesis

B.2.1

Loose part(s) exist in downcomer with sufficient downcomer flow forces to cause impacting of the loose part on heat transfer tubes.

B.2.2

Impacting of the loose part on peripheral tubes causes surface damage on the exposed face of the tubes.

- a) Surface damage is generally of a peening nature, with possible metal loss.
- b) Some I.D. surface disturbance may be present due to the impacting.
- c) Work hardening of metal grains on O.D. surface will exist.
- d) Free iron pick-up on the O.D. tube surface may exist.
- e) Local dings may occur due to particularly heavy impacts which distort the tube through the entire tube wall thickness.

B.2.3

Distortion of the tube from its original circular shape occurs due to force of impacts and/or due to bowing of the tube under peening action and bending moment caused by resistance to bowing at the support plate elevation. The distorted shape would be generally, but not necessarily exactly, in an oval form with the long axis of the oval generally parallel to the tube bundle periphery. The distorted shape would begin only some distance above the tube sheet, since the tube is restrained to a circular shape by the tube sheet hole.

B.2.4 (Case 1)

The tube is plugged due to false ECT indications of I.D. tube wall defects. False indications are caused by:

- a) Vector additions in the ECT test of several forms of tube wall distortion, or

- b) A combination of work hardening of the O.D. surface changing the tube conductivity and/or free iron pick-up on the tube O.D. surface, or
- c) Copper deposits on the tube O.D.

ECT indications of a "bulge" are caused by the distorted tube shapes mentioned in three above.

B.2.5 (Case 2)

The tube is plugged due to I.D. defects caused by coriou cracking. Coriou cracking results from high tensile strains at the tube I.D. due to some combination of:

- a) An axial tensile load in the tube during transients, caused by locking of the tube in the support plate in the hot condition. Locking may be in part due to the reaction to bending loads caused by bowing of the tube under the peening action.
- b) High I.D. tensile strains existing at local dings in the tube wall caused by particularly heavy impacts (see B.2.2e).
- c) Other tensile stresses resulting from internal pressure, tube vibration, distorted shape, etc.

(Note that, if tubes become locked into the support plate at full power, then compressive loads are developed in active tubes)

B.2.6

Tubes are plugged preferentially at welded lug locations because of hydraulic pertubations in the downcomer flow from upstream effects (flow eddy created below connection to the shell) and downstream effects (absence of flow holes in the support plate changes the flow drawn into the tube bundle at these locations). These hydraulic pertubations cause the loose part to dwell at these locations for most of the time rather than continue an otherwise random movement around the downcomer annulus.

B.2.7

Once plugged, tubes without a breach in the primary-secondary boundary are under external pressure during power operation (approximately 770 psi at full load and 970 psi at hot standby).

B.2.8

Plugged peripheral tubes experience local collapse due to some combination of:

- a) External pressure.
- b) Local bending moments, tube ovality, or deformation (Items 2.e. and 3. above).
- c) Axial tensile load (Item B.2.5b).
- d) Particularly heavy impacts from the loose part occurring after the tube is plugged.

B.2.9

Flow vibration effects on the locally collapsed tube result in fatigue failure of the tube in the collapse region.

B.2.10

Fatigue failures progress to the point of parting the tube, allowing that portion of the tube above the failure elevation to behave as a cantilevered tube under flow vibration forces.

B.2.11

The failed tube acts as a "loose part", subjecting itself and neighboring tubes to impact and wear damage. Neighboring tubes are subsequently plugged due to ECT indications resulting from the damage.

B.2.12

Progressive tube plugging, tube failure, and damage to additional neighboring tubes occurs, resulting in conditions observed during the current outage. The tube wall in R42 C55 had likely experienced considerable metal loss by wear or impacting prior to failure, creating conditions which result in a rupture of the length observed.

B.3 3-D-Plate and Tube Analysis

B.3.1 Statement of Problem

The purpose of this study was to determine the loads on the steam generator tubes as a result of the tubes becoming locked into the support plate.

B.3.2 Summary and Conclusions

The loads considered in this analysis were the result of a thermal expansion mismatch between the tubes and the stub barrel, and the thermal expansion mismatch between the hot tubes and the cold (plugged) tubes.

The tubes were considered locked in hot (100% steady state) condition. The first condition analyzed was shutdown condition

(70°F) prior to certain tubes being plugged. The tubes closer to the hard spots were found to be under most tensile loads. The second condition analyzed was 100% steady state condition after a certain number of tubes were plugged. The cold (plugged) tubes were found to be under tension whereas hot (active) tubes surrounding the cold tubes were under compression.

B.3.3 Results

The results of this analysis is presented in graphical form in Figures B.1 and B.2.

Figure B.1 presents the worst loads for the shutdown (70°F) condition prior to any tube plugging. The loads were as a result of initial $\Delta T = 72^\circ F$ between the tubes and the stub barrel.

Figure B.2 presents the worst loads for the 100% operating steady state condition after certain tubes were plugged ($T_{SHELL} = 483^\circ F$, $T_{TUBE} = 555^\circ F$, $T_{PLUGGED\ TUBE} = 474.7^\circ F$).

B.4 Single Tube Model for Vibration and Fluid-Elastic Instability Study

B.4.1 Statement of Problem

The purpose of this study is to evaluate a multi-supported single tube loaded in compression to determine its vibration characteristics and susceptibility to flow induced fluid-elastic vibrations.

B.4.2 Summary

The single tube unloaded configuration has a first mode natural frequency of vibration of 24 HZ. If the tube is assumed to be locked in at support plate elevations 1, 3, and 5, during application of a uniformly distributed axial load, buckling occurs in one of the upper spans at a force of 1360 lbs. If the tube is assumed to be locked-in at the first support elevation only, buckling occurs at 3340 lbs.

The axial loads necessary for initiation of fluid-elastic instability are, 1300 lbs. and 3220 lbs. respectively, for the two conditions discussed above. For these loads, the critical velocity is equal to gap velocity, 11.5 feet per second.

B.4.3 Results

Figure B.3 shows the variation in natural frequency with compressive load in the tube. Curve A was obtained by restraining vertical movement at support plate (S.P.) #1. All supports restrain lateral motion. Buckling occurs in the first span above the tube sheet for an axial load of 3340 lbs. Curve B was obtained by restraining vertical motion at SP-1, 3 and 5. A uniform axial load was applied in all spans from SP-5 downward. Buckling occurs in one of the upper spans at 1360 lbs. (Frequency = 0 at

(buckling load). Figure B.4 shows the variation in critical flow velocity with compressive load. Curves A and B were generated using the frequency-load results presented in Figure B.3.

For Curve A of Figure B.4, S.P. #1 locked, the axial compressive load required for initiation of fluid-elastic instability is about 3200 lbs. at 11.5 feet per second. Curve B with S.P. #1, 3, & 5 locked shows a required axial load of only 1300 lbs.

B.5 Thermal Analysis of Secondary Shell-Tube Sheet Juncture Region (Hot Leg Side)

B.5.1 Statement of Problem

This calculation presents a thermal analysis of the secondary shell-tube sheet juncture region for the Ginna steam generator for the purpose of comparing mean shell temperatures with secondary tube temperatures for use in a stress analysis. Several operating conditions are investigated.

B.5.2 Summary and Conclusions

A brief summary of the pertinent results of the analysis is presented below including the mean shell temperatures and tube temperatures for comparison. The end points of the 100°F/hr transients are presented here:

Transient	T_m Shell	T_m Active Tube	T_m Plugged Tube	Remarks
a. Plant Heatup	529°F	545°F	545°F	End of 70°F to 545°F Ramp at 4.75 hr.
b. 0% Load S.S.	545°F	545°F	545°F	Isothermal at 545°F
c. Plant Cooldown	86°F	70°F	70°F	End of 545°F to 70°F Ramp at 4.75 hr.
d. Cold Feed at Hot Standby S.S.	150°F	530°F	131°F	200 GPM Flow at 40°F
e. 100% Load S.S.	475°F	555°F	475°F	CR = 3.75; 81% of F.W. to Hot Side
f. 100% Load S.S.	485°F	555°F	484°F	CR = 4.70; 81% of F.W. to Hot Side

B.5.3 Results

Computer output showing representative temperature distributions for the various loading conditions and from which the summary of results in Section B.5.2 was obtained is presented in Figure B.5, sheets 1 through 9. Figure B.6 shows the computer print pattern corresponding to the element layout of Figure B.7. Detailed

temperature vs. time curves, including the outermost tube temperatures, are presented in Figure B.8, sheets 1 through 3.

B.6 Thermal Analysis of Downcomer Annulus

B.6.1 Statement of Problem

Determination of stresses in both active and plugged tubes is part of the investigation into the damage in the Ginna steam generator. The temperature of the downcomer annulus flow during steady state and transient conditions is needed to establish shell and tube temperatures for these stress calculations.

B.6.2 Summary of Conditions

The analysis was performed to evaluate the temperature of flow in the downcomer annulus for the conditions analyzed. The results were used directly to establish tube temperatures and indirectly by providing input temperatures for the secondary shell - tube sheet analysis. During hot standby at 544.6°F (1000 psia) without recirculation, 40°F feedwater to the hot side is heated to 130.7°F. At 100% power, the temperature of the mixed feedwater and recirculating saturated water increased only 0.2°F.

B.6.3 Results

The temperature distributions for the three conditions analyzed are presented in Figures B.9 through B.11. The results of the transient downcomer outlet temperatures vs. time are plotted in Figure B.12.

B.7 Tube Wall Temperatures

B.7.1 Statement of Problem

Average tube wall temperatures for the length between the tube sheet and the support plate are needed to calculate stresses due to axial loads.

B.7.2 Summary and Conclusions

The average temperature of plugged tubes is the same as that of the surrounding fluid, while active tubes and plugged tubes are the same temperature for heatup, 0% load steady state, and cooldown.

At 100% power, there is boiling - either sub-cooled or saturated - from the tube sheet to the first support, the length of interest. The computer program SGTUBE shows an average heat flux of 116,260 Btu/hr-ft² for this length. The average wall temperature for this value of heat flux is 555°F.

In cold feed at hot standby, the average tube wall temperature is calculated to be 529.7°F. The primary temperature is at the secondary saturation temperature, and heat transfer to the sub-cooled secondary is by natural convection.

B.7.3 Results

<u>T_{sec}, F</u>	<u>ΔT, F</u>	<u>ΔQ, Btu</u>	<u>Flux Btu/hr-ft²</u>	<u>L.M. Flux Btu/hr-ft²</u>	<u>L, in.</u>	<u>T_{wall}, F</u>
130.8	378.16		59,466			
		1926.6		50,644	19.67	525.4
250	268.98		42,741			
		1601.6		34,356	24.10	531.6
350	178.32		27,146			
		1710.4		18,206	48.57	534.3(1)
450	87.70		11,485			

(1) The wall temperature at T_{sec} = 350°F is extrapolated for the 8.04" to the support plate.

B.8 Feedwater Distribution to Hot and Cold Leg Side Downcomer

B.8.1 Statement of Problem

The feedwater rings on the Ginna steam generators have been modified to offset the feedwater flow to achieve a 80%/20% flow split to the hot leg/cold leg sides of the downcomer. Also, J-tubes have been installed on the top of the feedwater ring to reduce the probability of occurrence of water hammer. The purpose of this analysis is to calculate the feedwater distribution for 100% power operation to verify reported values and to calculate the flow distribution for hot standby with 200 GPM feedwater flow.

B.8.2 Summary and Conclusions

Results of the calculation for the modified feedring with J-tubes show that 81% of the feedwater is distributed to the hot side and 19% to the cold side for 100% power conditions. This confirms the prediction that the J-tube modification does not change the previously achieved flow split. The flow split for 200 GPM feed flow at hot standby was calculated to be 80%/20% to the hot leg/cold leg sides.

B.8.3 Results

The following is a tabulation of results from RINGFLO. The flow shown is one half the total since by symmetry, only one half the feedwater ring was used in the model.

COLD LEG SIDE

HOT LEG SIDE

100% Power

Hot Standby

Nozzle No.	Flow lb/hr	% Flow	Σ % Flow	Flow lb/hr	% Flow	Σ % Flow
Vent	63915	4.65		2506	4.99	
1	64393	4.68		2462	4.90	
2	65614	4.77	19.0	2480	4.94	19.8
3	66800	4.86		2499	4.98	
4	67835	4.93		2509	5.00	
5	69102	5.03		2542	5.06	
6	70296	5.11		2574	5.13	
7	71415	5.19		2605	5.19	
8	72457	5.27		2633	5.24	
9	73419	5.34		2659	5.30	
10	74298	5.40		2684	5.34	
11	75092	5.46	81.0	2706	5.39	80.2
12	75800	5.51		2726	5.43	
13	76418	5.56		2743	5.46	
14	76946	5.60		2758	5.49	
15	77381	5.63		2771	5.52	
16	77723	5.65		2781	5.54	
17	77968	5.67		2788	5.55	
18	78067	5.68		2791	5.56	

B.9 Downcomer Flow VelocitiesB.9.1 Problem

Tube damage in the steam generator may be caused by vibration and by impaction from heavy objects. Both of these causes are dependent on the velocity of the downcomer flow.

B.9.2 Summary and Conclusions

The velocity of the circulating flow exiting the downcomer is calculated to range from 11.08 to 16.35 feet per second, depending on the secondary steam flow specified and the circulation ratio. These give velocity heads or impact pressures of .66 to 1.38 psi. As the net weight per square inch of 7/16 inch thick iron or steel is .112 pounds, turbulence and deflected flows could easily lift such as plate.

The approach and gap velocities as calculated are an average based on the opening below the wrapper. Actual velocities will vary axially, due to the jetting action of the fluid leaving the downcomer.

During hot standby, there is a flow of 200 GPM of 40°F feedwater. Assuming no recirculation, the downcomer velocity is .086 feet per second, and approach and gap velocities are .013 and .044 feet per second, respectively.

B.10 Steam Generator Thermal-Hydraulic Analysis

B.10.1 Statement of Problem

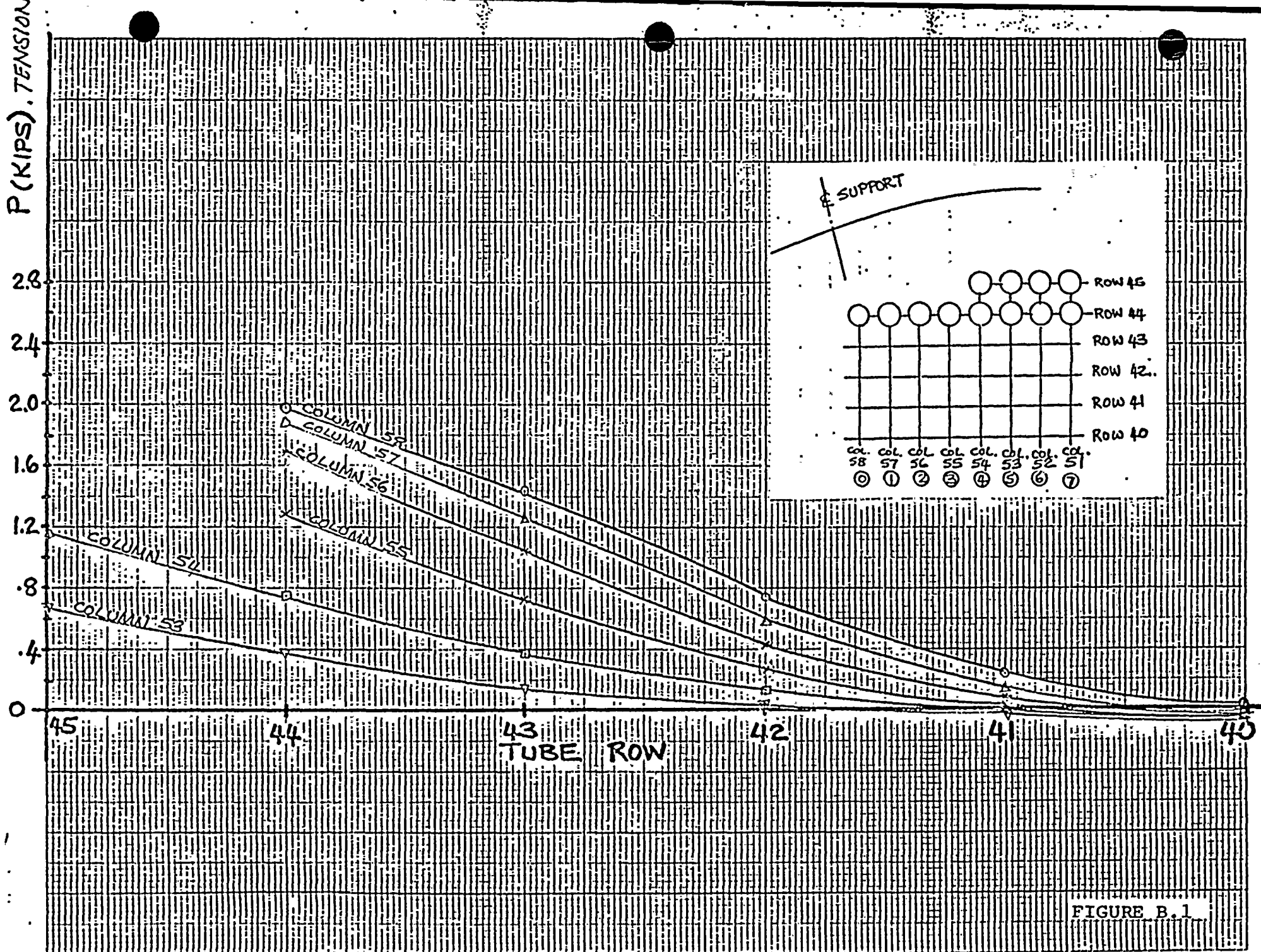
The thermal-hydraulic characteristics of the Westinghouse U-tube vertical steam generator were calculated in order to understand various phenomena observed during inspection of the R.E. Ginna nuclear steam generator.

B.10.2 Summary and Conclusions

The vector components of the secondary fluid velocities, the quality, and the vapor fraction of the two-phase mixture near the tube sheet and through the first tube support device were calculated in detail to determine the contribution of fluid conditions to the observed phenomena. No unusual trends were observed. However, the analysis and extensions of it may be useful in understanding contributions due to the loose objects discovered in the steam generator.

B.10.3 Results

The radial and axial velocities of the secondary fluid, the quality, and the void fraction at select locations in the steam generator are presented in the following line printer plots (Figure B.13 - Figure B.26). The key for interpreting these plots is shown at the top of each figure. Each plot integer spans 10% of the range of the variable in that figure. Even integers are omitted to enhance clarity.



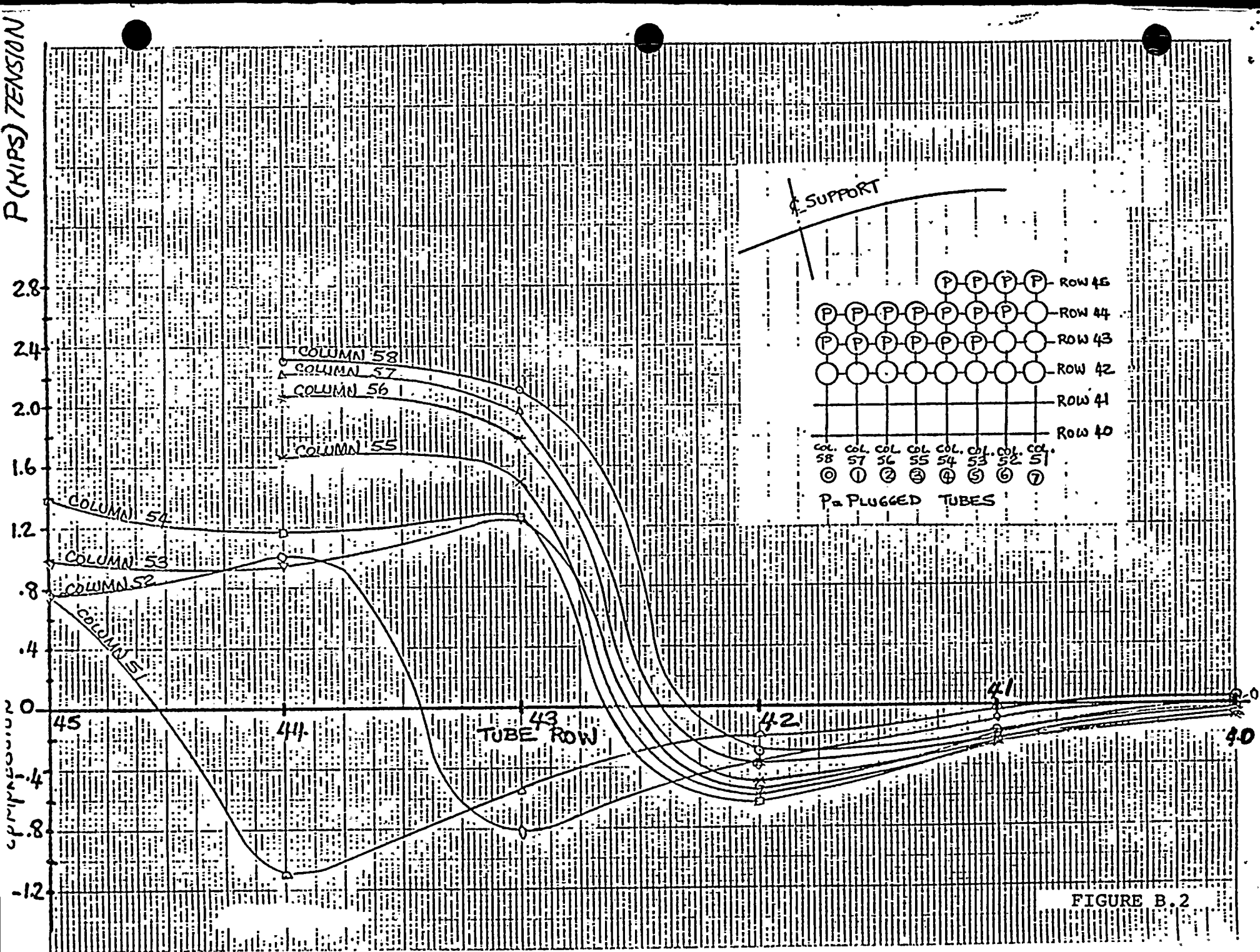
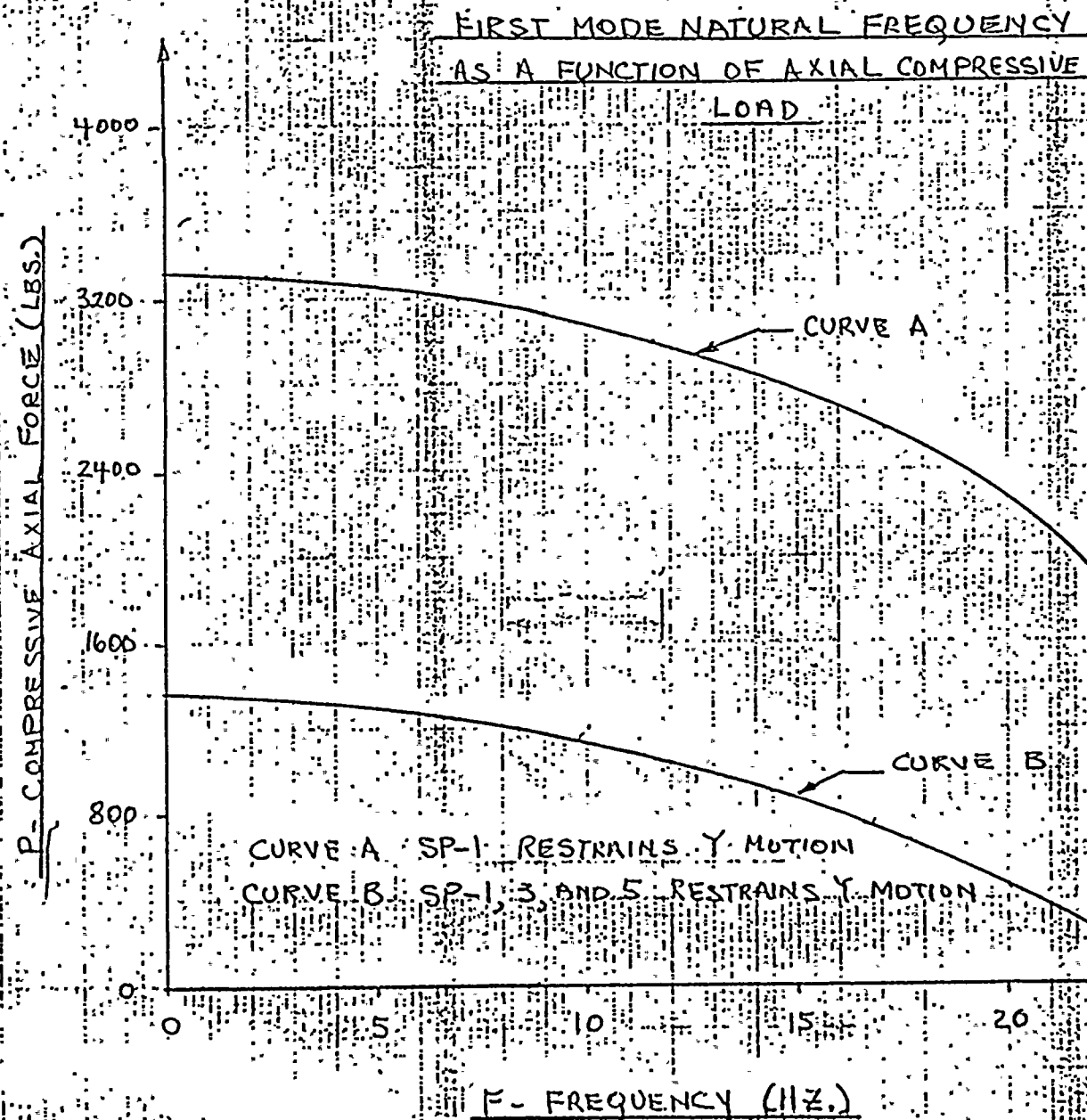


FIGURE B.2



SINGLE TUBE FINITE ELEMENT
MODEL

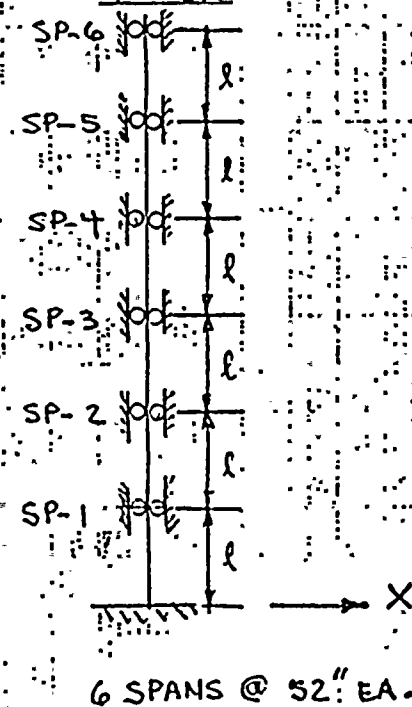


FIGURE B.3

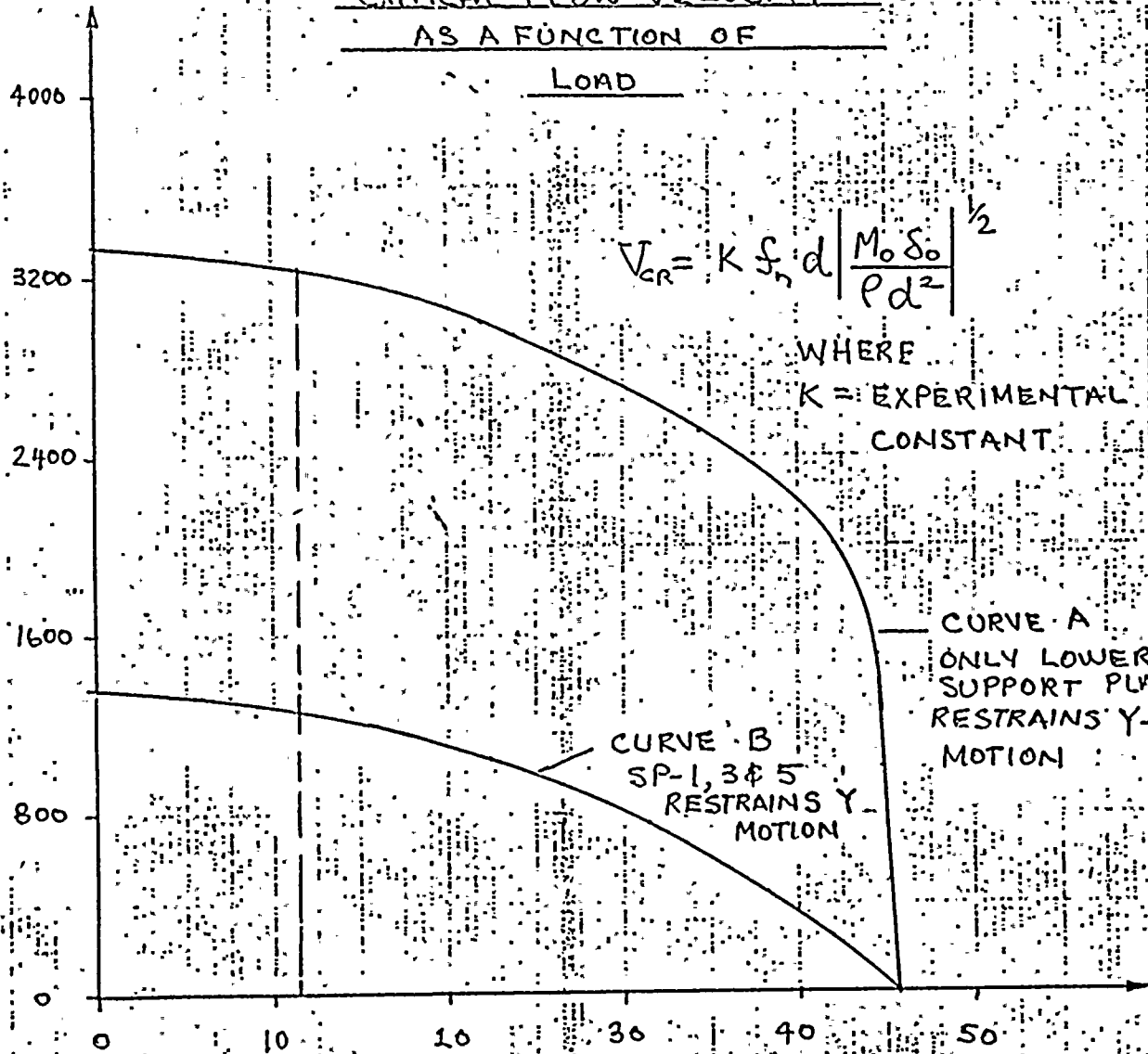
FLUID-ELASTIC VIBRATIONS

CRITICAL FLOW VELOCITY

AS A FUNCTION OF

LOAD

P - COMPRESSIVE AXIAL FORCE (LBS.)



$$V_{CR} = K f_n d \left| \frac{M_0 \delta_0}{\rho d^2} \right|^{1/2}$$

WHERE

K = EXPERIMENTAL CONSTANT

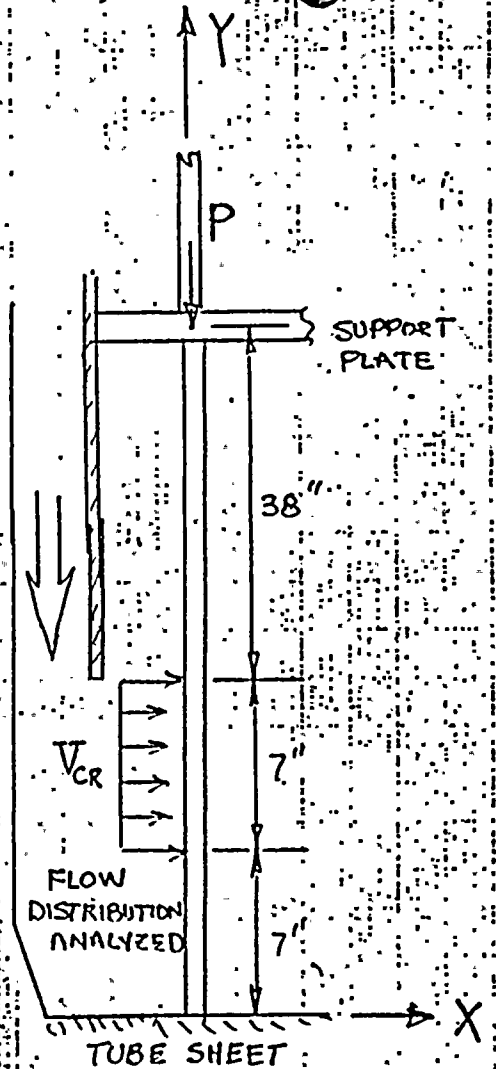


FIGURE B.3 SHOWS LOCATION & NOMENCLATURE FOR UPPER SUPPORTS

FIGURE B.4

TIME 4.750000HRS

534.1

534.1

545.0

534.1

534.1

534.1

534.1

545.0

534.1

534.1

533.8

545.0

532.6

529.2

528.1

545.0

527.6

527.4

527.3

545.0

527.0

526.4

524.9

545.0

521.3

511.3 529.2

504.9 523.6

502.7 522.2

545.0

503.9 523.0

508.9 527.2

518.2

519.3

545.0

545.0

545.0

545.0

545.0

545.0

545.0

545.0

545.0

545.0

545.0

545.0

545.0

545.0

545.0

545.0

545.0

545.0

545.0

545.0

545.0

545.0

545.0

545.0

545.0

545.0

545.0 545.0

545.0 545.0

545.0 545.0

545.0

545.0 545.0

545.0 545.0

545.0

545.0

545.0

86.9

80.9

70.0

80.9

80.9

80.9

80.9

70.0

80.9

80.9

81.2

70.0

82.4

85.8

86.9

70.0

87.4

87.6

87.7

70.0

88.0

88.6

90.1

70.0

93.7

103.7 85.8

110.1 91.4

112.3 92.8

70.0

111.1 92.0

106.1 87.8

96.8

95.7

70.0

TIME 10.00 MINS

468.5

468.5 229.0

468.5

468.5

471.9

471.9 240.0

472.3

474.7

475.3 250.0

476.3

497.9

500.6 259.0

501.2

502.2

502.5 266.0

502.5

502.6

503.1 266.0

507.9

538.2 519.6

544.1 542.6

544.6 544.6

544.6 544.6

544.6 544.6

544.6

544.6 544.6

FIGURE B.5 Sheet 4 of 9

SINHA 86

CALC COLD(40F)FEED AT

STANDRY

DATE

DIV

DEPT

TIME 22.00 HINS

299.3

299.3

150.9

299.3

300.2

302.0

302.9

165.5

303.4

306.8

310.6

171.5

324.1

352.9

363.1

176.6

367.7

369.9

370.8

180.6

372.2

375.6

385.7

180.6

412.6

490.4 406.4

529.9 531.8

541.5 542.1

544.6

544.1 544.2

544.5 544.5

544.4

544.6

544.6

FIGURE B.5 Sheet 5 of 9

TIME 0000 HRS

176.1

176.2 132.0

176.5

177.5

179.2

180.4 137.0

182.0

185.6

190.9 142.0

201.6

217.6

225.4 145.0

230.8

235.3

239.7 148.0

246.3

258.6

282.6 148.0

329.0

435.8 467.1

500.9 519.4

528.7 536.4 544.6

539.4 542.0

543.1 543.9

544.3

544.5 544.6

FIGURE B.5 Sheet 6 of 9



ITER 24 DELTA T MAX .0091 AT NODE 12

117.5

117.6

117.4

117.9

118.7

120.6

121.6

121.6

122.6

124.4

125.6

125.2

127.2

129.6

131.6

128.3

134.5

139.3

146.7

130.8

158.7

178.9

213.5

130.8

272.6

397.1 453.6

473.4 508.5

513.0 529.3

574.6

530.5 538.0

538.8 542.1

542.8

543.9

544.6

FIGURE B.5 Sheet 7 of 9

ITER 20 DELTA T MAX .0062 AT NODE 22

473.3

473.3 473.3

473.3

473.3

473.3

473.3 473.3

473.3

473.3

473.3 473.3

473.3

473.3

473.3 473.3

473.3

473.4

473.6 473.3

474.1

475.6

479.7 473.3

491.6

533.0 544.8

567.8 581.4

585.8 593.4 601.5

594.5 598.1

598.6 600.3

600.6

601.2 601.5

FIGURE B.5 Sheet 8 of 9

ITER 20 DELTA T MAX .0062 AT NODE 22

483.7

483.7 483.7

483.7

483.7

483.7

483.7 483.7

483.7

483.7

483.7 483.7

483.7

483.7

483.7 483.7

483.7

483.8

483.9 483.7

484.4

485.7

489.5 483.7

500.3

538.4 549.2

570.4 583.0

587.0 594.1 601.5

595.0 598.4

598.8 600.4

600.7

601.2 601.5

FIGURE B.5 Sheet 9 of 9

2 33

3

4

5

6

34

7

8

9

35

10

11

COMPUTER PRINT PATTERN

12

36

13

14

15

37

16

17

18

38

19

20

21

22

23

24

25

32

26

27

28

29

30

31

32

FIGURE B.6

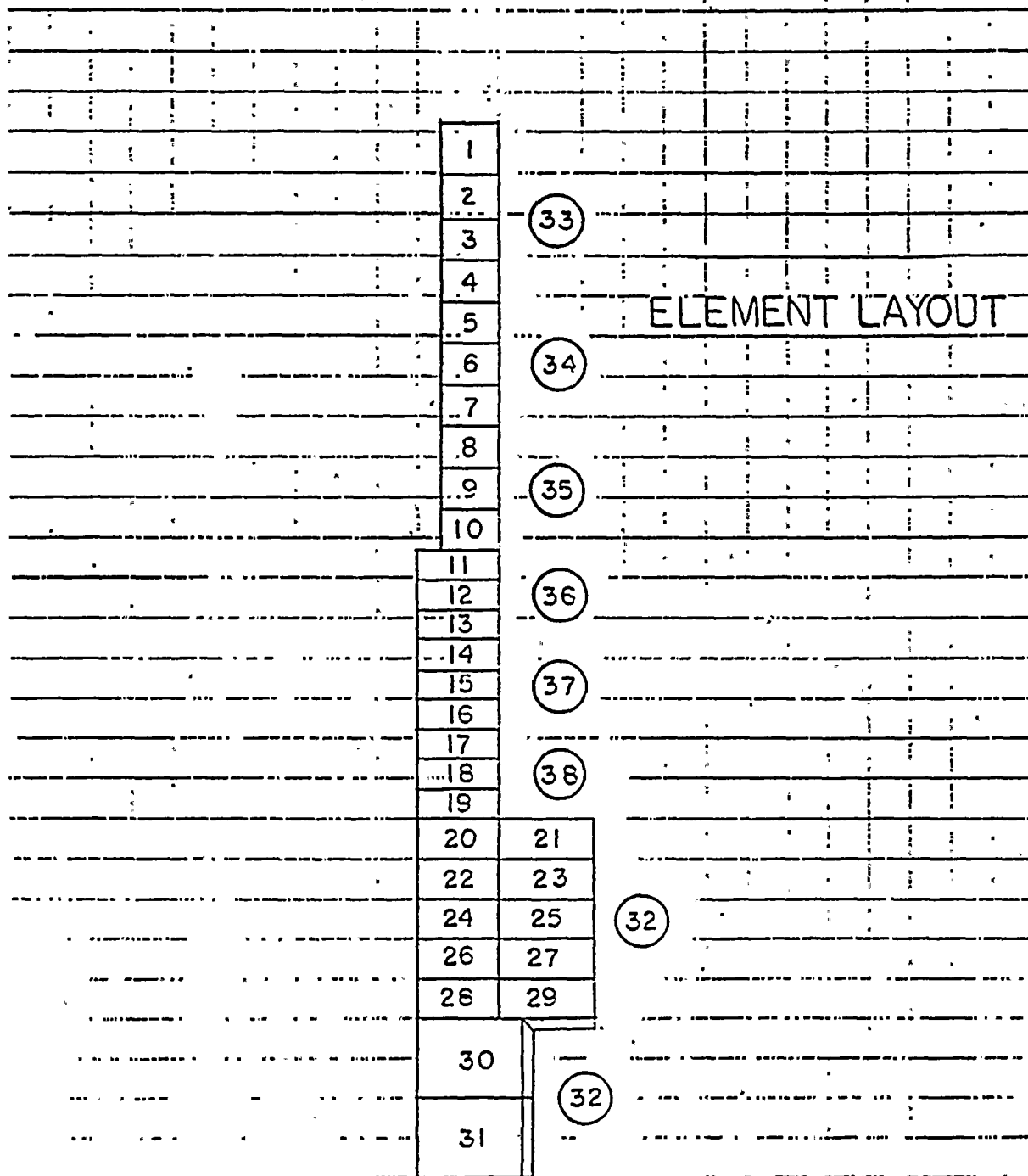


FIGURE B.7

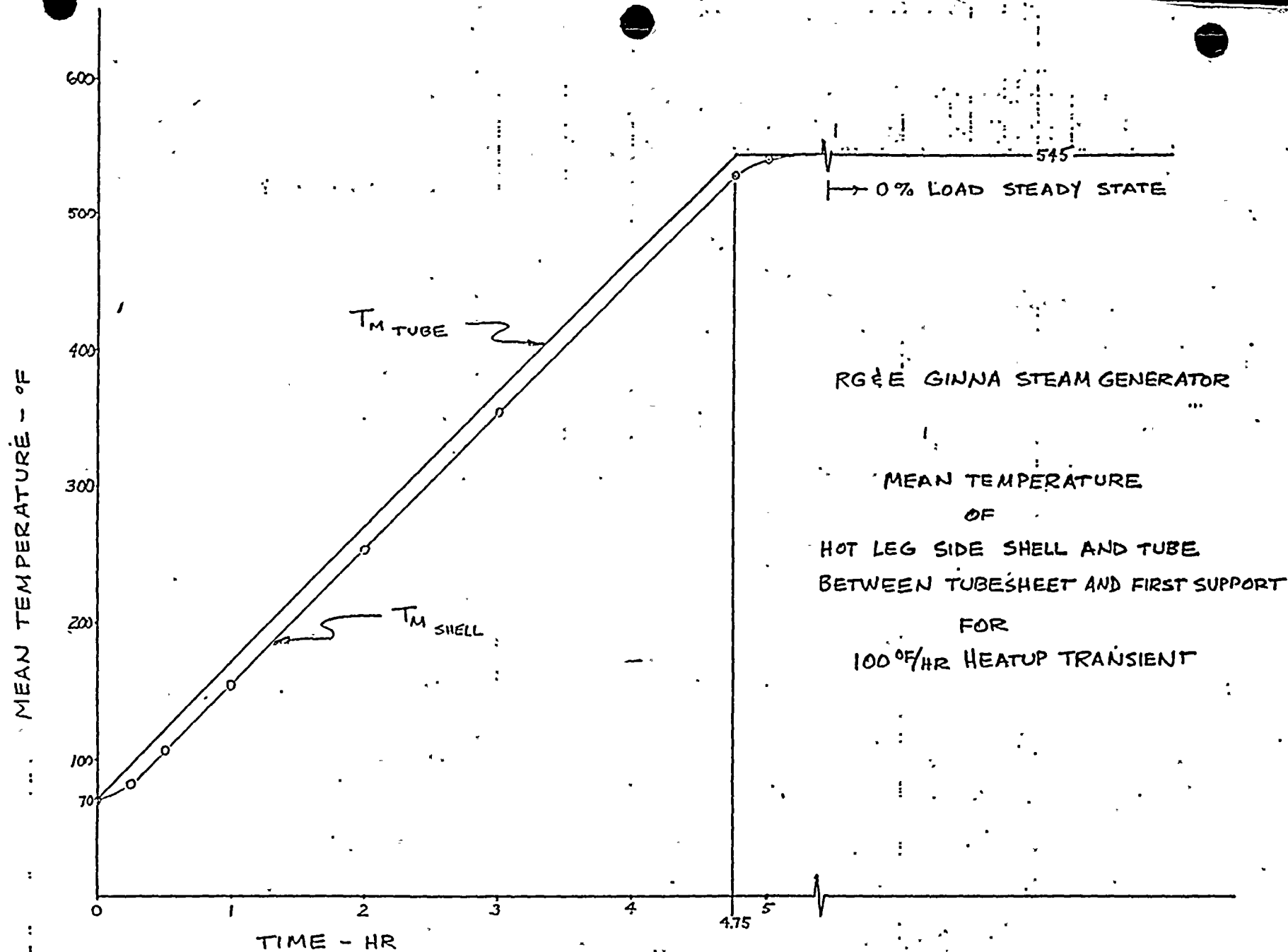


FIGURE B.8 Sheet 1 of 3

RG & E GINNA STEAM GENERATOR

MEAN TEMPERATURE
OF
HOT LEG SIDE SHELL AND TUBE
BETWEEN TUBESHEET AND FIRST SUPPORT
FOR
100 °F/HR COOLDOWN TRANSIENT

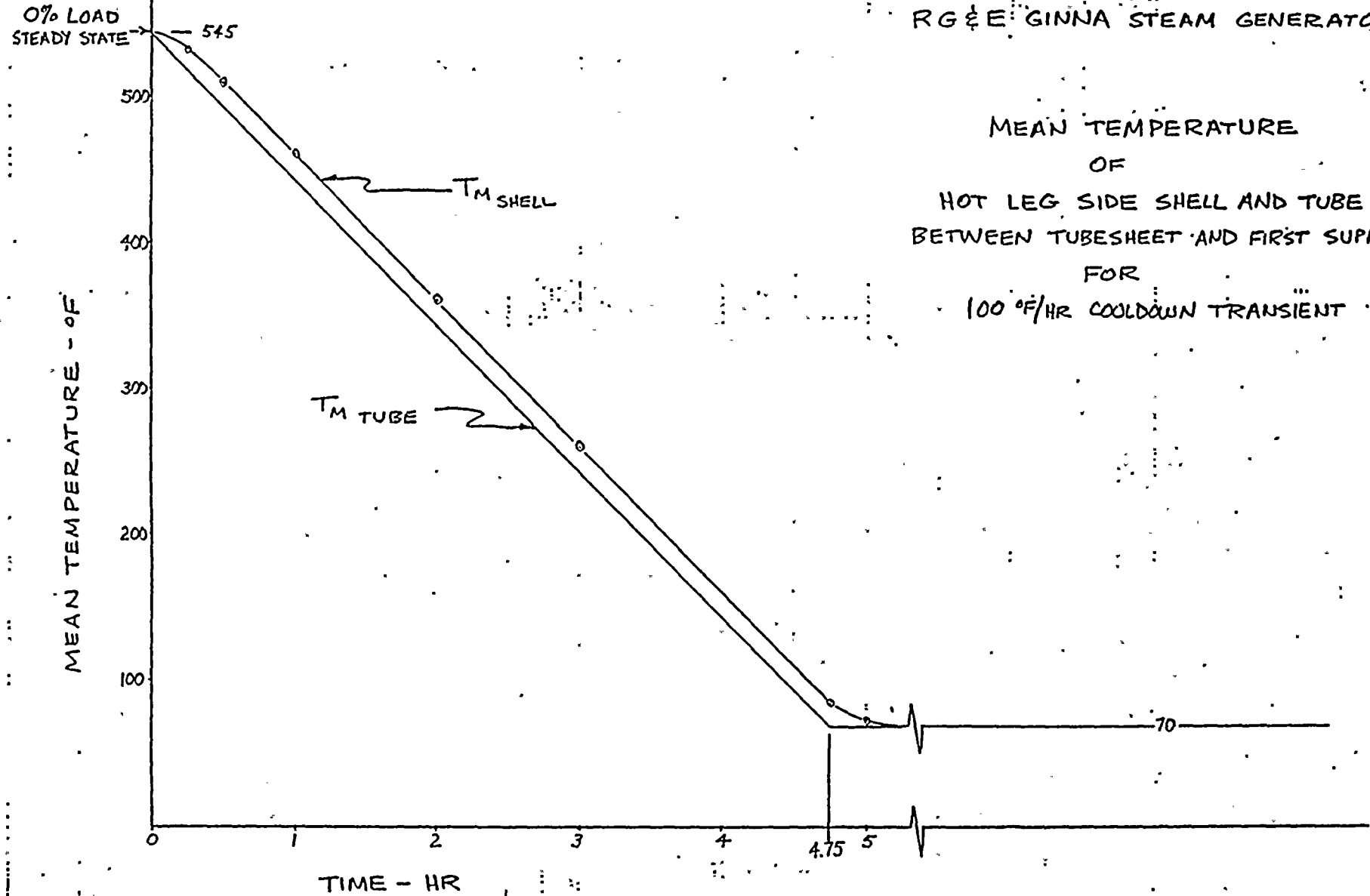
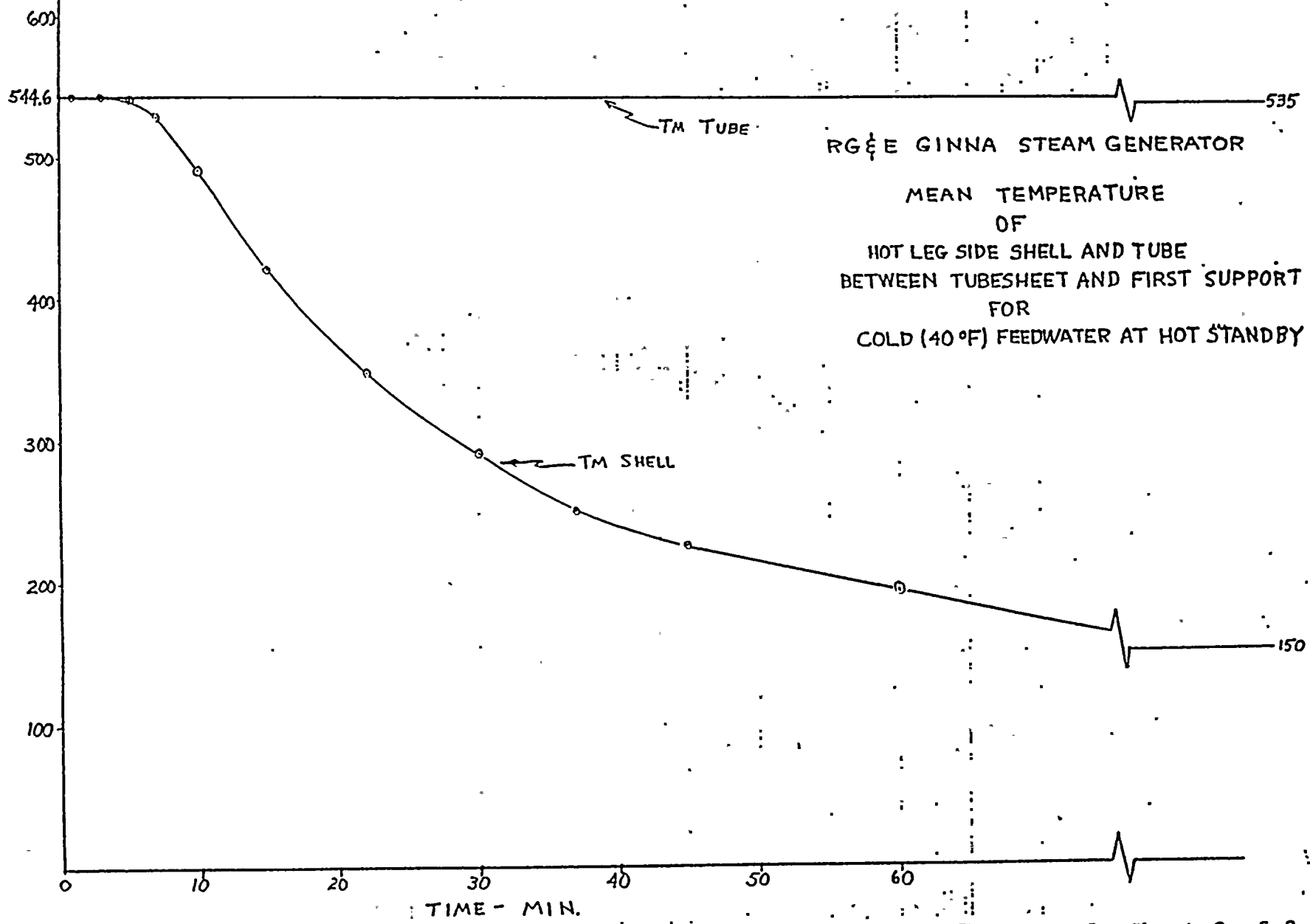


FIGURE B.8 Sheet 2 of 3

MEAN TEMPERATURE - °F



40.0 40.0

47.2 47.2 47.1 42.4 482.8

47.8 47.8 47.8 44.8 481.4

49.0 49.0 49.0 47.3 480.7

50.6 50.6 50.6 49.8 479.4

52.7 52.7 52.7 52.4 478.8

55.1 55.1 55.1 55.0 477.5

57.8 57.8 57.8 57.8 475.4

60.5 60.5 60.5 60.5 475.7

63.4 63.4 63.4 63.4 473.7

66.2 66.2 66.2 66.2 474.1 544.6

69.2 69.2 69.2 69.2 472.2

100.3 100.3 100.3 100.3 466.3

72.1 72.1 72.1 72.1 472.6

103.6 103.6 103.6 103.6 466.8

75.1 75.1 75.1 75.1 470.7

106.9 106.9 106.9 106.9 465.4

78.1 78.1 78.1 78.1 471.2

110.3 110.3 110.3 110.3 466.0

81.2 81.2 81.2 81.2 469.4

113.6 113.6 113.6 113.6 464.7 544.6

84.3 84.3 84.3 84.3 469.9

117.0 117.0 117.0 117.0 465.3

87.5 87.5 87.5 87.5 468.3

120.4 120.4 120.4 120.4 463.9

90.6 90.6 90.6 90.6 468.8

123.9 123.9 123.9 123.9 465.1

93.8 93.8 93.8 93.8 467.2

127.8 127.7 127.7 127.3 463.7

97.1 97.1 97.1 97.0 467.7

135.3 135.1 134.8 134.5 130.7 464.4

160.6

FIGURE B.9

CONTRACT

CALC. 100% POWER S.S.

DATE 2-15-82-DIV 04 DEPT 625

ITER 291 DELTA T MAX .0099 AT NODE 91

415.1 517.7

473.7 473.7 473.7 473.7 496.4

473.5 473.5 473.5 473.5 496.4

473.3 473.3 473.3 473.3 496.4

473.2 473.2 473.2 473.2 496.4

473.1 473.1 473.1 473.1 496.4

473.1 473.1 473.1 473.1 496.5

473.1 473.1 473.1 473.1 496.5

473.1 473.1 473.1 473.1 496.5

473.1 473.1 473.1 473.1 496.5

473.1 473.1 473.1 473.1 496.5 517.7

473.1 473.1 473.1 473.1 496.5

473.2 473.2 473.2 473.2 496.5

473.1 473.1 473.1 473.1 496.5

473.2 473.2 473.2 473.2 496.5

473.2 473.2 473.2 473.2 496.5

473.2 473.2 473.2 473.2 496.5

473.2 473.2 473.2 473.2 496.5

473.2 473.2 473.2 473.2 496.5

473.2 473.2 473.2 473.2 496.5

473.2 473.2 473.2 473.2 496.5 517.7

473.2 473.2 473.2 473.2 496.5

473.3 473.3 473.3 473.3 496.5

473.2 473.2 473.2 473.2 496.5

473.3 473.3 473.3 473.3 496.5

473.2 473.2 473.2 473.2 496.5

473.3 473.3 473.3 473.3 496.5

473.2 473.2 473.2 473.2 496.5

473.3 473.3 473.3 473.3 496.5

473.2 473.2 473.2 473.2 496.5

474.4 474.3 474.2 474.1 473.3 496.5

483.1

FIGURE B.10

CONTRACT

CALC TRANSIENT (RUN #2)

DATE 2-15-66

TIME 45.00 MINS

COLD FEED AT HOT STANDBY

40.0 40.0

472.1 470.9 469.0 42.7 482.8

458.1 456.6 454.3 45.0 481.1

436.0 434.3 431.4 48.3 480.4

401.7 399.4 395.8 51.4 478.8

383.2 380.4 375.8 54.5 478.1

286.0 282.5 276.8 57.9 478.6

181.1 177.7 172.2 61.3 474.0

152.3 149.3 144.4 64.7 474.5

149.0 146.1 141.4 68.1 472.2

151.3 148.4 143.8 71.6 472.7 544.6

149.9 147.1 142.5 75.1 470.5

148.5 145.9 141.8 112.3 464.7

152.6 149.8 145.3 78.8 471.1

172.2 169.7 165.5 116.1 465.4

152.0 149.3 144.8 82.5 469.0

174.1 171.5 167.4 120.0 464.0

155.0 152.3 147.9 85.9 469.6

177.9 175.3 171.3 123.8 464.7

155.1 152.4 148.1 89.6 467.7

180.0 177.5 173.4 127.9 463.4 544.6

158.3 155.6 151.3 93.2 468.3

183.9 181.4 177.4 131.6 464.1

158.9 156.3 152.0 97.0 466.6

186.3 183.8 179.8 135.8 462.8

162.3 159.7 155.5 100.8 467.2

190.5 188.0 184.0 139.8 464.0

163.4 160.8 156.7 104.6 465.6

193.9 191.2 188.9 143.6 462.7

167.0 164.4 160.3 108.4 466.2

229.3 226.4 220.7 214.0 148.1 463.6

229.0

FIGURE B.11

COLD FW (40°F) DURING HOT STANDBY
DOWNCOMER ANNULUS OUTLET TEMPERATURE VS. TIME

FEEDWATER FLOW RATE = 5368.6 #/HR

RECIRC. FLOW RATE = 0

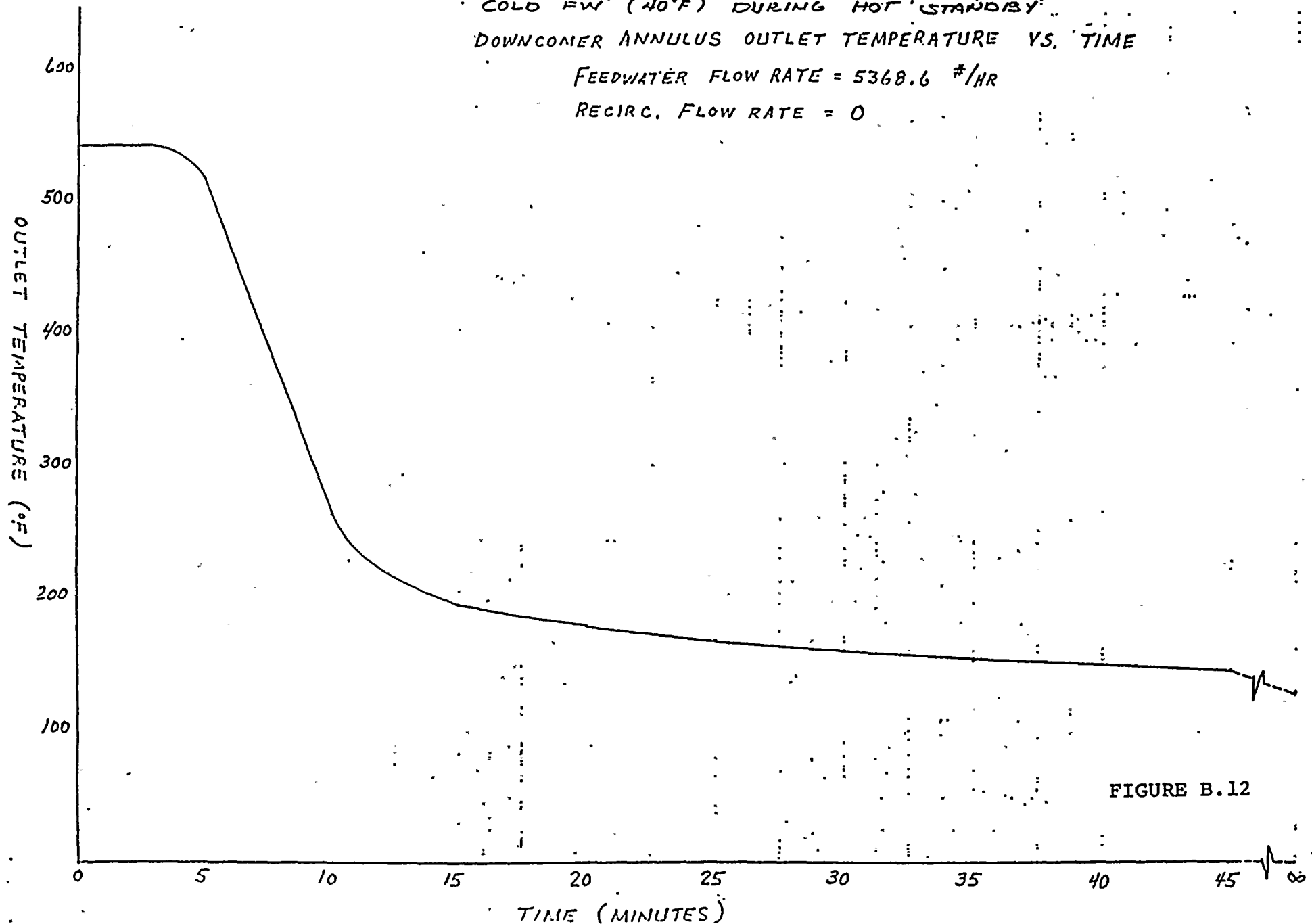


FIGURE B.12

AT THE HORIZONTAL PLANE $IZ = 1$

RANGE OF THE FIELD IS $-3.68E-01$ TO $2.268E-01$

BAND SCALES ARE	1	- .368E-01 TO	- .305E-01
	3	- .241E-01 TO	- .178E-01
	5	- .114E-01 TO	- .510E-02
	7	- .125E-02 TO	- .760E-02
	9	- .139E-01 TO	- .203E-01

[illegible][illegible]

```

1.....1      3333      5555      333      1111111111111111.....1
1.....1,      3333      555555555555      333      111111111111.....1
1.....      3333      5555      555      333      111111111111.....1

```

[illegible]

I	7	999	999	7	5555555	3333
I			9	7	55555555	
I			9		5555	

HOT SIDE

COLD SIDE

Quality at 7.in above tubesheet (CR = 3.76)

Note: Downcomer opening is 14 in high.

FIGURE B.13

RADIAL VELOCITY (MIXTURE) AT THE HORIZONTAL PLANE $z=1$

RANGE OF THE FIELD IS $-.520$ TO $.445$ meter/sec

BAND SCALES ARE	1	.520	TO	.424
	3	.328	TO	.231
	5	.135	TO	.388E-01
	7	.576E-01	TO	.154
	9	.250	TO	.347

[illegible]

. Radial velocity (m/sec) at 7 in above tubesheet (CR = 3.76)

Note: Downcomer opening is 14 in high.

FIGURE B.14

AXIAL VELOCITY

(MIXTURE)

AT THE HORIZONTAL PLANE $z=1$

RANGE OF THE FIELD IS

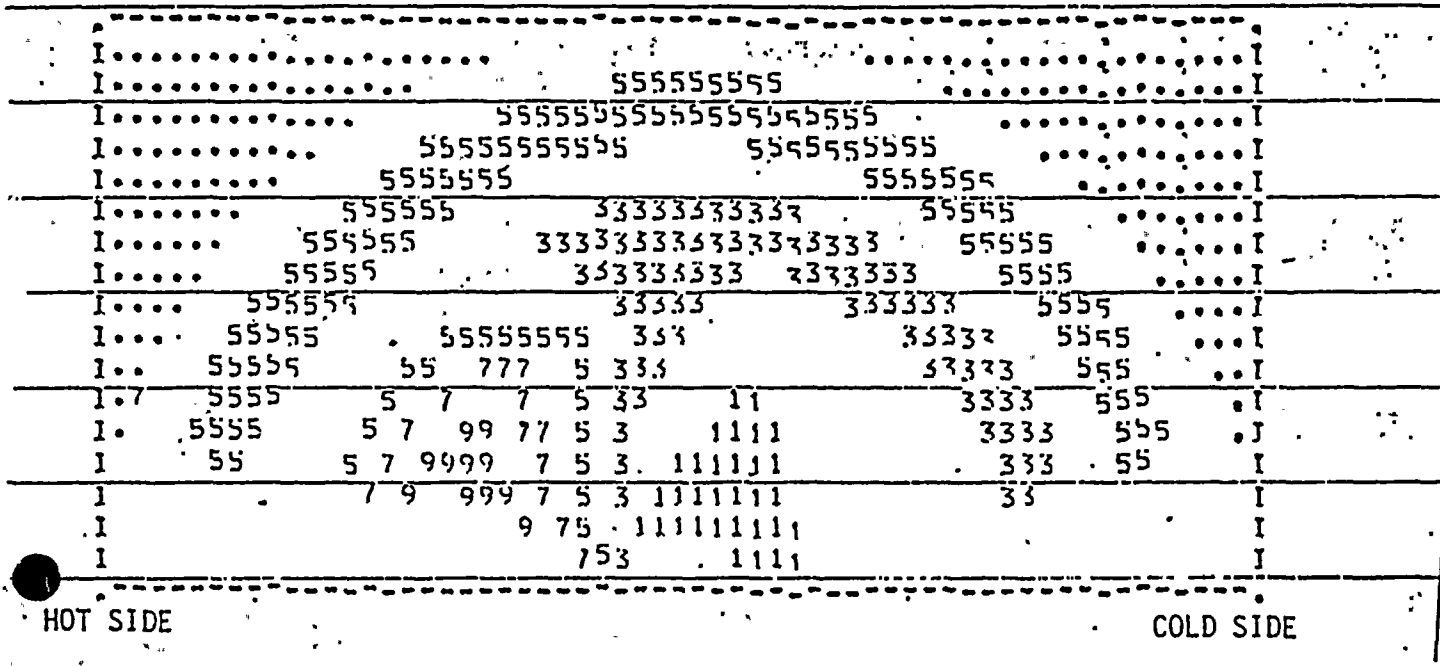
-0.205

TO

1.22 meter/sec

BAND SCALES ARE

1	-0.205	TO	$-0.626E-01$
3	$-0.194E-01$	TO	0.221
5	0.363	TO	0.505
7	0.647	TO	0.789
9	0.931	TO	1.07



Axial velocity (m/sec) at 14 in above tubesheet (CR = 3.76)

Note: Downcomer opening is 14 in high.

FIGURE B.15

VOID FRACTION (RG)

AT THE HORIZONTAL PLANE $IZ = 1$

RANGE OF THE FIELD IS 0. TO .430

BAND SCALES ARE	1	0.	TO	.429E-01
	3	.050E-01	TO	.129
	5	.172	TO	.214
	7	.257	TO	.300
	9	.343	TO	.386

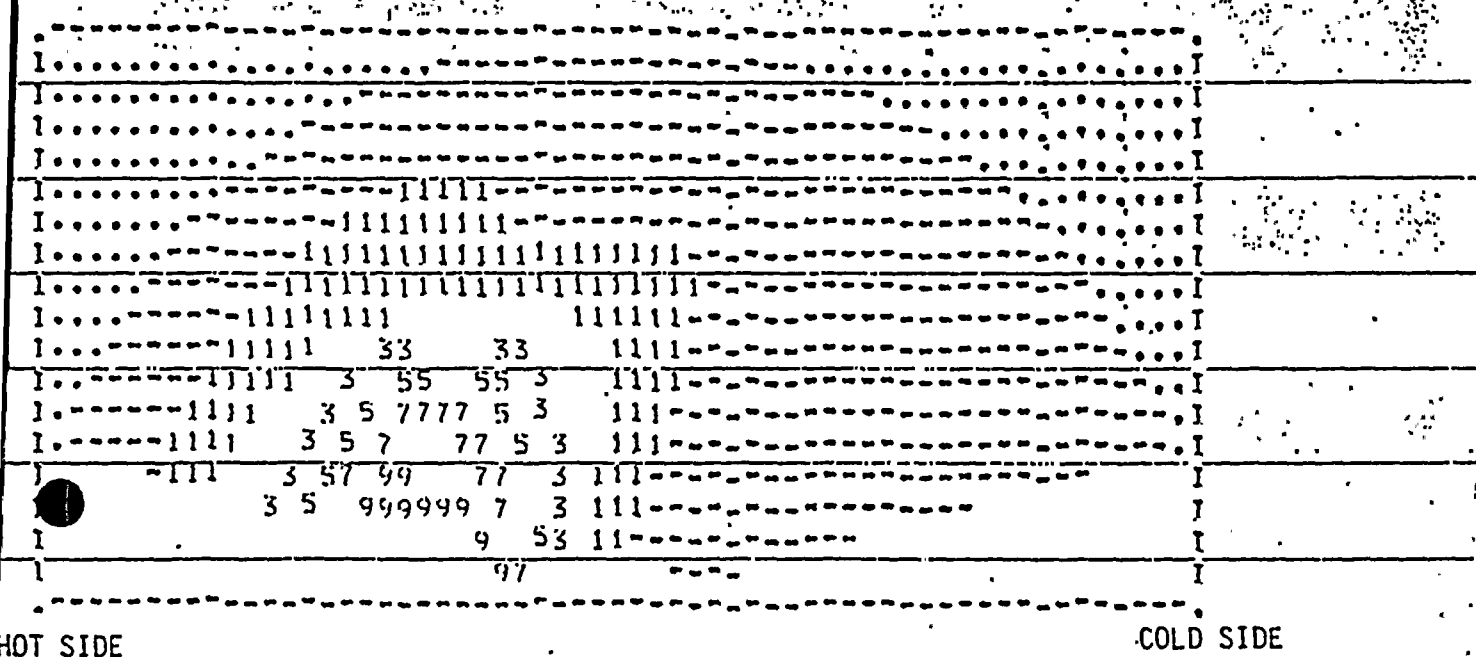


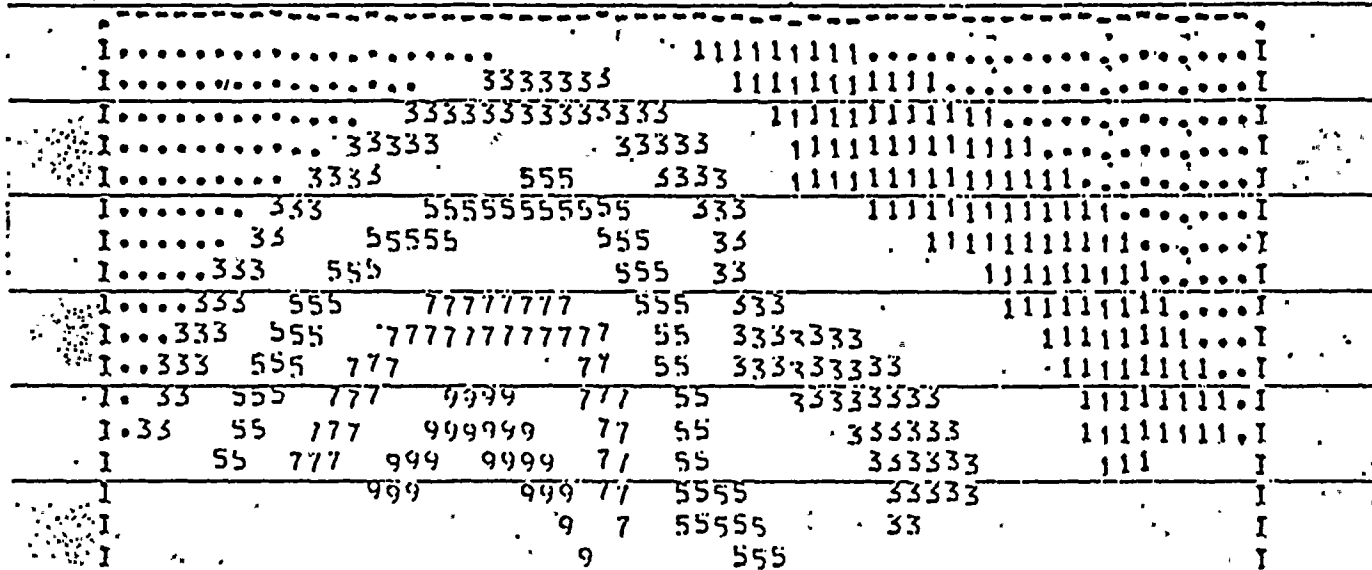
FIGURE B.16

MASS QUALITY

AT THE HORIZONTAL PLANE $IZ = 2$

RANGE OF THE FIELD IS $-.342E-01$ TO $.325E-01$

BAND SCALES ARE	1	$-.342E-01$ TO	$.276E-01$
	3	$-.209E-01$ TO	$.143E-01$
	5	$-.760E-02$ TO	$.948E-03$
	7	$.570E-02$ TO	$.124E-01$
	9	$.190E-01$ TO	$.257E-01$



HOT SIDE

COLD SIDE

Quality at 20 in above tubesheet (CR = 3.76)

FIGURE B.17

AXIAL VELOCITY

(MIXTURE)

AT THE HORIZONTAL PLANE $z = 2$

RANGE OF THE FIELD IS

-0.229

TO

1.89 meter/sec

BAND SCALES ARE

1

-0.229

TO

-0.169E-01

3

0.195

TO

0.407

5

0.619

TO

0.831

7

1.04

TO

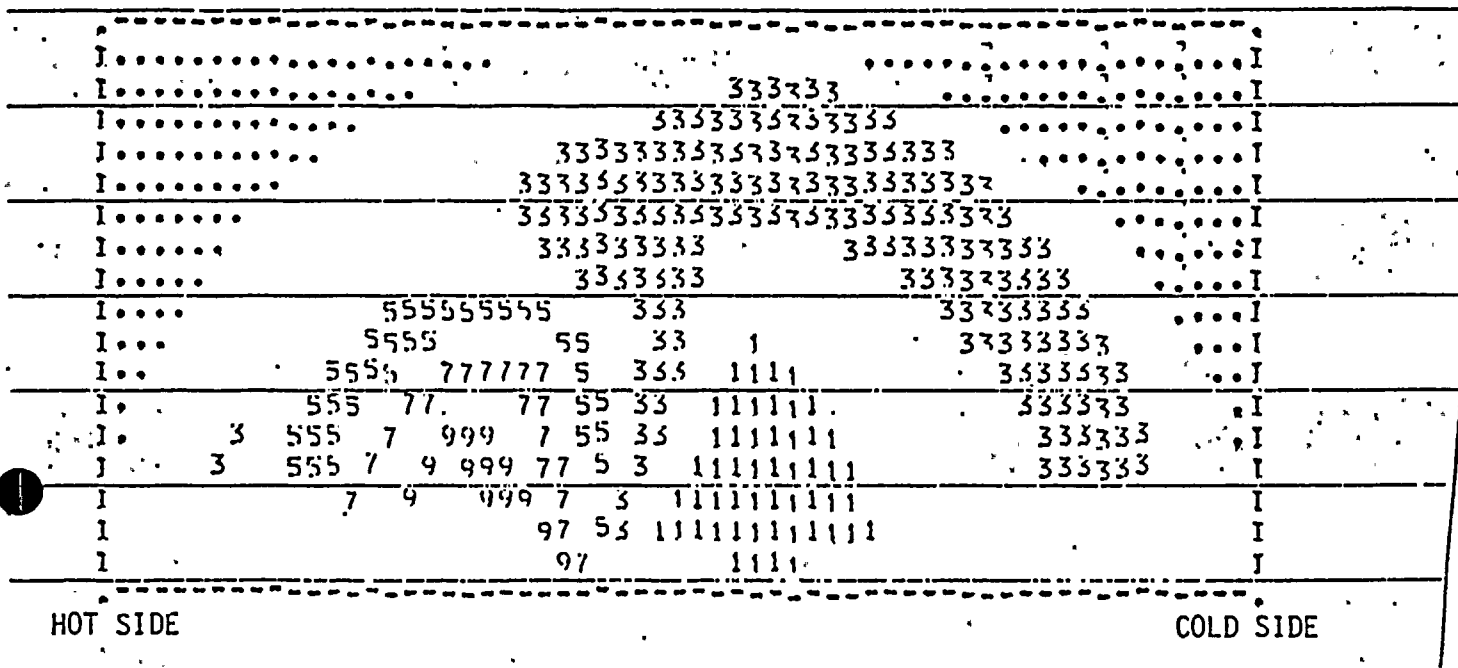
1.25

9

1.47

TO

1.68



Axial velocity (m/sec) at 27 in above tubesheet (CR = 3.76)

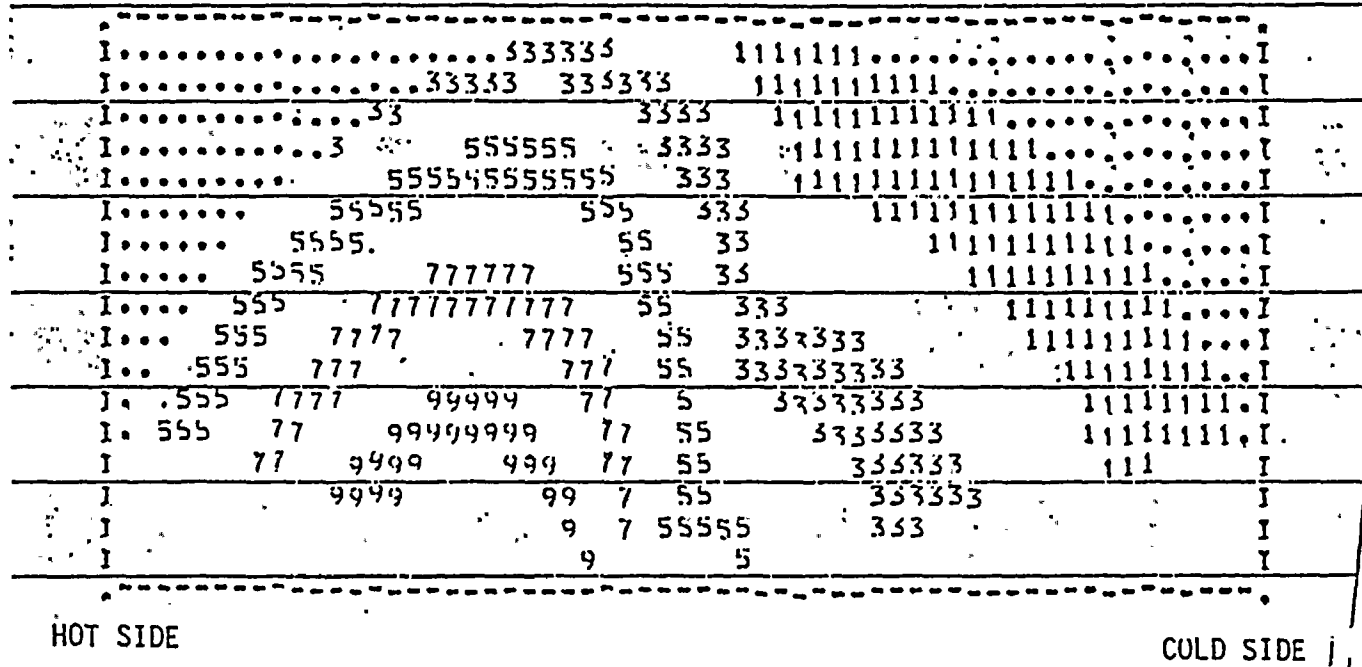
FIGURE B.19

MASS QUALITY

AT THE HORIZONTAL PLANE $IZ = 3$

RANGE OF THE FIELD IS $-0.311E-01$ TO $0.395E-01$

BAND SCALES ARE	1	$-0.311E-01$ TO	$0.240E-01$
	3	$-0.170E-01$ TO	$0.994E-02$
	5	$-0.290E-02$ TO	$0.414E-02$
	7	$0.112E-01$ TO	$0.182E-01$
	9	$0.253E-01$ TO	$0.323E-01$



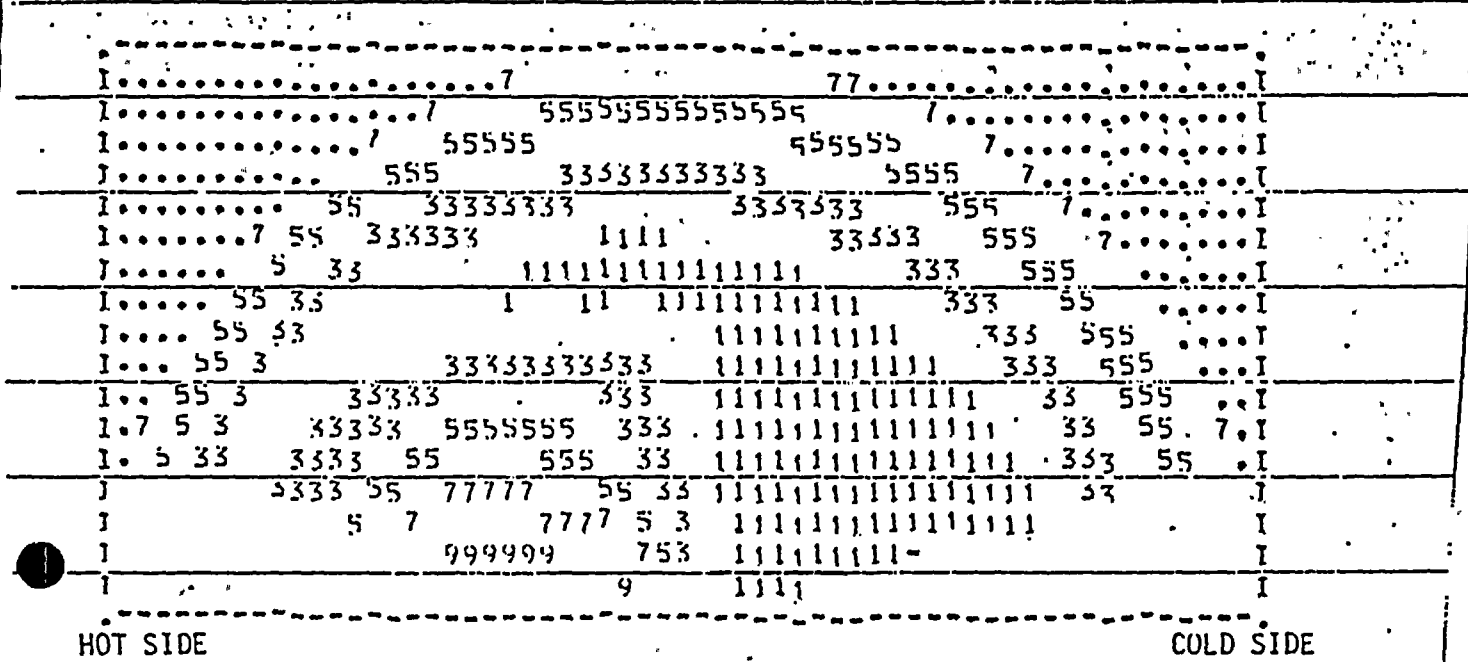
Quality at 33 in above tubesheet (CR = 3.76)

FIGURE B.20

RADIAL VELOCITY (MIXTURE) AT THE HORIZONTAL PLANE $z = 3$

RANGE OF THE FIELD IS -0.192 TO 0.113 meter/sec

BAND SCALES ARE	1	-0.192	TO	-0.162
	3	-0.131	TO	-0.101
	5	$-0.092E-01$	TO	$-0.0397E-01$
	7	$-0.029E-02$	TO	$0.212E-01$
	9	$0.516E-01$	TO	$0.821E-01$



Radial velocity (m/sec) at 33 in above tubesheet (CR = 3.76)

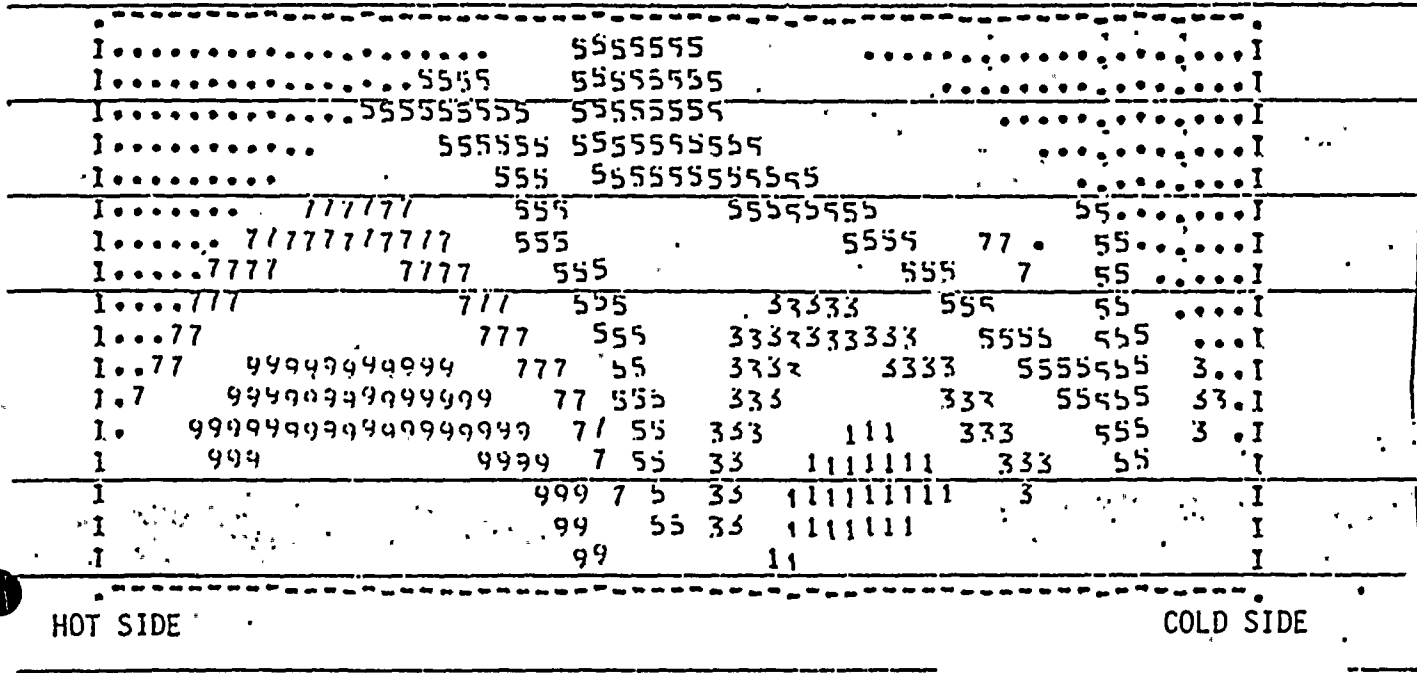
FIGURE B.21

MASS QUALITY

AT THE HORIZONTAL PLANE $17 = 6$

RANGE OF THE FIELD IS .305E-01 TO .821E-01

BAND SCALES ARE	1	.305E-01 TO	.357E-01
	3	.408E-01 TO	.460E-01
	5	.511E-01 TO	.563E-01
	7	.614E-01 TO	.665E-01
	9	.717E-01 TO	.768E-01



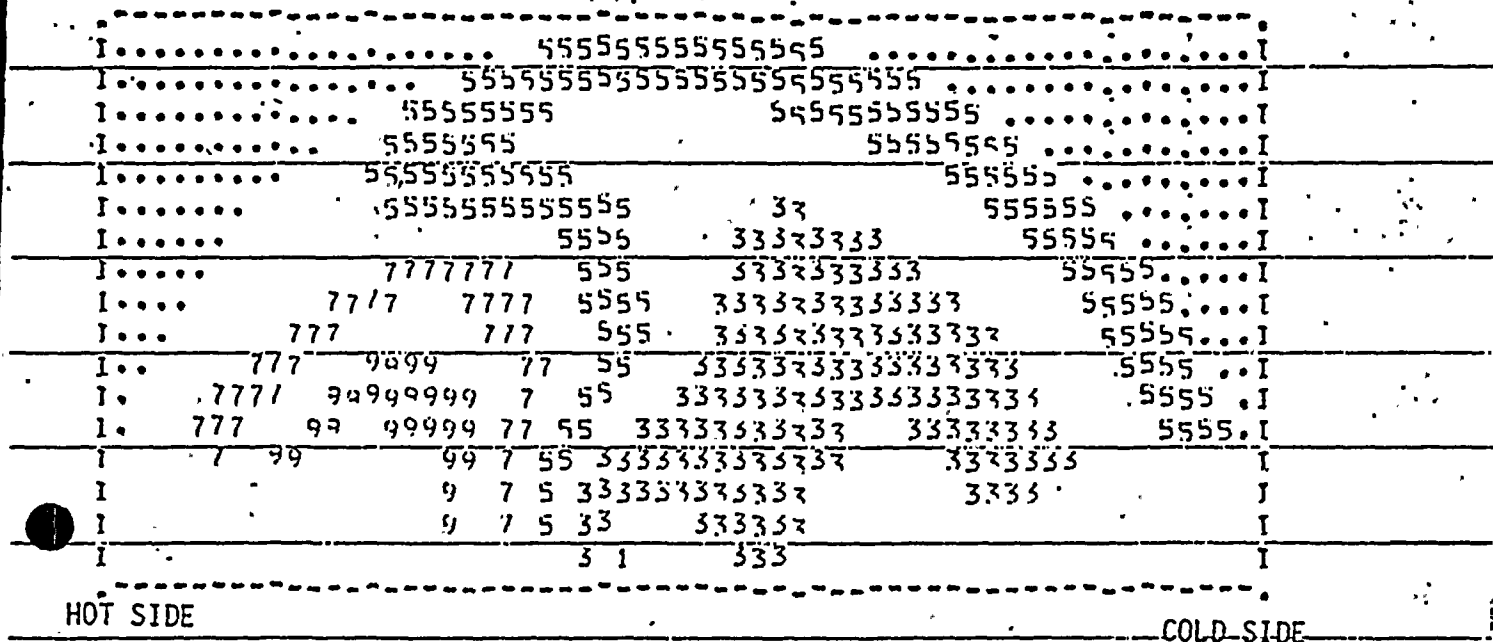
Quality at 91 in above tubesheet (CR = 3.76)

FIGURE B.22

RADIAL VELOCITY (MIXTURE) AT THE HORIZONTAL PLANE $IZ = 4$

RANGE OF THE FIELD IS $\sim .500$ TO $.279$ meter/sec

BAND SCALES ARE	1	$\sim .300$	10	$\sim .242$
	3	$\sim .184$	10	$\sim .127$
	5	$\sim .089E-01$	10	$\sim .111E-01$
	7	$\sim .466E-01$	10	$\sim .104$
	9	$\sim .162$	10	$\sim .220$



Radial velocity (m/sec) at 46 in above tubesheet (CR = 3.76)

Note: The first tube support device is at 51.8 in above tubesheet.

FIGURE B.23

AXIAL VELOCITY

(MIXTURE)

AT THE HORIZONTAL PLANE $IZ = 4$

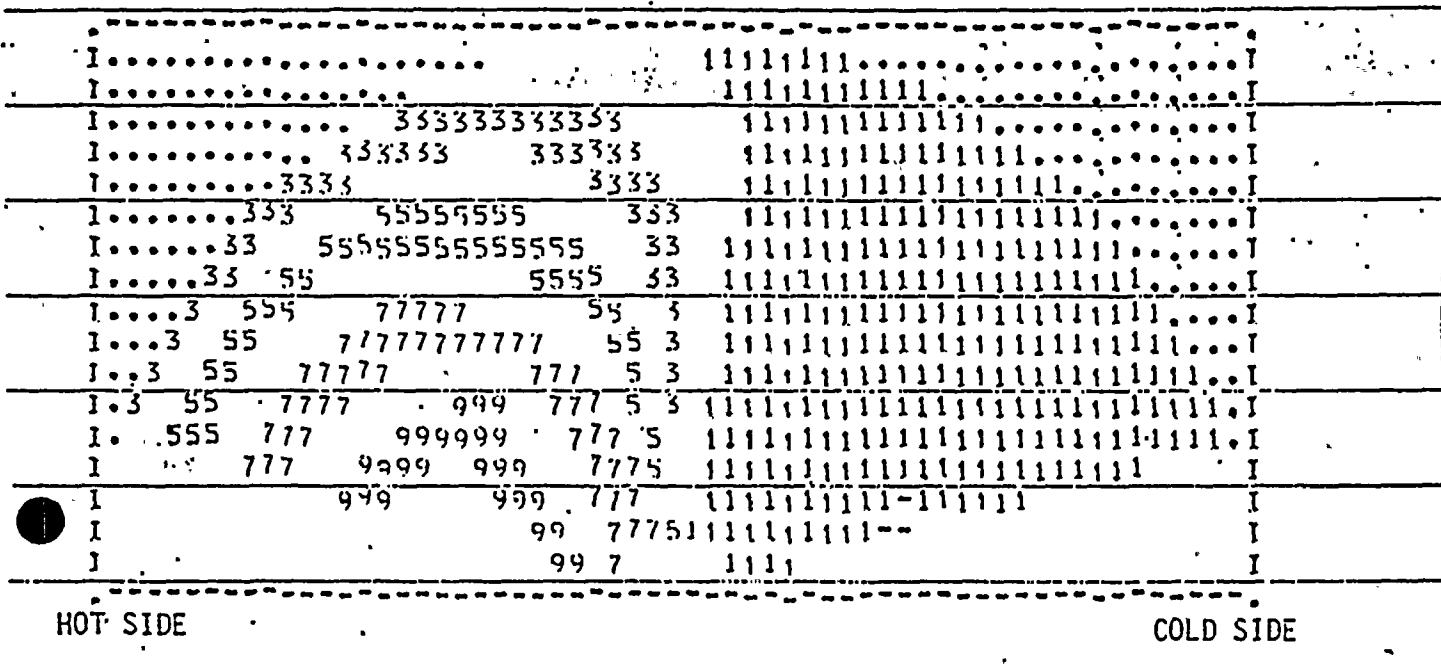
RANGE OF THE FIELD IS

.846E-01 TO

2.02 meter/sec

BAND SCALES ARE

1	.846E-01	TO	.278
3	.472	TO	.666
5	.859	TO	1.05
7	1.25	TO	1.44
9	1.63	TO	1.83



Axial velocity (m/sec) at 51.8 in above tubesheet (CR = 3.76)

Note: The first tube support device is at 51.8 in above tubesheet.

FIGURE B.24

7ASS QUALITY

AT THE HORIZONTAL PLANE $IZ = 4$

RANGE OF THE FIELD IS $-2.68E-01$ TO $.476E-01$

BAND	SCALES ARE			
1	- .268E-01	T0	- .194E-01	
3	- .119F-01	T0	- .447E-02	
5	.298F-02	T0	.104E-01	
7	- .179E-01	T0	.253E-01	
9	- .328E-01	T0	.402E-01	

1	3333333	111111.....
1	3333	11111111.....
1	55555555	333 1111111111.....
1	5555555555555555	333 111111111111.....
1	5555 555 333	11111111111111.....
1	555 77 555 333	11111111111111.....
1	55 7777777777 555 33	111111111111.....
1	5 77777777777777 55 33	1111111111.....
1	777 777777 55 33	1111111111.....
1	777 777 55 335333	1111111111.....
1	777 99999 77 55 33533333	1111111111.....
1	777 999999999999 77 55 33533333	1111111111.....
1	777 9999999 99999 77 5 33333333	1111111111.....
1	99999 9999 1 5 333333	1111.....
1	99 999 5 33333333
1	9999 3333
1	99

HOT SIDE

COLD SIDE

Quality at 46 in above tubesheet (CR = 3.76)

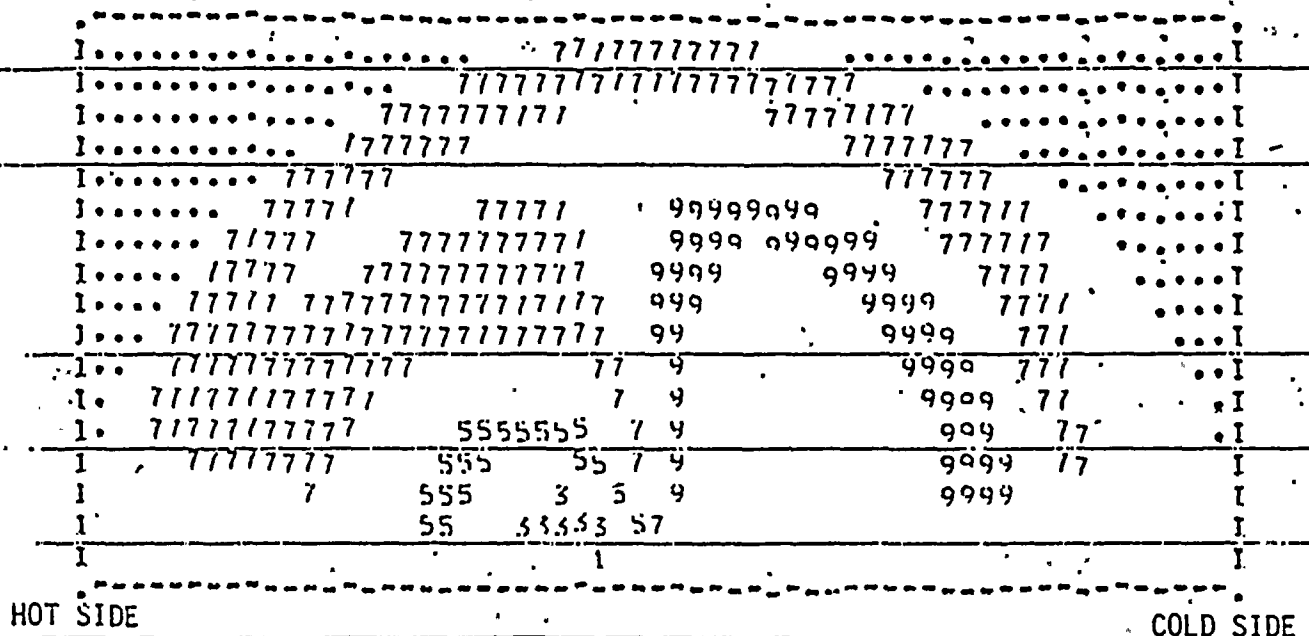
Note: The first tube support device is at 51.8 in above tubesheet.

FIGURE B.25

RADIAL VELOCITY (MIXTURE) AT THE HORIZONTAL PLANE $z = 6$

RANGE OF THE FIELD IS -0.463 TO 0.355 meter/sec

BAND SCALES ARE	1	-0.463	TO	-0.382
	3	-0.300	TO	-0.218
	5	-0.137	TO	$-0.552E-01$
	7	$-0.264E-01$	TO	0.108
	9	-0.190	TO	0.271



Radial velocity (m/sec) at 91 in above tubesheet (CR = 3.76)

FIGURE B.26

APPENDIX C

GINNA STEAM GENERATOR EXTERNAL TUBE LOADING TEST

C.1 Summary

Work under this program is concerned with performing a detailed analysis of the effects of axial load and loose part impacting on the Ginna steam generator tube's propensity for local buckling. Quantitative shot peening parameters such as shot size, velocity and duration will be developed which correctly simulate the tube distress caused by the loose metal piece found in the Ginna steam generator. Tubes representative of the various intensities of peening will be metallurgically examined to quantify the depth of affected metal and characterize the tube surface condition. Examination will include light microscopy and microhardness of tube wall cross sections as well as scanning electron microscopy of the peened surface. In addition, destructive metallography will be carried out as part of this effort.

C.2 Methodology

Two series of tests will be performed using the external tube loading test apparatus shown in Figure C.1. In the first test, the Axial Compressive Load Only Test, a tube sample with no peening is rigidly clamped at the tube sheet level with the first two supports positioned for a predetermined offset. An axial load is applied by mechanical torquing through a load cell until the tube sustains permanent deformation or until the maximum displacement due to differential temperature is reached. During the loading process, periodic data sets are taken. The test is repeated using offsets of zero, 1/4", 1/2" and other offset values as may be required.

The second test, Parameter Combination Test, involves samples that are peened at a predetermined amount. A predetermined axial load is then applied and the tube is subjected to external pressure until a sharp pressure reduction indicates local tube buckling or the maximum equipment test pressure capacity is reached. During the test, periodic data sets are taken at appropriate stop points in the loading sequence. Testing input variables will include:

a) Axial Load

- (1) Direction - tension or compression
- (2) Magnitude - from zero to 3,000 lb. using a load cell
- (3) Eccentricity - support offset, zero to 1/2 inch

b) Peening

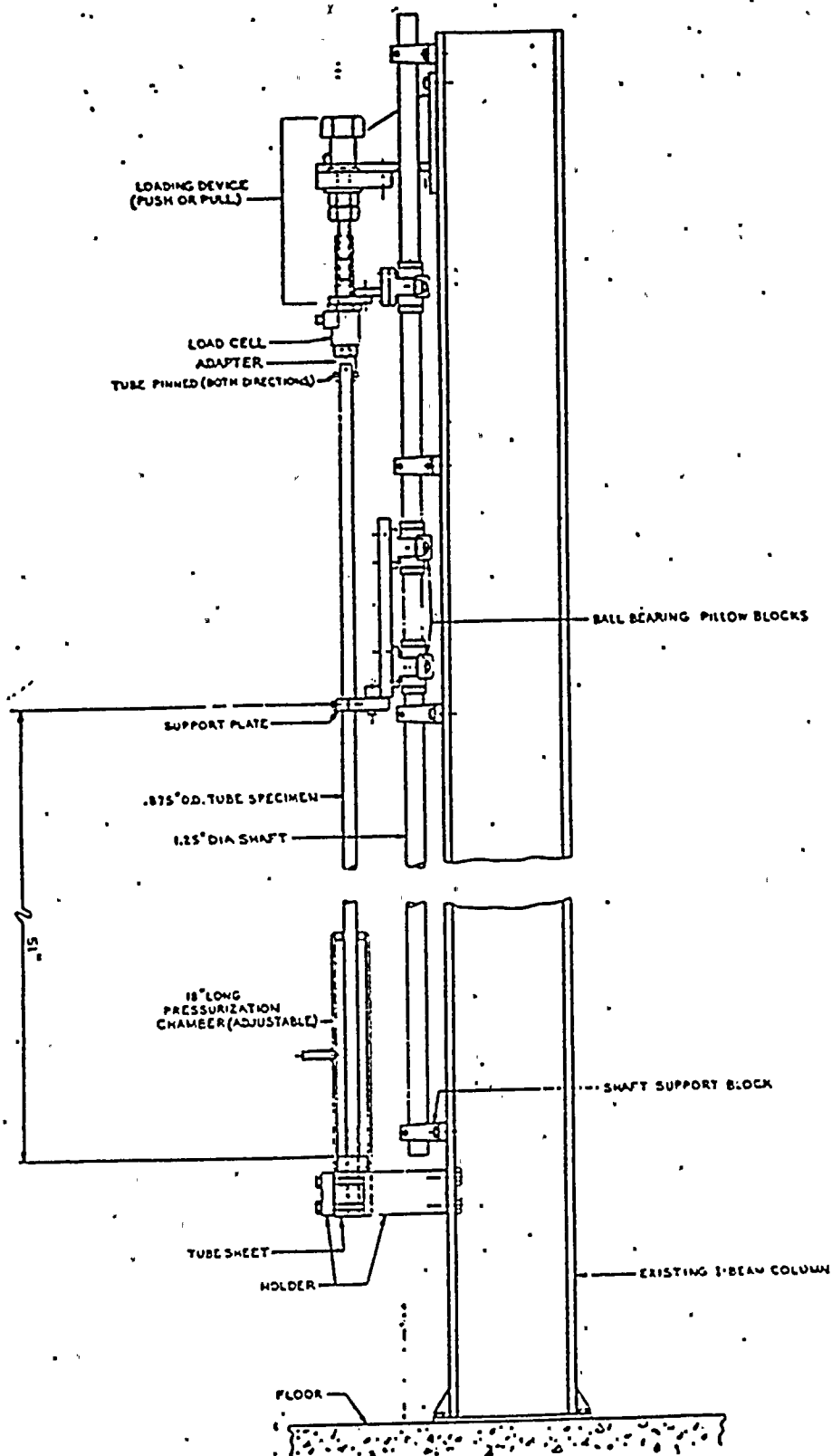
- (1) Area Covered
- (2) Shot size, shot velocity and shot duration based on comparison of RG&E input with peening bench test.
- (3) Metal Removal - to be finalized later

c) External Pressure

External Pressure will be applied in increments up to a value exceeding the Ginna steam generator secondary side design pressure.

Measured output data is to include the following:

- a) Forces developed at supports (leads to calculation of bending moment).
- b) Tube bowing (deflections taken at various vertical positions).
- c) Cross-section dimensions in peened region (micrometer and profilometer).
- d) ECT readings to determine (1) loss of wall thickness, (2) section irregularity and (3) surface distress (background noise).
- e) Load required to move "adjustable tube support" vertically (tendency to lock up).
- f) Visual and photographic record.
- g) Tube collapse pressure (local buckling).



EXTERNAL TUBE LOADING TEST APPARATUS

